Journal of Ophthalmology

Translational Devices, Technologies, and Medicines in Clinical Ophthalmology

Guest Editors: George M. Saleh, M. Reza Vagefi, and Ioannis Athanasiadis

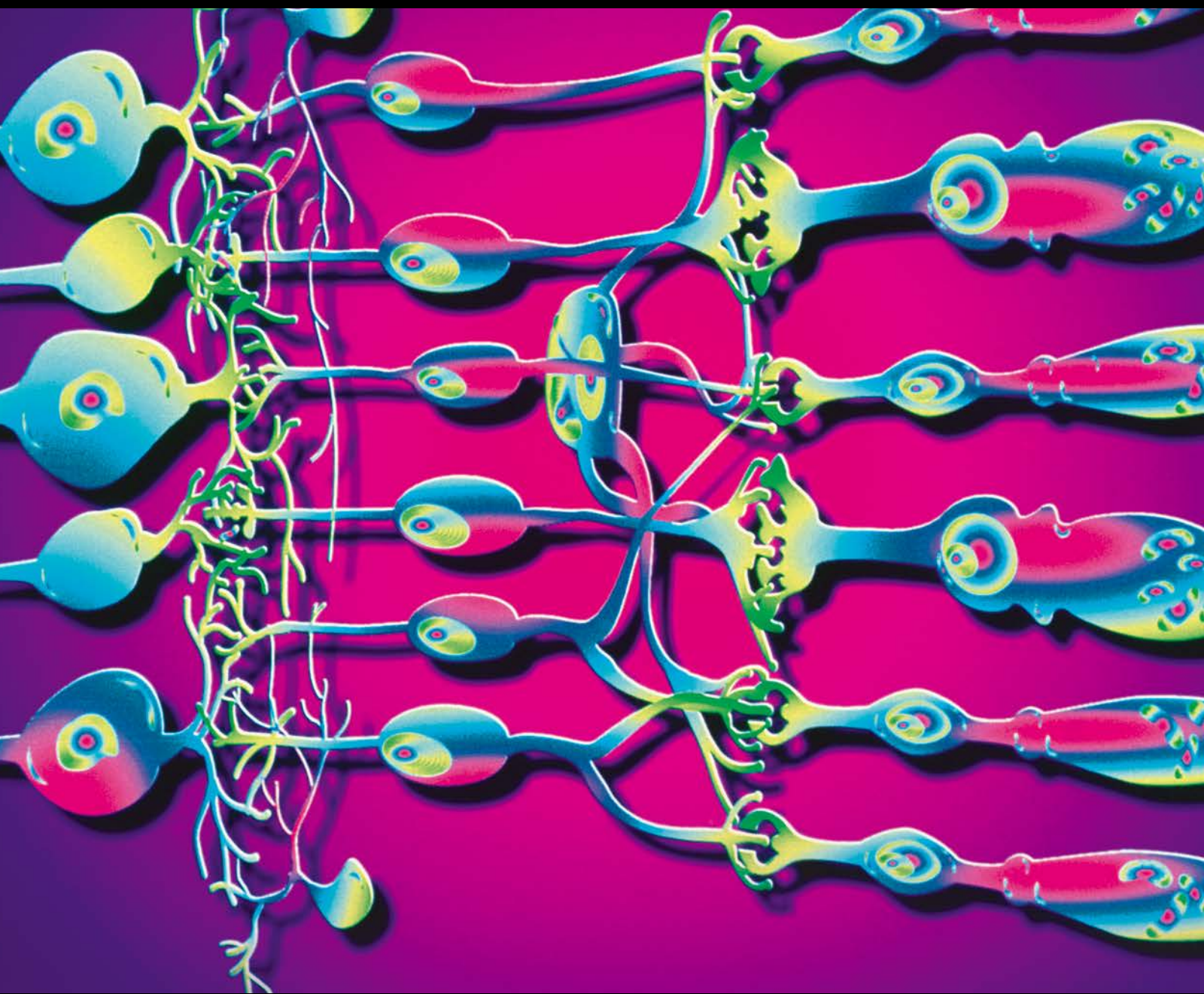

Translational Devices, Technologies, and Medicines in Clinical Ophthalmology

Journal of Ophthalmology

Translational Devices, Technologies, and Medicines in Clinical Ophthalmology

Guest Editors: George M. Saleh, M. Reza Vagefi, and Ioannis Athanasiadis

Editorial Board

Contents

Hindawi Publishing Corporation
Journal of Ophthalmology
Volume 2017, Article ID 2876896, 2 pages
http://dx.doi.org/10.1155/2017/2876896

Editorial

Translational Devices, Technologies, and Medicines in Clinical Ophthalmology

George M. Saleh,[1] M. Reza Vagefi,[2] and Ioannis Athanasiadis[3]

[1]*The National Institute for Health Research Biomedical Research Centre at Moorfields Eye Hospital and UCL Institute of Ophthalmology, London, UK*
[2]*Oculofacial Plastic, Orbital and Reconstructive Surgery, University of California, San Francisco, San Francisco, CA, USA*
[3]*Modern Ophthalmic Practice, Thessaloniki, Greece*

Correspondence should be addressed to George M. Saleh; george.saleh@moorfields.nhs.uk

Received 21 July 2016; Accepted 21 July 2016; Published 15 January 2017

Over the last few decades, there has been a rapid advance in the technologies contributing to clinical ophthalmology ranging from novel hardware and software to new imaging and laser modalities with the emergence of nanotechnologies and drug innovations. The stated aim of translational research is to apply discoveries from basic science to enhance medical practice and human health, with many of these already having a major impact. We are presently witnessing an array of developments emerging on the horizon that have the potential to enhance patient care, improve diagnosis, and deliver treatments.

Wearable sensors for health and activity monitoring are growing in popularity with a multitude of devices, such as Fitbit and Withings, coming to market able to monitor vitals and measure activity levels and calorific consumption and expenditure. Their scope is now being extended to monitor disease as well. The application of contact lens sensors in ocular diagnostics offers a minimally invasive platform for constant monitoring of pertinent disease indices [1]. Advances in materials, electronics, and microfabrication techniques have expanded the remit of this medical device from a visual corrective aid in isolation to one that has diagnostic potential. The possibilities of its application have even caught the interests of Google, Novartis, and Microsoft [2–4]. Within this issue, S. C. Xu and colleagues review the applications of contact lens sensors (CLS) in detecting 24-hour intraocular pressure with its potential to change our approach and understanding in glaucoma. CLS have also been used to quantify blink rate and limbal strain and measure the circadian rhythm in a variety of disease states including normal tension glaucoma and thyroid eye disease.

The ever-increasing power of computational hardware (as described by Moore's Law) coupled with accelerating advances in software engineering has allowed swift evolution of this technology in ophthalmology. This special issue provides a report on an automated diabetic retinopathy detection software system using singular spectrum analysis to focus on microaneurysms. When applied to over 17,000 retinal images across different racial groups from six different countries, the authors report high levels of performance and the potential for scalability in diverse populations. Computational power also underpins virtual reality modeling and simulation has been used with success in nonmedical domains such as aerospace and the military. Inroads with this technology are now being made in medicine with cancer and surgical applications [5–7]. In this issue, E. Lanchares et al. describe a finite element model of the eye to analyze the myopic effects of scleral buckling, concluding that the wider the band, the greater the induced myopia. This and other ophthalmic models will likely grow in power as further clinical correlation is sought, a greater understanding of ocular biomechanics is ascertained, and improved boundary conditions are applied.

Optical coherence tomography angiography (OCTA) involves noninvasive imaging that rapidly generates high-resolution volumetric angiography and visualization of blood flow without injection of a contrast agent. As a result, an

indirect representation of the vascular morphology of the retina and choroid is generated. This nascent technology has wide potential applicability for retinal vascular disease; however, OCTA requires higher imaging speeds than what most currently available OCT systems can provide in order to obtain a densely sampled volume. Its current limitations also include a relatively small field of view, inability to show leakage, and proclivity for image artifact due to patient movement. Nevertheless, with recent developments in equipment and software, OCTA can now measure the size of choroidal neovascularization (CNV). Q. Chen et al. assess the morphology of idiopathic choroidal neovascularization (ICNV) by OCTA in 17 patients undergoing intravitreal anti-vascular endothelial growth factor treatment. Future work will continue to define the applications of this contrast-free angiography to retinal disease.

Crowdsourcing is a relatively novel, cost-effective endeavour involving the distribution of work ("outsourcing") to a large group of people (the "crowd") typically via the Internet where the collective intelligence and combined efforts of networked communities are used for specific purposes such as data analysis. Crowdsourcing is increasingly used commercially and more recently for scientific research such as the Zooniverse project [8, 9]. Due to the strict regulation governing medical research, crowdsourcing has been slow to be adopted but still has significant potential in medicine and ophthalmology [10]. In this issue, A. Y. Lee et al. evaluate the feasibility of using Mechanical Turk to perform manual segmentation of macular OCT images. The Amazon Mechanical Turk, which derives its name from the fake chess-playing automaton of the 18th century, is one of the most popular crowdsourcing Internet marketplaces for the coordinated use of human intelligence tasks (HITs) that computers are currently unable to do. This novel proof-of-concept study concludes that Mechanical Turk provides a cost-effective, scalable, high-availability infrastructure for manual segmentation of OCT images. As large data sets are becoming increasingly common with today's clinical studies and multicenter trials, rapid, reliable, cost-effective methods of interpretation will be crucial.

In this special issue on translational devices, technologies, and medicines in clinical ophthalmology, various potential breakthrough developments are reported in diverse spheres of ophthalmic practice. It is an exciting time for ophthalmology as we sit on the precipice of many significant advances that will steer the progress of our discipline. These innovations will inevitably improve the detection of disease and provide cutting-edge medical therapeutics and surgical interventions for our patients.

George M. Saleh
M. Reza Vagefi
Ioannis Athanasiadis

References

[1] N. M. Farandos, A. K. Yetisen, M. J. Monteiro, C. R. Lowe, and S. H. Yun, "Contact lens sensors in ocular diagnostics," *Advanced Healthcare Materials*, vol. 4, no. 6, pp. 792–810, 2015.

[2] B. P. Otis and B. A. Parviz, "Introducing our smart contact lens project," http://googleblog.blogspot.co.uk.

[3] Microsoft Research Connections, "Functional Contact Lens Moni-tors Blood Sugar Without Needles," http://research.microsoft.com.

[4] Novartis International AG Press Release, "Novartis to license Google 'smart lens' technology," 2014.

[5] T. Kawamorita, K. Shimizu, and N. Shoji, "Effect of hole size on fluid dynamics of a posterior-chamber phakic intraocular lens with a central perforation by using computational fluid dynamics," *Graefe's Archive for Clinical and Experimental Ophthalmology*, vol. 254, no. 4, pp. 739–744, 2016.

[6] D. Lockington, X. Luo, H. Wang, N. A. Hill, and K. Ramaesh, "Mathematical and computer simulation modelling of intracameral forces causing pupil block due to air bubble use in Descemet's Stripping Endothelial Keratoplasty: the mechanics of iris buckling," *Clinical and Experimental Ophthalmology*, vol. 40, no. 2, pp. 182–186, 2012.

[7] H. G. Colt, S. W. Crawford, and O. Galbraith III, "Virtual reality bronchoscopy simulation: a revolution in procedural training," *Chest*, vol. 120, no. 4, pp. 1333–1339, 2001.

[8] A. Swanson, M. Kosmala, C. Lintott, and C. Packer, "A generalized approach for producing, quantifying, and validating citizen science data from wildlife images," *Conservation Biology*, vol. 30, no. 3, pp. 520–531, 2016.

[9] https://www.zooniverse.org.

[10] X. Wang, L. Mudie, and C. J. Brady, "Crowdsourcing: an overview and applications to ophthalmology," *Current Opinion in Ophthalmology*, vol. 27, no. 3, pp. 256–261, 2016.

Hindawi Publishing Corporation
Journal of Ophthalmology
Volume 2017, Article ID 7982051, 6 pages
http://dx.doi.org/10.1155/2017/7982051

Research Article

Suppression of Human Tenon Fibroblast Cell Proliferation by Lentivirus-Mediated VEGF Small Hairpin RNA

Zhongqiu Li, Wen Hua, Xuedong Li, and Wei Wang

Department of Ophthalmology, Chaoyang Hospital, Capital Medical University, Beijing, China

Correspondence should be addressed to Zhongqiu Li; lizhqiu@outlook.com

Received 24 March 2016; Revised 27 August 2016; Accepted 22 September 2016; Published 11 January 2017

Academic Editor: George M. Saleh

Purpose. The functions of vascular endothelial growth factor (VEGF) in scar formation after trabeculectomy were investigated in a human Tenon fibroblast cell line from glaucoma patients using lentivirus-mediated VEGF shRNA. *Methods*. Human Tenon fibroblast (HTF) cells were isolated from scar tissue of glaucoma patients during secondary surgery. Lentivirus-VEGF-shRNA was constructed and transfected into HTF cells. Subsequently, VEGF mRNA and protein expression were analyzed using quantitative RT-PCR and western blotting, respectively, and the effects of VEGF knockdown were analyzed. The inhibition of HTF proliferation was monitored according to total cell numbers using ScanArray. *Results*. Both mRNA and protein levels of VEGF were reduced by lentivirus-mediated VEGF-shRNA, and proliferation of HTF cells was inhibited. *Conclusions*. Primary cultures of human Tenon fibroblast (HTF) were established, and proliferation was decreased following inhibition of VEGF. VEGF may be a suitable therapeutic target for reducing scar tissue formation in glaucoma patients after filtration surgery.

1. Introduction

Glaucoma is a common cause of blindness, and filtration surgery remains the most effective therapy for reducing intraocular pressure (IOP). Bleb scarring is the leading cause of surgical failure [1], and corticosteroids and antimetabolites, such as triamcinolone, mitomycin C (MMC), and 5-fluorouracil (5-FU), are currently used to inhibit the proliferation of fibroblasts and to increase success rates of surgery [2]. However, the side effects of intraocular toxicity, bleed leakage, postoperative shallow anterior chamber, and necrosis of conjunctiva and sclera warrant studies of safer, more targeted, and effective antifibrosis agents [3, 4].

Vascular endothelial growth factor (VEGF) plays an important role in scar formation. In a previous study, we showed that VEGF levels were significantly increased in the aqueous humor of the anterior chamber of primary open angular glaucomas (POAG) in patients and rabbits at surgery. Expression of the VEGF receptors VEGFR-1 (Flt-a) and VEGFR-2 (KDR/Flk-1) in Tenon fibroblasts was increased and fibroblast proliferation was stimulated following *in vitro* delivery of VEGF. This suggested that Tenon fibroblasts are direct targets of VEGF during scar formation after filtration surgery [5]. Moreover, higher VEGF expression in Tenon tissue was associated with failure of surgery [6], indicating that isoforms of VEGF play differing roles in scar formation after filtration surgery [7].

The use of anti-VEGF agents to control scar formation after trabeculectomy remains controversial [8–12]. How et al. used the VEGF monoclonal antibody bevacizumab with 5-FU injections into the subconjunctiva to inhibit experimental surgical glaucoma scarring [13]. Nilforushan et al. found that both trabeculectomy with subconjunctival bevacizumab and MMC are effective in controlling IOP profiles. However, the effects of adjunctive subconjunctival bevacizumab were less prominent than those of MMC [14]. In a randomized, controlled clinical trial, local conjunctival necrosis was reported in the subconjunctival bevacizumab group [15]. Contraindications, such as pregnancy, breast feeding, and uncontrolled systemic hypertension, are also important considerations when using bevacizumab. Recently, ranibizumab was used as an anti-VEGF agent after filtration surgery and led to severe hypotony and bleb leak [16], indicating the requirement of safer, more potent anti-VEGF agents.

RNA interference (RNAi) has emerged as a powerful tool to induce loss-of-function phenotypes by posttranscriptional silencing of gene expression and has been used to suppress VEGF-induced retinal neovascularization [17]. In the present study, we used a lentiviral vector expressing a small hairpin RNA (shRNA) to inhibit the expression of VEGF in human Tenon fibroblast (HTF) cells.

2. Material and Methods

The tenets of the Declaration of Helsinki were upheld, approval was granted by the IRB committee, and informed consent was obtained for all human experiments.

2.1. Human Tenon Fibroblast Isolation and Quality Control. Scar tissues were obtained from eight bleb-scarring patients who had secondary surgeries after trabeculectomy. There was no difference in terms of harvesting HTF between the patients with the primary and secondary surgeries. Primary cells were cultured as tissue adherence explants. For series quality control, observations of cell morphology, immunofluorescence cell validation using mouse antihuman vimentin monoclonal antibody (ZF-0512, Zhongbin Golden), mycoplasma testing (Huyuan Biotech), and stability testing were performed and growth curves, proliferation, and population doubling times were determined in isolated primary cells. Primary HTF cells were mycoplasma free and no significant changes in cell morphology or growth rates were observed between passage 5 and passage 15 cells.

2.2. Lentivirus Vectors for VEGF Small Hairpin RNA. Five VEGF probes were designed and synthesized based on the released sequence from RNAi Codex as follows:

shRNA-1: 5′-CCGGGCGCAAGAAATCCCGGTATAACTCGAGTTATACCGGGATTTCTTGCGCTTTTT-3′

shRNA-2: 5′-CCGGGACGTGTAAATGTTCCTGCAACTCGAGTTGCAGGAACATTTACACGTCTTTTT-3′

shRNA-3: 5′-CCGGATGCGGATCAAACCTCACCAACTCGAGTTGGTGAGGTTTGATCCGCATTTTTTT-3′

shRNA-4: 5′-CCGGCAAGATCCGCAGACGTGTAAACTCGAGTTTACACGTCTGCGGATCTTGTTTTTT-3′

shRNA-5: 5′-CCGGCAAGATCCGCAGACGTGTAAACTCGAGTTTACACGTCTGCGGATCTTGTTTTTT-3′

Positive control miR-214 was designed according to the methods described in Yang et al. [18]. Subsequently, miR-shRNA probes were inserted into pEn-TmiRC3 vectors using PCR and were cloned into pSLIK-Zeo using LR recombination methods. Transformations of the LR reaction were performed using DH10B and recombinant vectors were confirmed using Sanger sequencing.

2.3. HTF Cell Transfection and RNAi Efficacy. Recombinant VEGF-shRNA plasmids were transiently transfected into HTF cells, and shRNAs were screened using a pSLIK miRNA-based vector that lacked VEGF interference sequences as a negative control.

Both transiently and stably infected cell lines were grown in 6-well plates with no selection of drug for validation using qRT-PCR and western blotting. DOX was added to cell cultures at a final contraction of 1 μg/mL and the cells were incubated for at least 72 h as necessary. The cells were harvested at indicated times after induction, and cell extracts were prepared using RNeasy Kits (Qiagen) for qRT-PCR or using RIPA buffer for western blotting. Standard protocols were used for qRT-PCR and western blot analyses.

All five VEGF shRNAs reduced VEGF mRNA expression in HTF cells, and shRNA-2 and shRNA-3a reduced expression to 41.0% and 36.5%, respectively, and were selected for subsequent VEGF functional knockdown experiments.

2.4. Cell Culture and Transfection. Lenti-neo-GFP with the same backbone as pSLIK-VEGF-shRNA was used as the control titer. Viruses with recombinant target sequences and Lenti-neo-GFP were produced in parallel. Virus titers were determined using FACs analysis, and lentiviral titers of pSLIK-neo-GFP were 1.3×10^5 TU/mL.

Primary HTF cells were cultured in Dulbecco's Modified Eagle Medium containing high glucose (Gibco BRL) and 10% fetal bovine serum. Cells were incubated in a humidified incubator at 37°C in 5% CO_2 and 95% air. HTF cells were infected with lentivirus-shRNAs at MOI = 1. At 96 h after transfection, 1 μg/mL of DOX was added to the cultures to induce the transcription of shRNA.

2.5. Western Blot Analysis. At four days after induction with DOX, transfected HTF cells were collected and lysed in buffer containing 150 mM NaCl, 50 mM Tris-HCl (pH 7.4), 2 mM EDTA, 1% NP-40, and protease inhibitors (Boehringer Mannheim, Germany). Total protein in extracts was measured using the Bradford method. Aliquots of total proteins were resolved using SDS polyacrylamide gel electrophoresis and were then transferred onto immobilon P membrane using an SD semidry transfer apparatus according to the manufacturer's instructions. Membranes were incubated with polyclonal antihuman VEGF antibody (Cat. #AF-293-NA, R&D Systems, USA) and monoclonal antihuman β-actin (1 : 10,000 dilution; Sigma). Peroxidase-conjugated secondary antibodies were used as secondary detection reagents with an enhanced chemiluminescence kit (Cat. #20-500, Biological Industries, Israel). X-ray films were developed to visualize chemiluminescence signals.

2.6. Proliferation Experiments in HTF Cells after VEGF Knockdown. HTF cells were seeded into 96-black well plates at 30,000 cells per well. Cells were then infected with lentivirushRNA-2 and shRNA-3. After four days of induction with DOX, cell quantities were determined using ArrayScan and curves were calculated using PRISMBIOLAB.

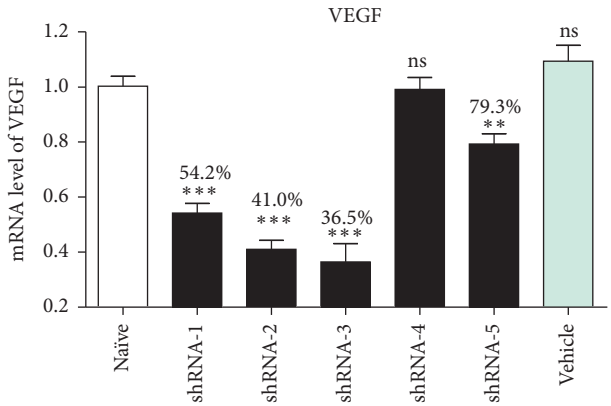

Figure 1: RNA interference after transfection with VEGF-shRNA. $^{**}p < 0.1$; $^{***}p < 0.01$.

3. Results

3.1. Comparisons of Interference Efficacy between Designs of Lentivirus-shRNA. Interference efficiencies were compared between various transfected VEGF-shRNA plasmid constructs in cultured HTF cells. VEGF mRNA levels were measured using quantitative RT-PCR.

"Naïve" indicates relative VEGF mRNA expression in nontransfected controls and vehicle indicates that of samples transfected with vehicle only. With the exception of shRNA-4, all VEGF-shRNAs significantly reduced VEGF mRNA levels, and VEGF-shRNA-2 and VEGF-shRNA-3 inhibited expression to 41.0% and 36.5%, respectively, and were selected for functional analyses; see Figure 1.

3.2. Suppression of VEGF Expression by VEGF-shRNA-2 and VEGF-shRNA-3. Lentivirus-carrying VEGF-shRNA-2 and VEGF-shRNA-3 were transfected into cultured HTF cells. VEGF protein expression was then investigated using western blotting, which showed reduced VEGF protein expression in HTF cells transfected with lentivirus VEGF-shRNA (Figure 2).

In these experiments, shRNA-2 and shRNA-3 significantly knocked down VEGF protein expression after 96 h of DOX treatment.

3.3. Suppression of HTF Proliferation by Lentivirus Transfected VEGF shRNA. Lentivirus-VEGF was transfected into cultured HTF cells. After 96 h, DOX was added to the culture medium to induce the transcription of shRNA.

Numbers of vehicle transfected HTF cells did not significantly differ from those of naïve HTF cells. However, total numbers of VEGF-shRNA-2 and VEGF-shRNA-3 transfected HTF cells were suppressed, particularly with VEGF-shRNA-3; see Figure 3.

4. Discussion

Filtration surgery remains the most effective choice for glaucoma patients. However, excessive scarring remains a leading cause of surgical failure [19–21]. Antimitotic agents, such as mitomycin C (MMC) and 5-fluorouracil (5-FU), have been used to prevent postsurgical scarring and improve surgical outcomes. However, nonselective cell death and apoptosis caused by these agents may lead to serious complications and limit their use [22–24].

Among wound healing factors, angiogenesis plays a key role and VEGF is a key factor because it stimulates angiogenesis, inflammation, and fibrosis at operative sites in glaucoma patients. Several VEGF isoforms and three high affinity VEGF receptors have been identified [25]. In particular, VEGF-R2 mediates most VEGF related-biological responses, and anti-VEGF agents, such as monoclonal antibodies and VEGF traps, have been used as antiangiogenic treatments [26–30]. Previously, we showed that VEGF receptors are expressed in human and rabbit Tenon fibroblasts, which are the main effector cells of ocular scar formation after filtration surgery. At filtration sites, VEGF modified fibroblast activity and caused collagen deposition and contraction, leading to scar formation; moreover, VEGF stimulated Tenon fibroblast proliferation *in vitro*. Accordingly, bevacizumab has been administered to inhibit Tenon fibroblast proliferation but requires repetitive injections [5]. The main complication of trabeculectomy is postoperative scar formation. We found that in our clinic, even with the same operator and same procedures, some patients had postoperative scars while others did not have. Regarding this and comparing with our previous study, we collected the Tenon tissues from patients with secondary surgeries in this study. Although systemic administration of bevacizumab for certain cancers has reported side effects, such as proteinuria, edema, and hypertension, intravitreal usage of bevacizumab has been reported as effective and safe [31–33]. However, long-term safety remains unclear, and RPE tears and other complications have been reported in treated patients [34, 35].

In the present study, we demonstrated that inhibition of VEGF expression using lentivirus-mediated shRNA suppresses the proliferation of human Tenon fibroblast cells. These observations may reflect binding of VEGF to VEGFR-2, leading to activation of the MAPK/ERK pathway, which is a key signaling pathway of cell proliferation, differentiation, and apoptosis. VEGFR-2 dimerization activates the intracellular serine/threonine kinase Raf, the dual specificity MAPK kinase (MEK), and the MAPK-ERK pathway upon stimulation, leading to increased DNA synthesis and cell proliferation. In addition, inhibition of ERK phosphorylation limits proliferation of Tenon fibroblasts, indicating that VEGF stimulates the proliferation of Tenon fibroblasts via the MAPK/ERK pathway. Phosphorylated ERK is translocated into the nucleus and phosphorylates growth factors, such as c-fos, c-Jun, c-myc, and ATF2, which lead to increased nucleotide synthesis, activated transcription and translation, and enhanced cell cycle progression [36, 37]. VEGF has also been shown to affect TGF-beta1/Smad/Snail pathways and trigger myofibroblast transformation [38].

We used lentivirus-mediated VEGF-shRNA to suppress VEGF mRNA expression. Previous studies of RNAi for VEGF show inhibition of neovascularization in ocular angiogenic diseases and demonstrate significant specific inhibition of

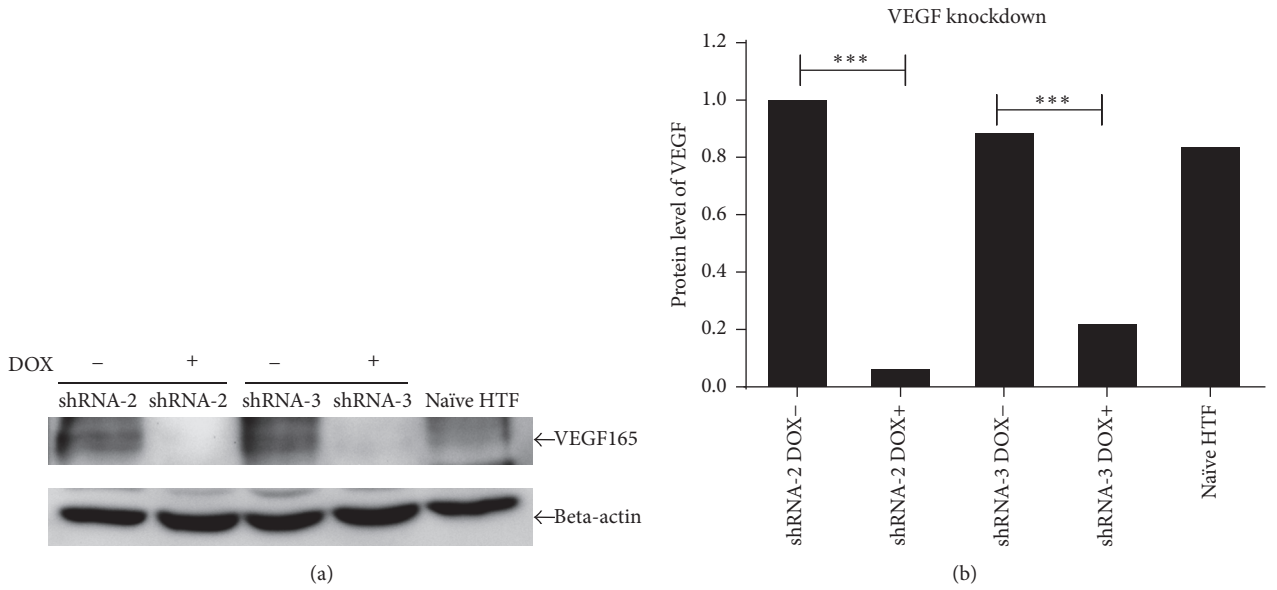

Figure 2: Western blot analysis of the effects of RNA interference on VEGF expression in HTF cells. (a) Relative expression of VEGF in cells treated with shRNA-2 and shRNA-3; (b) protein expression levels in treated groups and naïve HTF controls. *** $p < 0.01$.

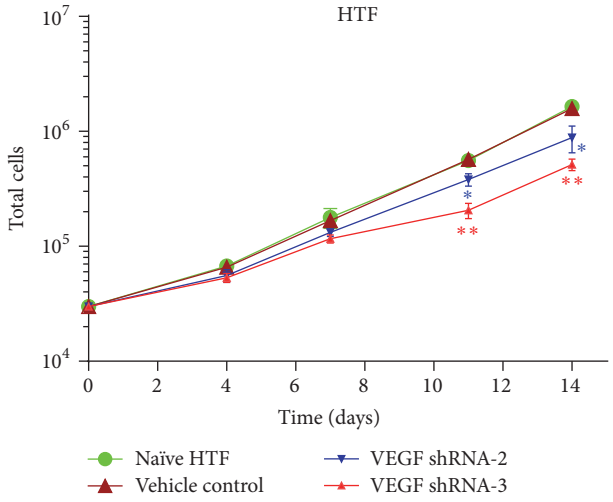

Figure 3: Cell growth curves. Total cell numbers were counted at 4, 7, 11, and 14 days after addition of DOX to cultures. Curves represent total cell numbers of naïve HTF cells, vehicle transfected HTF cells, VEGF-shRNA-2 transfected HTF cells, and VEGF-shRNA-3 transfected HTF cells. ∗ means p value < 0.5 compared to vehicle control. ∗∗ means p value < 0.1 compared to vehicle control.

VEGF by siRNAs [17, 39]. However, to the best of our knowledge, the present data are the first to show that inhibition with VEGF-shRNA also inhibits fibrosis. RNAi is a powerful emerging tool for gene knockdown, and since the 1990s, more than 50 RNA and RNA-derived therapeutics have reached clinical trials [40].

Efficiency and specificity of delivery represent a significant obstacle to therapeutic RNAi. In the present study, a lentivirus-mediated VEGF-shRNA system was used for the following reasons: lentiviruses efficiently transfect cells [41], lentiviral delivery of siRNA is suitable for local administration in ocular tissue, and the vector is transcribed in a DOX-dependent manner allowing easy control of shRNA transcription. Off-target effects of *in vivo* siRNA delivery are another obstacle to siRNA therapies. However, proprietary modifications of siRNA QPI-1007 structure and chemistry have been reported, with similar drug efficacy and reduced off-target effects [42].

The main surgical failure of using MMC or 5-FU is bleb leaking, which is followed by complications as infections and hypotony-related maculopathy. In the previous study, we observed the postoperative effect of inhibiting VEGF in rabbit model. In addition, no bleb leakages were found. In the future study, we will research on lentivirus VEGF-shRNA inhibiting scarring after trabeculectomy in animal models. The comparative research will be also designed in antiproliferative effects between shRNA and MMC.

In summary, lentivirus VEGF-shRNA was successfully used to knock down VEGF expression in Tenon fibroblasts from patient glaucomas, and fibroblast proliferation was suppressed. Subsequent inhibition of ERK phosphorylation had a similar effect, indicating that VEGF stimulates Tenon fibroblast proliferation via the MAPK/ERK pathway. RNAi technology may produce an adjunct agent that improves outcomes of glaucoma filtration surgery, especially secondary surgery for patient with postoperative scar formation.

Competing Interests

The authors declare that there is no conflict of interests regarding the publication of this manuscript.

Acknowledgments

This paper is supported by grants from Nature Science Fund of China (81000377), Advanced Science and Technology Activities Program for Overseas Returnees of Beijing (2001163), and Key Project on Foundation and Clinical Research Collaboration of Capital Medical University (10JL05).

References

[1] R. Daneshvar, "Anti-VEGF agents and glaucoma filtering surgery," *Journal of Ophthalmic and Vision Research*, vol. 8, no. 2, pp. 182–186, 2013.

[2] J. G. Crowston, "Long-term outcomes of trabeculectomy," *Clinical and Experimental Ophthalmology*, vol. 36, no. 8, pp. 705–706, 2008.

[3] J. Min, Z. L. Lukowski, M. A. Levine et al., "Prevention of ocular scarring post glaucoma filtration surgery using the inflammatory cell and platelet binding modulator saratin in a rabbit model," *PLoS ONE*, vol. 7, no. 4, Article ID e35627, 2012.

[4] A. M. Palanca-Capistrano, J. Hall, L. B. Cantor, L. Morgan, J. Hoop, and D. WuDunn, "Long-term outcomes of intraoperative 5-fluorouracil versus intraoperative mitomycin c in primary trabeculectomy surgery," *Ophthalmology*, vol. 116, no. 2, pp. 185–190, 2009.

[5] Z. Li, T. van Bergen, S. van de Veire et al., "Inhibition of vascular endothelial growth factor reduces scar formation after glaucoma filtration surgery," *Investigative Ophthalmology and Visual Science*, vol. 50, no. 11, pp. 5217–5225, 2009.

[6] H.-Y. Lopilly Park, J. H. Kim, M. D. Ahn, and C. K. Park, "Level of vascular endothelial growth factor in tenon tissue and results of glaucoma surgery," *Archives of Ophthalmology*, vol. 130, no. 6, pp. 685–689, 2012.

[7] T. Van Bergen, E. Vandewalle, S. Van de Veire et al., "The role of different VEGF isoforms in scar formation after glaucoma filtration surgery," *Experimental Eye Research*, vol. 93, no. 5, pp. 689–699, 2011.

[8] E. Vandewalle, L. A. Pinto, T. Van Bergen et al., "Intracameral bevacizumab as an adjunct to trabeculectomy: a 1-year prospective, randomised study," *British Journal of Ophthalmology*, vol. 98, no. 1, pp. 73–78, 2014.

[9] W. Suh and C. Kee, "The effect of bevacizumab on the outcome of trabeculectomy with 5-fluorouracil," *Journal of Ocular Pharmacology and Therapeutics*, vol. 29, no. 7, pp. 646–651, 2013.

[10] C. Ozgonul, T. Mumcuoglu, and A. Gunal, "The effect of bevacizumab on wound healing modulation in an experimental trabeculectomy model," *Current Eye Research*, vol. 39, no. 5, pp. 451–459, 2014.

[11] B. E. Chua, D. Q. Nguyen, Q. Qin et al., "Bleb vascularity following post-trabeculectomy subconjunctival bevacizumab: a pilot study," *Clinical and Experimental Ophthalmology*, vol. 40, no. 8, pp. 773–779, 2012.

[12] T. Zarnowski and M. Tulidowicz-Bielak, "Topical bevacizumab is efficacious in the early bleb failure after trabeculectomy," *Acta Ophthalmologica*, vol. 89, no. 7, pp. e605–e606, 2011.

[13] A. How, J. L. L. Chua, A. Charlton et al., "Combined treatment with bevacizumab and 5-fluorouracil attenuates the postoperative scarring response after experimental glaucoma filtration surgery," *Investigative Ophthalmology and Visual Science*, vol. 51, no. 2, pp. 928–932, 2010.

[14] N. Nilforushan, M. Yadgari, S. K. Kish, and N. Nassiri, "Subconjunctival bevacizumab versus mitomycin C adjunctive to trabeculectomy," *American Journal of Ophthalmology*, vol. 153, no. 2, pp. 352–357.e1, 2012.

[15] S. Sengupta, R. Venkatesh, and R. D. Ravindran, "Safety and efficacy of using off-label bevacizumab versus mitomycin C to prevent bleb failure in a single-site phacotrabeculectomy by a randomized controlled clinical trial," *Journal of Glaucoma*, vol. 21, no. 7, pp. 450–459, 2012.

[16] I. Georgalas, D. Papaconstantinou, I. Tservakis, C. Koutsandrea, and I. Ladas, "Severe hypotony and filtering bleb leak after intravitreal injection of ranibizumab," *Therapeutics and Clinical Risk Management*, vol. 5, no. 1, pp. 17–19, 2009.

[17] H. Xu, J. Liu, S. Xiong, Y.-Z. Le, and X. Xia, "Suppression of retinal neovascularization by lentivirus-mediated netrin-1 small hairpin RNA," *Ophthalmic Research*, vol. 47, no. 3, pp. 163–169, 2012.

[18] Z. Yang, S. Chen, X. Luan et al., "MicroRNA-214 is aberrantly expressed in cervical cancers and inhibits the growth of HeLa cells," *IUBMB Life*, vol. 61, no. 11, pp. 1075–1082, 2009.

[19] A. Choudhary and P. K. Wishart, "Non-penetrating glaucoma surgery augmented with mitomycin C or 5-fluorouracil in eyes at high risk of failure of filtration surgery: long-term results," *Clinical and Experimental Ophthalmology*, vol. 35, no. 4, pp. 340–347, 2007.

[20] M. B. Sherwood, "A sequential, multiple-treatment, targeted approach to reduce wound healing and failure of glaucoma filtration surgery in a rabbit model (an American Ophthalmological Society thesis)," *Transactions of the American Ophthalmological Society*, vol. 104, pp. 478–492, 2006.

[21] M. C. Gillies and T. Su, "Cytokines, fibrosis and the failure of glaucoma filtration surgery," *Australian and New Zealand Journal of Ophthalmology*, vol. 19, no. 4, pp. 299–304, 1991.

[22] Z. Wu, S. Li, N. Wang, W. Liu, and W. Liu, "A comparative study of the safety and efficacy effect of 5-fluorouracil or mitomycin C mounted biological delivery membranes in a rabbit model of glaucoma filtration surgery," *Clinical Ophthalmology*, vol. 7, pp. 655–662, 2013.

[23] J. C. Watson, O. A. Kadri, and M. J. Wilcox, "Effects of mitomycin C on glaucoma filtration capsules," *Biomedical Sciences Instrumentation*, vol. 41, pp. 394–399, 2005.

[24] P. T. Khaw, J. W. Doyle, M. B. Sherwood, M. F. Smith, and S. McGorray, "Effects of intraoperative 5-fluorouracil or mitomycin C on glaucoma filtration surgery in the rabbit," *Ophthalmology*, vol. 100, no. 3, pp. 367–372, 1993.

[25] I. Zachary, "VEGF signalling: integration and multi-tasking in endothelial cell biology," *Biochemical Society Transactions*, vol. 31, no. 6, pp. 1171–1177, 2003.

[26] J. Y. Choi, J. Choi, and Y.-D. Kim, "Subconjunctival bevacizumab as an adjunct to trabeculectomy in eyes with refractory glaucoma: a case series," *Korean Journal of Ophthalmology*, vol. 24, no. 1, pp. 47–52, 2010.

[27] D. Vasudev, M. P. Blair, J. Galasso, R. Kapur, and T. Vajaranant, "Intravitreal bevacizumab for neovascular glaucoma," *Journal of Ocular Pharmacology and Therapeutics*, vol. 25, no. 5, pp. 453–458, 2009.

[28] S. Grover, S. Gupta, R. Sharma, V. S. Brar, and K. V. Chalam, "Intracameral bevacizumab effectively reduces aqueous vascular endothelial growth factor concentrations in neovascular glaucoma," *British Journal of Ophthalmology*, vol. 93, no. 2, pp. 273–274, 2009.

[29] D. P. Smit and D. Meyer, "Intravitreal bevacizumab: an analysis of the evidence," *Journal of Clinical Ophthalmology*, vol. 1, no. 3, pp. 273–284, 2007.

[30] J. Cao, L. Zhao, Y. Li et al., "A subretinal matrigel rat choroidal neovascularization (CNV) model and inhibition of CNV and associated Inflammation and fibrosis by VEGF Trap," *Investigative Ophthalmology & Visual Science*, vol. 51, no. 11, pp. 6009–6017, 2010.

[31] R. A. Costa, R. Jorge, D. Calucci, J. A. Cardillo, L. A. S. Melo Jr., and I. U. Scott, "Intravitreal bevacizumab for choroidal neovascularization caused by AMD (IBeNA Study): results of a phase 1 dose-escalation study," *Investigative Ophthalmology & Visual Science*, vol. 47, no. 10, pp. 4569–4578, 2006.

[32] Y. Sugimoto, H. Mochizuki, H. Okumichi et al., "Effect of intravitreal bevacizumab on iris vessels in neovascular glaucoma patients," *Graefe's Archive for Clinical and Experimental Ophthalmology*, vol. 248, no. 11, pp. 1601–1609, 2010.

[33] A. L. Moraczewski, R. K. Lee, P. F. Palmberg, P. J. Rosenfeld, and W. J. Feuer, "Outcomes of treatment of neovascular glaucoma with intravitreal bevacizumab," *British Journal of Ophthalmology*, vol. 93, no. 5, pp. 589–593, 2009.

[34] D. Brouzas, C. Koutsandrea, M. Moschos, S. Papadimitriou, I. Ladas, and M. Apostolopoulos, "Massive choroidal hemorrhage after intravitreal administration of bevacizumab (Avastin) for AMD followed by controlateral sympathetic ophthalmia," *Clinical Ophthalmology*, vol. 3, no. 1, pp. 457–459, 2009.

[35] D. Kook, A. Wolf, A. S. Neubauer et al., "Retinal pigment epithelial tears after intravitreal injection of bevacizumab for AMD. Frequency and progress," *Ophthalmologe*, vol. 105, no. 2, pp. 158–164, 2008.

[36] F. Huang, J. Cao, Q. Liu, Y. Zou, H. Li, and T. Yin, "MAPK/ERK signal pathway involved expression of COX-2 and VEGF by IL-1β induced in human endometriosis stromal cells in vitro," *International Journal of Clinical and Experimental Pathology*, vol. 6, no. 10, pp. 2129–2136, 2013.

[37] A. M. Doanes, D. D. Hegland, R. Sethi, I. Kovesdi, J. T. Bruder, and T. Finkel, "VEGF stimulates MAPK through a pathway that is unique for receptor tyrosine kinases," *Biochemical and Biophysical Research Communications*, vol. 255, no. 2, pp. 545–548, 1999.

[38] H.-Y. L. Park, J. H. Kim, and C. K. Park, "VEGF induces TGF-β1 expression and myofibroblast transformation after glaucoma surgery," *American Journal of Pathology*, vol. 182, no. 6, pp. 2147–2154, 2013.

[39] M.-K. Yuan, Y. Tao, W.-Z. Yu, W. Kai, and Y.-R. Jiang, "Lentivirus-mediated RNA interference of vascular endothelial growth factor in monkey eyes with iris neovascularization," *Molecular Vision*, vol. 16, pp. 1743–1753, 2010.

[40] D. Peer and J. Lieberman, "Special delivery: targeted therapy with small RNAs," *Gene Therapy*, vol. 18, no. 12, pp. 1127–1133, 2011.

[41] P. Salmon, V. Kindler, O. Ducrey, B. Chapuis, R. H. Zubler, and D. Trono, "High-level transgene expression in human hematopoietic progenitors and differentiated blood lineages after transduction with improved lentiviral vectors," *Blood*, vol. 96, no. 10, pp. 3392–3398, 2000.

[42] Y. Guo, S. M. Srinivasula, A. Druilhe, T. Fernandes-Alnemri, and E. S. Alnemri, "Caspase-2 induces apoptosis by releasing proapoptotic proteins from mitochondria," *The Journal of Biological Chemistry*, vol. 277, no. 16, pp. 13430–13437, 2002.

Hindawi Publishing Corporation
Journal of Ophthalmology
Volume 2016, Article ID 4176547, 5 pages
http://dx.doi.org/10.1155/2016/4176547

Research Article

An Automated Detection System for Microaneurysms That Is Effective across Different Racial Groups

George Michael Saleh,[1,2,3] James Wawrzynski,[4] Silvestro Caputo,[1] Tunde Peto,[2,3] Lutfiah Ismail Al Turk,[5] Su Wang,[2] Yin Hu,[2] Lyndon Da Cruz,[1,3,6] Phil Smith,[2] and Hongying Lilian Tang[2]

[1]*Moorfields Eye Hospital NHS Foundation Trust, London, UK*
[2]*Department of Computing, Faculty of Engineering, University of Surrey, Guildford, UK*
[3]*National Institute for Health Research Biomedical Research Centre, Moorfields Eye Hospital NHS Foundation Trust and UCL Institute of Ophthalmology, London, UK*
[4]*Barking, Havering and Redbridge University Hospitals Trust, London, UK*
[5]*Statistics Department, Faculty of Sciences, King Abdulaziz University, Jeddah, Saudi Arabia*
[6]*Institute of Ophthalmology, UCL, London, UK*

Correspondence should be addressed to George Michael Saleh; george.saleh@moorfields.nhs.uk

Received 22 March 2016; Revised 28 June 2016; Accepted 10 July 2016

Academic Editor: Neil Lagali

Patients without diabetic retinopathy (DR) represent a large proportion of the caseload seen by the DR screening service so reliable recognition of the absence of DR in digital fundus images (DFIs) is a prime focus of automated DR screening research. We investigate the use of a novel automated DR detection algorithm to assess retinal DFIs for absence of DR. A retrospective, masked, and controlled image-based study was undertaken. 17,850 DFIs of patients from six different countries were assessed for DR by the automated system and by human graders. The system's performance was compared across DFIs from the different countries/racial groups. The sensitivities for detection of DR by the automated system were Kenya 92.8%, Botswana 90.1%, Norway 93.5%, Mongolia 91.3%, China 91.9%, and UK 90.1%. The specificities were Kenya 82.7%, Botswana 83.2%, Norway 81.3%, Mongolia 82.5%, China 83.0%, and UK 79%. There was little variability in the calculated sensitivities and specificities across the six different countries involved in the study. These data suggest the possible scalability of an automated DR detection platform that enables rapid identification of patients without DR across a wide range of races.

1. Introduction

Patients without diabetic retinopathy (DR) represent a large proportion of the caseload seen by the DR screening service and can be time consuming to identify for human graders [1]. Microaneurysms (MAs) are the first visible sign of DR and their detection has been widely described in the literature as an important factor in identifying the onset of DR [2, 3]. As such, reliable recognition of the absence of microaneurysms initially on FFA [4] and subsequently in digital fundus images [5] (DFIs) has been a prime focus of automated DR screening research for many years.

DR detection is partly undertaken through contrast of the MA with the background field of the DFIs. The appearance of the background field in DFIs is highly variable and is influenced by many factors including the degree of pigmentation in the retinal pigment epithelium and choroid, the size of the pupil, unevenness in illumination, poor transparency of the ocular media in corneal disease and cataract, and the camera type and its settings [6]. Variability in the background field is further complicated by well-reported racial variance, for example, in the calibre of retinal blood vessels [7–9].

The effect of differing racial and image influences have not previously been evaluated in the domain of DR identification

Table 1: Prevalence of microaneurysms within each studied image dataset as determined by human graders.

	Prevalence of microaneurysms as detected by human graders
Kenya	9.2%
Botswana	30.4%
Norway	9.6%
Mongolia	11.3%
China	8.2%
UK	11.7%

using automated screening algorithms. As the racial variance in pigmentation is known to influence the background field that automated systems use to operate it is important to know whether this will influence their performance of this important detection task [10]. Better defining these potential effects will be central to the future functionality and clinical usefulness of these platforms.

The aim of this study is to investigate the use of an automated DR detection algorithm to assess retinal DFIs and to evaluate its performance across patients of different racial backgrounds relative to a human observer.

2. Materials and Methods

This was a retrospective, masked, and controlled image-based study. Full Institutional Review Board approval was obtained for this study. The retrospective use of anonymized retinal images from data banks did not require ethics approval.

2.1. Subjects. A dataset from Moorfields Eye Hospital of digital fundal images of patients from six different countries and of varying race was retrospectively identified. In total 17,850 digital fundus images from population studies in six different countries were identified. The number of images from each country was Kenya 12,587, Botswana 500, Norway 840, Mongolia 1636, China 1079, and UK 1208. The images from Kenya and Norway originate from population screening, while those from Botswana and Mongolia originate from DR screening. The images from the UK and China originate from patients attending ophthalmic clinics: in the case of the UK, all patients had diabetes. All patients were aged 18 or over. In all cases patients were almost exclusively of the racial group that predominates in the relevant country as follows: Kenya and Botswana: African; Norway and the UK: Caucasian; China: Chinese; and Mongolia: Mongolian.

The prevalence of microaneurysms in the images as determined by human graders (the current gold standard) was as shown in Table 1.

These images were presented to the automated system described below in order to identify the eyes that did not have any evidence of microaneurysms.

2.2. Digital Fundus Photographs. One fovea centred digital fundus photograph was taken of each eye. The present study examined the fovea centred images. The resolution of the images varied from 3888 × 2592 pixels in Mongolia to 768 × 576 pixels in the UK.

2.3. The Daphne Automated Microaneurysm Detection System. The Daphne automated microaneurysm detection system assesses digital fundus images in order to detect microaneurysms. It is a noncommercialised software package newly developed in the Department of Computer Science within the Faculty of Engineering and Physical Science at the University of Surrey [11]. The aim of the system is to detect microaneurysms with high sensitivity, thus allowing any images where no microaneurysms are detected to be considered free of DR.

2.3.1. System Development. The automated system was built to detect microaneurysms in a three-stage process as described below. The system was then calibrated by presenting it with 50 digital fundus photographs from the retinopathy online challenge (ROC). Each image had already been graded by humans allowing feedback on the system's performance. The results from the 50 training cases were used to fine-tune the system's parameters. The system was then tested using unseen retinal photographs from the datasets described above.

2.3.2. Technical Specifications. The processing time per image on a computer equipped with an Intel Core i5 processor running at 2.2 GHz was one minute. The method is currently implemented using MATLAB. This software is currently only available for research.

2.3.3. Three-Stage Process of Microaneurysm Detection

(1) Image Preprocessing. Images are assessed for quality and those that do not meet the required quality standard are excluded from further analysis. Image quality is acceptable if the retinal vasculature could be visualised and they were correctly centred on the disc or fovea as appropriate. Images of varying resolutions are then automatically resized and cropped to a standard size and resolution.

Colour digital fundus photographs meeting the quality criteria are passed through a red-free filter in order to render microaneurysms and other vascular features as dark lesions. A Gaussian filter is then applied to the red-free image in order to enhance small and dark structures, which include microaneurysms. Bright lesions (such as cotton wool spots and exudates) are removed from the image using a shade correction algorithm [12] in order to prevent small darker gaps between two adjacent bright lesions being confused for a microaneurysm.

(2) Extraction of All Potential Microaneurysm Candidate Lesions. All lesions in the preprocessed photograph that are possible microaneurysms are detected. This is achieved by passing the image through a multilayered dark object filtering method [11, 13] which was set to search for dark lesions approximately seven pixels in diameter. This step has a high sensitivity but low specificity for microaneurysms.

(3) Selection of True Microaneurysms from Candidate Pool. The pool of candidate lesions (possible microaneurysms) is

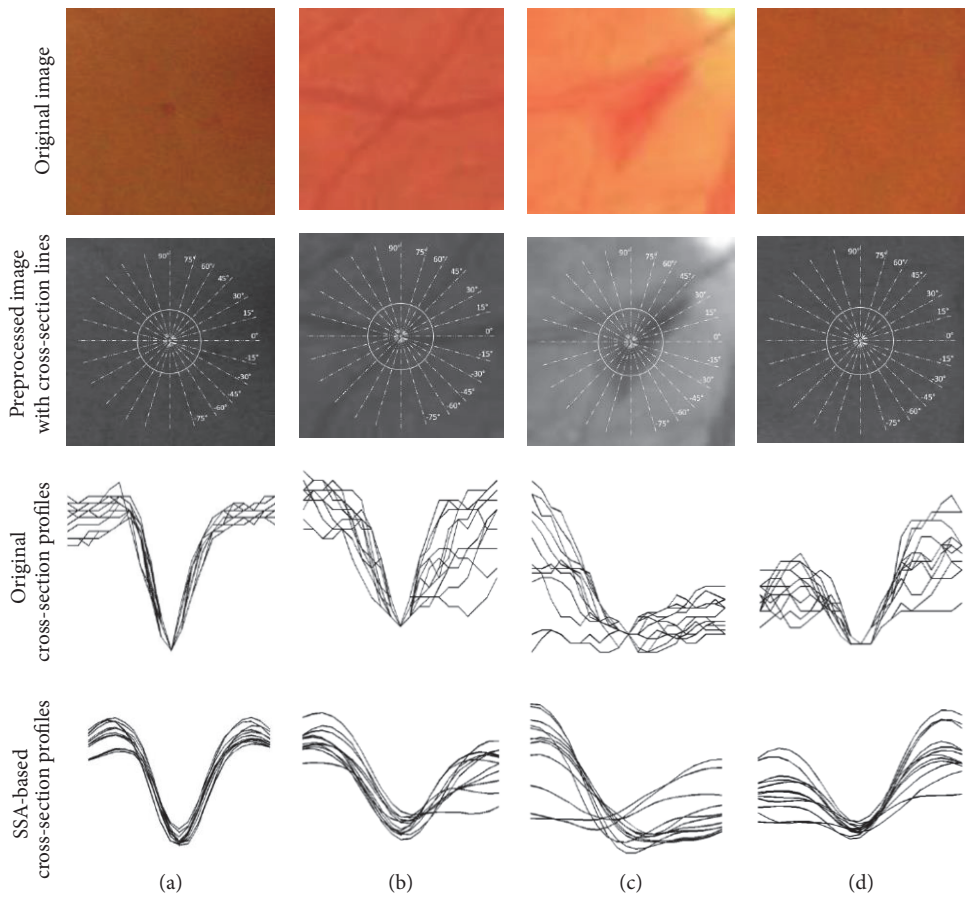

Figure 1: SSA cross-section profiles of different objects. (a) MA, (b) blood vessels crossing, (c) haemorrhage (an elongated non-MA structure), and (d) a retinal background. The white circles in the middle of the images indicate the actual cross-section scanning regions with 31-pixel diameter.

further processed to separate the true positives from the false positives. The candidate lesions are analysed using singular spectrum analysis (SSA) [14]. SSA involves profiling the intensity of the candidates by generating several cross-sectional profiles through the candidate in different orientations. Microaneurysms tend to differ from other dark lesions such as haemorrhages or small blood vessels in that they display a high level of rotational symmetry. Therefore, a candidate was determined to be a microaneurysm when there was a high level of similarity between all cross-sectional intensity profiles at all orientations. This is demonstrated graphically in Figure 1.

2.4. Classification of the Images by Trained Human Graders. A human grader classified the fundus photographs into two groups based on the presence or absence of DR according to the UK national screening guidelines for diabetic retinopathy. A second human grader reclassified a minimum of 10% of randomly selected images for quality control. Human graders were based at the Reading Centre at Moorfields Eye Hospital, London, UK, and at the Department of Computer Science, University of Surrey, UK. All human graders had undergone standard training as required to be a grader for the UK's DR screening programme.

In cases where there was disagreement between machine and human grading, a senior human grader decided the appropriate grading.

2.5. Statistical Analysis. The sensitivity and specificity of the automated system's ability to detect DR were analysed for each of the populations studied, taking the human graders' results as the gold standard. The sensitivity and specificity values and their standard deviations across different races were analysed using R Studio software, R consortium, Boston, MA, USA [15]. Standardised positive and negative predictive values of the automated system were also calculated for each country based on the known prevalence of DR amongst patients with diabetes within the relevant racial group, as reported by Yau et al. 2012 [16]: 27% for China and Mongolia, 56% for Kenya and Botswana, and 47% for Norway and the UK.

3. Results

The sensitivities, defined as the proportion of patients classified as having microaneurysms by human graders that were correctly identified by the automated system, were as follows: Kenya 92.8%, Botswana 90.1%, Norway 93.5%, Mongolia

91.3%, China 91.9%, and UK 90.1%. The standard deviation in the sensitivity values across the six countries was 1.3%.

The specificities, defined as to the proportion of patients classified as not having microaneurysms by human graders that were correctly identified as such by the automated system, were Kenya 82.7%, Botswana 83.2%, Norway 81.3%, Mongolia 82.5%, China 83.0%, and UK 79.0%. The standard deviation in the specificity values across the six countries was 1.5%.

The positive predictive values were Kenya 87%, Botswana 87%, Norway 82%, Mongolia 66%, China 67%, and UK 79%. The negative predictive values were Kenya 90%, Botswana 87%, Norway 93%, Mongolia 96%, China 97%, and UK 90%.

4. Discussion

The prevalence of diabetes is increasing worldwide due to population growth and increasing rates of obesity and physical inactivity. Projections suggest that the prevalence of diabetes in the USA will rise from 14% (in 2010) to between 25% and 28% by 2050 [12] and the worldwide prevalence will rise from 2.8% (in 2000) to 4.4% by 2030, with an expected worldwide population of 366 million people with diabetes. The most significant increase over the three decades is expected to involve the Middle East (+163%), Sub-Saharan Africa (+161%), China (+104%), and India (+151%) [17]. 2011 census data shows a rise in the English and Welsh population of people of middle eastern, Sub-Saharan African, and Indian origin, which may further accelerate the rise in the prevalence of diabetes in the UK [18].

DR screening programmes have been recognized as an effective method for disease detection at the earliest stage of the disease to potentially prevent permanent visual loss. However, due to a rapidly expanding population of patients with diabetes, the screening programme will require significant annual increases in investment, along with the recruitment and training of an increasing number of qualified human graders. In order to alleviate this problem, several attempts have been made to develop an automated system to assist human graders [19].

The specificity of our automated system remained consistent across all the racial groups examined with standard deviation of only 1.3% and results ranging from 83.2% in Botswana to 81.3% in Norway confirming its ability to accurately detect normal images irrespective of the race of the patient. Its sensitivity ranged from 91.1% in Botswana and the UK to 93.5% in Norway, with a standard deviation of 1.5%, demonstrating that it does not miss DR in the vast majority of cases and was again consistent across the different racial groups studied. In some cases, DR that was missed by human graders was detected by the system. In such cases a human grader reevaluated the images.

The standardised negative predictive value of the system was highly consistent across all countries varying from 87% in Botswana to 97% in China, suggesting that negative results (no MAs) are highly likely to be accurate. Conversely the positive predictive value ranged between 66% in Mongolia and 87% in Kenya and Botswana, suggesting that positive results (presence of MAs) would require further human grading. Thus, the value of this system lies chiefly in its ability to rapidly and reliably identify the absence of MAs, a task which may take a human grader much longer than identifying MAs when they are present. Given that the majority of patients attending screening do not have DR, the use of such a system has the potential to vastly reduce the number of images requiring human grading.

One key limitation in this study is that the performance of the system was evaluated only relative to human grading of the same images rather than additional modalities such as other automated systems or FFA. Therefore, it is only possible to conclude that the system tends to give very similar results to humans when grading DFIs without retinopathy across a wide range of racial groups. It cannot account for any possible systematic errors in grading if humans are also susceptible to those same mistakes. In addition, although the system was built to detect microaneurysms, it is impossible to compare which exact MAs the automated system detected compared to humans.

The previously reported structural and anatomical retinal differences amongst different racial groups including macular pigment distribution [10], the presence of the parafoveal ring, and the retinal microvascular calibre variation [7, 8] along with clinically visible differences in pigmentation do not appear to have impacted significantly on the performance of this automated system, which performed well across a wide range of different racial groups. This represents a significant advantage of the Daphne system that has not been specifically tested for in previous automated systems. Similarly, differences in image quality and illumination have not had a significant effect on the automated detection of DR.

5. Conclusions

The data presented here suggests the possible scalability of an automated microaneurysm detection platform that enables rapid identification of patients without DR across a wide range of races.

Disclosure

The views expressed are those of the authors and not necessarily those of the NHS, the NIHR, or the Department of Health.

Competing Interests

The authors declare that they have no conflict of interests.

Acknowledgments

This research was partly funded and supported by the National Institute for Health Research (NIHR) Biomedical Research Centre based at Moorfields Eye Hospital NHS Foundation Trust and UCL Institute of Ophthalmology. This work has been carried out in collaboration with the Reading Centre, Department of Research and Development, National Institute for Health Research (NIHR) Biomedical Research Centre at Moorfields Eye Hospital NHS Foundation Trust, and UCL Institute of Ophthalmology, UK. The authors

would like to thank the Mongolia, Kenya, Norway, China, UK, and Botswana medical study teams who contributed either by providing images or carrying out manual grading for this study. This project was funded by the National Plan for Science, Technology and Innovation (MAARIFAH), King Abdulaziz City for Science and Technology, Saudi Arabia, award number (10-INF1262-03). The authors also acknowledge with thanks Science and Technology Unit, King Abdulaziz University, for technical support. The authors would like to thank the Engineering and Physical Sciences Research Council (EPSRC) in the UK for supporting the foundation of this work. Grant information is EPSRC NIHR DRN 805.

References

[1] H. L. Tang, J. Goh, T. Peto et al., "The reading of components of diabetic retinopathy: an evolutionary approach for filtering normal digital fundus imaging in screening and population based studies," *PLoS ONE*, vol. 8, no. 7, Article ID e66730, 2013.

[2] E. M. Kohner, M. Sleightholm, and Kroc Collaborative Study Group, "Does microaneurysm count reflect severity of early diabetic retinopathy?" *Ophthalmology*, vol. 93, no. 5, pp. 586–589, 1986.

[3] R. Klein, S. M. Meuer, S. E. Moss, and B. E. K. Klein, "The relationship of retinal microaneurysm counts to the 4-year progression of diabetic retinopathy," *Archives of Ophthalmology*, vol. 107, no. 12, pp. 1780–1785, 1989.

[4] C. E. Baudoin, B. J. Lay, and J. C. Klein, "Automatic detection of microaneurysms in diabetic fluorescein angiography," *Revue d'Epidemiologie et de Sante Publique*, vol. 32, no. 3-4, pp. 254–261, 1984.

[5] M. U. Akram, S. Khalid, and S. A. Khan, "Identification and classification of microaneurysms for early detection of diabetic retinopathy," *Pattern Recognition*, vol. 46, no. 1, pp. 107–116, 2013.

[6] A. Goatman Keith, A. David Whitwam, A. Manivannan, A. John, and F. Peter, "Colour normalisation of retinal images," in *Proceedings of the Medical Image Understanding and Analysis*, pp. 49–52, 2003.

[7] Y. W. Tien, F. M. A. Islam, R. Klein et al., "Retinal vascular caliber, cardiovascular risk factors, and inflammation: the multi-ethnic study of atherosclerosis (MESA)," *Investigative Ophthalmology and Visual Science*, vol. 47, no. 6, pp. 2341–2350, 2006.

[8] N. Cheung, F. M. A. Islam, S. M. Saw et al., "Distribution and associations of retinal vascular caliber with ethnicity, gender, and birth parameters in young children," *Investigative Ophthalmology and Visual Science*, vol. 48, no. 3, pp. 1018–1024, 2007.

[9] T. Tillin, R. M. Evans, N. W. Witt et al., "Ethnic differences in retinal microvascular structure," *Diabetologia*, vol. 51, no. 9, pp. 1719–1722, 2008.

[10] U. E. K. Wolf-Schnurrbusch, N. Röösli, E. Weyermann, M. R. Heldner, K. Höhne, and S. Wolf, "Ethnic differences in macular pigment density and distribution," *Investigative Ophthalmology and Visual Science*, vol. 48, no. 8, pp. 3783–3787, 2007.

[11] S. Wang, H. Tang, L. Al Turk et al., "Localising microaneurysms in fundus images through singular spectrum analysis," *IEEE Transactions on Biomedical Engineering*, 2016.

[12] J. P. Boyle, T. J. Thompson, E. W. Gregg, L. E. Barker, and D. F. Williamson, "Projection of the year 2050 burden of diabetes in the US adult population: dynamic modeling of incidence, mortality, and prediabetes prevalence," *Population Health Metrics*, vol. 8, no. 1, article 29, 2010.

[13] M. Vlachos and E. Dermatas, "Multi-scale retinal vessel segmentation using line tracking," *Computerized Medical Imaging and Graphics*, vol. 34, no. 3, pp. 213–227, 2010.

[14] N. Golyandina, V. Nekrutkin, and A. Zhigljavsky, *Analysis of Time Series Structure: SSA and Related Techniques*, vol. 90 of *Monographs on Statistics and Applied Probability*, CRC Press, Boca Raton, Fla, USA, 2001.

[15] RStudio: integrated development environment for R (Version 0.98.501), (Computer software), Boston, Mass, USA, http://www.rstudio.org/.

[16] J. W. Y. Yau, S. L. Rogers, R. Kawasaki et al., "Global prevalence and major risk factors of diabetic retinopathy," *Diabetes Care*, vol. 35, no. 3, pp. 556–564, 2012.

[17] S. Wild, G. Roglic, A. Green, R. Sicree, and H. King, "Global prevalence of diabetes: estimates for the year 2000 and projections for 2030," *Diabetes Care*, vol. 27, no. 5, pp. 1047–1053, 2004.

[18] "Ethnicity and National Identity in England and Wales 2011," [office for national statistics].

[19] T. Teng, M. Lefley, and D. Claremont, "Progress towards automated diabetic ocular screening: a review of image analysis and intelligent systems for diabetic retinopathy," *Medical and Biological Engineering and Computing*, vol. 40, no. 1, pp. 2–13, 2002.

Hindawi Publishing Corporation
Journal of Ophthalmology
Volume 2016, Article ID 3548039, 7 pages
http://dx.doi.org/10.1155/2016/3548039

Research Article

Man versus Machine: Software Training for Surgeons—An Objective Evaluation of Human and Computer-Based Training Tools for Cataract Surgical Performance

Nizar Din,[1] Phillip Smith,[2] Krisztina Emeriewen,[3] Anant Sharma,[3] Simon Jones,[4] James Wawrzynski,[5] Hongying Tang,[2] Paul Sullivan,[1] Silvestro Caputo,[3] and George M. Saleh[1,2,6]

[1]*Moorfields Eye Hospital, 162 City Road, London EC1V 2PD, UK*
[2]*Department of Computer Science, University Of Surrey, Guildford, UK*
[3]*Moorfields Eye Hospital, Bedford, UK*
[4]*NYU Langone Medical Center, New York, USA*
[5]*Royal Free Hospital, London, UK*
[6]*NIHR Biomedical Research Centre at Moorfields Eye Hospital and the UCL Institute of Ophthalmology, London, UK*

Correspondence should be addressed to George M. Saleh; george.saleh@moorfields.nhs.uk

Received 25 March 2016; Revised 1 July 2016; Accepted 24 August 2016

Academic Editor: Takaaki Hayashi

This study aimed to address two queries: firstly, the relationship between two cataract surgical feedback tools for training, one human and one software based, and, secondly, evaluating microscope control during phacoemulsification using the software. Videos of surgeons with varying experience were enrolled and independently scored with the validated PhacoTrack motion capture software and the Objective Structured Assessment of Cataract Surgical Skill (OSACCS) human scoring tool. Microscope centration and path length travelled were also evaluated with the PhacoTrack software. Twenty-two videos correlated PhacoTrack motion capture with OSACCS. The PhacoTrack path length, number of movements, and total procedure time were found to have high levels of Spearman's rank correlation of −0.6792619 ($p = 0.001$), −0.6652021 ($p = 0.002$), and −0.771529 ($p = 0001$), respectively, with OSACCS. Sixty-two videos evaluated microscope camera control. Novice surgeons had their camera off the pupil centre at a far greater mean distance (SD) of 6.9 (3.3) mm, compared with experts of 3.6 (1.6) mm ($p \ll 0.05$). The expert surgeons maintained good microscope camera control and limited total pupil path length travelled 2512 (1031) mm compared with novices of 4049 (2709) mm ($p \ll 0.05$). Good agreement between human and machine quantified measurements of surgical skill exists. Our results demonstrate that surrogate markers for camera control are predictors of surgical skills.

1. Introduction

In recent years objective feedback for trainees in surgical procedures has become increasingly important for the training of new surgeons, not only to overcome the learning curve at an earlier stage, but also due to the environment of reduced training opportunities and stringent clinical commitments. Two broad systems have emerged, one is human and the other is machine based, but to date no study has compared the two on the same dataset.

One group of systems, termed the objective structured tools, are based on trainer led rating with tools which have defined scores. The Objective Structured Assessment of Cataract Surgical Skill (OSACSS) is one such tool and has been shown to statistically significantly discriminate between junior and senior surgeons [1]. The OSACSS has

also been used as the platform for the construction of the International Council of Ophthalmology's Ophthalmology Surgical Competency Assessment Rubrics (ICO-OSCAR) scheme that is currently being applied worldwide and available to download for free online in a multitude of different languages [2]. The OSACSS was used as opposed to the ICO-OSCAR, as the original OSACSS study [1] included construct validation (the differentiation based on experience), which is directly related to the objectives of this study for comparing OSACSS with PhacoTracking and the OSACSS was designed as a quantitative rating tool. Conversely, ICO-OSCAR was designed as a formative feedback tool, designed to provide feedback and progress whilst learning and hence was less appropriate for this study.

The other group of systems used was motion analysis, allowing movements of a surgeon's hands, instrument, or camera view to be evaluated with metrics such as path length, time, and number of movements being derived. These machine based tools are purely quantitative and have also been shown to statistically significantly discriminate between different surgical skill levels [3, 4]. The PhacoTrack software is one example where computer vision tracking has been applied to phacoemulsification surgery and successfully differentiated between junior and senior surgeons [5]. This methodology has been applied to other ophthalmic procedures including endoscopic dacryocystorhinostomy surgery [6]. Motion tracking also underpins high fidelity simulators such as the EyeSi simulator (VRmagic Holding AG, Mannheim, Germany), which are growing in importance and relevance in eye surgery [7–10].

Key to both of these measurement tools is the concept of validity. By definition, validity provides an overall evaluative judgment of the degree to which empirical evidence and theoretical rationales support the *adequacy* and *appropriateness* of *interpretations* and *actions* based on test scores or other modes of assessment [11, 12]. The popularised Messick validity tool encompasses five different aspects emphasizing content, substantive, structural, external, and consequential aspects of construct validity. In effect, these *five* aspects function as general validity criteria or standards for all educational and psychological measurement. In this study, we examine instrument motion metrics relationships to other variables in one group and internal structure is investigated in a second group by investigating a subset of motion metrics regarding microscope control. PhacoTrack and OSACSS demonstrate validity for measuring surgical skill to varying degrees. Identifying differences in validity for each method will enable us to understand how such methods could be combined to provide more valid means of measuring surgical skill.

Objective structured systems are based upon the human experts' structured evaluation; in contrast measurements of skill through motion analysis utilise machine feedback. Whilst both have been independently validated these two distinct tools have not been previously applied to the same set of data; thus there is a poor understanding of their interrelationship. This study aimed to explore two related aspects. Firstly, to assess how both human and machine tools relate to each other in cataract surgery, this would help establish content and substantive validity and ascertain how well the two systems work together. Thereafter, the aim was to select a component of training that had not previously been specifically tested but was an explicit component of the human OSACSS tool that could be clearly tested by the PhacoTrack. Microscope control, which is an explicit stem of the OSACSS, was chosen. The applicability of microscope motion tracking in live cataract surgery between junior and senior surgeons, using the PhacoTracking tool (5), was then evaluated. The hypothesis was that those surgeons, who have a low path length and reduced number of movements as dictated by the PhacoTrack software, would have a higher OSACCS score. Equally, the hypothesis was that senior surgeons would keep the microscope in the central field of view with minimal movement compared with junior surgeons, as recorded by the PhacoTracking software.

2. Methods

Full IRB and ethics approval were awarded for this study.

2.1. Subjects. Videos from surgeons with varying experience were used in this study. A junior surgeon was defined as an operator with <200 completed cases whilst a senior surgeon was one with >1000 completed cases.

2.2. Videos. These were captured through the microscope-viewing platform with standard recording equipment, which captured the surgeons' operative perspective. All cataract cases were deemed suitable for junior surgeons to allow for a fair comparison.

The following inclusion and exclusion criteria were applied to all patients who had given informed consent, whilst undergoing routine phacoemulsification cataract surgery.

Inclusion Criteria. Inclusion criteria for both groups of systems included adult patients who had given informed consent, prior to undergoing routine phacoemulsification cataract surgery. Surgeons operated only on straightforward cases, and the inclusion criteria for patients were as follows: pupils fully dilating; mild to moderate cataract (1+ nuclear sclerosis or cortical lens opacity only); ability to fully lie flat and still for the duration of surgery; and no ocular comorbidity (e.g., glaucoma or pseudoexfoliation) [4].

Exclusion Criteria. Exclusion criteria included a patient unable to give informed consent or not wishing to participate; nonroutine cataract (e.g., secondary to previous trauma or previous intraocular surgery); concurrent pathology that would exclude a clear view (e.g., corneal pathology); and complex cases not suitable for the less experienced surgical grade (e.g., very small pupil, mature cataracts, and patients with pseudoexfoliation) [4].

Group 1. In this group the motion tracking software was compared with OSACSS on the same set of surgical videos.

(1) Motion Analysis. Software analysis using computer vision tracking methodology, which has been previously described in full, was employed [5]. A combination of SURF point

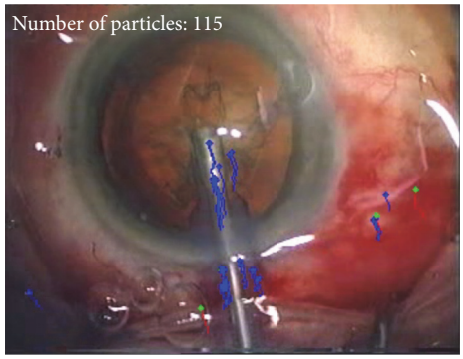

Figure 1: Screenshot of the PhacoTracking tool tracking the phacoemulsification probe.

detection [6] and Kanade-Lucas-Tomasi tracking [7] was applied to measure the motion of instruments used throughout the procedure in a fully automatic manner. The system analyses the full video of the surgery one frame at a time and measures the movement of each instrument within the field of view between frames. These measurements are used to calculate the instrument path length, the number of movements, and the total time accrued during each operation [5] (Figure 1).

(2) OSACSS Scoring. The same videos were anonymised, randomised, and then passed on to an independent expert (PS) who graded the skill level according to the objective structured assessment of cataract surgical skill (OSACSS) [1]. This tool consists of both global and phacoemulsification task-specific elements and is rated on a 5-point Likert scale totalling 100 potential points for the whole procedure (Figure 2) [1].

Group 2

(1) Microscope Tracking. In the second group of subjects, a computer vision algorithm that tracks the location of the iris was applied [7, 13]. A set of "histogram of orientated gradients" (HoG) detectors was applied to locate the pupil position [14]. Five different regions of the eye were detected in order to add robustness to the system (see Figure 3). These included superior, inferior, nasal, and temporal regions of the pupil, and an average of these values was computed to provide an estimate of the centre of the eye. From this tracking result, the distance from the centre of the pupil to the centre of the frame was then calculated for each frame along with the path length of the operative camera during the procedure. Similar analysis was used to calculate the total path length of the camera during the surgical video. The surgeons were split into novices (<200 cases) and experts (>1000 cases) with the camera tracking tool applied to each video.

Statistical Analysis. Mean, standard deviation (SD), and 95% confidence intervals were computed based on the recorded scores from each task. Spearman rank correlation was used to establish the relationship between OSACSS and PhacoTrack (for path length and movement).

Bland-Altman analysis comparing levels of agreement between the OSACCS and PhacoTrack ±1.96 standard deviation was undertaken. As the scale of both path length and number of movements is different than OSACCS, a linear model was found between the two measurements. The Bland-Altman plots use fitted OSACCS values for both path length and number of movements. The Bland-Altman provides a graphical representation of the levels of agreement/disagreement between the PhacoTrack and OSACSS within the defined margins. If there is little or no agreement then clinically they are not overlapping enough to make measurements comparable and usefully applicable to the same dataset. Conversely, if they agree 100% then there is no point in having two systems as they will be doing much the same thing.

A Mann–Whitney U test with significance at $p < 0.05$ was undertaken to test for a statistically significant difference in the total path length and mean decentration of the microscope between junior and senior surgeons. Python 2.7 and Scipy 1.9 statistical software were employed.

3. Results

Group 1. In the first group of systems, comparing PhacoTracking instruments with OSACSS, 22 videos from 22 surgeons (11 novices, 11 experts) were enrolled and analysed in the study.

In all cases, there was a strong negative correlation meaning a higher OSACSS corresponded with fewer instrument movements, a reduced path length, and shorter operative time. A strong correlation between the natural logarithm of the number of instrument movements (as measured by PhacoTrack motion analysis) and the total OSACSS score was observed with Spearman's rank correlation coefficient giving a result of −0.6652021 ($p = 0.002$). This suggests that the number of movements was inversely proportional to the surgeon's OSACSS score. A correlation between the path length of the instruments travelled as measured by PhacoTrack motion analysis and the total OSACSS score was observed with Spearman's rank correlation coefficient giving a result of −0.6792619 ($p = 0.001$). This strongly suggests that the path length was inversely proportional to the surgeon's OSACSS score. The time taken for the procedure was inversely correlated to the score as measured by the OSACCS with Spearman's rank correlation of −0.771529 ($p = 0.001$). This strongly suggests that the time was inversely proportional to the surgeon's OSACSS score.

Figure 4 shows a Bland-Altman plot comparing the level of agreement for the OSACCS and PhacoTrack scores. The Bland-Altman plot describes the level of agreement between two quantitative measurements by constructing limits of agreement. Both Figures 4(a) and 4(b) demonstrate a strong agreement within limits of agreement due to 95% of the data points lying within the tight range of ±1.96 standard deviation. The path length measurements may overestimate/underestimate a surgeon's OSACSS score by 14.55 units, whilst for the log of number of movements, an overestimate/underestimate of a surgeon's OSACSS score by 68% was found. The Bland-Altman plot for number of movements

	Poorly or inadequately performed		Performed with some errors or hesitation		Performed well with no prompting or hesitation	Tick if not performed
Draping: surgical field clear of lashes	1	2	(3)	4	5	
Incision and paracentesis: formation and technique	1	2	3	(4)	5	
Viscoelastic: appropriate use and safe insertion	1	2	3	(4)	5	
Capsulorhexis: commencement of flap	1	2	(3)	4	5	
Capsulorhexis: formation and circular completion	1	2	3	(4)	5	
Hydrodissection: visible fluid wave and free nuclear rotation	1	2	3	4	(5)	
Phacoemulsification probe and second instrument: insertion into eye	1	2	3	(4)	5	
Phacoemulsification probe and second instrument: effective use and stability within the eye	1	2	3	4	(5)	
Nucleus: sculpting or primary chop	1	(2)	3	4	5	
Nucleus: rotation and manipulation	1	2	(3)	4	5	

Figure 2: OSACCS scoring tool independently evaluating phacoemulsification.

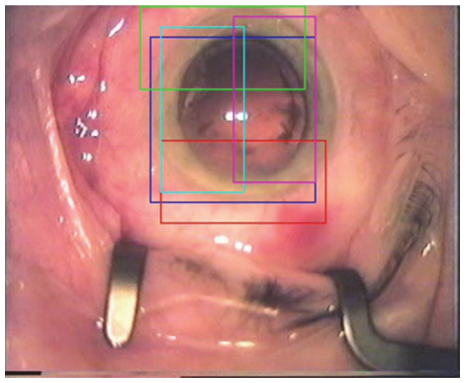

Figure 3: Snapshot of the iris tracking algorithm components.

to OSACSS score displayed signs of the differences being proportional to the mean, as such we take the log of number of movements and OSACSS score [15].

Group 2. In the second group of systems, looking into operative microscope control between junior and senior surgeons, 62 participants were enrolled (31 experts, 31 novices). The comparison between novices and experts for average pupil centre to frame centre distance is shown in Figure 5. Novice surgeons had an average of 6.9 mm pupil centration with a standard deviation of 3.3 mm. In contrast, experts had good camera control minimising movements by keeping pupil centration on average 3.6 mm from the frame with a standard deviation of 1.6 mm. When analysing path length of the operative camera, novice surgeons had an average of pupil path length of 4049 mm with a standard deviation of 2709 mm. Expert surgeons had an average path length of 2512 mm with a standard deviation of 1031 mm. Hence, the novice group showed a greater total path length and a larger variation in length compared with experts who were more consistent. The p values for a Mann–Whitney U test between the two groups (novices and experts) were statistically significant at $p \ll 0.05$.

4. Discussion

This study is the first in which an explicit investigation comparing two different methodologies, one human and the other machine, for measuring cataract surgical skill has been undertaken. Our results suggest a moderate correlation between surgical skills marked by a human expert as compared to the motion metrics found with computer vision algorithms. This is also the first study in which control of the operating microscope has been objectively analysed using motion analysis. A positive relationship between good camera control and surgical skill is reported.

The OSACSS was used as opposed to the ICO-OSCAR, as the original OSACSS study [1] included construct validation (the differentiation based on experience), which is directly related to the objectives of this study for comparing OSACSS with PhacoTracking and the OSACSS was designed as a quantitative rating tool. Conversely, ICO-OSCAR was designed as a formative feedback tool, designed to provide feedback and progress whilst learning and hence was less appropriate for this study.

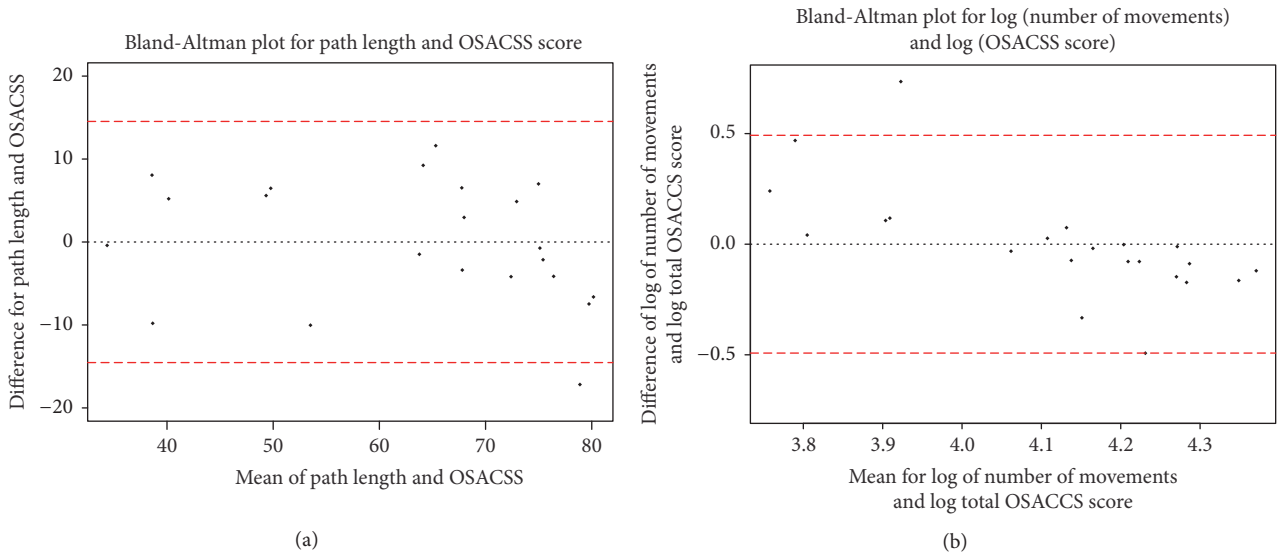

Figure 4: (a) Bland-Altman plot of OSACSS score to PhacoTrack path length (fitted by linear model to OSACSS score). Red lines represent the limits of agreement from −1.96s to +1.96s and dotted line is the mean difference. (b) Bland-Altman plot of Log OSACSS score to log PhacoTrack number of movements (fitted by linear model to OSACSS score). Red lines represent the limits of agreement from −1.96s to +1.96s and dotted line is the mean difference.

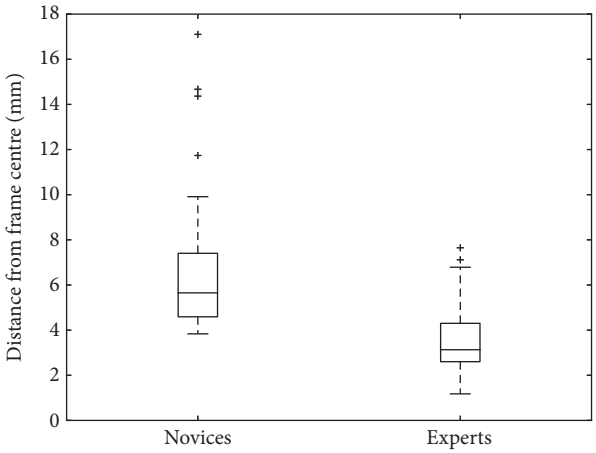

Figure 5: Box and whisker plot showing average pupil centre distance from frame centre between novices and experts. The horizontal line within each box is the median value, and the top and bottom borders of the box are ±1 SD with limit lines showing 95% CIs (±2 SDs).

The results presented indicate a strong link between the machine based instrument motion and the human based surgical skill rating. A higher OSACSS score was inversely proportional to the path length of the instruments [−0.68 (p = 0.001)], inversely proportional to the number of movements the instruments made [−0.67 (p = 0.002)], and inversely proportional to the total time to complete the procedure [−0.77 (p = 0001)]. This suggests that those with greater experience as defined by their OSACSS score [1] were more efficient in their use of instruments and quicker to complete the procedure [5]. These results are strongly in keeping with previous work in this field validating these tools.

This relationship was also clearly illustrated on an individual basis, for example, in subject 16 who obtained an OSACSS score of 88, and demonstrated efficient motion (path length = 3677.771 mm, number of movements = 4646). In contrast subject 2 had a lower OSACSS score of 35 and was found to be less efficient with PhacoTrack (path length = 10146.134 mm, number of movements = 9819). Critically this is the first time that these two complementary rubrics have been evaluated on the same dataset. This may offer respective individuals a more significant amount of data by way of feedback for learning purposes than has traditionally been available to date.

The OSACCS tool is a validated method of assessing trainees' surgical competency and the level of agreement with the PhacoTrack scoring tool is illustrated in Figure 4 on the Bland-Altman plot showing agreement between the two methods, for both path lengths. Figure 4(a) demonstrates a 14.55-point over/underestimation for path length instrument; this would not move an average surgeon's score for each cohort into a different group. In Figure 4(b) we observe that less skilled surgeons have larger percentage difference between the log total OSACSS and log of number of movements score whereas PhacoTrack overestimates the score of a novice. We hypothesise that in the case of novice surgeon's OSACSS scores are being influenced by information that does not influence the number of movements. The number of movements has an overestimation/underestimation of 68%; this would be likely to change the interpretation of a score. Hence, we strongly advocate using both human marked and motion based metrics systems concurrently, as they offer complimentary information.

The disagreements between motion based metrics and human marked metrics are not surprising. A human grader offers lower scores with the OSACCS tool when a combination of errors and inefficiencies is observed. PhacoTrack's quantitative measurements reproducibly and

objectively track instruments without a surgical trainer's context. Thus, a trainee may proceed more cautiously in the context of a potentially complicated situation (and be scored appropriately and highly with OSACSS) whereas another may slow down due to inefficiency (and would score lower with OSACSS). With the purely objective PhacoTrack they may both take the same amount of time and similar number of movements and thus be rated comparably. In this paper we investigate PhacoTrack's validity in regard to its relationship to other variables and internal structure as evidence of validity provided by the original model introduced by Messick. Previous tracking work has not been undertaken in conjunction with human tools and so correlation has not been possible [9, 10, 13, 14]. Better understanding the difference in approach will potentially provide a basis to form combined measurements of surgical skill and may well prove useful in enhancing formative feedback through the two methods.

Of the 62 participants evaluated we found that novice surgeons had a higher average pupil path length and pupil centre from frame centre distance than expert surgeons who kept the surgical field through the microscope statistically significantly better centre. The measurements recorded were able to discriminate between different skill levels of surgeons and hence demonstrate construct validity (content validity is the ability of a tool to measure what it is supposed to not discriminate, not sure where this change came from). This is further exemplified by the wider spread of results found in novice surgeons. The results show that surrogate markers for camera control including lower pupil centre to frame centre measurements and a small path length all contribute to higher surgical performance. Hence, objective automated markers of both PhacoTrack parameters of instrument path length and movements and camera control data can be a useful tool for formative feedback.

Despite its crucial role in ophthalmic surgery, structured instruction of microscope camera control is often an underrepresented part of surgical training. Motion analysis of camera control may offer complementary information to be used alongside existing tools, to provide more comprehensive and structured formative feedback of microscope control intraoperatively. This technique offers an accessible system based on standard operative microscope recording equipment and, similar to simulators, an objective and numerical benchmark with an individual score breakdown (detailing parameters explaining where improvements can be made).

There are a few limitations to the study that need considering. Whilst the automated system measures efficiency of a surgeon's performance and agrees with human assessment tools, it does not provide feedback for specific tasks, which need further investigation. In addition, the automatic method does not detect any surgical errors that would be readily identified by the human observer. Whilst objective raw values of path length and number of movements provide a gross indication of surgical performance, these data values fail to identify the complexity of the case in question, the technique employed, or the critical intraoperative decision-making. We also do not know how useful these metrics are for surgeons and whether this type of feedback would improve surgical performance in the long term. This provides a further case for computational methods being used in conjunction with human based tools but further investigation will better help elucidate this.

This is the first time that an objective quantitative system has been compared with a human marked scheme for surgical skill in actual cataract surgery with promising results. Both the instrument and camera motion analysis have the potential to measure surgical skill, in a manner that is in agreement with established human methodologies. In time, automatically measured motion metrics may prove to be a useful adjunct tool to augment human marked schemes that are currently in use. The addition of a new surgical skill measure that is derived independently of existing methods can provide objective quantitative feedback to aid in the training of surgeons that complements feedback from an experienced surgeon. This is already taking place in simulators, such as the EyeSi (VR Magic, Maheim), which uses tracking metrics inside the simulated eye to form its numerical score and feedback.

Although encouraging, further work needs to be undertaken to evaluate its usefulness and applicability in surgical education and training. As motion technology develops, the operating microscope of the future may well incorporate similar algorithms allowing continuous and instant formative feedback to be available.

Disclosure

The views expressed are those of the authors and not necessarily those of the NHS, the NIHR, or the Department of Health.

Competing Interests

The authors declare that there is no conflict of interests regarding the publication of this manuscript.

Acknowledgments

This research was partly funded and supported by the National Institute for Health Research (NIHR) Biomedical Research Centre based at Moorfields Eye Hospital NHS Foundation Trust and UCL Institute of Ophthalmology. This work was also partly supported by the NIHR CRN Eastern through network support. The authors acknowledge an unrestricted grant from the Special Trustees of Moorfields Eye Hospital.

References

[1] G. M. Saleh, V. Gauba, A. Mitra, A. S. Litwin, A. K. K. Chung, and L. Benjamin, "Objective structured assessment of cataract surgical skill," *Archives of Ophthalmology*, vol. 125, no. 3, pp. 363–366, 2007.

[2] International Council of Ophthalmology, "Surgical Assessment Tool: ICO-OSCAR in English, Chinese, Portuguese, Russian, Spanish, Vietnamese, and French," http://www.icoph.org/resources/230/Surgical-Assessment-Tool-ICO-OSCAR-in-English-Spanish-Chinese-Portuguese-Vietnamese-and-French.html.

[3] G. M. Saleh, Y. Voyazis, J. Hance, J. Ratnasothy, and A. Darzi, "Evaluating surgical dexterity during corneal suturing," *Archives of Ophthalmology*, vol. 124, no. 9, pp. 1263–1266, 2006.

[4] G. M. Saleh, V. Gauba, D. Sim, D. Lindfield, M. Borhani, and S. Ghoussayni, "Motion analysis as a tool for the evaluation of oculoplastic surgical skill: evaluation of oculoplastic surgical skill," *Archives of Ophthalmology*, vol. 126, no. 2, pp. 213–216, 2008.

[5] P. Smith, L. Tang, V. Balntas et al., "'PhacoTracking:' an evolving paradigm in ophthalmic surgical training," *JAMA Ophthalmology*, vol. 131, no. 5, pp. 659–661, 2013.

[6] H. Bay, A. Ess, T. Tuytelaars, and L. Van Gool, "Speeded-Up Robust Features (SURF)," *Computer Vision and Image Understanding*, vol. 110, no. 3, pp. 346–359, 2008.

[7] T. Carlo and T. Kanade, "Detection and tracking of point features," Carnegie Mellon University Technical Report CMU-CS-91-132, 1991.

[8] J. R. Wawrzynski, P. Smith, L. Tang et al., "Tracking camera control in endoscopic dacryocystorhinostomy surgery," *Clinical Otolaryngology*, vol. 40, no. 6, pp. 646–650, 2015.

[9] G. M. Saleh, J. Lamparter, P. M. Sullivan et al., "The international forum of ophthalmic simulation: developing a virtual reality training curriculum for ophthalmology," *British Journal of Ophthalmology*, vol. 97, no. 6, pp. 789–792, 2013.

[10] M. Selvander and P. Åsman, "Virtual reality cataract surgery training: Learning curves and concurrent validity," *Acta Ophthalmologica*, vol. 90, no. 5, pp. 412–417, 2012.

[11] S. Messick, "Validity," in *Educational Measurement*, R. L. Linn, Ed., pp. 13–103, American Council on Education and Macmillan, New York, NY, USA, 3rd edition, 1989.

[12] D. A. Cook, R. Brydges, B. Zendejas, S. J. Hamstra, and R. Hatala, "Technology-enhanced simulation to assess health professionals: a systematic review of validity evidence, research methods, and reporting quality," *Academic Medicine*, vol. 88, no. 6, pp. 872–883, 2013.

[13] N. Dalal and B. Triggs, "Histograms of oriented gradients for human detection," in *Proceedings of the IEEE Computer Society Conference on Computer Vision and Pattern Recognition (CVPR '05)*, vol. 1, 2005.

[14] J. Bergqvist, A. Person, A. Vestergaard, and J. Grauslund, "Establishment of a validated training programme on the Eyesi cataract simulator. A prospective randomized study," *Acta Ophthalmologica*, vol. 92, no. 7, pp. 629–634, 2014.

[15] J. Martin Bland and D. Altman, "Statistical methods for assessing agreement between two methods of clinical measurement," *The Lancet*, vol. 327, no. 8476, pp. 307–310, 1986.

Hindawi Publishing Corporation
Journal of Ophthalmology
Volume 2016, Article ID 3436415, 7 pages
http://dx.doi.org/10.1155/2016/3436415

Clinical Study

A Combination of Intrastromal and Intracameral Injections of Amphotericin B in the Treatment of Severe Fungal Keratitis

Jianzhang Hu, Jingjin Zhang, Yanling Li, Xiaoli Han, Weidong Zheng, Juan Yang, and Guoxing Xu

The Eye Center of the First Affiliated Hospital of Fujian Medical University, Fujian Eye Institute, 20 Chazhong Road, Fuzhou 350005, China

Correspondence should be addressed to Guoxing Xu; fjmuxuguoxing@hotmail.com

Received 7 March 2016; Accepted 13 June 2016

Academic Editor: George M. Saleh

Purpose. To evaluate the efficacy of a combination of intrastromal and intracameral injections of amphotericin B in the treatment of severe recalcitrant fungal keratitis. *Methods*. Patients with severe fungal keratitis who were resistant to conventional antifungal medical treatments and needed potential surgical intervention were recruited at the First Affiliated Hospital of Fujian Medical University between January 2012 and July 2013. The patients were treated with a combination of intrastromal and intracameral injections of amphotericin B (25 μg/mL and 50 μg/mL, resp.). Selectively repeated injections were performed as necessary. The efficacy, complications, and outcome were evaluated. *Results*. Nine patients (9 eyes) were involved in this study. All 9 cases responded favorably, and the clinical appearance of serious corneal damage and intraocular extension was resolved after the treatment. Four eyes required only 1 injection, and 5 eyes required repeated injections. Seven corneal ulcers healed with leucoma, and 2 healed with adherent leucoma. All of our cases had a marked increase in the anterior chamber reaction and pain immediately after the injection. There was no obvious clinical evidence of corneal or lenticular toxicity in any patient. *Conclusions*. A combination of intrastromal and intracameral injections of amphotericin B may be safe and effective for the treatment of severe fungal keratitis that is resistant to conventional therapy.

1. Introduction

Fungal keratitis is one of the major causes of blindness in developing agricultural countries and is usually difficult to treat [1, 2]. Some patients who live in remote and economically impoverished regions may delay visiting the hospital; some are underdiagnosed and inappropriately treated and often suffer serious consequences. The keratitis may aggravate and lead to serious complications such as corneal staphyloma, descemetocele, endophthalmitis, perforation, and blindness.

The most frequently isolated causes of fungal keratitis are *Fusarium* and *Aspergillus*, which are highly virulent microorganisms and are partially resistant to most antifungal medications [3]. The hypha is capable of penetrating the intact Descemet's membrane and rapidly entering the anterior chamber. In such cases, conventional treatment such as the use of antifungal medications, including fluconazole, topical natamycin, amphotericin B, or the combination with oral fluconazole, seems to obtain poor results. Moreover, the corneal penetration and bioavailability of many of the available topical antifungal preparations are suboptimal, making it difficult to treat cases of deep mycotic keratitis [4, 5]. Keratoplasty may be an effective way to control the fungal infection [6]. However, because it is not as effective as an optical keratoplasty performed on a quiescent eye after healing [7], and partly because of the limited and erratic supply of donor corneas in China, it seems wise to try to postpone keratoplasty until after healing.

To overcome these problems, investigators have evaluated alternate routes such as intracameral or intrastromal amphotericin B injections to treat fungal keratitis [8–11]. When used as a topical antifungal agent, amphotericin B has broad-spectrum antifungal activity but strong cytotoxicity at high concentrations and poor corneal penetration [12, 13]. In our clinical experience, intrastromal injections of amphotericin B often obtain poor results in the treatment of severe fungal

keratitis when the hypha has invaded the anterior chamber and pupillary space. Additionally, intracameral injections of amphotericin B are not very effective at inhibiting the hypha growth in the stroma and usually cause some complications, including immediate anterior chamber reactions, secondary glaucoma, and cataract. In this study, we used a combination of intrastromal and intracameral injections of different concentrations of amphotericin B as an alternative to conventional therapies and evaluated its efficacy in the management of severe keratomycosis with serious corneal damage and intraocular extension which was resistant to conventional antifungal medical treatment and may have required potential surgical intervention.

2. Patients and Methods

2.1. Patients. From January 2012 through July 2013, 103 patients with fungal keratitis were hospitalized at the Eye Center at the First Affiliated Hospital of Fujian Medical University, Fujian Eye Institute, Fuzhou. As the largest referral eye center in Southeast China, this institution serves a large proportion of patients with eye diseases in Fujian province and in neighboring provinces. Institutional review board approval was obtained. Each of the patients gave informed consent for participation before treatment.

In this interventional case series, patients diagnosed of fungal keratitis involving serious corneal damage and visible fungal mass in the anterior chamber that were resistant to topical and/or systemic antifungal treatment underwent intrastromal combined with intracameral injections of amphotericin B at doses of 25 micrograms/0.1 mL and 50 micrograms/0.1 mL, respectively. The epidemiological characteristics, predisposing factors, clinical features, microbiological findings, treatment protocol, and final outcome data for each patient were collected.

2.2. Diagnostic Methods. The diagnosis of fungal keratitis was made on the basis of clinical evaluation, positive smear, and fungal cultures. The corneal scrapings were obtained aseptically from the leading edge or base of the ulcer. A portion of each scraping was examined microscopically for the presence of fungi by staining with 10% potassium hydroxide (KOH) or Gram stain. Another portion was subjected to fungal culture following inoculation onto Sabouraud glucose agar (SGA) and strain identification.

2.3. Initial Medical Treatment. Once the diagnosis of fungal keratitis was established, medical treatment with antifungal agents was initiated. Patients received 0.5% fluconazole every half hour, combined with 5% natamycin or 0.25% amphotericin B every two hours. The patients were also treated with 200 mg of oral itraconazole daily for 21 days. Those with hypopyon received an intravenous injection of fluconazole (100 mg) twice daily and atropine drops once daily. If the infection was not controlled or continued to deteriorate with intensive antifungal therapy, intrastromal or intracameral amphotericin B injection, intrastromal combined with intracameral amphotericin B injection, or surgical intervention was performed according to the state of infection.

2.4. Inclusion Criteria. Combined intrastromal and intracameral injection of amphotericin B was recommended if the infection was not controlled with 1 week of the antifungal therapy described above, showed a tendency to aggravation, and presented with serious corneal damage and intraocular extension, such as severe corneal inflammation, diffuse edema and opacity, local staphyloma and descemetocele (an ulcer reaching Descemet's membrane), increasing endothelial plaque and hypopyon, or visible fungal mass in the anterior chamber and pupillary space.

Initially, we considered this form of management when a severe keratomycosis failed to respond to medical treatment, a donor cornea was not immediately available, and evisceration was most likely needed. After our successful treatment of the first case, and with our experience of single intrastromal or intracameral injection, we believed that a combination of intrastromal and intracameral injections might be beneficial and tried it in additional cases. Therapeutic keratoplasty was considered the next option if donor corneas were available.

2.5. Exclusion Criteria. Cases that had some involvement of adjacent sclera, frank corneal perforation, shallow anterior chamber, and presence of intravitreal fungal mass by B-ultrasound scanning were excluded from this management.

2.6. Injection Procedure. Amphotericin B was obtained in pure powder form and was reconstituted in 5% dextrose to obtain concentrations of 25 μg/mL and 50 μg/mL. All the injection procedure was carried out by Dr. Jianzhang Hu using an operating microscope after administering peribulbar and topical anesthesia under aseptic conditions.

Regarding intrastromal injection, with the bevel down, a 27-gauge needle was inserted obliquely from the uninvolved, clear area to reach just flush with the abscess at the midstromal level (intended level for drug deposit) in each case. Amphotericin B (25 μg/mL) was injected in 4–6 divided doses around the ulcer to form a drug deposit around the circumference of the lesion. The total amount of drug injected intrastromally ranged from 0.05 mL to 0.1 mL.

As for intracameral injection, a limbal incision was made with number 11 surgical blade at the clear corneal sides, and the endothelial plaque region, hypopyon, and fungal mass were gently aspirated and subsequently inoculated on SGA. A volume of 0.5 μg amphotericin B (50 μg/mL) in 0.1 mL was intracamerally injected using a 30-gauge needle on a tuberculin syringe.

2.7. Treatment and Evaluation after Injection. Selectively repeated intrastromal or intracameral or combined intrastromal and intracameral injections were performed as necessary on the basis of the clinical response. If there was an aggravating inflammation, edema, opacity, or ulcer in the cornea, repeated intrastromal injections were scheduled with an interval of more than 5 days. In addition, repeated intracameral injections were also scheduled until the endothelial plaque, hypopyon, and fungal mass in the anterior chamber disappeared or until the treatment was deemed to have failed. The interval between repeat intracameral injections was more than 3 days.

Topical natamycin, fluconazole, and atropine were continued along with the injections. All patients were evaluated daily, including visual acuity, intraocular pressure, complications, and situation of ocular infection. Follow-up ranged from 2 to 4 months. Treatment success was defined as resolution of the corneal infiltrate, disappearance of the anterior chamber inflammation, and healing of the epithelial defect.

3. Results

Nine patients (9 eyes) were involved in this study. Of the 9 patients in this study, the mean age at presentation was 55.22±8.6 years (range, 37 to 71 years). There were 6 males and 3 females. Five patients were farm workers, 2 patients were physical laborers, and 2 patients were temporary employees. The mean age of duration from the onset of symptoms to presentation at our institution ranged from 17 to 63 days (means, 39.22±10.45 days). The risk factors identified in these cases were corneal trauma with vegetable matter (5 eyes), contact lens use (1 eye), and unknown factors (3 eyes). Three patients had a history of diabetes mellitus, and 4 patients had previously received topical steroid therapy (Table 1).

Before injection, initial visual acuity was counting fingers or worse. The size of the ulcers varied from 4.0 to 8.0 mm, and the size of the infiltrate varied from 5.0 to 9.0 mm. In all 9 eyes, laboratory test results before injection showed a positive stain and/or culture for the presence of fungus. Of the 7 eyes with positive cultures, 3 scrapings grew *Fusarium* spp., 2 grew *Aspergillus* spp., 1 was identified as *Alternaria species*, and there was 1 unidentified species (Table 1). The aspirate from the anterior chambers of 8 eyes contained fungal elements.

3.1. Progress of Treatment. Four eyes healed after just 1 treatment with combined intrastromal and intracameral injections (Iii), and 5 eyes needed subsequent injections. Of the 4 eyes that required only 1 treatment, the inflammatory response was observed to weaken after 2 days, and hypopyon disappeared between 3 and 10 days after injection (mean, 6.17 ± 2.27 days). Of the 5 eyes that required more than 1 treatment, 1 eye required one additional combined intrastromal and intracameral injection, 1 eye required another 1 intrastromal injection, 2 eyes required another 2 intracameral injections, and 1 eye required another 2 intracameral injections and 1 intrastromal injection in succession (case 5; Table 1). Case 5, which was identified as *Aspergillus* spp. infection, responded well after the first injection, but the cornea showed no obvious improvement, and hypopyon and fungal mass showed slight increases on day 5. Therefore, the patient received 2 intracameral injections on day 7 and day 12 and 1 intrastromal injection on day 15, and the infection was controlled 7 days after the last intervention.

3.2. Complications. In each of the 9 patients, the procedure was performed successfully, and no severe intraoperative or postoperative complications were observed. In 2 patients (cases 2 and 3), there was minimal intrastromal bleeding in the inferior part of the cornea, but this resolved in 5–7 days. All patients complained of slight pain immediately after injection, and 4 patients reported a significant increase in pain following the injections. Marked uveitis was observed in all eyes with exudative membrane in the anterior chamber the day after the first injection, which decreased by the second day. Secondary glaucoma occurred in 6 eyes the day following every intracameral injection, especially in patients who received several intracameral injections, and the intraocular pressure was lowered by intravenous infusion of mannitol and application of Timolol Maleate drops twice daily.

3.3. Outcome of Treatment. In all 9 eyes, the clinical appearance of fungal invasion, including corneal infiltration, hypopyon, endothelial plaque, and fungal mass in the anterior chamber, resolved after the treatment. Seven corneal ulcers healed with leucoma, and 2 healed with adherent leucoma. Final visual acuity improved to hand movement to 20/40 depending on the location of the remaining scar (Table 1). The time from the first injection to complete resolution of the infection ranged from 18 to 53 days. None of the eyes exhibited vitreous opacity or band formation, and there was no evidence of either local or systemic toxic side effects. There was no recurrence of the infection after withdrawal of all of the antifungal agents. All patients ultimately developed a cataract.

4. Discussion

The primary treatment of fungal keratitis is still the use of antifungal medications, including topical natamycin, amphotericin B, or fluconazole, alone or combined with oral antifungal medications. This approach seems to be effective in the early stages of the disorder. The antifungal agents currently used for fungal keratitis possess a narrow spectrum of activity, toxicity, and lack of effective penetration into deeper layers of the cornea [4, 5]. In recent years, it was still much difficult to treat severe keratitis caused by antimycotic-resistant fungi, even though there was great development of new broad-spectrum antimycotics. To overcome these problems, attempts at site-directed drug deposition have been made in the form of intracameral injections, intrastromal injections, intravitreal injections, and posterior Sub-Tenon injections [8–11, 14–16].

Severe corneal infections may result in extensive corneal melting, acute perforation, endophthalmitis, and rapid visual loss [17]. Meanwhile, the hypha may be penetrating the intact Descemet's membrane and rapidly invading the anterior chamber. At this point, oral and/or intravenous and/or topical drops of antifungal agents obtain poor results, just as in cases reported here. In order to achieve adequate intracorneal concentrations of antifungals, intrastromal injections of antifungals have been tried [8, 14–16]. This treatment was used in infections which were mostly focused in the cornea and seldom invaded the anterior chamber. Additionally, to achieve adequate drug levels in the anterior chamber, subconjunctival and intraocular injections have been tried [9–11, 18]. Subconjunctival injections can produce long-standing periocular inflammation and can lead to epithelial ulcerations, with little penetration into the aqueous [18]. From clinical

Table 1: Clinical data of patients with severe fungal keratitis treated with combined intrastromal and intracameral amphotericin B.

Case number	Age (years)/gender	Risk factor for fungal keratitis	History	Duration of onset of symptoms (days)	Initial BCVA	Size of ulcer (mm)	Fungal identification	Repeated injection	Final BCVA	Healed with
1	37/F	Corneal trauma	Diabetes	27	CF	5 × 6	*Fusarium*	1 Isi	20/40	Leucoma
2	56/M	Unknown	Steroid	17	HM	5.5 × 6.5	Not identified	2 Ici	20/200	Leucoma
3	67/M	Corneal trauma	Diabetes	35	LP	6 × 7	*Alternaria*	1 Iii	CF	Leucoma
4	71/M	Unknown	No	33	HM	6 × 6	*Fusarium*	—	CF	Leucoma
5	57/F	Corneal trauma	Steroid	39	HM	7 × 8	*Aspergillus*	2 Isi + 1 Isi	HM	Adherent leucoma
6	63/F	Contact lens	Diabetes	46	LP	6 × 7	Negative	—	20/300	Leucoma
7	56/M	Corneal trauma	Steroid	63	LP	5 × 7	*Aspergillus*	2 Ici	HM	Adherent leucoma
8	47/M	Unknown	No	52	HM	5.5 × 6.5	*Fusarium*	—	CF	Leucoma
9	43/M	Corneal trauma	Steroid	41	CF	6 × 8	Negative	—	20/200	Leucoma

CF, counting fingers; F, female; HM, hand movements; Iii, combined intrastromal and intracameral injections; Isi, intrastromal injections; Ici, intracameral injections; LP, light perception; M, male.

experience, intracameral injections may achieve therapeutic concentrations in the aqueous, but they are suboptimal in the corneal stroma, where fungal invasion can easily lead to corneal perforation. Hence, in this study, a combination of intrastromal and intracameral injections was administered and successfully treated 9 severe cases without surgical intervention.

Amphotericin B has been shown to be effective in treating systemic mycosis caused by natamycin-resistant filamentous fungi [5, 19]. It has a wide spectrum of activity but has cytotoxicity and poor penetration [12, 13]. It remains to be a potent agent in the treatment of severe keratomycosis, and its efficacy is closely dependent on the ability to achieve optimal drug levels in the cornea [5, 19]. So, to improve the efficacy of amphotericin B, selecting a proper formulation and mode of application is the key [10].

In our series, none of the 9 severe cases had responded to topical antifungal therapy, and we therefore decided to proceed with combined intrastromal and intracameral drug delivery. Successful administration means a more focused concentration of amphotericin B on the side of infection, as well as more reduction of tissue damage. In our opinion, successful injection includes the following aspects. First, the drug should be injected around the abscess on the cornea to form a deposit and create a barrier around the circumference of the ulcer. Second, the needle should be inserted from the uninvolved area to reach just flush with the abscess. Third, to avoid piercing the cornea during intrastromal injection, the needle should be beveled down and inserted to the mid-stromal level slowly and accurately. Fourth, during intracameral injection, when the needle passes through the endothelium and reaches the anterior chamber without resistance, the clinician should stop advancing and begin injecting.

The ideal dose of amphotericin B for intrastromal and/or intracameral use is undetermined, but it should achieve maximum therapeutic effect with minimal side effects. Study has shown that intrastromal injection of amphotericin B at a concentration of less than 10 μg per 0.1 mL is safe in rabbit corneas [20], and at a concentration of 5 μg per 0.1 mL it does not appear to be deleterious to keratocytes or endothelial cells in the clinic [8]. Up to 50 μg of intracamerally injected amphotericin B is also well tolerated by rabbit eyes, and it causes only reversible iritis and clouding of the lens [21]. Some reports showed that the clinical dose recommended for intracameral injections of amphotericin B is 10 to 30 μg in 0.1 to 0.2 mL [9–11]. In our cases, up to 2.5 μg of amphotericin B was intrastromally injected and up to 5.0 μg was intracamerally injected, and a therapeutic concentration was readily delivered without significant adverse effects. The reason that the concentration of amphotericin B used for intrastromal injection (25 μg/mL) was lower than that for intracameral injection (50 μg/mL) is that, first, lower concentrations cause less cornea toxicity and damage. Otherwise, for these severe cases, high concentrations of amphotericin B may easily have led to cornea perforation. Second, amphotericin B in the anterior chamber may penetrate the endothelium into the stroma and gradually increase the concentration of amphotericin B in the stroma to achieve a therapeutic effect. Although this option was not attempted, our study has shown that this treatment was very effective.

Several studies reported the use of intracameral or intrastromal amphotericin B injection in the treatment of fungal keratitis and found that all patients responded favorably with complete clearing of corneal infection and hypopyon and no evidence of corneal or lenticular toxicity [8–11]. In our study, we also found that injections of amphotericin B were safe. None of our patients developed systemic toxic effects from the drug after the injection. No corneal decompensation was shown. Animal studies have shown that low doses of intracameral amphotericin B injection could cause reversible iritis and clouding of the lens [21]; however, a recent similar preliminary study did not report any immediate increase in pain or inflammation [10]. We speculated that complications may be related to the severity of the fungal infection. In this study, all 9 cases involved serious infection. All of our cases had marked increases in the anterior chamber reaction and pain immediately after injection, consistent with a report by Kuriakose et al. [11]. The pain mostly resolved in 12 hours and was presumed to be related to the stimulation of the ciliary body by amphotericin B. The anterior chamber reaction accompanied by exudative membrane was speculated to be caused by three factors: one was the toxic effect of amphotericin B on the iris-ciliary body; one was the stimulation of the iris-ciliary body by the degradation products of fungus decomposed by the drug; and one may have been exudation from the inflamed dilated iris vessels secondary to the decompression caused by the procedure. The anterior chamber reaction may also result in a transient increase of intraocular pressure, which is mainly caused by obstruction of aqueous humor drainage.

Case 5 was the most severe case in this study; he received 2 intrastromal and 3 intracameral injections, and the infection was finally controlled. In our clinical experience, a total of 3 intrastromal and/or 3 intracameral injections may be generally sufficient for the management of severe keratomycosis, thus avoiding complications related to possible toxicity which might result from increased doses of amphotericin B. In addition, the interval between repeat injections should be sufficient to allow adequate healing time of wounds caused by the procedure. We thought that intervals of more than 5 and 3 days between repeat intracameral and intrastromal injections, respectively, were appropriate.

The keratitis in the patients in this study was so severe that they needed potential surgical interventions such as keratoplasty, or even evisceration, in our experience. Our treatment allows the clinician to avoid keratoplasty as a primary mode of treatment, and avoidance of this surgery was beneficial on several counts. However, our treatment only resolved the infection at an acute stage of fungal keratitis and saved the eyeball, but it could not improve the patients' visual acuity. Most of the corneal ulcers healed with leucoma and had extensive corneal scarring after resolution of the infection. This outcome was also common for serious corneal damage. All patients ultimately developed a cataract, which was most likely related to an inflammatory reaction, amphotericin B toxicity, and/or injection trauma. Thus, optical keratoplasty and cataract extraction should be considered the next option.

Of the cases in this study, the mean duration from the onset of symptoms to presentation at our institution was 39.2 ± 10.5 days, much longer than that in a previous report of a spectrum of fungal keratitis in North China which was 26.6 ± 19.0 days. There, 5 eyes still required more than 1 injection for successful resolution of the infection. The patients who needed repeated injections had a preexisting history of diabetes mellitus (1 case) or previous topical steroid therapy (4 cases). It was reported that steroids may increase disease severity and may delay fungal clearance [22, 23]. It seems that a long disease course, a history of diabetes mellitus, and previous topical steroid therapy may aggravate the keratitis and increase the difficulty of injection therapy. It was reported that *Aspergillus* spp. have a stronger virulence than *Fusarium* spp. and *Alternaria species* [24]. In our study, the cases identified as *Aspergillus* spp. infection all needed repeated injections, such as cases 5 and 7. Therefore, an understanding of these potential risk factors may provide ophthalmologists with valuable information before injection and help properly evaluate the treatment.

In summary, the results from this study showed that a combination of intrastromal and intracameral injections of amphotericin B was safe and effective in the treatment of severe fungal keratitis that was resistant to conventional therapy. Different concentrations of amphotericin B can be used in the intrastromal and intracameral injections. Repeated injections may be necessary in some cases. Adept injection skills and correct recognition of complications and potential risk factors are important for successful treatment.

Competing Interests

The authors declare that there are no competing interests regarding the publication of this paper.

Acknowledgments

The authors thank Yulang Lin (the First Affiliated Hospital of Fujian Medical University) for her laboratory assistance. This study is supported in part by the National Natural Science Foundation of China, Beijing, China (Grant no. 81270976), and Fujian Province Medical Project for Middle-Aged and Young Talents (BC), Fuzhou, China (Grant no. 2015-ZQN-ZD-20).

References

[1] L. Xie, W. Zhong, W. Shi, and S. Sun, "Spectrum of fungal keratitis in North China," *Ophthalmology*, vol. 113, no. 11, pp. 1943–1948, 2006.

[2] A. Chowdhary and K. Singh, "Spectrum of fungal keratitis in North India," *Cornea*, vol. 24, no. 1, pp. 8–15, 2005.

[3] H.-C. Lin, P.-H. Chu, Y.-H. Kuo, and S.-C. Shen, "Clinical experience in managing Fusarium solani keratitis," *International Journal of Clinical Practice*, vol. 59, no. 5, pp. 549–554, 2005.

[4] U. Pleyer, J. Grammer, J. H. Pleyer et al., "Amphotericin B—bioavailability in the cornea. Studies with local administration of liposome incorporated amphotericin B," *Ophthalmologe*, vol. 92, no. 4, pp. 469–475, 1995.

[5] P. A. Thomas, "Fungal infections of the cornea," *Eye*, vol. 17, no. 8, pp. 852–862, 2003.

[6] L. Xie, H. Zhai, and W. Shi, "Penetrating keratoplasty for corneal perforations in fungal keratitis," *Cornea*, vol. 26, no. 2, pp. 158–162, 2007.

[7] A. Panda, R. B. Vajpayee, and T. S. Kumar, "Critical evaluation of therapeutic keratoplasty in cases of keratomycosis," *Annals of Ophthalmology*, vol. 23, no. 10, pp. 373–376, 1991.

[8] E. Garcia-Valenzuela and C. D. Song, "Intracorneal injection of amphothericin B for recurrent fungal keratitis and endophthalmitis," *Archives of Ophthalmology*, vol. 123, no. 12, pp. 1721–1723, 2005.

[9] S. Yilmaz, M. Ture, and A. Maden, "Efficacy of intracameral amphotericin B injection in the management of refractory keratomycosis and endophthalmitis," *Cornea*, vol. 26, no. 4, pp. 398–402, 2007.

[10] S. Kaushik, J. Ram, G. S. Brar, A. K. Jain, A. Chakraborti, and A. Gupta, "Intracameral amphotericin B: initial experience in severe keratomycosis," *Cornea*, vol. 20, no. 7, pp. 715–719, 2001.

[11] T. Kuriakose, M. Kothari, P. Paul, P. Jacob, and R. Thomas, "Intracameral amphotericin B injection in the management of deep keratomycosis," *Cornea*, vol. 21, no. 7, pp. 653–656, 2002.

[12] L. Qu, L. Li, and H. Xie, "Corneal and aqueous humor concentrations of amphotericin B using three different routes of administration in a rabbit model," *Ophthalmic Research*, vol. 43, no. 3, pp. 153–158, 2010.

[13] S. D. Schwartz, S. A. Harrison, R. E. Engstrom Jr., R. E. Bawdon, D. A. Lee, and B. J. Mondino, "Collagen shield delivery of amphotericin B," *American Journal of Ophthalmology*, vol. 109, no. 6, pp. 701–704, 1990.

[14] N. Sharma, P. Agarwal, R. Sinha, J. S. Titiyal, T. Velpandian, and R. B. Vajpayee, "Evaluation of intrastromal voriconazole injection in recalcitrant deep fungal keratitis: case series," *British Journal of Ophthalmology*, vol. 95, no. 12, pp. 1735–1737, 2011.

[15] N. Sharma, J. Chacko, T. Velpandian et al., "Comparative evaluation of topical versus intrastromal voriconazole as an adjunct to natamycin in recalcitrant fungal keratitis," *Ophthalmology*, vol. 120, no. 4, pp. 677–681, 2013.

[16] G. Prakash, N. Sharma, M. Goel, J. S. Titiyal, and R. B. Vajpayee, "Evaluation of intrastromal injection of voriconazole as a therapeutic adjunctive for the management of deep recalcitrant fungal keratitis," *American Journal of Ophthalmology*, vol. 146, no. 1, pp. 56–59.e2, 2008.

[17] D. Dursun, V. Fernandez, D. Miller, and E. C. Alfonso, "Advanced Fusarium keratitis progressing to endophthalmitis," *Cornea*, vol. 22, no. 4, pp. 300–303, 2003.

[18] D. M. O'Day, "Fungal keratitis," in *Ocular Infection and Immunity*, J. S. Pepose, G. N. Holland, and K. R. Wilhelmus, Eds., pp. 1048–1061, Mosby Year-Book, St. Louis, Mo, USA, 1996.

[19] R. W. Yee, D. E. Boone, and M. G. Rinaldi, "Antifungal agents," in *Infections of the Eye*, K. F. Tabbara and R. A. Hyndiuk, Eds., pp. 249–267, Little Brown, Boston, Mass, USA, 1996.

[20] L. Qu, L. Li, and H. Xie, "Toxicity and pharmacokinetics of intrastromal injection of amphotericin B in a rabbit model," *Current Eye Research*, vol. 39, no. 4, pp. 340–347, 2014.

[21] J. B. Foster, E. Almeda, M. L. Littman, and M. E. Wilson, "Some intraocular and conjunctival effects of amphotericin B in man and in the rabbit," *Archives of Ophthalmology*, vol. 60, no. 4, pp. 555–564, 1958.

[22] T. G. Wu, V. V. Keasler, B. M. Mitchell, and K. R. Wilhelmus, "Immunosuppression affects the severity of experimental

Fusarium solani keratitis," *Journal of Infectious Diseases*, vol. 190, no. 1, pp. 192–198, 2004.

[23] H. Kiryu, S. Yoshida, Y. Suenaga, and M. Asahi, "Invasion and survival of *Fusarium solani* in the dexamethasone-treated cornea of rabbits," *Journal of Medical and Veterinary Mycology*, vol. 29, no. 6, pp. 395–406, 1991.

[24] X. Dong, W. Shi, Q. Zeng, and L. Xie, "Roles of adherence and matrix metalloproteinases in growth patterns of fungal pathogens in cornea," *Current Eye Research*, vol. 30, no. 8, pp. 613–620, 2005.

Hindawi Publishing Corporation
Journal of Ophthalmology
Volume 2016, Article ID 3513794, 8 pages
http://dx.doi.org/10.1155/2016/3513794

Clinical Study

Low-Fluence Photodynamic Therapy versus Subthreshold Micropulse Yellow Wavelength Laser in the Treatment of Chronic Central Serous Chorioretinopathy

Emin Özmert, Sibel Demirel, Özge Yanık, and Figen Batıoğlu

Department of Ophthalmology, Faculty of Medicine, Ankara University, 06620 Ankara, Turkey

Correspondence should be addressed to Emin Özmert; eozmert56@gmail.com

Received 15 February 2016; Accepted 5 July 2016

Academic Editor: George M. Saleh

Purpose. To compare the efficacy and safety of subthreshold micropulse yellow wavelength laser (SMYL) and low-fluence photodynamic therapy (PDT) in the treatment of chronic central serous chorioretinopathy (CSC). *Methods*. Thirty-three eyes of 30 patients with chronic CSC received either PDT (18 eyes) or SMYL (15 eyes) therapy. Best corrected visual acuity (BCVA), subretinal fluid (SRF) height, and central macular thickness (CMT) were evaluated at the baseline visit and one, three, six, nine, and 12 months after the therapy. *Results*. After 12 months, mean BCVA improved from 67.3 ± 14.2 to 71.5 ± 21.4 ETDRS letters in SMYL group and from 60.7 ± 16.3 to 64.4 ± 24.9 ETDRS letters in PDT group ($p = 0.285$ and $p = 0.440$, resp.). Mean CMT decreased from 242.8 ± 80 μm to 156.9 ± 60 μm in the PDT group and from 287.3 ± 126 μm to 138.0 ± 40 μm in the SMYL group ($p = 0.098$ and $p = 0.003$, resp.). SRF resolved completely in 72.2% and 80.0% of the eyes in the PDT and SMYL groups, respectively. Mean SRF height decreased from 117.2 ± 58 μm to 31.3 ± 56 μm in the PDT group and from 130.0 ± 104 μm to 12.5 ± 21 μm in the SMYL group ($p = 0.031$ and $p = 0.014$, resp.). *Conclusions*. Subthreshold micropulse yellow wavelength laser seems to be effective in the treatment of chronic CSC without any side effect and results in the resorption of SRF without causing visible retinal scarring.

1. Introduction

Central serous chorioretinopathy (CSC) is a disorder of unknown etiology characterized by detachment of the neurosensory retina due to accumulation of serous fluid between the retinal pigment epithelium (RPE) and photoreceptor layers. The disease can present in acute or chronic form. Acute CSC is generally self-limited with spontaneous regression, and it causes minimal sequelae. In chronic CSC, the long-term persistence (longer than six months) of subretinal fluid (SRF) can result in atrophy of the RPE, cystoid retinal degeneration, choroidal neovascularization, and permanent vision loss [1, 2].

Management of chronic CSC includes various options, such as risk factor modification (discontinuation of steroids) [3], medical treatment (carbonic anhydrase inhibitors) [4], conventional focal laser [5], photodynamic therapy (PDT) [6, 7], and intravitreal injection of vascular endothelial growth factor inhibitors [6, 8]. It has been reported that PDT with verteporfin induces the resorption of SRF by reducing choroidal vascular hyperpermeability [9, 10]. However, it has the potential for serious side effects, such as choroidal ischemia, RPE atrophy, and iatrogenic choroidal neovascularization [11, 12]. To avoid these complications, newer PDT protocols, including half-dose [13] and low-fluence [14] applications, have been developed.

Nowadays, micropulse laser (MPL) photocoagulation is another possible treatment option for chronic CSC [15, 16]. The mechanism of action depends on targeting a train of ultrashort laser pulses at the particular tissue of interest. These repetitive bursts prevent damage to adjacent tissues from thermal effects, minimize total energy use, and provide time for tissue cooling between pulses [17]. This technology can be paired with either 810 nm or 577 nm wavelength lasers. The first studies on MPL for CSC used an 810 nm diode laser as the laser source [15, 16, 18]. Subthreshold

micropulse yellow wavelength (577 nm) laser (SMYL) is a newer technology that offers major advantages such as peak absorption of oxyhemoglobin, minimal xanthophyll absorption in the macula, and better penetration [19]. The aim of this study was to compare the efficacy and safety of SMYL and low-fluence PDT in the treatment of chronic CSC. This is the first study that compares the treatment outcomes of SMYL and PDT in patients with chronic CSC.

2. Methods

This retrospective comparative case series included 33 eyes of 30 patients with chronic CSC treated with either low-fluence PDT (18 eyes) or SMYL (15 eyes) therapy at the Ankara University Faculty of Medicine, Department of Ophthalmology, between January 2012 and January 2015. The study was conducted in accordance with the Declaration of Helsinki.

The diagnosis of chronic CSC was confirmed by clinical examination, spectral domain optical coherence tomography (SD-OCT) (Spectralis; Heidelberg Engineering, Inc., Heidelberg, Germany), fundus fluorescein angiography (FA), indocyanine green angiography (ICGA), and fundus autofluorescence (FAF) imaging (Heidelberg Retina Angiograph 2; Heidelberg Engineering, Heidelberg, Germany).

Inclusion criteria were as follows:

(1) Visual impairment history lasting at least six months.

(2) CSC with SRF involving the fovea and documented by SD-OCT.

(3) Presence of single or multiple active leakage sites and/or RPE changes on baseline FA.

(4) Absence of prior history of micropulse laser or PDT therapies.

(5) Follow-up period of at least 12 months after both treatment modalities.

There were not any criteria such as disease severity for selection of the treatment modalities. Patients with a history of comorbid ocular conditions such as age-related macular degeneration, diabetic macular edema, advanced glaucoma, optic neuropathy, or intraocular surgery within the previous six months were excluded.

In the micropulse treatment group (15 eyes), SMYL treatment (Supra Scan 577; Quantel Medical, Clermont-Ferrand, France) had been performed by the same experienced surgeon (EO), using the following parameters: low-intensity (5% duty cycle) and high-density (confluent spots) treatment with 200 msn duration and 160 μm spot size on the slit-lamp adaptor. The power was initially increased upward to the minimum threshold value to cause a barely visible burn on micropulse mode, and then it was adjusted to half of that value. An OCT-guided approach was preferred, and in this manner, an appropriate scan shape was chosen to cover the edematous area entirely on the OCT thickness map.

In the low-fluence PDT group (18 eyes), verteporfin (Visudyne; Novartis, Basel, Switzerland) was administered intravenously at a dose of 6 mg/m^2 over ten minutes. Fifteen minutes after the start of the infusion, a 689 nm laser was delivered for 83 seconds at a reduced light dose of 25 J/cm^2 and an intensity of 300 mW/cm^2. The same experienced specialist (FB) performed the procedure on all of the patients in this group. The PDT application location was based on choroidal hyperpermeability identified by ICGA. After the treatment, the patients were instructed to avoid sunlight exposure for five days.

All of the patients were examined at the baseline visit and one, three, six, nine, and 12 months after undergoing the SMYL or PDT therapy. At each visit, each participant underwent a complete ophthalmic examination that included best corrected visual acuity (BCVA) with Early Treatment Diabetic Retinopathy Study (ETDRS) charts, slit-lamp biomicroscopy, intraocular pressure measurements, dilated fundus examination, FAF imaging, and OCT; FA was repeated as needed. The morphologic results of the treatment were evaluated with SD-OCT in terms of SRF height and central macular thickness (CMT). Subretinal fluid height was measured manually between the outer segment of the photoreceptor layer and the apical face of the RPE layer.

The patients were divided into three groups according to response to treatment: complete response, incomplete response, and unresponsive to therapy. Complete response was defined as complete resolution of SRF in the central 1000 micron area. Any change in SRF within ±100 μm was defined as unresponsive. If the SRF decreased more than 100 μm but was not fully resorbed, the treatment response was defined as incomplete resolution.

The main outcome measures were changes in BCVA and SRF height between the baseline and follow-up examinations. The second outcome measure was to compare the complete anatomic resolution, recurrence, and complication rate between treatment modalities at the end of the 1 year.

Data are shown as mean and standard deviation for continuous variables. For visual acuity assessment, BCVA was converted to logarithm of the minimum angle of resolution (logMAR) equivalents; in addition, ETDRS letters were used in the statistical analysis. Statistical analysis was performed using SPSS software for Windows version 15.0 (SPSS, Inc., Chicago, IL). A p value <0.05 was considered statistically significant. Specific differences in mean values between different treatment groups were tested for significance using Mann-Whitney U test with Bonferroni's correction of p values for multiple comparison. The changes in the same group throughout the follow-up visits were compared using the Friedman test. Kruskal-Wallis test was used for the evaluation of singly ordered categorical data.

3. Results

Thirty-three eyes of 30 patients with chronic CSC were analyzed in this study. The patient group included 22 (73%) male patients and eight (27%) female patients. The mean age (±SD) of the patients at presentation was 49.9 ± 11.1 (31–73) years. The PDT group was older than the SMYL group (52.7 ± 11.2 years versus 44.7 ± 9.5, resp.; $p = 0.037$), and the duration of chronic CSC prior to treatment was longer in the PDT group (18.8 ± 13.5 months versus 13.0 ± 9.1 months, resp.; $p = 0.330$). None of the patients in the SMYL group

Table 1: Final best corrected visual acuity changes in low-fluence photodynamic therapy and subthreshold micropulse yellow laser therapy groups.

BCVA change	Low-fluence PDT n (%)	SMYL n (%)
Increase ≥ 5 ETDRS letters	6 (33.3%)	10 (66.7%)
Stable (within ±4 ETDRS letters)	6 (33.3%)	1 (6.7%)
Decrease ≥ 5 ETDRS letters	6 (33.3%)	4 (26.7%)
Total	18	15
		$p = 0.101$

Table 2: Treatment responses based on SRF resolution in low-fluence photodynamic therapy and subthreshold micropulse yellow laser therapy groups at the end of one-year follow-up period.

Treatment response	Low-fluence PDT n (%)	SMYL n (%)
Complete resolution of SRF	13 (72.2%)	12 (80.0%)
Incomplete resolution of SRF	1 (5.6%)	1 (6.7%)
Unresponsive	3 (16.7%)	None
Recurrence	1 (5.6%)	2 (13.3%)
Total	18	15
		$p = 0.486$

underwent previous therapy. Ten patients in the PDT group had previously received intravitreal ranibizumab injections, but the last injection was performed at least three months prior to PDT. The mean number of ranibizumab injections was 4.7 ± 3.2.

Initial mean visual acuity was 0.47 ± 0.32 logMAR units in the PDT group and 0.32 ± 0.29 logMAR units in the SMYL group ($p = 0.126$). All patients had at least a 12-month follow-up after treatment. In the PDT group, BCVA improved at least 5 ETDRS letters in six eyes (33.3%) and remained stable (within ±4 ETDRS letters) in six eyes (33.3%) (Table 1). In the SMYL group, BCVA improved at least 5 ETDRS letters in ten eyes (66.7%) and remained stable in one eye (6.7%) ($p = 0.101$). Mean BCVA improved from 67.3 ± 14.2 to 71.5 ± 21.4 ETDRS letters in SMYL group and improved from 60.7 ± 16.3 to 64.4 ± 24.9 ETDRS letters in PDT group ($p = 0.285$, $p = 0.440$). The changes in logMAR visual acuity scores and ETDRS letters throughout the follow-up period are shown in Figure 1; there were no statistical differences between the groups ($p = 0.079$ for both groups).

Mean SRF height decreased from 117.2 ± 59 μm to 31.3 ± 57 μm in the PDT group and from 130.0 ± 105 μm to 12.6 ± 21 μm in the SMYL group. The reduction in SRF from baseline to the 12th month was statistically significant in both groups ($p = 0.031$ and $p = 0.014$, resp.). The changes in SRF height throughout the follow-up period are shown in Figure 2; there were no statistical differences between the treatment groups ($p = 0.735$). Mean CMT decreased from 242.9 ± 80 μm to 156.9 ± 61 μm in the PDT group and from 287.3±126 μm to 138.0±41 μm in the SMYL group ($p = 0.098$ and $p = 0.003$, resp.). There were no statistical differences between the treatment groups throughout follow-up ($p = 0.338$).

Treatment responses based on SRF resolution were evaluated at the 12-month follow-up (Table 2). In the PDT group, 13 eyes (72.2%) achieved complete anatomic resolution of SRF in the central macula (Figure 3) and one eye (5.6%) had incomplete resolution, confirmed by OCT. Recurrence of SRF after complete resolution occurred in one eye (5.6%); three eyes (16.7%) were unresponsive to PDT. Of these unresponsive eyes, one eye received one more seance of PDT; however, the patient was unresponsive to the treatment again. The other patients were not retreated. In the SMYL group, 12 eyes (80.0%) achieved complete anatomic resolution of SRF in the central macula (Figure 4) and one eye (6.7%) had incomplete resolution. Subthreshold micropulse yellow wavelength laser treatment was repeated in this eye. However, complete anatomic response could not be achieved again. Recurrence of SRF after complete resolution occurred in two eyes (13.3%); no eyes were unresponsive to SMYL. There

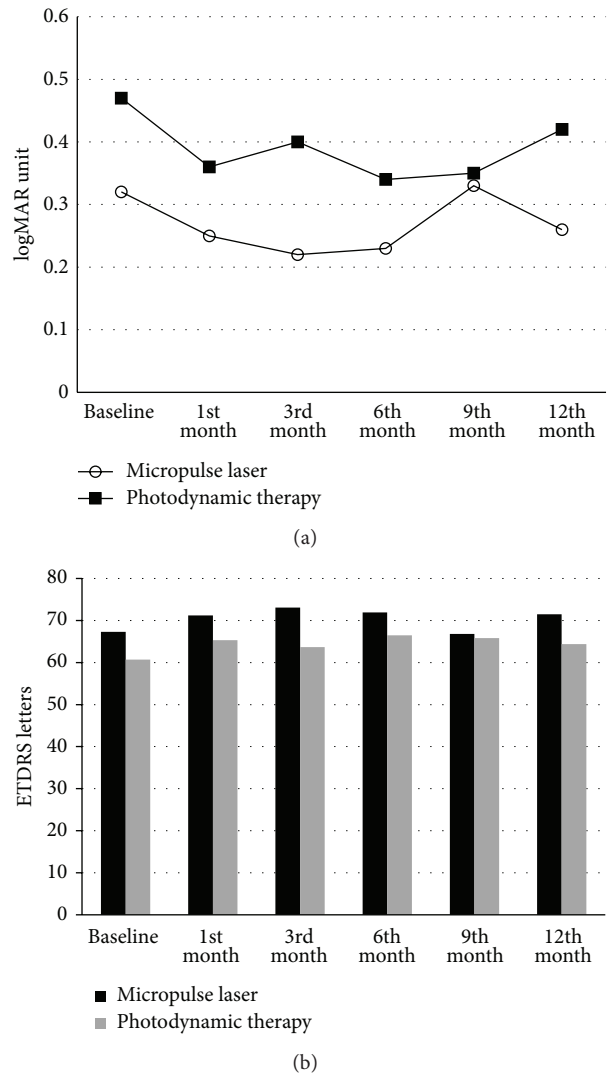

Figure 1: The changes in logMAR visual acuity scores (a) and ETDRS letters (b) throughout follow-up were shown.

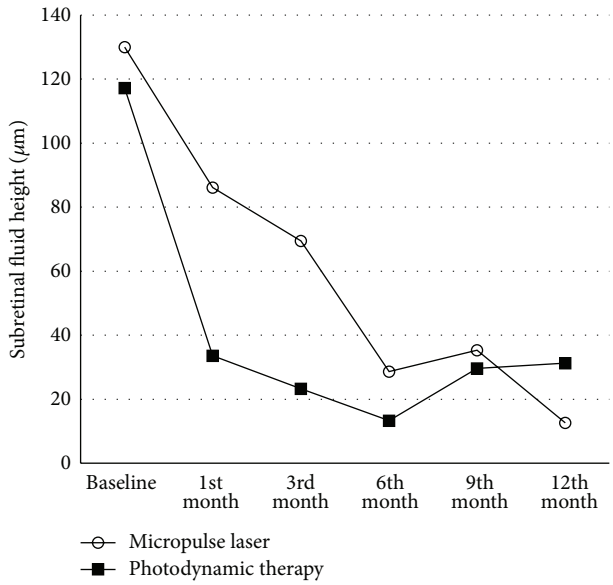

Figure 2: The changes in subretinal fluid height throughout follow-up were shown.

was no statistical difference between the PDT and SMYL groups in terms of treatment response ($p = 0.486$). Fundus autofluorescence imaging used to determine the safety profile of the SMYL group revealed hypofluorescent laser spots that were not visible in the fundus examination in one case. There were no significant side effects in the PDT group.

4. Discussion

In the present study, the treatment outcomes of chronic CSC patients treated with either low-fluence PDT or SMYL were compared, and changes in logMAR visual acuity scores, ETDRS letters, SRF height, and CMT throughout the follow-up were analyzed. To our knowledge, this is the first study in the literature to compare SMYL and low-fluence PDT treatment results in chronic CRC patients. The results of the study indicate that there were no statistically significant differences in the parameters listed above between the two treatment modalities. Subthreshold micropulse yellow wavelength laser seems to be an effective modality in treatment response, visual acuity improvement, and SRF reduction.

The exact pathophysiologic changes that lead to the characteristic RPE leakage associated with CSC remain unclear. However, ICGA has demonstrated the effect of choroidal circulatory abnormalities in the development of CSC, such as hyperpermeability from choriocapillaris [20], venous dilation [21], and vascular congestion [22]. In the treatment of CSC, the aim is to induce absorption of SRF and to improve or stabilize visual acuity.

Photodynamic therapy with verteporfin has proven to be effective according to several reports [11, 23, 24]. The mechanism of action of PDT depends on transient choroidal hypoperfusion leading to choroidal vascular remodeling and the reduction of choroidal exudation [6, 23, 25]. However, the conventional PDT protocol has several potential serious adverse effects, including RPE changes, permanent choroidal ischemia, and secondary choroidal neovascularization [11, 12, 23]. To reduce the risk of these potential adverse effects, modified PDT protocols have been developed, such as half-dose verteporfin administration [13, 26, 27] and low-fluence rate [28, 29]. It has been reported that low-fluence PDT reduces choroidal hypoperfusion without causing significant differences in treatment efficacy [28]. Photodynamic therapy is a relatively invasive procedure that requires the intravenous injection of verteporfin. Also, ICG may cause anaphylactic and urticarial reactions in patients both with and without a history of allergy, and hepatic diseases, hemodialysis, and pregnancy are relative contraindications for ICG [30]. A low-fluence PDT protocol was used in the present study, with complete resolution of SFR achieved in 72.2% of the patients.

The subthreshold MPL technique introduced the term "photostimulation," as opposed to "photocoagulation" [18]. The mechanism depends on low-intensity, high-density laser applications in envelopes of repetitive short pulses [31]. These pulses stimulate the production of intracellular antiangiogenic and restorative biological factors without causing visible laser scars [32, 33]. Wavelengths of either 810 or 577 nm can be used as the laser source in micropulse photostimulation. This technique has been used with promising results in the treatment of macular edema in diabetic retinopathy and branch retinal vein occlusion [34–36]. Chen et al. [15] studied subthreshold diode MPL in 26 eyes of 25 CSC patients and reported it to be effective in the presence of point source leakage. However, a less favorable response was noted in eyes with diffuse leakage. Another study reported that, after ICG dye-enhanced subthreshold MPL, neuroepithelial detachment was completely resolved in five of seven patients with CSC within four to eight weeks [16]. In a recent study comparing the outcomes of subthreshold MPL and intravitreal bevacizumab injections, subthreshold MPL photocoagulation was found to be superior to intravitreal injections of 1.25 mg bevacizumab in the treatment of CSC [18]. All of these promising findings define subthreshold MPL as a possible treatment option for chronic CSC.

Subthreshold micropulse yellow wavelength laser is a quite different modality than subthreshold micropulse diode laser. The yellow wavelength (577 nm) laser produces combined absorption by both melanin and oxyhemoglobin, which leads to maximum absorption in the pigment epithelium and choriocapillaris [37]. It also has negligible xanthophyll absorption, which allows repeated treatment close to the fovea [19]. While the longer wavelength provides better penetration, it also leads to energy concentration in a smaller volume and allows a shorter pulse duration. The major advantages of the procedure are the tissue-sparing effect and repeatability of the sessions after three to six months in case of recurrence of SRF or unresponsiveness to therapy. Subthreshold micropulse yellow wavelength laser might also lead to an increase in retinal sensitivity in the macular area [38]. In the present study, the effects of the SMYL therapy on macular sensitivity could not be evaluated, due to the lack of availability of a microperimetry device. However, we believe

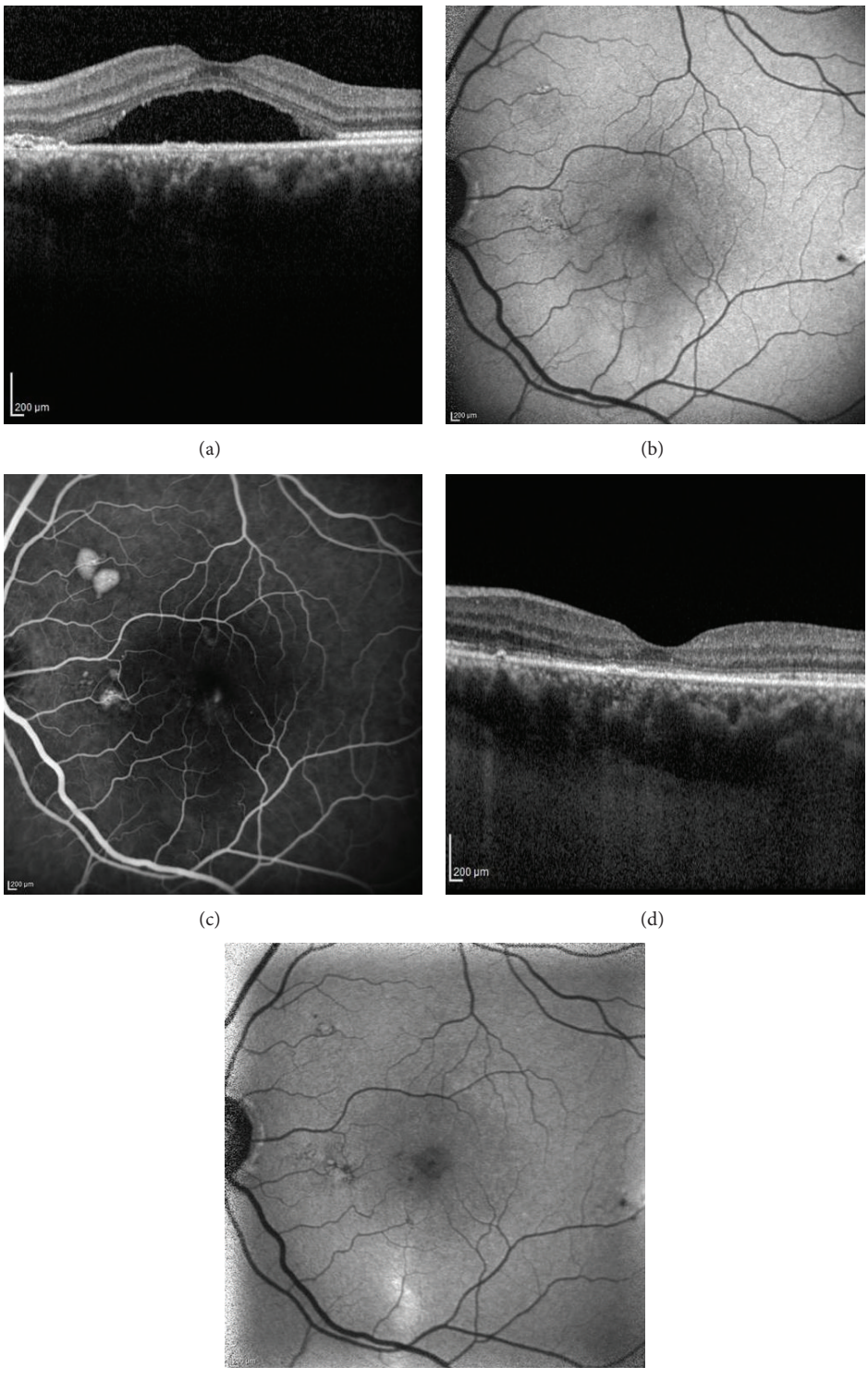

Figure 3: Spectral domain optical coherence tomography (SD-OCT), fundus autofluorescence (FAF), and fluorescein angiography (FA) images of a 47-year-old female patient with CSC for 7 months. Left eye before photodynamic therapy (PDT): chronic subretinal fluid on SD-OCT (a), hypoautofluorescence on FAF image due to the blockage effect of the subretinal fluid (b), and focal leakage of fluorescein and two small pigment epithelial detachments at the late phase of FA (c). Eight months after PDT treatment: complete resolution of the subretinal fluid (d) and disappearance of hypoautofluorescence on FAF (e).

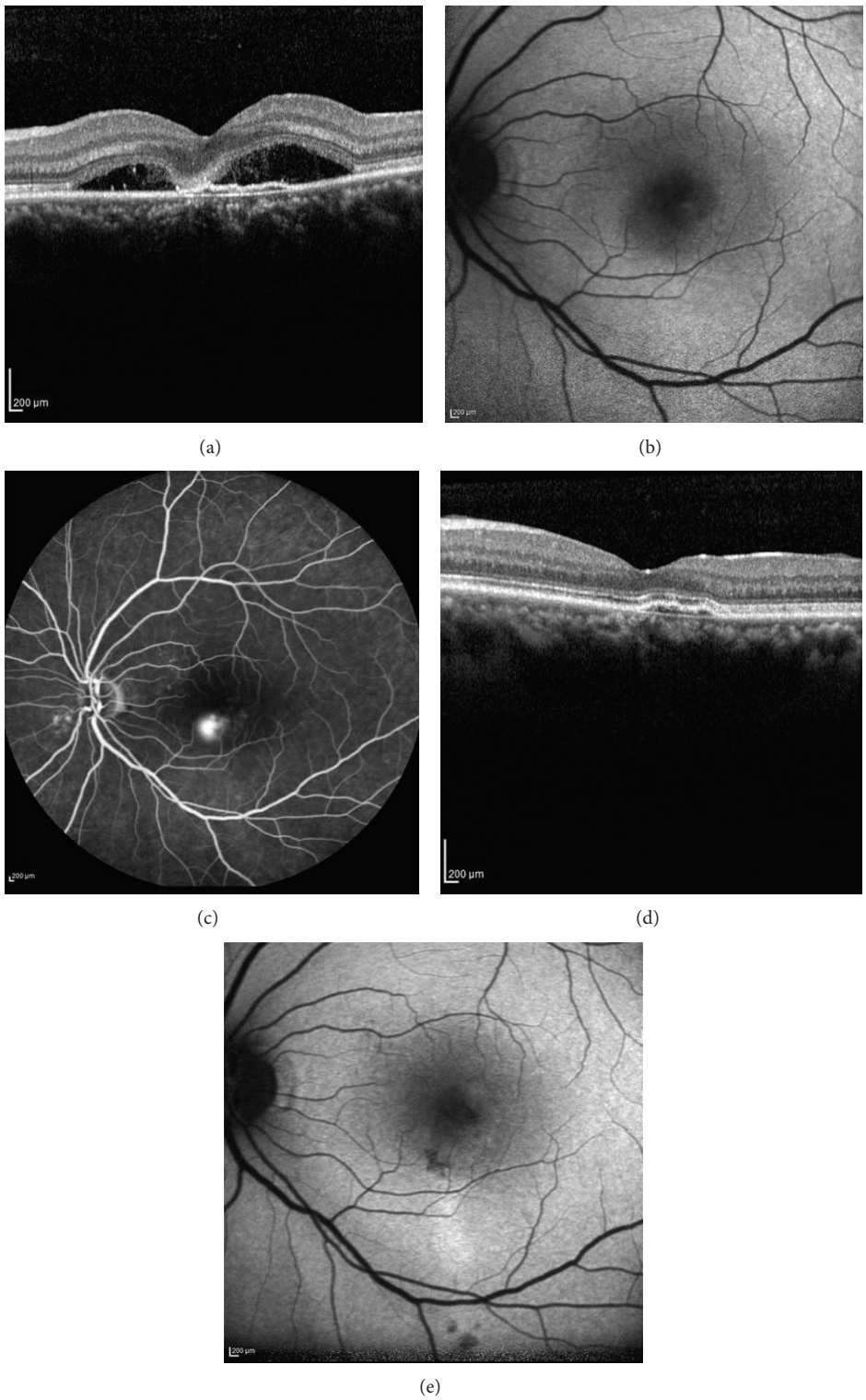

Figure 4: Spectral domain optical coherence tomography (SD-OCT), fundus autofluorescence (FAF), and fluorescein angiography (FA) images of a 42-year-old female patient with CSC for 7 months. Left eye before subthreshold micropulse yellow wavelength laser (SMYL) treatment: chronic subretinal fluid with fibrin accumulation on SD-OCT (a), increased hypoautofluorescence on FAF image due to the blockage effect of the subretinal fluid (b), and focal leakage of fluorescein at the late phase of FA (c). Nine months after SMYL treatment: complete resolution of the subretinal fluid (d) and hypoautofluorescence spots due to RPE atrophies at the previous leakage area on FAF (e).

SMYL therapy may improve retinal sensitivity in addition to increasing visual acuity.

Only two studies in the literature have reported the efficacy of SMYL in chronic CSC patients. The first study included 15 eyes of 13 patients who had CSC for more than three months. The mean follow-up period was eight weeks, and the researchers reported a reduction in mean SRF height from 232 to 49 μm at the final visit. They determined that the procedure was safe and that it caused no obvious changes in RPE as seen on OCT and FAF [38]. In the second study, the authors reported the results of ten eyes of ten chronic or chronic recurrent CSC patients who received SMYL with a 15% duty cycle. The logMAR visual acuity scores improved from 0.21 ± 0.21 to 0.035 ± 0.063 at the end of the follow-up period (mean, 8 months; range, 3–18 months) [39]. The present study is the first study to compare the treatment outcomes of low-fluence PDT and SMYL, with follow-up period of 12 months. In this study, 80% of the eyes in the SMYL group achieved complete resorption of SRF (72.2% in PDT group), and all of the eyes were responsive to therapy. However, two patients experienced recurrence of CSC, and in another patient, FAF revealed hypofluorescent laser spots that were not visible in the fundus examination. Retinal laser spots on FAF could occur in rare circumstances as a result of RPE changes. The occurrence of retinal burn depends on the pigmentation of the individual and the applied laser power. Several methods were developed for MPL power adjustment. Some authors adjust laser power upward to the minimum threshold value for a visible burn in a continuous wave mode and then switch the apparatus to micropulse model [15, 38, 40]. Other researchers have also used the micropulse mode for power titration and applied 50–80% of the minimum threshold power to cause a barely visible burn [39, 41]; that power adjustment method was used in the present study. However, further studies are needed to determine a standard power titration protocol in SMYL applications.

The major limitation of the present study is the retrospective design. A randomized prospective controlled trial will be more rational to compare the treatment modalities. Also the longer duration of the disease and the presence of eyes previously treated with intravitreal anti-VEGF therapy in PDT group are the other main limitations of the study.

In conclusion, SMYL seems to be effective in providing resorption of SRF in the treatment of chronic CSC. Although not statistically significant, the rate of complete resolution of SRF and ≥ 5 increase in ETDRS letters were higher in SMYL group. Also, in contrast to the PDT group, no eyes were unresponsive to SMYL. Major advantages of SMYL are having a tissue-sparing effect, being a noninvasive procedure, and allowing safe repetition of the therapy after three to six months. In addition to improving BCVA, SMYL may also improve retinal sensitivity in the macular area without causing collateral chorioretinal damage. Further prospective studies are needed to investigate the correlation between changes in visual acuity and macular sensitivity on microperimetry after SMYL in the treatment of CSC.

Competing Interests

No conflicting relationship exists for any author.

Authors' Contributions

All authors conceived the study, participated in its design and coordination, and revised the paper critically for important intellectual content. All authors read and approved the final paper.

References

[1] F. C. Piccolino, R. R. De La Longrais, G. Ravera et al., "The foveal photoreceptor layer and visual acuity loss in central serous chorioretinopathy," *American Journal of Ophthalmology*, vol. 139, no. 1, pp. 87–99, 2005.

[2] M. S. M. Wang, B. Sander, and M. Larsen, "Retinal atrophy in idiopathic central serous chorioretinopathy," *American Journal of Ophthalmology*, vol. 133, no. 6, pp. 787–793, 2002.

[3] J. Levy, M. Marcus, N. Belfair, I. Klemperer, and T. Lifshitz, "Central serous chorioretinopathy in patients receiving systemic corticosteroid therapy," *Canadian Journal of Ophthalmology*, vol. 40, no. 2, pp. 217–221, 2005.

[4] J. Pikkel, I. Beiran, A. Ophir, and B. Miller, "Acetazolamide for central serous retinopathy," *Ophthalmology*, vol. 109, no. 9, pp. 1723–1725, 2002.

[5] E. Burumcek, A. Mudun, S. Karacorlu, and M. O. Arslan, "Laser photocoagulation for persistent central serous retinopathy: results of long-term follow-up," *Ophthalmology*, vol. 104, no. 4, pp. 616–622, 1997.

[6] S. H. Bae, J. W. Heo, C. Kim et al., "A randomized pilot study of low-fluence photodynamic therapy versus intravitreal ranibizumab for chronic central serous chorioretinopathy," *American Journal of Ophthalmology*, vol. 152, no. 5, pp. 784–792.e2, 2011.

[7] E. Ozmert and F. Batioglu, "Fundus autofluorescence before and after photodynamic therapy for chronic central serous chorioretinopathy," *Ophthalmologica*, vol. 223, no. 4, pp. 263–268, 2009.

[8] J. W. Lim, S. J. Ryu, and M. C. Shin, "The effect of intravitreal bevacizumab in patients with acute central serous chorioretinopathy," *Korean Journal of Ophthalmology*, vol. 24, no. 3, pp. 155–158, 2010.

[9] Z. Alkin, I. Perente, A. Ozkaya et al., "Comparison of efficacy between low-fluence and half-dose verteporfin photodynamic therapy for chronic central serous chorioretinopathy," *Clinical Ophthalmology*, vol. 8, pp. 685–690, 2014.

[10] R. M. Silva, J. M. Ruiz-Moreno, F. Gomez-Ulla et al., "Photodynamic therapy for chronic central serous chorioretinopathy: a 4-year follow-up study," *Retina*, vol. 33, no. 2, pp. 309–315, 2013.

[11] F. C. Piccolino, C. M. Eandi, L. Ventre, R. C. Rigault de La Longrais, and F. M. Grignolo, "Photodynamic therapy for chronic central serous chorioretinopathy," *Retina*, vol. 23, no. 6, pp. 752–763, 2003.

[12] M. Colucciello, "Choroidal neovascularization complicating photodynamic therapy for central serous retinopathy," *Retina*, vol. 26, no. 2, pp. 239–242, 2006.

[13] W.-M. Chan, T. Y. Y. Lai, R. Y. K. Lai, D. T. L. Liu, and D. S. C. Lam, "Half-dose verteporfin photodynamic therapy for acute central serous chorioretinopathy: one-year results of a randomized controlled trial," *Ophthalmology*, vol. 115, no. 10, pp. 1756–1765, 2008.

[14] M. Reibaldi, F. Boscia, T. Avitabile et al., "Low-fluence photodynamic therapy in longstanding chronic central serous chorioretinopathy with foveal and gravitational atrophy," *European Journal of Ophthalmology*, vol. 19, no. 1, pp. 154–158, 2009.

[15] S.-N. Chen, J.-F. Hwang, L.-F. Tseng, and C.-J. Lin, "Subthreshold diode micropulse photocoagulation for the treatment of chronic central serous chorioretinopathy with juxtafoveal leakage," *Ophthalmology*, vol. 115, no. 12, pp. 2229–2234, 2008.

[16] F. Ricci, F. Missiroli, F. Regine, M. Grossi, and G. Dorin, "Indocyanine green enhanced subthreshold diode-laser micropulse photocoagulation treatment of chronic central serous chorioretinopathy," *Graefe's Archive for Clinical and Experimental Ophthalmology*, vol. 247, no. 5, pp. 597–607, 2009.

[17] S. Sivaprasad, M. Elagouz, D. McHugh, O. Shona, and G. Dorin, "Micropulsed diode laser therapy: evolution and clinical applications," *Survey of Ophthalmology*, vol. 55, no. 6, pp. 516–530, 2010.

[18] M. J. Koss, I. Beger, and F. H. Koch, "Subthreshold diode laser micropulse photocoagulation versus intravitreal injections of bevacizumab in the treatment of central serous chorioretinopathy," *Eye*, vol. 26, no. 2, pp. 307–314, 2012.

[19] M. A. Mainster, "Decreasing retinal photocoagulation damage: principles and techniques," *Seminars in Ophthalmology*, vol. 14, no. 4, pp. 200–209, 1999.

[20] R. F. Spaide, L. Hall, A. Haas et al., "Indocyanine green videoangiography of older patients with central serous chorioretinopathy," *Retina*, vol. 16, no. 3, pp. 203–213, 1996.

[21] A. Giovannini, B. Scassellati-Sforzolini, E. D'Altobrando, C. Mariotti, T. Rutili, and R. Tittarelli, "Choroidal findings in the course of idiopathic serous pigment epithelium detachment detected by indocyanine green videoangiography," *Retina*, vol. 17, no. 4, pp. 286–293, 1997.

[22] C. Prunte and J. Flammer, "Choroidal capillary and venous congestion in central serous chorioretinopathy," *American Journal of Ophthalmology*, vol. 121, no. 1, pp. 26–34, 1996.

[23] W.-M. Chan, D. S. C. Lam, T. Y. Y. Lai, B. S. M. Tam, D. T. L. Liu, and C. K. M. Chan, "Choroidal vascular remodelling in central serous chorioretinopathy after indocyanine green guided photodynamic therapy with verteporfin: a novel treatment at the primary disease level," *British Journal of Ophthalmology*, vol. 87, no. 12, pp. 1453–1458, 2003.

[24] L. A. Yannuzzi, J. S. Slakter, N. E. Gross et al., "Indocyanine green angiography-guided photodynamic therapy for treatment of chronic central serous chorioretinopathy: a pilot study," *Retina*, vol. 23, no. 3, pp. 288–298, 2003.

[25] M. Taban, D. S. Boyer, E. L. Thomas, and M. Taban, "Chronic central serous chorioretinopathy: photodynamic therapy," *American Journal of Ophthalmology*, vol. 137, no. 6, pp. 1073–1080, 2004.

[26] T. Y. Y. Lai, W.-M. Chan, H. Li, R. Y. K. Lai, D. T. L. Liu, and D. S. C. Lam, "Safety enhanced photodynamic therapy with half dose verteporfin for chronic central serous chorioretinopathy: a short term pilot study," *British Journal of Ophthalmology*, vol. 90, no. 7, pp. 869–874, 2006.

[27] K. Fujita, M. Yuzawa, and R. Mori, "Retinal sensitivity after photodynamic therapy with half-dose verteporfin for chronic central serous chorioretinopathy: short-term results," *Retina*, vol. 31, no. 4, pp. 772–778, 2011.

[28] M. Reibaldi, N. Cardascia, A. Longo et al., "Standard-fluence versus low-fluence photodynamic therapy in chronic central serous chorioretinopathy: a nonrandomized clinical trial," *American Journal of Ophthalmology*, vol. 149, no. 2, pp. 307–315.e2, 2010.

[29] J. Y. Shin, S. J. Woo, H. G. Yu, and K. H. Park, "Comparison of efficacy and safety between half-fluence and full-fluence photodynamic therapy for chronic central serous chorioretinopathy," *Retina*, vol. 31, no. 1, pp. 119–126, 2011.

[30] S. L. Owens, "Indocyanine green angiography," *British Journal of Ophthalmology*, vol. 80, no. 3, pp. 263–266, 1996.

[31] G. Dorin, "Subthreshold and micropulse diode laser photocoagulation," *Seminars in Ophthalmology*, vol. 18, no. 3, pp. 147–153, 2003.

[32] N. Ogata, J. Tombran-Tink, N. Jo, D. Mrazek, and M. Matsumura, "Upregulation of pigment epithelium-derived factor after laser photocoagulation," *American Journal of Ophthalmology*, vol. 132, no. 3, pp. 427–429, 2001.

[33] A. K. Yu, K. D. Merrill, S. N. Truong, K. M. Forward, L. S. Morse, and D. G. Telander, "The comparative histologic effects of subthreshold 532- and 810-nm diode micropulse laser on the retina," *Investigative Ophthalmology & Visual Science*, vol. 54, no. 3, pp. 2216–2224, 2013.

[34] K. Inagaki, K. Ohkoshi, S. Ohde, G. A. Deshpande, N. Ebihara, and A. Murakami, "Subthreshold micropulse photocoagulation for persistent macular edema secondary to branch retinal vein occlusion including best-corrected visual acuity greater than 20/40," *Journal of Ophthalmology*, vol. 2014, Article ID 251257, 10 pages, 2014.

[35] K. Ohkoshi and T. Yamaguchi, "Subthreshold micropulse diode laser photocoagulation for diabetic macular edema in Japanese patients," *American Journal of Ophthalmology*, vol. 149, no. 1, pp. 133–139, 2010.

[36] M. B. Parodi, S. Spasse, P. Iacono, G. Di Stefano, T. Canziani, and G. Ravalico, "Subthreshold grid laser treatment of macular edema secondary to branch retinal vein occlusion with micropulse infrared (810 nanometer) diode laser," *Ophthalmology*, vol. 113, no. 12, pp. 2237–2242, 2006.

[37] M. A. Mainster, "Wavelength selection in macular photocoagulation. Tissue optics, thermal effects, and laser systems," *Ophthalmology*, vol. 93, no. 7, pp. 952–958, 1986.

[38] N. K. Yadav, C. Jayadev, A. Mohan et al., "Subthreshold micropulse yellow laser (577 nm) in chronic central serous chorioretinopathy: safety profile and treatment outcome," *Eye*, vol. 29, no. 2, pp. 258–265, 2015.

[39] J. Y. Kim, H. S. Park, and S. Y. Kim, "Short-term efficacy of subthreshold micropulse yellow laser (577-nm) photocoagulation for chronic central serous chorioretinopathy," *Graefe's Archive for Clinical and Experimental Ophthalmology*, vol. 253, no. 12, pp. 2129–2135, 2015.

[40] L. Roisman, F. P. Magalhães, D. Lavinsky et al., "Micropulse diode laser treatment for chronic central serous chorioretinopathy: a randomized pilot trial," *Ophthalmic Surgery Lasers and Imaging Retina*, vol. 44, no. 5, pp. 465–470, 2013.

[41] B. Gupta, M. Elagouz, D. McHugh, V. Chong, and S. Sivaprasad, "Micropulse diode laser photocoagulation for central serous chorio-retinopathy," *Clinical and Experimental Ophthalmology*, vol. 37, no. 8, pp. 801–805, 2009.

Hindawi Publishing Corporation
Journal of Ophthalmology
Volume 2016, Article ID 4727423, 8 pages
http://dx.doi.org/10.1155/2016/4727423

Review Article

The Application of a Contact Lens Sensor in Detecting 24-Hour Intraocular Pressure-Related Patterns

Sarah C. Xu,[1,2] Angela C. Gauthier,[1] and Ji Liu[1]

[1]*Department of Ophthalmology and Visual Science, Yale University School of Medicine, New Haven, CT 06510, USA*
[2]*Department of Ophthalmology, Mayo Clinic, Rochester, MN 55905, USA*

Correspondence should be addressed to Ji Liu; liu.ji@yale.edu

Received 25 March 2016; Accepted 22 June 2016

Academic Editor: George M. Saleh

Glaucoma is one of the leading causes of blindness worldwide. Recent studies suggest that intraocular pressure (IOP) fluctuations, peaks, and rhythm are important factors in disease advancement. Yet, current glaucoma management remains hinged on single IOP measurements during clinic hours. To overcome this limitation, 24-hour IOP monitoring devices have been employed and include self-tonometry, permanent IOP, and temporary IOP monitoring. This review discusses each IOP measuring strategy and focuses on the recently FDA-approved contact lens sensor (CLS). The CLS records IOP-related ocular patterns for 24 hours continuously. Using the CLS, IOP-related parameters have been found to be associated with the rate of visual field progression in primary open-angle glaucoma, disease progression in primary angle-closure glaucoma, and various clinical variables in ocular hypertension. The CLS has been used to quantify blink rate and limbal strain and measure the circadian rhythm in a variety of disease states including normal-tension glaucoma and thyroid eye disease. The effects of various IOP-lowering interventions were also characterized using the CLS. CLS provides a unique, safe, and well-tolerated way to study IOP-related patterns in a wide range of disease states. IOP-related patterns may help identify patients most at risk for disease progression and assist with the development of tailored treatments.

1. Introduction

Glaucoma is a progressive optic neuropathy characterized by visual field loss and structural changes to the optic nerve. It is one of the leading causes of blindness worldwide along with cataracts and age-related macular degeneration [1–4]. Population-based studies on glaucoma have reported a prevalence rate in the range of 1.5–4.2% throughout the world with developing nations carrying a greater burden of bilateral blindness from glaucoma [5–9]. It has been estimated that 80 million people will be diagnosed with glaucoma and 11.2 million will be blinded by the disease by 2020 [10]. This troubling prediction is mainly due to aging and a growing world population.

Although it is no longer part of the modern definition of glaucoma, uncontrolled intraocular pressure (IOP) remains the single most important risk factor for glaucoma development and progression. Recent studies suggest that IOP fluctuations and peaks are associated with disease advancement. Nouri-Mahdavi et al. found that large IOP fluctuations and age carry significant odds ratios for visual field loss in the Advanced Glaucoma Intervention Study [11]. Similarly, De Moraes et al. found that IOP peak and fluctuation were associated with an increased risk for visual field progression in the Glaucoma Progression Study. Peak IOP was also found to be a significant risk factor in the multivariable model for visual field loss (OR = 1.13), along with thinner central corneal thickness, disc hemorrhage, and beta-zone parapapillary atrophy [12]. The association between IOP peaks and disease progression highlights the importance of studying IOP parameters during a 24-hour period.

Clinicians have realized the limitations in our current IOP measurement method for quite a few years. In most clinical practices in the United States, IOP is measured once during a patient's clinic visit using Goldmann applanation tonometry. The Goldmann tonometer measures the force needed to deform the spherical cornea to a standardized diameter based on the Imbert-Fick law [13]. The office measurements provide only cross-sectional views of patients' fluctuating IOP.

Additionally, IOP measurements obtained by the Goldmann tonometer are operator dependent and influenced by patient position and ocular factors, such as astigmatism and central corneal thickness [14–16]. As a result, clinical details such as short-term IOP fluctuations within a 24-hour period and other IOP parameters remain hidden by our current IOP measurements using the Goldmann tonometer. This review discusses innovative approaches to measuring IOP during a 24-hour period, particularly the use of a contact lens sensor (CLS).

2. Strategies in 24-Hour Pressure Monitoring

Given the limitations of our current IOP measurement method, researchers and clinicians have devised three main strategies of 24-hour IOP monitoring: self-tonometry by the patient, permanent IOP monitoring, and temporary IOP monitoring [17]. In terms of self-tonometry, the Pulsair-Keeler was one device invented for patients to measure IOP at home to supplement the office visit IOP. The Pulsair-Keeler tonometer is a hand-held noncontact tonometer that measured IOP by indenting the cornea using a puff of air from the machine held 2 cm from the cornea [17]. However, self-tonometry was only achieved 75% of the time due to difficulty with usage. Of the measurements obtained, only 73% were accurate within 1 mmHg of measurements from the Goldmann tonometer [18]. Consequently, this device was not adopted for clinical use. Other self-tonometers trialed include the Proview Eye Pressure Monitor (also known as phosphine self-tonometry) and Ocuton S, both of which were based on the same principle of applanation, like the Goldmann tonometer. Despite training, 41% to 47% of patients could not perform self-tonometry with Ocuton S [19, 20]. Numerous studies have showed limited correlation in the IOP readings from Proview and Goldmann, thus questioning the effectiveness of the Proview tonometer [8, 21, 22]. A self-tonometer offering good correlation with the Goldmann is the iCare rebound tonometer [23]. It is a hand-held device that measures IOP through deceleration of a magnetized probe after it rebounds from the cornea. Out of 76 subjects, 74% were able to correctly preform the self-tonometry. Central corneal thickness below 500 μm or above 600 μm was correlated with greater difference between Goldmann and iCare [23]. Despite the various self-tonometers available, these devices do not allow continuous measurement of 24-hour IOP patterns during undisturbed sleep. Furthermore, they are limited by challenges of usability and IOP recording accuracy.

Implantable, permanent IOP sensors provide the second strategy in IOP monitoring. Chen et al. in 2006 designed an intraocular sensor that can be fixed to the iris. The principle behind this device is the use of a Bourdon tube that mechanically deforms depending on the IOP [24]. Another permanent sensor is designed as an artificial intraocular lens with an embedded sensor, which detects IOP-induced stress and causes a change in the resistance of the circuit [25–27]. The advantage of these devices is that they would allow continuous, direct measurement of true IOP, particularly during undisturbed sleep. However, these devices require surgical implantation, which is associated with risks including infection, bleeding, inflammation, and device failure. To date, none of the designs have advanced to the human trials phase [8].

Finally, temporary IOP devices have the most potential to be widely used given that no surgical intervention is necessary and the sensor is easily reversible. Leonardi et al. designed and tested the first contact lens sensor [28]. A soft contact lens is embedded with strain gauges to measure the circumferential changes at the corneoscleral junction. The principle behind the device is that a change in IOP of 1 mmHg is associated with a 3 μm change in the corneal curvature radius [29, 30]. The electrical output (mV Eq) change from the sensor has been shown to significantly correlate with IOP changes. Leonardi et al. showed in 2009 that, in enucleated pig eyes, electrical output from the contact lens sensor had good sensitivity and correlation with IOP in the range of 17 to 29 mmHg [31]. Since then, the device has also shown good sensitivity and tolerability in human clinical trials [32].

3. What Is the Triggerfish® 24-Hour Contact Lens Sensor?

The Triggerfish is a soft contact lens sensor tested by Leonardi et al. [28]. This CLS provides a minimally invasive method to record IOP-related ocular patterns for 24 hours continuously [31]. The CLS consists of resistive platinum-titanium strain gauges embedded in the soft silicon contact lens (Figure 1(a)). Depending on the patient's cornea steepness, three different sizes of the contact lens are available to allow for an appropriate fit. The device is placed on the cornea as shown in Figure 1(b). The CLS sends electrical signals via Bluetooth® to an antenna which is patched periorbitally, before transmitting and storing the information in a recorder (Figure 1(c)). Patients wear the device for 24 hours with minimal restriction in activities. The 24-hour IOP-related ocular pattern data are retrieved after connecting the recorder to a computer. The CLS produces electric output in millivolts (mV). When the output is trended over time, the resulting graph is termed IOP-related patterns or profiles. The output has been hypothesized to measure a composite of IOP, anterior volume change, and ocular biomechanical properties [32–34]. Thus far, this CLS has been used safely and effectively in healthy subjects, patients with open-angle glaucoma, and patients with angle-closure glaucoma [32, 34–36]. It has also been used to show the effect of IOP-lowering interventions during a 24-hour period, particularly the nocturnal period [37].

4. Safety, Reproducibility, and Accuracy

The most common adverse events include conjunctival hyperemia, blurred vision, and superficial punctate keratitis as reported by Mansouri et al. [38]. In the initial clinical study, one case of corneal erosion in a patient with severe dry eye disease and four cases of superficial punctate keratitis were reported in a cohort of 15 patients, all of which resolved within 24 hours [39]. In our study that fitted 17 ocular hypertensive patients with the CLS unilaterally, all patients experienced self-resolving, mild conjunctival hyperemia [40]. In a study that examined the safety and tolerability of the CLS in patients

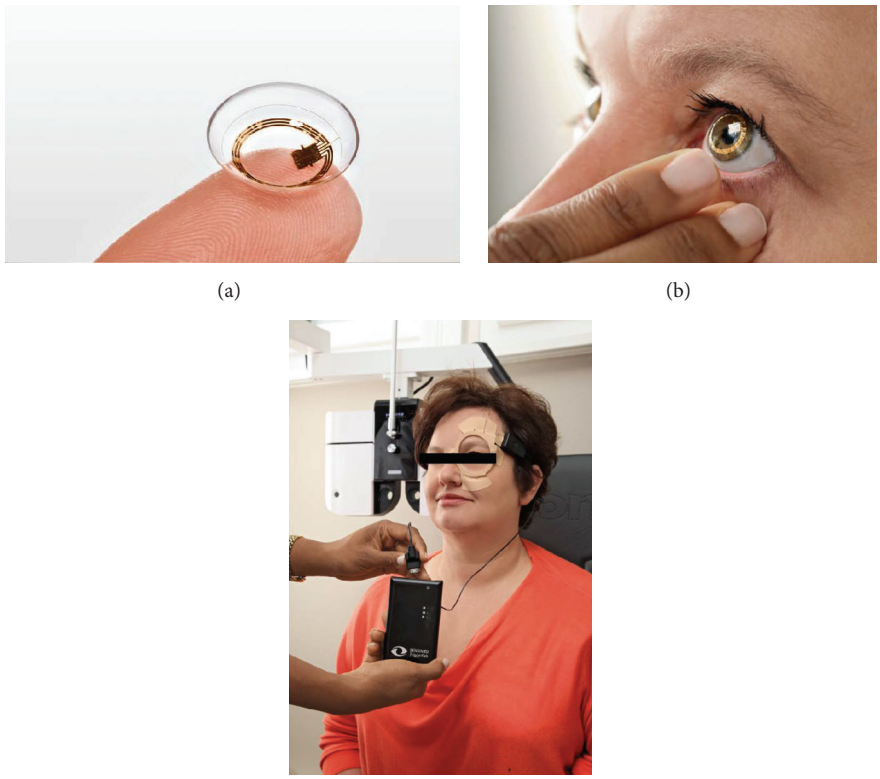

(a) (b) (c)

Figure 1: (a) SENSIMED Triggerfish contact lens sensor. (b) The contact lens sensor worn on the eye. (c) The device system consists of a wireless contact lens sensor, a periorbital antenna, data cable, and a recorder. Images are reproduced from SENSIMED Triggerfish with permission from the company.

with glaucoma, Mansouri et al. found that 82% of participants developed blurred vision, 80% conjunctival hyperemia, and 15% superficial punctate keratitis after CLS use [38].

The CLS has been found to be an accurate and reproducible method to characterize the nyctohemeral IOP rhythm. In a cross-sectional study of 12 young healthy volunteers, Mottet et al. found fair-to-good agreement (i.e., 95% confidence interval) between CLS measurements in separate recording sessions [32]. By comparing output from the CLS to output from a noncontact tonometry (Pulsair-Keeler) in the fellow eye, Mottet et al. showed that the CLS tended to overestimate the high IOP changes in comparison with the noncontact tonometry [32]. The authors postulated that the difference is likely a result of the higher frequency of data acquisition by the CLS, thus reducing the influence of outliers.

24-hour CLS use has been shown to cause overnight corneal swelling, particularly in the central and midperipheral zones. However, Freiberg et al. did not find a correlation between pre- and postcentral corneal thickness and CLS output difference. These data suggest continuous CLS output is not significantly affected by differences in corneal thickness that occurred during overnight CLS wear [41].

Furthermore, output from the CLS has been used to accurately identify sleep and wake periods. Gisler et al. derived an algorithm to process the output and was able to identify sleep periods with 95% accuracy [42]. The authors also quantified eye blinks using CLS output and validated the measurements with simultaneous video recording in a subset of the participants.

5. Clinical Applications

In glaucoma patients, output from the CLS has been used to predict the rate of visual field loss. In a prospective cross-sectional study, 34 treated, open-angle glaucoma patients with at least 8 recorded 24-2 Humphrey visual field tests over 2 years wore the CLS for 24 hours [43]. Based on visual field tests, the patients were divided into "fast progressors" and "slow progressors." Various CLS parameters were measured, including the number of large peaks (excludes smaller peak artifacts) and the mean peak ratio (a higher mean peak height to time-to-peak indicates quick spikes in mV equivalents). "Fast progressors" tended to be predicted by the number of long peaks and the mean peak ratio. This indicates that CLS may be used to identify patients more likely to advance quickly in their disease so they can be treated more aggressively. A summary of this and studies below is provided in Table 1.

Glaucoma patients may be at higher risk of eye damage during sleep, especially if they lie face down, which can increase pressure on the eye. CLS has been used to investigate

Table 1: Summary of studies using the CLS in the discovery of risk factors, characterization of circadian rhythm, and investigation of effects of IOP-lowering interventions.

Study	Study design	*n*	Mean age (yr)	Disease	Outcome measures	Main findings
De Moraes et al. [43]	Cross-sectional	34	66.8	Primary open-angle glaucoma	Rates of visual field change and CLS parameters	Number of long peaks and mean peak ratio were best predictors of faster progression
Flatau et al. [36]	Nonrandomized comparative trial	33	62.6	Glaucoma	Changes in limbal strain and sleeping head position	Limbal strain increased in glaucoma eyes with face down position, particularly those eyes with progressive visual field loss
Lee et al. [44]	Prospective cohort	18	65.1	Normal-tension glaucoma (NTG)	IOP-related pattern in nocturnal and diurnal periods	NTG patients have IOP-related pattern unique to diurnal/nocturnal period: greater diurnal variability and fewer nocturnal peaks
Tan et al. [45]	Nonrandomized comparative trial	25	69.1	Primary angle-closure glaucoma	Glaucoma progression and CLS parameters	Patients with progressive disease differ from stable patients in gradients of IOP fluctuation curve during specific time periods
Xu et al. [40]	Nonrandomized comparative trial	17	59	Ocular hypertension	Baseline clinical factors and CLS parameters	Poorer visual field mean deviation associated with steeper sleep to wake slopes; higher number of peaks associated with greater IOP fluctuations between office visits
Parekh et al. [46]	Prospective nonrandomized trial	10	61.8	Thyroid eye disease	Safety, tolerability, and IOP-related pattern	Well-tolerated and safe CLS; 50% of patients experience nocturnal acrophase with peak at 6:30 am
Mansouri et al. [37]	Randomized controlled trial	23	63.8	Primary open-angle glaucoma	Effect of different groups of medications	Bimatoprost uniquely decreased the IOP-related slope during the wake-to-sleep period
Pajic et al. [35]	Nonrandomized trial	5	62	Normal-tension Glaucoma	Effect of different groups of medications	Treatment with latanoprost, travoprost, and/or dorzolamide altered the IOP-related slope during the wake-to-sleep period
Lee et al. [47]	Prospective cohort	18	65.1	Normal-tension Glaucoma	Effect of SLT	Amplitude of CLS fitted curve was reduced by 24.6% in successful treatment group
Mansouri et al. [48]	Case report	1	59	Primary open-angle glaucoma	Effect of prostaglandin-pilocarpine	Prostaglandin-pilocarpine reduced nighttime IOP peaks and relieved patient's symptoms

this risk in a study of 22 glaucoma patients and 11 age-matched controls [36]. First, the Tono-Pen was used to help determine that the glaucoma and control subjects' baseline IOPs while sitting and lying were similar. Then, the participants wore the CLS for approximately 3 hours while alternating positions of sitting, lying supine, and lying face down. Subjects with glaucoma experienced a sustained increase in CLS values while lying face down, but control subjects did not. This rise was equivalent to a mean IOP increase of 2.5 mmHg. Future efforts may be directed at identifying which glaucoma patients are most susceptible to this increased strain and developing therapies to mitigate it.

CLS has also been used to monitor the IOP-related profile in normal-tension glaucoma patients, which may help elucidate why they experience visual field loss seemingly without elevations in IOP. In one study, 18 subjects wore the CLS for 24 hours and data were collected detailing variability from the mean and the number of peaks and troughs that occurred during the day and night [44]. It found that there was 48.9% less variability and 54.7% less peaks during the night compared to the day. This may be due to less eye and body movements at night. The study also discovered that going to sleep was associated with a higher rate of increase in the IOP-related pattern than the decrease in such pattern associated with waking up. The authors postulated that the difference in IOP-related pattern change may be due to IOP increase from postural change. Further research aided by CLS may eventually help optimize treatment timing for each patient based on his/her IOP-related pattern throughout the day.

In primary angle-closure glaucoma, CLS has been used to study how differences in IOP fluctuations are associated with rates of disease progression. Tan et al. had 25 patients with primary angle-closure glaucoma wear the CLS for 24 hours, while they went about their daily activities [45]. The patients were classified as having "progressive" or "stable" glaucoma by measuring mean deviation, visual field index, and retinal nerve fiber layer thickness changes every 6 months. Progressive patients as defined by a significant change in the mean deviation had significantly different gradients (1st derivative) of the IOP fluctuation curve during the hours of 10:00 pm to 11:00 pm and 7:00 am to 8:00 am compared to stable patients. They also had significant differences in the curvature (2nd derivative) of the IOP curve between the hours of 11:00 pm and 12:00 am, as well as 8:00 am and 9:00 am. Significant differences were found between progressive and stable patients using the visual field index and retinal nerve fiber layer thickness criteria during several other hours as well. Overall, the CLS helped illustrate that patients with progressive glaucoma experienced larger variations in IOP fluctuation than the stable group during bedtime and waking hours.

The use of CLS is not limited to glaucoma patients; it has also been used to study patients with ocular hypertension. CLS monitoring in 17 untreated ocular hypertension patients revealed that patients who had poorer visual field mean deviation had steeper sleep to wake slopes [40]. In addition, a higher number of peaks within the 24 hours of monitoring were associated with greater fluctuations in IOP between office visits. Similar to glaucoma patients, ocular hypertension patients with worse disease may be more easily identified by CLS IOP-related patterns.

CLS may also be used to help patients with thyroid eye disease. Grave's Disease often involves ocular manifestations such as proptosis and diplopia due to mucopolysaccharide and lymphocyte infiltrates into the extraocular muscles. These infiltrates apply pressure to the globe, which may increase IOP. Goldmann applanation tonometry may produce inaccurate IOP readings because of the increased force required to pull the eye against the fibrotic and constrained extraocular muscles [46]. However, CLS can provide a more accurate way to follow IOP in these patients, as long as it is safe and well tolerated. A prospective study of 10 patients with thyroid eye disease used the CLS to monitor ambulatory IOP in the patients' more proptotic eye for 24 hours [46]. The study found that CLS was very well tolerated, achieving a score of 1.5 ± 0.7 on a scale of 0 (no discomfort) to 10 (very severe discomfort). In addition, it was deemed safe, as the most frequent adverse effects were only mild blurred vision (50% of patients), mild hyperemia of the bulbar and palpebral conjunctiva (100% of patients), and superficial punctate keratitis (20% of patients), all of which resolved after CLS removal. Fifty percent of the patients experienced nocturnal acrophase, with the peak occurring at 6:30 am. The timing of acrophase differs from glaucoma patients, who typically experience a peak between 1:00 am and 3:00 am [33]. This indicates that patients with thyroid eye disease may have a unique circadian IOP rhythm compared to those with glaucoma.

6. Effect of Interventions during a 24-Hour Period

The CLS was used to study the circadian IOP-related effects of ocular hypotensive medications. Mansouri et al. found in a cohort of 23 patients with primary open-angle glaucoma that prostaglandin analogues uniquely flattened the IOP-related increase during the wake-to-sleep period [37]. All patients initially underwent a four-week wash-out and then were fitted with the CLS for baseline measurements. Patients were randomly assigned to use bimatoprost 0.01% nightly, brimonidine 0.1% twice daily, brinzolamide 1% twice daily, or timolol 0.25% nightly for 1 month prior to a second CLS fitting. Patients treated with bimatoprost had a significant decrease in the slope during wake-to-sleep period, something which other treatment groups did not experience. This finding adds to the growing literature that prostaglandin analogues alter the nocturnal IOP-related pattern. A case series involving five normal-tension glaucoma patients showed flattening of the nocturnal IOP increase in three of the patients after introduction of a mixed group of medications, including prostaglandin analogue eye drops [35]. Another case study reported the IOP-related pattern change after treatment with prostaglandin-pilocarpine combination [48]. The patient presented with ocular pain after ab interno trabeculotomy (Trabectome™) surgery. Through the use of CLS, a significantly lower, nocturnal IOP-related pattern was associated with patient's improvement in symptoms.

The 24-hour effect of selective laser trabeculoplasty (SLT) has been examined in patients with normal-tension glaucoma using the CLS. Eighteen patients were fitted with CLS before and 1 month after SLT. The IOP-related pattern amplitude was reduced in patients with a successful SLT treatment (>20% in IOP reduction by Goldmann applanation). In contrast, the amplitude increased in patients with nonsuccessful SLT treatment [47]. Higher diurnal, local IOP-related variability and flatter sleep-to-wake slope were observed after SLT in patients with nonsuccessful treatment. This CLS study revealed the association between SLT treatment success and amplitude of IOP-related patterns.

7. Advantages and Limitations

Recently, the Triggerfish has gained the U.S. Food and Drug Administration (FDA) approval for its CLS application. It is currently the only FDA-approved, nonimplantable device for continuous 24-hour IOP-related pattern measurements. The CLS is indicated to detect the peak patterns of variation in intraocular pressure over a maximum period of 24 hours to identify the window of time to measure intraocular pressure by conventional clinical methods [49]. In addition to helping determine the most critical time of day for clinicians to measure a patient's IOP, parameters calculated using CLS output enhance our understanding of medication effects and identify patients with higher risk of disease progression.

As summarized above, CLS is a revolutionary tool in ophthalmology, especially in the glaucoma field, but the current cost of the device can be an obstacle for its wide use. Although every glaucoma patient may benefit from CLS for disease management, this device will be most helpful to those with faster disease progression or those who are less responsive to IOP-lowering therapy by the current standard. For most patients, glaucoma is a slow, progressive optic nerve disease. However, some patients may show worrisome faster visual function loss than average patients, even if their IOP seems adequately reduced during office visits. The CLS recording may help identify the ocular patterns of these patients and provide guidance to administer medicine more precisely to suppress IOP outside office hours. This could completely control intraocular pressure in this group of patients and also decrease the chance of exposing them to more aggressive and/or more invasive therapy. Similarly, the CLS can help determine the effectiveness of an IOP-lowering medicine for a patient before switching or escalating therapy, especially for those patients with low pressure glaucoma. In addition, the application of CLS on ocular hypertensive patients may help identify those who are more likely to develop glaucoma. This can help many patients in this group avoid unnecessary therapy, as studies showed ocular hypertension might not lead to glaucoma in every patient [50]. Therefore, as an approach to deliver precision medicine, the CLS may potentially decrease the total cost of glaucoma management and treatment risks.

One major limitation of the CLS is that its output cannot be converted to millimeter mercury (mmHg) to allow for direct clinical interpretation. However, because the ocular pattern recorded by CLS is highly correlated to the IOP rhythm, the readings obtained from the CLS can be used to guide clinicians to determine the critical time for IOP measurement during the 24-hour period, as stated by FDA [48]. In addition, current studies indicate that the IOP-related CLS profile itself can be used as an ocular perimeter for individualized glaucoma management. More studies are needed to determine which biomechanical properties determine the CLS output and whether the output is associated with corneoscleral properties, such as corneal hysteresis.

8. Conclusions

Using the CLS, IOP-related parameters have been found to be associated with the rate of visual field progression in primary open-angle glaucoma, disease progression in primary angle-closure glaucoma, and various clinical variables in ocular hypertension. The CLS has been used to quantify blink rate and limbal strain and measure the circadian rhythm in a variety of disease states including normal-tension glaucoma and thyroid eye disease. The effects of various IOP-lowering interventions were also characterized using the CLS. CLS provides a unique, safe, and well-tolerated way to study IOP-related patterns in many conditions. With its recent clearance from the FDA, wider usage of CLS may lead to a change of current practice patterns in glaucoma. IOP-related patterns may help identify patients most at risk for disease progression and assist with the development of tailored treatments.

Competing Interests

The authors declare that there are no competing interests regarding the publication of this paper.

References

[1] R. Varma, M. Ying-Lai, B. A. Francis et al., "Prevalence of open-angle glaucoma and ocular hypertension in Latinos: the Los Angeles Latino Eye Study," *Ophthalmology*, vol. 111, no. 8, pp. 1439–1448, 2004.

[2] J. M. Tielsch, A. Sommer, J. Katz, R. M. Royall, H. A. Quigley, and J. Javitt, "Racial variations in the prevalence of primary open-angle glaucoma: the Baltimore eye survey," *Journal of the American Medical Association*, vol. 266, no. 3, pp. 369–374, 1991.

[3] M. Coffey, A. Reidy, R. Wormald, W. X. Xian, L. Wright, and P. Courtney, "Prevalence of glaucoma in the west of Ireland," *British Journal of Ophthalmology*, vol. 77, no. 1, pp. 17–21, 1993.

[4] R. Ramakrishnan, P. K. Nirmalan, R. Krishnadas et al., "Glaucoma in a rural population of Southern India: the aravind comprehensive eye survey," *Ophthalmology*, vol. 110, no. 8, pp. 1484–1490, 2003.

[5] R. R. Buhrmann, H. A. Quigley, Y. Barron, S. K. West, M. S. Oliva, and B. B. O. Mmbaga, "Prevalence of glaucoma in a rural east African population," *Investigative Ophthalmology and Visual Science*, vol. 41, no. 1, pp. 40–48, 2000.

[6] P. J. Foster, F. T. S. Oen, D. Machin et al., "The prevalence of glaucoma in chinese residents of singapore: a cross-sectional population survey of the tanjong pagar district," *Archives of Ophthalmology*, vol. 118, no. 8, pp. 1105–1111, 2000.

[7] H. A. Quigley, S. K. West, J. Rodriguez, B. Munoz, R. Klein, and R. Snyder, "The prevalence of glaucoma in a population-based study of Hispanic subjects: proyecto VER," *Archives of Ophthalmology*, vol. 119, no. 12, pp. 1819–1826, 2001.

[8] Y. B. Liang, D. S. Friedman, Q. Zhou et al., "Prevalence of primary open angle glaucoma in a rural adult chinese population: The Handan Eye Study," *Investigative Ophthalmology and Visual Science*, vol. 52, no. 11, pp. 8250–8257, 2011.

[9] L. Dandona, R. Dandona, P. Mandal et al., "Angle-closure glaucoma in an urban population in southern India: the andhra pradesh eye disease study," *Ophthalmology*, vol. 107, no. 9, pp. 1710–1716, 2000.

[10] H. Quigley and A. T. Broman, "The number of people with glaucoma worldwide in 2010 and 2020," *British Journal of Ophthalmology*, vol. 90, no. 3, pp. 262–267, 2006.

[11] K. Nouri-Mahdavi, D. Hoffman, A. L. Coleman et al., "Predictive factors for glaucomatous visual field progression in the

Advanced Glaucoma Intervention Study," *Ophthalmology*, vol. 111, no. 9, pp. 1627–1635, 2004.

[12] C. G. V. De Moraes, V. J. Juthani, J. M. Liebmann et al., "Risk factors for visual field progression in treated glaucoma," *Archives of Ophthalmology*, vol. 129, no. 5, pp. 562–568, 2011.

[13] H. Goldmann, "A new applanation tonometer," *Bulletins et Mémoires de la Société Française d'Ophtalmologie*, vol. 67, pp. 477–478, 1954.

[14] J. T. Holladay, M. E. Allison, and T. C. Prager, "Goldmann applanation tonometry in patients with regular corneal astigmatism," *American Journal of Ophthalmology*, vol. 96, no. 1, pp. 90–93, 1983.

[15] Y. M. Buys, T. Alasbali, Y.-P. Jin et al., "Effect of sleeping in a head-up position on intraocular pressure in patients with glaucoma," *Ophthalmology*, vol. 117, no. 7, pp. 1348–1351, 2010.

[16] H. H. Mark and T. L. Mark, "Corneal astigmatism in applanation tonometry," *Eye*, vol. 17, no. 5, pp. 617–618, 2003.

[17] S. Y.-W. Liang, G. A. Lee, and D. Shields, "Self-tonometry in glaucoma management—past, present and future," *Survey of Ophthalmology*, vol. 54, no. 4, pp. 450–462, 2009.

[18] B. Boles Carenini, B. Brogliatti, C. Tonetto, and E. Renis, "The Pulsair-Keeler non-contact tonometer in self-tonometry: preliminary results," *International Ophthalmology*, vol. 16, no. 4-5, pp. 295–297, 1992.

[19] R. Vogt and G. I. W. Duncker, "Usability of self-tonometry using 'Ocuton S®' for diurnal IOP profiles at home," *Klinische Monatsblätter für Augenheilkunde*, vol. 222, no. 10, pp. 814–821, 2005.

[20] I. Theofylaktopoulos, M. Diestelhorst, and G. K. Krieglstein, "Self-tonometry with the Ocuton S versus Goldmann tonometry," *Graefe's Archive for Clinical and Experimental Ophthalmology*, vol. 237, no. 9, pp. 720–724, 1999.

[21] M. Baskaran, K. K. Ramani, S. Ve Ramesh, R. George, and L. Vijaya, "Comparison of proview phosphene tonometer with the goldmann applanation tonometer in myopic and non-myopic eyes," *Asian Journal of Ophthalmology*, vol. 8, no. 2, pp. 57–61, 2006.

[22] T. L. Alvarez, S. A. Gollance, G. A. Thomas et al., "The Proview phosphene tonometer fails to measure ocular pressure accurately in clinical practice," *Ophthalmology*, vol. 111, no. 6, pp. 1077–1085, 2004.

[23] P. L. Dabasia, J. G. Lawrenson, and I. E. Murdoch, "Evaluation of a new rebound tonometer for self-measurement of intraocular pressure," *British Journal of Ophthalmology*, vol. 100, no. 8, pp. 1139–1143, 2016.

[24] P.-J. Chen, D. C. Rodger, M. S. Humayun, and Y.-C. Tai, "Unpowered spiral-tube parylene pressure sensor for intraocular pressure sensing," *Sensors and Actuators, A: Physical*, vol. 127, no. 2, pp. 276–282, 2006.

[25] P. Walter, U. Schnakenberg, G. Vom Bögel et al., "Development of a completely encapsulated intraocular pressure sensor," *Ophthalmic Research*, vol. 32, no. 6, pp. 278–284, 2000.

[26] C. C. Collins, "Miniature passive pressure transensor for implanting in the eye," *IEEE Transactions on Biomedical Engineering*, vol. 14, no. 2, pp. 74–83, 1967.

[27] K. Hille, J. Draeger, T. Eggers, and P. Stegmaier, "Construction, calibration and results of a new sensor in an intraocular lens with telemetric transmission of the intraocular pressure," *Klinische Monatsblätter für Augenheilkunde*, vol. 218, no. 5, pp. 376–380, 2001.

[28] M. Leonardi, P. Leuenberger, D. Bertrand, A. Bertsch, and P. Renaud, "First steps toward noninvasive intracular pressure monitoring with a sensing contact lens," *Investigative Ophthalmology and Visual Science*, vol. 45, no. 9, pp. 3113–3117, 2004.

[29] J. O. Hjortdal and P. K. Jensen, "In vitro measurement of corneal strain, thickness, and curvature using digital image processing," *Acta Ophthalmologica Scandinavica*, vol. 73, no. 1, pp. 5–11, 1995.

[30] A. K. C. Lam and W. A. Douthwaite, "The effect of an artificially elevated intraocular pressure on the central corneal curvature," *Ophthalmic and Physiological Optics*, vol. 17, no. 1, pp. 18–24, 1997.

[31] M. Leonardi, E. M. Pitchon, A. Bertsch, P. Renaud, and A. Mermoud, "Wireless contact lens sensor for intraocular pressure monitoring: assessment on enucleated pig eyes," *Acta Ophthalmologica*, vol. 87, no. 4, pp. 433–437, 2009.

[32] B. Mottet, F. Aptel, J.-P. Romanet, R. Hubanova, J.-L. Pépin, and C. Chiquet, "24-hour intraocular pressure rhythm in young healthy subjects evaluated with continuous monitoring using a contact lens sensor," *JAMA Ophthalmology*, vol. 131, no. 12, pp. 1507–1516, 2013.

[33] K. Mansouri, J. H. K. Liu, R. N. Weinreb, A. Tafreshi, and F. A. Medeiros, "Analysis of continuous 24-hour intraocular pressure patterns in glaucoma," *Investigative Ophthalmology and Visual Science*, vol. 53, no. 13, pp. 8050–8056, 2012.

[34] K. Mansouri, R. N. Weinreb, and J. H. K. Liu, "Efficacy of a contact lens sensor for monitoring 24-H intraocular pressure related patterns," *PLoS ONE*, vol. 10, no. 5, Article ID e0125530, 2015.

[35] B. Pajic, B. Pajic-Eggspuchler, and I. Haefliger, "Continuous IOP fluctuation recording in normal tension glaucoma patients," *Current Eye Research*, vol. 36, no. 12, pp. 1129–1138, 2011.

[36] A. Flatau, F. Solano, S. Idrees et al., "Measured changes in limbal strain during simulated sleep in face down position using an instrumented contact lens in healthy adults and adults with glaucoma," *JAMA Ophthalmology*, vol. 134, no. 4, pp. 375–382, 2016.

[37] K. Mansouri, F. A. Medeiros, and R. N. Weinreb, "Effect of glaucoma medications on 24-hour intraocular pressure-related patterns using a contact lens sensor," *Clinical and Experimental Ophthalmology*, vol. 43, no. 9, pp. 787–795, 2015.

[38] K. Mansouri, F. A. Medeiros, A. Tafreshi, and R. N. Weinreb, "Continuous 24-hour monitoring of intraocular pressure patterns with contact lens sensor: safety, tolerability, and reproducibility in patients with glaucoma," *Archives of Ophthalmology*, vol. 130, no. 12, pp. 1534–1539, 2012.

[39] K. Mansouri and T. Shaarawy, "Continuous intraocular pressure monitoring with a wireless ocular telemetry sensor: initial clinical experience in patients with open angle glaucoma," *British Journal of Ophthalmology*, vol. 95, no. 5, pp. 627–629, 2011.

[40] S. C. Xu, S. X. Wang, J. S. Maslin et al., "Twenty-four-hour ocular dimensional profiles correlate with early visual field defects and IOP fluctuations between office visits in ocular hypertensive patients," in *Proceedings of the American Academy of Ophthalmology Annual Meeting*, Las Vegas, Nev, USA, 2015.

[41] F. J. Freiberg, J. Lindell, L. A.-L. Thederan, S. Leippi, Y. Shen, and T. Klink, "Corneal thickness after overnight wear of an intraocular pressure fluctuation contact lens sensor," *Acta Ophthalmologica*, vol. 90, no. 7, pp. e534–e539, 2012.

[42] C. Gisler, A. Ridi, J. Hennebert, R. N. Weinreb, and K. Mansouri, "Automated detection and quantification of circadian eye blinks

using a contact lens sensor," *Translational Vision Science & Technology*, vol. 4, no. 1, article 4, 2015.

[43] C. G. De Moraes, J. V. Jasien, S. Simon-Zoula, J. M. Liebmann, and R. Ritch, "Visual field change and 24-hour IOP-related profile with a contact lens sensor in treated glaucoma patients," *Ophthalmology*, vol. 123, no. 1, pp. 744–753, 2016.

[44] J. W. Lee, L. Fu, J. W. Shum, J. C. Chan, and J. S. Lai, "Continuous 24-hour ocular dimensional profile recording in medically treated normal-tension glaucoma," *Journal of Clinical Ophthalmology*, vol. 29, no. 9, pp. 197–202, 2015.

[45] S. Tan, M. Yu, N. Baig, P. P. Chan, F. Y. Tang, and C. C. Tham, "Circadian intraocular pressure fluctuation and disease progression in primary angle closure glaucoma," *Investigative Ophthalmology & Visual Science*, vol. 56, no. 8, pp. 4994–5005, 2015.

[46] A. S. Parekh, K. Mansouri, R. N. Weinreb, A. Tafreshi, B. S. Korn, and D. O. Kikkawa, "Twenty-four-hour intraocular pressure patterns in patients with thyroid eye disease," *Clinical and Experimental Ophthalmology*, vol. 43, no. 2, pp. 108–114, 2015.

[47] J. W. Y. Lee, L. Fu, J. C. H. Chan, and J. S. M. Lai, "Twenty-four-hour intraocular pressure related changes following adjuvant selective laser trabeculoplasty for normal tension glaucoma," *Medicine*, vol. 93, no. 27, article e238, 2014.

[48] K. Mansouri, F. A. Medeiros, and R. N. Weinreb, "Twenty-four-hour intraocular pressure patterns in a symptomatic patient after ab interno trabeculotomy surgery," *Clinical Ophthalmology*, vol. 8, pp. 2195–2197, 2014.

[49] FDA permits marketing of device that senses optimal time to check patient's eye pressure, 2016, http://www.fda.gov/NewsEvents/Newsroom/PressAnnouncements/ucm489308.htm.

[50] M. A. Kass, D. K. Heuer, E. J. Higginbotham et al., "The Ocular Hypertension Treatment Study: a randomized trial determines that topical ocular hypotensive medication delays or prevents the onset of primary open-angle glaucoma," *Archives of Ophthalmology*, vol. 120, no. 6, pp. 701–713, 2002.

Hindawi Publishing Corporation
Journal of Ophthalmology
Volume 2016, Article ID 5072781, 7 pages
http://dx.doi.org/10.1155/2016/5072781

Research Article

Expression of TSLP and Downstream Molecules IL-4, IL-5, and IL-13 on the Eye Surface of Patients with Various Types of Allergic Conjunctivitis

Xiaofen Zheng, Juan Yao, and Bing Li

Department of Corneal Diseases, Shanxi Eye Hospital, Fu Dong Street No. 100, Xinghualing District, Taiyuan City, Shanxi Province, China

Correspondence should be addressed to Bing Li; libingeye@126.com

Received 12 March 2016; Accepted 17 June 2016

Academic Editor: George M. Saleh

Background. The pathogenesis of allergic conjunctivitis has not been clearly established. Moreover, previous studies fail to consider human models of allergic conjunctivitis. This study investigated the expression of thymic stromal lymphopoiet in TSLP and its downstream molecules in conjunctival scrappings and tear. *Methods.* This cross-sectional study compares patients with vernal keratoconjunctivitis (VKC), seasonal allergic conjunctivitis (SAC), and perennial allergic conjunctivitis (PAC) with normal controls. There are 80 people recorded in Shanxi Eye Hospital. Increasingly, 20 are with VKC, 20 are with SAC, 20 are with PAC, and the remaining 20 are normal controls. Conjunctiva were harvested for total RNA extraction and gene expression by real-time polymerase chain reaction. Epithelial cells were collected to make pathological sections for immunohistochemical staining. Human tears were evaluated by Luminex microbead assay. A P value less than 0.05 from Dunnett's post hoc test in SPSS means a statistical significant distinction. *Results.* Positive expression in conjunctival cells of patients with allergic conjunctivitis. The expression of TSLP and IL-4, IL-5, and IL-13 mRNA shows a statistically significant difference ($P < 0.05$). TSLP and IL-4, IL-5, and IL-13 concentrations show a statistically significant difference ($P < 0.01$). *Conclusions.* This study suggests that TSLP and downstream molecules are expressed in patients with various types of allergic conjunctivitis.

1. Introduction

Allergic conjunctivitis is one of the most common ocular surface diseases. In recent years, the incidence of allergic conjunctivitis showed an increasing trend with the damage of natural environment, increase in the regional haze, frequent use of poor-quality cosmetics, wearing contact lenses, and other factors [1]. The disease ranges in severity from mild forms, such as seasonal allergic conjunctivitis (SAC) and perennial allergic conjunctivitis (PAC) that can still interfere significantly with the quality of life, to severe cases, such as vernal keratoconjunctivitis (VKC) [2] and atopic keratoconjunctivitis [3] that may be complicated by corneal damage and may have the potential to cause permanent vision loss. Allergic conjunctivitis pathogenesis is very complex, but the mechanism is still not very clear. Little was known about the regulation of the development of Th2 type allergic inflammation locally at mucosal surfaces until studies identified a novel proallergic molecule, thymic stromal lymphopoietin (TSLP), a kind of interleukin 7-like cytokine, which can strongly activate dendritic cells through interaction with TSLP receptor (TSLPR) expressed by dendritic cells [4, 5], and then TSLP-treated dendritic cells express OX40 ligands (OX40L) that interact with OX40 to prime CD4+ T cells to produce proallergic cytokines IL-4, IL-13, and IL-5 to induce an inflammatory Th2 type response and initiate allergic inflammation [6–9]. In recent years, short ragweed pollen-triggered allergic conjunctivitis mouse models were excited and MyD88 knockout (MyD88−/−) ones were established. In the animal tests, scholars [10–13] confirmed that TLR4 was produced by conjunctival epithelium through TLR4-dependent innate immune pathways and then stimulated Th2 cell-mediated allergic inflammation of the ocular surface through TSLP-TSLPR and OX40L-OX40 signaling pathways. In regard to basic research aspects, although there are related studies using human corneal epithelial cells [13], they can

only simulate the pathological process of similar state close to the human body. For the human experiment of different severity, different stages of acute or chronic condition, and different types of patients with allergic conjunctivitis, further exploration is also needed. The present study sought to investigate the expression of TSLP and its downstream molecules IL-4, IL-13, and IL-5 in the conjunctival tissue of patients with allergic conjunctivitis and tear.

2. Material and Methods

2.1. Inclusion Criteria [14]

(1) Vernal Keratoconjunctivitis (VKC). It typically appears in boys between the ages of 4 and 12 years and disappears after puberty. Intense itching, tearing, and photophobia are the typical symptoms of VKC. Disease exacerbation can be triggered either by allergen reexposure or, more frequently, by nonspecific stimuli such as sunlight, wind, and dust. The tarsal form of VKC is characterized by irregularly sized hypertrophic papillae, leading to a cobblestone appearance of the upper tarsal plate. The limbal form Horner-Trantas dots and papillae are deposited at the limbus, which may appear thickened and opacified for 360°. Punctate keratitis, epithelial macroerosions, ulcers, and plaques are signs of corneal involvement and resolve with different levels of scarring.

(2) SAC. It is more prevalent from the spring to fall seasons when pollen levels are high. The hallmark symptom is intermittent itching; however, tearing, conjunctival redness, eyelid swelling, and small papillary hypertrophy of tarsal conjunctiva are common but are nonspecific signs. Signs and symptoms arise and subside depending on the patient's exposure to the offending allergen(s). An accurate medical history followed by allergy testing may identify the specific sensitization.

(3) PAC. It is present all year round due to allergens, such as dust mites, animal dander, and molds, or due to multiple sensitization instances. It is characterized by the same signs and symptoms as SAC; however, PAC is a chronic condition, with persistent, frequently mild symptoms, enhanced by higher or longer exposure to allergens and exacerbated by nonspecific irritating factors.

2.2. The Exclusion Criteria [15]. The exclusion criteria are as follows:

(1) Exclusion of people with a history of other keratoconjunctivitis in addition to allergic conjunctivitis.

(2) Eczema, atopic dermatitis, urticaria, systemic lupus erythematosus, rheumatoid arthritis, and other systemic allergic case histories.

(3) Tear and lacrimal duct diseases.

(4) Eye surgery and medication history.

(5) The history of wearing contact lens.

The cross-sectional study was conducted on all patients presenting to the clinic at the Shanxi Eye Hospital in China from May 2013 to August 2014. A total of 20 patients (40 eyes) were selected with vernal keratoconjunctivitis (VKC), as well as 20 patients (40 eyes) with SAC, 20 patients (40 eyes) with PAC, and 20 normal controls (40 eyes; these patients had no eye disease). The study was conducted in accordance with the provisions of the Declaration of Helsinki for research involving human subjects. The Ethical Review Committee of the Shanxi Ophthalmic Center approved the study (approval ID: 2013064), and written informed consent was obtained from all study participants.

2.3. Immunohistochemical Staining. After completing the examination of patients with allergic conjunctivitis and complex standard normal population, conjunctival scrapings were collected from conjunctival epithelial cells using immunohistochemical methods. Proparacaine hydrochloride eye drops (Alcon, Puurs, BE) were instilled in the ocular surface of the patients' eyes 1-2 times at intervals of 3 minutes. After the materials were scraped, they were immediately applied to the slides, naturally dried for 10 minutes, and then placed in 95% alcohol for 20 minutes to immersion fixation. Cell cultures were permeabilized with 0.2% Triton X-100 in phosphate-buffered saline at room temperature for 10 minutes. Indirect immunostaining was performed according to previously published methods [16–18] with primary rabbit antibodies against human TSLP, IL-4, IL-5, and IL-13 (all at 1 : 500; 1 Ug/mL) for the night at 4°C; primary antibody was applied and incubated for 1 hour at room temperature and for 30 minutes at room temperature, then dropping the goat anti-rabbit biotinylated second antibody (Poway, CA) for 30 minutes. The samples were incubated for 5 minutes with diaminobenzidine (DAB) to give a brown or red stain (optimized for each antibody) and were counterstained with Mayer's hematoxylin, as well as 100% and 95% gradient alcohol dehydration two times. The antibody dilution was used as control. Then, each group was examined and photographed with a microscope equipped with a digital camera (Eclipse E400 with a DS-Fi1, Nikon, NY, USA).

2.4. Total RNA Extraction, Reverse Transcription, and Quantitative Real-Time Polymerase Chain Reaction. Conjunctival epithelial cells were collected by impression cytology. Proparacaine hydrochloride eye drops (Alcon, Puurs, BE) were used for topical anesthesia. Sterile microforceps gripping disinfection trapezoid nitrocellulose membrane (Shanxi Medical University Laboratories, Taiyuan, CN) were lightly attached to the conjunctiva of the eye in patients with temporal side, top, and bottom for 10 s and then removed. The conjunctiva cells were obtained, and their epithelia were dissolved in the lysis buffer (Buffer RLT, RNeasy Kit, Qiagen, Valencia, CA) without homogenizing to prevent stromal cell contamination. Total RNA was extracted (RNeasy Micro or Mini Kit, Qiagen) according to the manufacturer's instructions, quantified by a spectrophotometer (NanoDrop ND-1000, Thermo Scientific, MA, USA), and stored at −80°C before use. First-strand cDNA was synthesized by M-MuLV

reverse transcription with random hexamers (Ready-To-Go You-Prime First-Strand Beads, GE Healthcare, NJ, USA), as previously described.

Real-time polymerase chain reaction (PCR) was performed with specific primers and probes (using TaqMan Gene Expression Assays and TaqMan Gene Expression Master Mix (Applied Biosystems, CA, USA) in a QPCR System (StepOnePlus, Stratagene, CA, USA)). IDs (TaqMan Gene Expression Assay IDs, Applied Biosystems) for human glyceraldehyde-3-phosphate dehydrogenase (GAPDH), TSLP, IL-4, IL-5, and IL-13 were hs99999905_m1, hs00263639_m1, Hs00174122_m1, Hs01548712_g1, and Hs00174379_m1, respectively. Results were analyzed by the comparative threshold cycle method [19, 20] and normalized by GAPDH, as previously reported [21, 22].

2.5. Luminex Detection Tear TSLP, IL-4, IL-5, and IL-13 Cytokine Levels. A total of 4 μL of conjunctival scrapings was collected from the patient's eye using a 1 μL capillary tube, which was quickly transferred into the Eppendorf tube containing 6 μL of 1% BSA solution and stored at −80°C. For using in the assay, the sample was thawed at room temperature and was added to the tear sample assay buffer in a 1 : 1 dilution; detection of cytokines was performed in strict accordance with the Luminex kit instructions.

2.6. Statistical Analysis. The statistical analysis was performed using SPSS for Windows 17.0 (SPSS Inc.). The relative expression and protein concentration values of TSLP, IL-4, IL-5, and IL-13 in the normal control, VKC, SAC, and PAC groups were normal as confirmed by the Kolmogorov-Smirnov test ($P > 0.05$) (results shown were the mean ± standard deviation [SD]). The one-way analysis of variance test was used to make comparisons among three or more groups, followed by Dunnett's post hoc test. P values <0.05 were considered statistically significant.

3. Results

3.1. Immunohistochemistry of TSLP, IL-4, IL-5, and IL-13. Immunohistochemical staining confirmed an increase in TSLP, IL-4, IL-5, and IL-13 production in the eyes with various types of allergic conjunctivitis. As shown in Figure 1, the conjunctival tissues of various types of allergic conjunctivitis displayed stronger TSLP, IL-4, IL-5, and IL-13 staining throughout the entire epithelium than did those of normal controls. These data indicated that TSLP, IL-4, IL-5, and IL-13 protein production by ocular surface epithelia increase in various types of allergic conjunctivitis, suggesting the possible involvement of TSLP, IL-4, IL-5, and IL-13 in allergic development.

3.2. mRNA Expression of TSLP, IL-4, IL-5, and IL-13 by Real-Time PCR. Significant differences were reported in the expression of TSLP, IL-4 mRNA, IL-5 mRNA, and IL-13 mRNA in the four groups of subjects ($F = 71.67, 51.32, 220.18$, and 162.49, $P < 0.001$). Compared with the control group, the VKC, SAC, and PAC groups had an increased expression of the ocular surface TSLP, IL-4 mRNA, IL-5 mRNA, and IL-13 mRNA; the differences were statistically significant ($P < 0.05$); the expression of TSLP, IL-4 mRNA, IL-5 mRNA, and IL-13 mRNA in the VKC group was significantly higher than in the SAC and PAC groups; the difference was statistically significant ($P < 0.05$). The expression of TSLP mRNA, IL-4 mRNA, IL-5 mRNA, and IL-13 mRNA in the SAC group was significantly higher than in the PAC group ($P < 0.05$). These results suggested that the expression of TSLP mRNA, IL-4 mRNA, IL-5 mRNA, and IL-13 mRNA increases in these three groups of allergic conjunctivitis, suggesting the possible involvement of TSLP, IL-4, IL-5, and IL-13 in allergic development (Figure 2).

3.3. Comparison of Protein Concentration Results of TSLP, IL-4, IL-5, and IL-13 in Tears. In the samples of the normal control group, the cytokines TSLP, IL-4, IL-5, and IL-13 were not detected; however, these cytokines were detected in all the samples in the VKC, SAC, and PAC groups (Table 1). Test results showed a significant difference in the tear TSLP, IL-4, IL-5, and IL-13 expression levels ($P < 0.001$) among the four groups. The tear TSLP, IL-4, IL-5, and IL-13 expression levels in different types of allergic conjunctivitis were found elevated to varying degrees in the VKC, SAC, and PAC compared with the control group; the differences were statistically significant ($P < 0.001$). TSLP, IL-4, IL-5, and IL-13 concentrations in the VKC group were significantly higher than in the SAC and PAC groups; the difference was statistically significant ($P < 0.001$). These concentrations were significantly higher in the SAC group than in the PAC group; the difference was statistically significant ($P < 0.001$).

4. Discussion

Allergic conjunctivitis is mainly mediated by lgE I-type hypersensitivity caused by a very common type of noninfectious ocular inflammatory disease. Its main symptoms are itching, often conjunctival hyperemia, edema, nipple eyelids, follicular hyperplasia, and other signs. It often causes significant eye discomfort, seriously affecting people's daily lives and work.

Classification of different types of allergic conjunctivitis has been controversial (Hannouche and Hoangxuan [23], etc.). According to the clinical manifestations, course, and prognosis differences, allergic conjunctivitis is divided into five types: SAC, PAC, VKC, giant papillary conjunctivitis, and atopic keratoconjunctivitis. Although the majority of allergic diseases are not serious ocular complications and the majority of patients can be clinically diagnosed and treated properly, there are still some patients that fail to be accurately diagnosed on time and hence do not get timely treatment. Long term use of antibiotics and other nontargeted drugs, side effects of drugs, and delayed diagnosis even cause irreversible visual impairment. Therefore, selected clinical trials are more common than the confusing three allergic conjunctivitis types: SAC, PAC, and VKC.

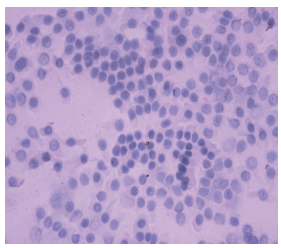

(a) No expression of TSLP in the normal control group

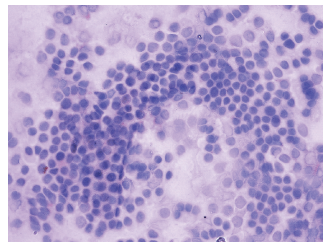

(b) No expression of IL-4 in the normal control group

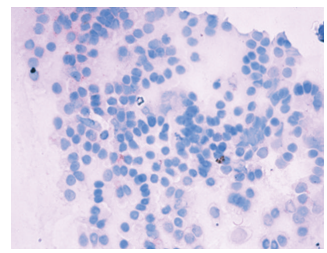

(c) No expression of IL-5 in the normal control group

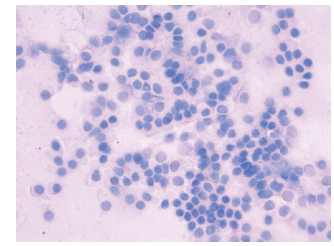

(d) No expression of IL-13 in the normal control group

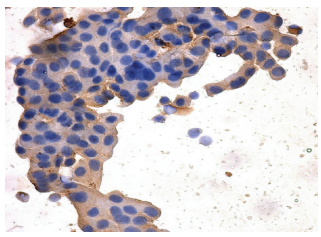

(e) Positive staining of TSLP in the VKC group

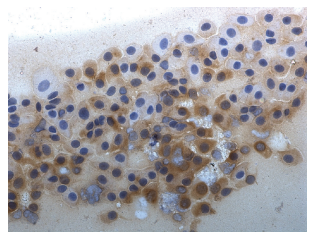

(f) Positive staining of IL-4 in the VKC group

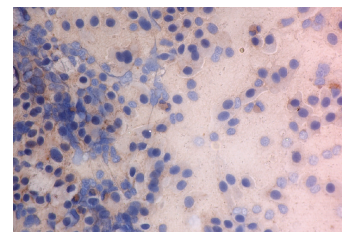

(g) Positive staining of IL-5 in the VKC group

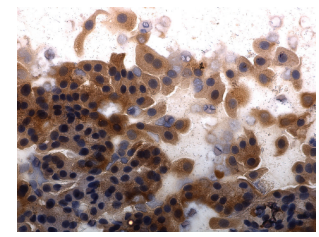

(h) Positive staining of IL-13 in the VKC group

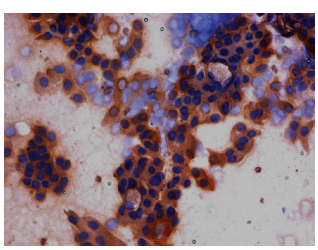

(i) Positive staining of TSLP in the SAC group

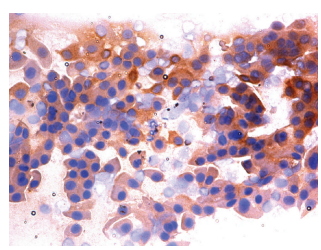

(j) Positive staining of IL-4 in the SAC group

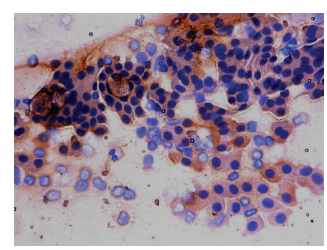

(k) Positive staining of IL-5 in the SAC group

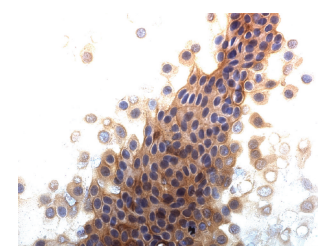

(l) Positive staining of IL-13 in the SAC group

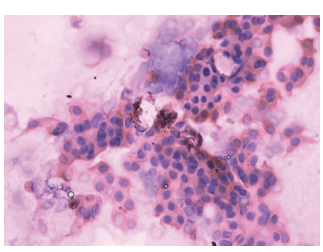

(m) Positive staining of TSLP in the PAC group

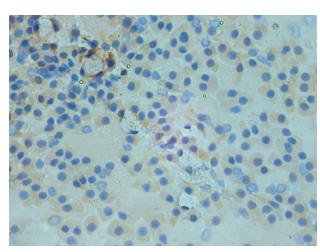

(n) Positive staining of IL-4 in the PAC group

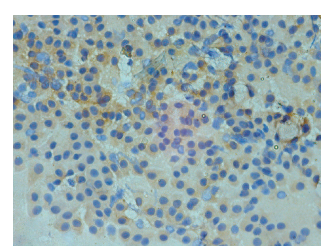

(o) Positive staining of IL-5 in the PAC group

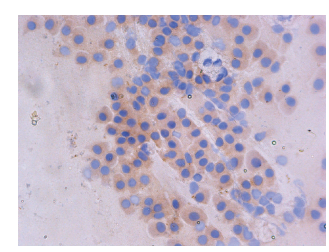

(p) Positive staining of IL-13 in the PAC group

Figure 1: Detection of TSLP, IL-4, IL-5, and IL-13 protein expression by immunohistochemistry (×400). ((a), (b), (c), (d)) No expression of TSLP, IL-4, IL-5, and IL-13 in the normal control group. ((e), (f), (g), (h)) Positive staining of TSLP, IL-4, IL-5, and IL-13 in the VKC group. ((i), (j), (k), (l)) Positive staining of TSLP, IL-4, IL-5, and IL-13 in the SAC group. ((m), (n), (o), (p)) Positive staining of TSLP, IL-4, IL-5, and IL-13 in the PAC group. Brown granules showed positive staining.

Immunohistochemistry, real-time PCR, and Luminex technology were used to measure the expression of TSLP, IL-4, IL-5, and IL-13 in the tears and conjunctival cell of the normal population and patients with three types of allergic conjunctivitis. Previous studies used enzyme-linked immunosorbent assay or flow cytometry to detect the concentrations of inflammation factors in tears. The Luminex chip technologies [24, 25] are integrated flow cytometry, laser technology, digital signal processing, and traditional chemical technology with the greatest features of high-throughput and high-flexibility. The study approved by Luminex detected TSLP and its downstream molecule concentrations in patients with three types of allergic conjunctivitis, but TSLP was not detected in the normal control group. The expression of four factors was significantly higher in patients with VKC than in patients with SAC and PAC. The expression of four factors was higher in patients with SAC than in patients with PAC. In this study, real-time PCR was used to detect the TaqMan probe method, which was highly specific and sensitive. TaqMan probe also detected that three types of allergic conjunctivitis conjunctival epithelial cells of patients had significantly increased TSLP and its downstream molecules

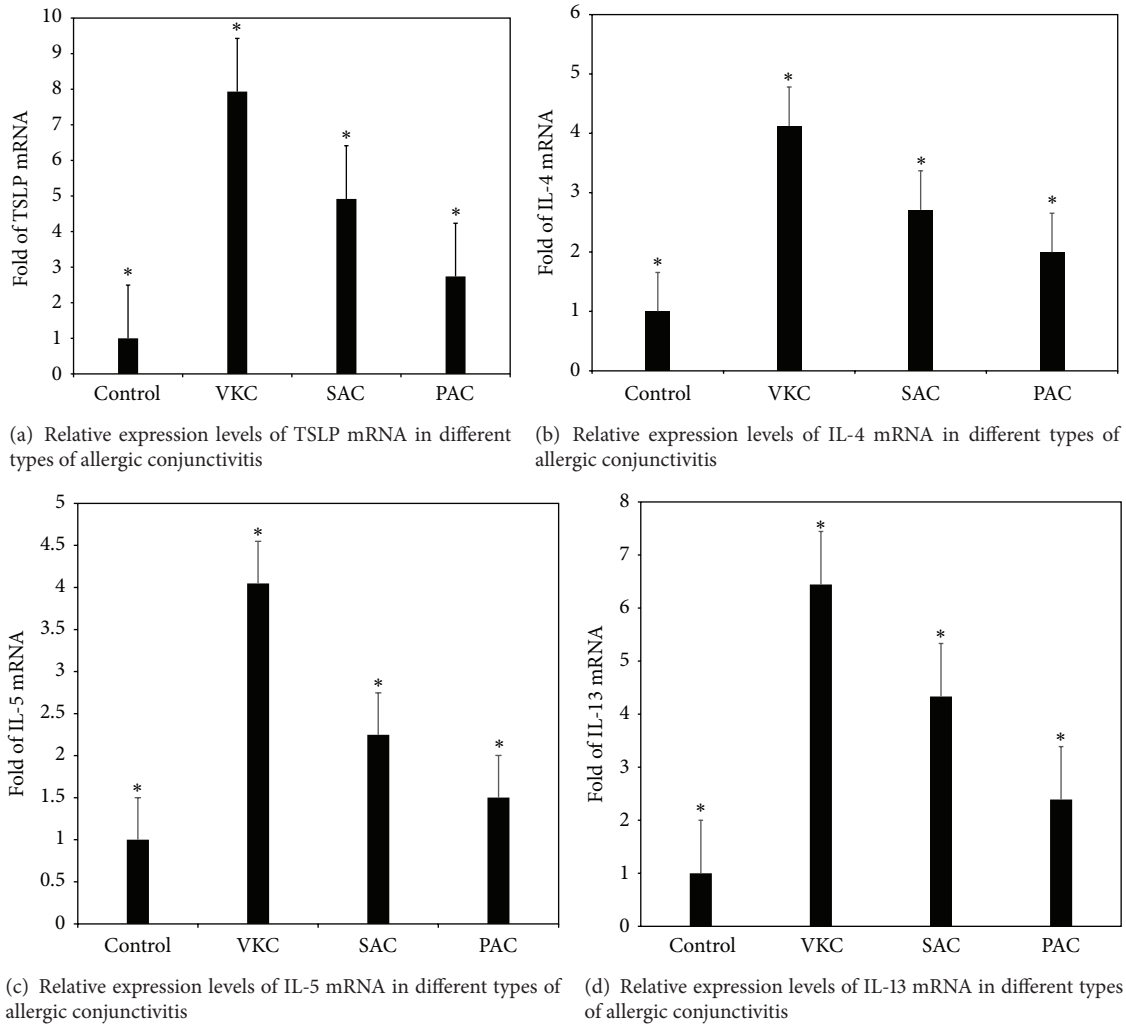

(a) Relative expression levels of TSLP mRNA in different types of allergic conjunctivitis

(b) Relative expression levels of IL-4 mRNA in different types of allergic conjunctivitis

(c) Relative expression levels of IL-5 mRNA in different types of allergic conjunctivitis

(d) Relative expression levels of IL-13 mRNA in different types of allergic conjunctivitis

Figure 2: Relative expression levels of TSLP mRNA, IL-4 mRNA, IL-5 mRNA, and IL-13 mRNA in different types of allergic conjunctivitis. TSLP mRNA, IL-4 mRNA, IL-5 mRNA, and IL-13 mRNA expression levels are presented as relative fold in various types of allergic conjunctivitis over the normal controls, which were evaluated by RT and real-time PCR using gene expression assay, with GAPDH as an internal control. Results shown are the mean ± SD. $^{*}P < 0.05$; each group $n = 20$.

compared with the normal population; the highest expression was observed in the VKC group and the lowest was observed in the PAC group, while the expression of TSLP and its downstream molecules was significantly higher in the VKC group than in the SAC and PAC groups, with the expression in the SAC group being higher than that in the PAC group. These results showed that, in allergic conjunctivitis, TSLP and its downstream molecules, as an important inflammatory factor, not only are involved in the pathogenesis of VKC, SAC, and PAC but also indicated that the expression level of these inflammatory factors was positively correlated with the severity of the disease. We found that TSLP in patients with VKC, whether from the mRNA expression or from protein expression, is significantly higher. Among the three types of conjunctivitis, signs and symptoms of VKC are the most severe ones, being more common in children and teenagers, with recurrent disease and delayed healing. Severe cases can damage the eyesight. The two types of allergic conjunctivitis are often associated with other histories of allergic diseases, such as allergic rhinitis, asthma, and atopic dermatitis. We found that, in patients with SAC and PAC, TSLP and its downstream molecules increased from mRNA levels and protein levels, but their expression was lower than that of VKC, which may be because the two types of allergic conjunctivitis are often associated with other histories of allergic diseases, such as allergic rhinitis, asthma, and atopic dermatitis, but the symptoms and signs of the patients were less than VKC. Our study also found that PAC was lower compared to SAC, which may be due to PAC in patients with mild clinical symptoms; PAC is characterized by mild symptoms, long duration of the disease, long term use of drugs, and other nontargeted drugs. Patients were less sensitive to drugs, so TSLP and downstream molecules IL-4, IL-5, and IL-13 levels were lower than those in SAC patients.

In short, although in the past animal models of allergic conjunctivitis were used, normal corneal epithelial cell

Table 1: Tear TSLP, IL-4, IL-5, and IL-13 cytokine concentrations in each group ($\overline{x} \pm s$, pg/mL).

Group	Sample size	TSLP	IL-4	IL-5	IL-13
Control group	20	0.00 ± 0.00	0.00 ± 0.00	0.00 ± 0.00	0.00 ± 0.00
VKC group	20	48.91 ± 7.45	14.06 ± 3.50	10.88 ± 1.82	34.28 ± 8.42
SAC group	20	24.63 ± 2.43	7.71 ± 0.65	5.10 ± 1.33	23.77 ± 6.29
PAC group	20	21.56 ± 2.72	3.30 ± 1.50	2.43 ± 1.28	17.67 ± 4.28
F		349.71	200.29	260.49	128.23
P		<0.001	<0.001	<0.001	<0.001

TSLP, IL-4, IL-5, and IL-13 concentrations in the control group were not detected, but these were detected in VKC, SAC, and PAC patient specimens. The results of the four different types of allergic conjunctivitis are shown as mean ± SD. The Luminex microbead assay confirmed that the patient groups had different degrees of the increase in concentration of the cytokines compared with the normal control group. $P < 0.001$; each group $n = 20$.
VKC: vernal keratoconjunctivitis; SAC: seasonal allergic conjunctivitis; PAC: perennial allergic conjunctivitis.

culture studies on the role and mechanisms of TSLP in the pathogenesis of allergic conjunctivitis played an irreplaceable role. However, these methods can simulate only the environmental conditions that are similar to human disease. The current study performed the human eye biopsy confirming directly the expression of TSLP and its downstream molecules in different types of patients with allergic conjunctivitis. This study provides clinical evidence for human ocular allergic diseases and provides a reference for conducting similar research work on ocular allergic diseases later. However, identifying the roles of TSLP and its downstream molecules in different types of allergic conjunctivitis needs more research.

Competing Interests

The authors declare that they have no actual or potential conflict of interests.

Authors' Contributions

Xiaofen Zheng and Juan Yao contributed equally to this work.

Acknowledgments

This research was supported by the Natural Science Foundation of Shanxi Province (2013011059-6) and the authors are very grateful for that support.

References

[1] Z. Liu, Y. Yao, and B. Sun, "The clinical characteristics of allergic conjunctivitis," *Chinese Journal of Practical Ophthalmology*, vol. 22, pp. 694–697, 2004.

[2] S. Bonini, M. Coassin, S. Aronni, and A. Lambiase, "Vernal keratoconjunctivitis," *Eye*, vol. 18, no. 4, pp. 345–351, 2004.

[3] S. Bonini, "Atopic keratoconjunctivitis," *Allergy*, vol. 59, no. 78, supplement, pp. 71–73, 2004.

[4] L. S. Park, U. Martin, K. Garka et al., "Cloning of the murine thymic stromal lymphopoietin (TSLP) receptor: formation of a functional heteromeric complex requires interleukin 7 receptor," *The Journal of Experimental Medicine*, vol. 192, no. 5, pp. 659–670, 2000.

[5] G. R. Melum, L. Farkas, C. Scheel et al., "A thymic stromal lymphopoietin-responsive dendritic cell subset mediates allergic responses in the upper airway mucosa," *The Journal of Allergy and Clinical Immunology*, vol. 134, no. 3, pp. 613–621.e7, 2014.

[6] Y.-J. Liu, "Thymic stromal lymphopoietin and OX40 ligand pathway in the initiation of dendritic cell-mediated allergic inflammation," *Journal of Allergy and Clinical Immunology*, vol. 120, no. 2, pp. 238–246, 2007.

[7] Y.-J. Liu, V. Soumelis, N. Watanabe et al., "TSLP: an epithelial cell cytokine that regulates t cell differentiation by conditioning dendritic cell maturation," *Annual Review of Immunology*, vol. 25, pp. 193–219, 2007.

[8] Y.-H. Wang and Y.-J. Liu, "OX40-OX40L interactions: a promising therapeutic target for allergic diseases?" *The Journal of Clinical Investigation*, vol. 117, no. 12, pp. 3655–3657, 2007.

[9] Y.-H. Wang, T. Ito, Y.-H. Wang et al., "Maintenance and polarization of human T_H2 central memory T cells by thymic stromal lymphopoietin-activated dendritic cells," *Immunity*, vol. 24, no. 6, pp. 827–838, 2006.

[10] P. Ma, F. Bian, Z. Wang et al., "Human corneal epithelium-derived thymic stromal lymphopoietin links the innate and adaptive immune responses via TLRs and Th2 cytokines," *Investigative Ophthalmology and Visual Science*, vol. 50, no. 6, pp. 2702–2709, 2009.

[11] X. Zheng, P. Ma, C. S. de Paiva et al., "TSLP and downstream molecules in experimental mouse allergic conjunctivitis," *Investigative Ophthalmology and Visual Science*, vol. 51, no. 6, pp. 3076–3082, 2010.

[12] D.-Q. Li, L. Zhang, S. C. Pflugfelder et al., "Short ragweed pollen triggers allergic inflammation through Toll-like receptor 4-dependent thymic stromal lymphopoietin/OX40 ligand/OX40 signaling pathways," *Journal of Allergy and Clinical Immunology*, vol. 128, no. 6, pp. 1318–1325, 2011.

[13] A. Matsuda, N. Ebihara, N. Yokoi et al., "Functional role of thymic stromal lymphopoietin in chronic allergic keratoconjunctivitis," *Investigative Ophthalmology & Visual Science*, vol. 51, no. 1, pp. 151–155, 2010.

[14] A. Leonardi, E. Bogacka, J. L. Fauquert et al., "Ocular allergy: recognizing and diagnosing hypersensitivity disorders of the ocular surface," *Allergy*, vol. 67, no. 11, pp. 1327–1337, 2012.

[15] S. Liu, *Introduction to Immunology*, People's Health Publishing Press, Beijing, China, 2003.

[16] M. Dinowitz, R. Rescigno, and L. Bielory, "Ocular allergic diseases: differential diagnosis, examination techniques, and testing," *Clinical Allergy and Immunology*, vol. 15, pp. 127–150, 2000.

[17] H.-S. Kim, X. J. Song, C. S. De Paiva, Z. Chen, S. C. Pflugfelder, and D.-Q. Li, "Phenotypic characterization of human corneal epithelial cells expanded ex vivo from limbal explant and single cell cultures," *Experimental Eye Research*, vol. 79, no. 1, pp. 41–49, 2004.

[18] D.-Q. Li and S. C. G. Tseng, "Three patterns of cytokine expression potentially involved in epithelial-fibroblast interactions of human ocular surface," *Journal of Cellular Physiology*, vol. 163, no. 1, pp. 61–79, 1995.

[19] Z. Chen, C. S. De Paiva, L. Luo, F. L. Kretzer, S. C. Pflugfelder, and D.-Q. Li, "Characterization of putative stem cell phenotype in human limbal epithelia," *Stem Cells*, vol. 22, no. 3, pp. 355–366, 2004.

[20] B. Lowe, H. A. Avila, F. R. Bloom, M. Gleeson, and W. Kusser, "Quantitation of gene expression in neural precursors by reverse-transcription polymerase chain reaction using self-quenched, fluorogenic primers," *Analytical Biochemistry*, vol. 315, no. 1, pp. 95–105, 2003.

[21] K.-C. Yoon, C. S. De Paiva, H. Qi et al., "Expression of Th-1 chemokines and chemokine receptors on the ocular surface of C57BL/6 mice: effects of desiccating stress," *Investigative Ophthalmology and Visual Science*, vol. 48, no. 6, pp. 2561–2569, 2007.

[22] C. S. De Paiva, R. M. Corrales, A. L. Villarreal et al., "Corticosteroid and doxycycline suppress MMP-9 and inflammatory cytokine expression, MAPK activation in the corneal epithelium in experimental dry eye," *Experimental Eye Research*, vol. 83, no. 3, pp. 526–535, 2006.

[23] D. Hannouche and T. Hoangxuan, *Inflammatory Diseases of the Conjunctiva*, Srettgart, New York, NY, USA, 2001.

[24] S. A. Dunbar, C. A. Vander Zee, K. G. Oliver, K. L. Karem, and J. W. Jacobson, "Quantitative, multiplexed detection of bacterial pathogens: DNA and protein applications of the Luminex LabMAP™ system," *Journal of Microbiological Methods*, vol. 53, no. 2, pp. 245–252, 2003.

[25] A. Inic-Kanada, A. Nussbaumer, J. Montanaro et al., "Comparison of ophthalmic sponges and extraction buffers for quantifying cytokine profiles in tears using luminex technology," *Molecular Vision*, vol. 18, pp. 2717–2725, 2012.

Hindawi Publishing Corporation
Journal of Ophthalmology
Volume 2016, Article ID 5608250, 8 pages
http://dx.doi.org/10.1155/2016/5608250

Clinical Study

The Application of OCTA in Assessment of Anti-VEGF Therapy for Idiopathic Choroidal Neovascularization

Qin Chen,[1,2] Xiaobing Yu,[2] Zihan Sun,[2] and Hong Dai[2]

[1] *The Fifth School of Clinical Medicine, Peking University, Beijing 100730, China*
[2] *Department of Ophthalmology, Beijing Hospital, Beijing 100730, China*

Correspondence should be addressed to Xiaobing Yu; yuxiaobing@sina.com

Received 24 March 2016; Accepted 9 May 2016

Academic Editor: George M. Saleh

Purpose. To assess the morphology of idiopathic choroidal neovascularization (ICNV) by optical coherence tomography angiography (OCTA) and determine the therapeutic effects of intravitreal antivascular endothelial growth factor (anti-VEGF). *Method*. Patients with naive ICNV were assessed by spectral domain optical coherence tomography (SD-OCT) and OCTA in this observational study. The timing of observation was before treatment, 1 day after treatment with intravitreal anti-VEGF injection, and 1 month after the treatment. The central retina thickness (CRT) on SD-OCT, selected CNV area, and flow area on OCTA were measured. *Results*. A total of 17 eyes from 17 patients with ICNV were included in this study. OCTA showed visible irregular choroidal neovascularization with "tree-in-bud" form on outer retinal layer. After treatment, as well as in the 1-day follow-up, CNV decreased in size from the periphery, and the vessel density was reduced. As shown on OCTA, the selected CNV area and flow area were significantly reduced compared to pretreatment. The rate of CNV vessel area changes was higher on OCTA than the changes in CRT on SD-OCT at 1-day and 1-month follow-up. *Conclusion*. Intravitreal injection of anti-VEGF is effective for idiopathic choroidal neovascularization, and the treatment outcomes are observable after 1 day. OCTA provides a useful approach for monitoring and evaluating the treatment of intravitreal anti-VEGF for CNV.

1. Introduction

Idiopathic choroidal neovascularization (ICNV) occurs without clear causes in patients younger than 50 years. It is distinct from CNV secondary, pathological myopia, angioid streaks, multifocal choroiditis, punctate inner choroidopathy, presumed ocular histoplasmosis syndrome, and trauma [1, 2]. Choroidal neovascularization (CNV) causes exudation, hemorrhage, and fibrosis at the macula resulting in poor central vision and visual loss.

The pathological basis of ICNV is similar to age-related macular degeneration (AMD). Because vascular endothelial growth factor (VEGF) is part of the pathophysiology of CNV [3], anti-VEGF therapy has become the first-line treatment for ICNV patients [4]. Intravitreal injection of bevacizumab and ranibizumab improves and stabilizes the vision of patient with ICNV [1, 5, 6].

Optical coherence tomography angiography (OCTA) is a new, noninvasive imaging technique that plays an important role in clinical practice [7, 8]. Like ordinary optical coherence tomography (OCT), OCTA provides B-scans of the retina, but OCTA additionally offers rapid, high-resolution, repeated, and accurate visualization of blood flow without injection of a contrast agent, which provides indirect representation of the vascular morphology of the retina and choroid [9].

OCTA has been shown to be effective in the detection of CNV [7, 10]. Lumbroso et al. and Muakkassa et al. used OCTA to detect changes in CNV after anti-VEGF treatment [11, 12]. Furthermore, with recent developments in equipment and software, OCTA can now measure the size of CNV, so that it can be compared before and after anti-VEGF treatment.

Usually, fundus fluorescein angiography (FFA) and OCT are used to evaluate ICNV before and after treatment [6]. No systematic study has been performed on the assessment of ICNV by OCTA. The purpose of our study is to use OCTA to assess the changes in CNV morphology after intravitreal anti-VEGF therapy and compare the results to OCT images.

2. Materials and Methods

2.1. Subjects. This prospective study was arranged according to the Declaration of Helsinki and approved by the institutional review committee of Beijing Hospital. Informed consent was obtained from all patients. A total of 17 patients of Beijing Hospital with naïve ICNV from May 2015 to January 2016 were included in this study. The diagnosis of ICNV was established in each subject by clinical examination, spectral domain optical coherence tomography (SD-OCT) (RTVue XR AVANTI, Optovue Inc., Fremont, CA) with FFA, and indocyanine green angiography (ICGA) (HRA II, Heidelberg, Germany) when available. Every patient agreed to receive treatment of intravitreal ranibizumab (Lucentis). Every patient was examined three times by SD-OCT and OCTA: the first time was up to three days before treatment, and then the patient was followed 1 day after treatment and 1 month after treatment. To evaluate subretinal and intraretinal fluid, the central retinal thickness (CRT) was measured automatically by SD-OCT.

Exclusion criteria were previous therapy (laser, photodynamic therapy, or anti-VEGF), age-related macular degeneration, myopia, history of trauma, choroiditis, and any other cause of secondary CNV. Eyes that could not be imaged clearly by OCTA and eyes that could not be imaged serially were excluded.

2.2. Optical Coherence Tomography Angiography. OCTA images were obtained with an AngioVue OCTA device (RTVue XR AVANTI, Optovue, Fremont, CA, USA). AngioVue uses a split-spectrum amplitude-decorrelation algorithm to detect erythrocyte movement [9]. The macular angiography scan protocol covered a 3 mm × 3 mm area at 840 nm wavelength and 70,000 A-scans per second. The device produced 2 OCT volumes, each consisting of 304 × 304 A-scans with 2 B-scans captured in around 3 seconds. OCTA volumes of the outer retina were automatically segmented by AngioVue software between the Bruch membrane and the inner nuclear layer/outer plexiform layer junction. This region is devoid of blood vessels, so CNV-related abnormal blood flow signals are easy to distinguish. Using AngioAnalytics software, the CNV areas on the outer retina were manually selected by two independent qualified technicians. The selected CNV area values were the data according to the CNV size we chose, and the flow area value was automatically measured as just the detected flow signals within the selected area of CNV.

2.3. Statistics. Statistical evaluation was performed using SPSS software (IBM SPSS Statistic 22). All results, including age, gender, best correct visual acuity (BCVA), CRT, selected CNV area, and detected vessels area, were expressed as the mean ± standard deviations. The comparative t-test was used to compare CNV changes before and after treatment. To compare lesion changes seen on OCTA with those seen on OCT, the independent-samples t-test was used. In all analyses, $P < 0.05$ was considered to be statistically significant.

3. Results

This study observed 14 eyes of 14 female patients and 3 eyes of 3 male patients. The mean age of subjects was 34.24 ± 5.68 years. The mean baseline best corrected visual acuity (BCVA) was 59.29 ± 14.80 early treatment diabetic retinopathy study (ETDRS) letters.

All eyes had pure type 2 choroidal neovascular membranes based on SD-OCT, which showed a highly reflective region that exceeded the retinal pigment epithelium (RPE). Subretinal fluid accumulation around the lesions was seen in 11 eyes and 5 eyes had intraretinal fluid. OCTA presented an irregular or nearly round closed mass at the level of the outer retinal layer in all patients, with convoluted and intertwined vessels. 13 of all had irregular blood flow like small "tree-in-bud" inside lesions (Figure 1(a)). "Tree-in-bud" was defined as a short and discontinuous linearly branching flow signal. OCTA showed that highlighted peripheral flow signals connected to form a continuous line or ring around the vessel mass in 8 eyes (Figure 1(b)). Two eyes had "medusa-shaped" lesions (Figure 1(c)), which were defined as a compact zone of small new blood vessels with minimal internal hypodense structure. One eye had an obvious net of dendritic branch vessels, which branched from the trunk (Figure 1(d)).

All 17 eyes were treated with intravitreal ranibizumab. Follow-up images were obtained 1 day and 1 month after treatment. After 1 day, OCTA showed lesion shrinkage from peripheral vessels in 16 eyes and reduction in the number and density of vessels. Small vessels narrowed and fragmented. In some case, peripheral blood flow decreased and became filamentous. The average selected CNV area and flow area were significantly smaller than those before treatment ($t = 4.559$, $P < 0.01$; $t = 5.775$, $P < 0.01$). However, intraretinal and subretinal fluid as imaged by SD-OCT did not change or showed only a small amount of reduction. One month later, the mean BCVA for all patients increased by 7 letters to 66.11±10.86 ETDRS letters ($t = -1.533$, $P = 0.135$). SD-OCT showed reduction of retinal fluid. On the OCT angiogram, 14 of 17 eyes showed a continued decrease of visible vessels and CNV area size and in 1 eye the CNV had completely disappeared (Figure 2(1a–1c)). The vessel reduced with pruning of thinner peripheral flow. The network density decreased, but some vessels with large diameters were still retained. The selected CNV area and flow area became smaller than those before treatment ($t = 4.182$, $P < 0.01$; $t = 4.249$, $P < 0.01$) and were smaller than 1 day after treatment ($t = 3.591$, $P < 0.01$; $t = 2.823$, $P < 0.05$), and the difference was statistically significant (Table 1). However, in 3 eyes, OCTA showed that the flow area increased, comparing to 1-day follow-up. The small vessels inside the previous lesion and some peripheral vessels reappeared (Figure 2(2a–2c)).

During every visit, CRT on SD-OCT was also measured. The selected CNV area and flow area were reduced by 21.65% and 29.41%, respectively, compared to a 3.29% decrease in CRT 1 day after treatment. This was a larger, significant difference ($t = 5.651$, $P < 0.01$; $t = 7.732$, $P < 0.01$). Although there were signs of recurrence in 3 patients with CNV at the 1-month visit, on average, there was a 51.65% decrease in the selected CNV areas and a 49.00% decrease in the flow areas,

Table 1: Comparison of pretreatment and posttreatment measurements of ICNV.

	Pretreatment	1-day posttreatment	1-month posttreatment		t			P value	
BCVA letter (n)	59.29 ± 14.80	—	66.11 ± 10.86		−1.533***			0.135***	
Selected CNV area (mm^2)	0.41 ± 0.43	0.33 ± 0.38	0.19 ± 0.25	4.559*	3.591**	4.182***	<0.01*	<0.01**	<0.01***
Flow area (mm^2)	0.19 ± 0.19	0.14 ± 0.17	0.09 ± 0.11	5.775*	2.832**	4.249***	<0.01*	<0.05**	<0.01***

BCVA, best corrected visual acuity; CNV, choroidal neovascularization; *Comparing pretreatment to 1-day posttreatment measurements; **Comparing 1-day to 1-month posttreatment measurements; ***Comparing pretreatment to 1-month posttreatment measurements.

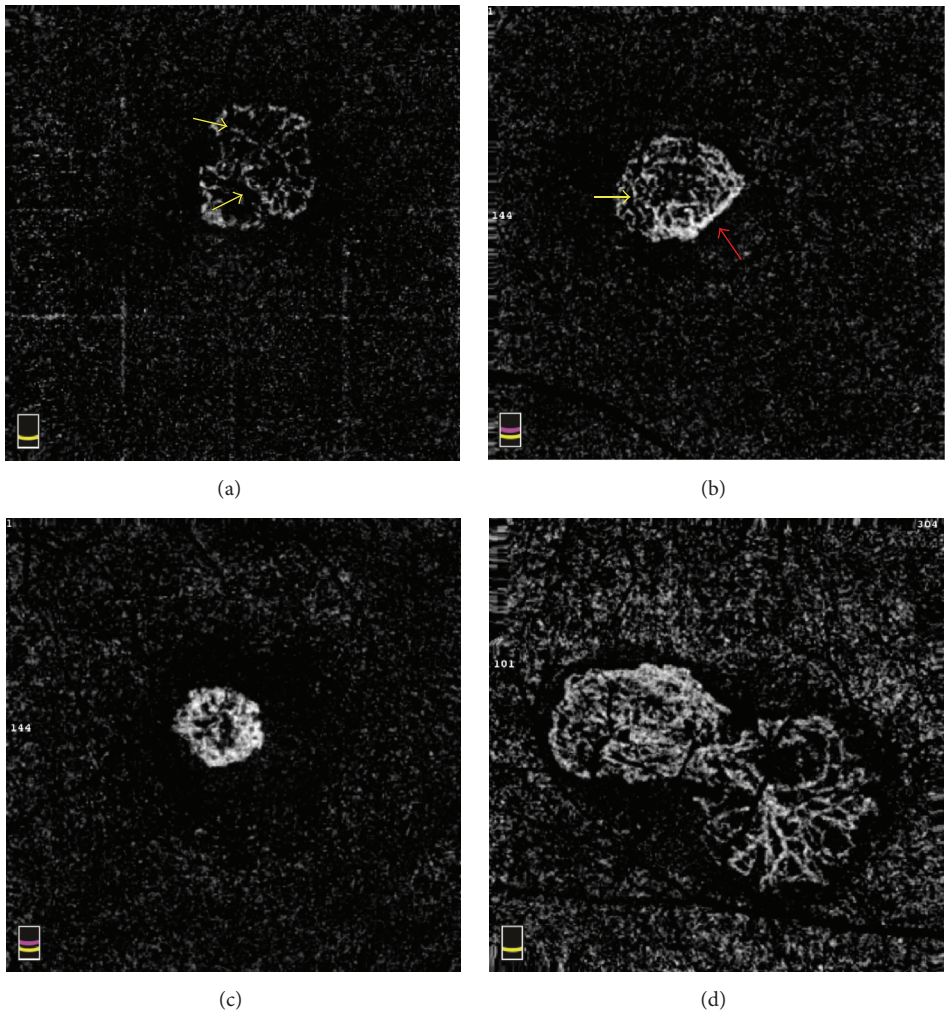

Figure 1: CNV structure of outer retinal layer on OCTA. (a) Irregular circumscribed CNV lesion with abnormal "tree-in-bud" blood flow inside (yellow arrows). (b) A round-like closed CNV with continuous linear peripheral flow (red arrow). (c) An irregular CNV as "medusa-shaped." (d) The CNV had obvious dendritic branch vessels net from the trunk.

which was significantly larger than the 20.88% decrease in CRT ($t = 4.256$, $P < 0.01$; $t = 3.674$, $P < 0.01$) (Figure 3).

One eye showed opposing results with OCTA versus OCT. OCTA indicated that the patient's CNV area was continuously increased after intravitreal treatment at the 1-day and 1-month follow-ups. BCVA was also reduced by 18 EDTRS letters. However, the subretinal fluid seemed to be absorbed and CRT dropped from 367 μm to 287 μm (Figure 4).

4. Discussion

Currently, in clinical situations, FFA and ICGA are the golden standards for detecting CNV [13, 14]. Both methods are invasive examinations that require injections and can cause nausea, vomiting, and, rarely, anaphylaxis. In contrast, OCTA is noninvasive and does not require dye injection. OCTA is a new technology that has provided layered angiograms of retinal and choroidal blood vessels. An OCTA-enabled method is called split-spectrum amplitude-decorrelation angiography (SSADA), which detects motion in the blood vessel lumen by measuring the variation in reflected OCT signal amplitude between consecutive cross-sectional scans. Moreover, OCTA is sensitive to observing the size and shape of CNV without obscured details due to dye leakage, as occurs with FFA and ICGA.

In ICNV patients, OCTA showed the CNV structures to be varied, mostly irregular, or nearly round closed masses with internal arborescent capillaries. This confirms some reports that OCTA visualized CNV as irregular, closely knit flow formations at the level of the outer retinal layer [15, 16]. Most abnormal vessels of ICNV had "tree-in-bud" blood flow. We hypothesized that CNVs of ICNV are composed of many tightly coiled blood vessels, where the blood flowing through multiple turns or knotted parts is likely to form turbulence. However, OCT-A measures only the linear blood flow [9]. Turbulent motion could present as a dark area, which impeded the conversion and representation of this flow on

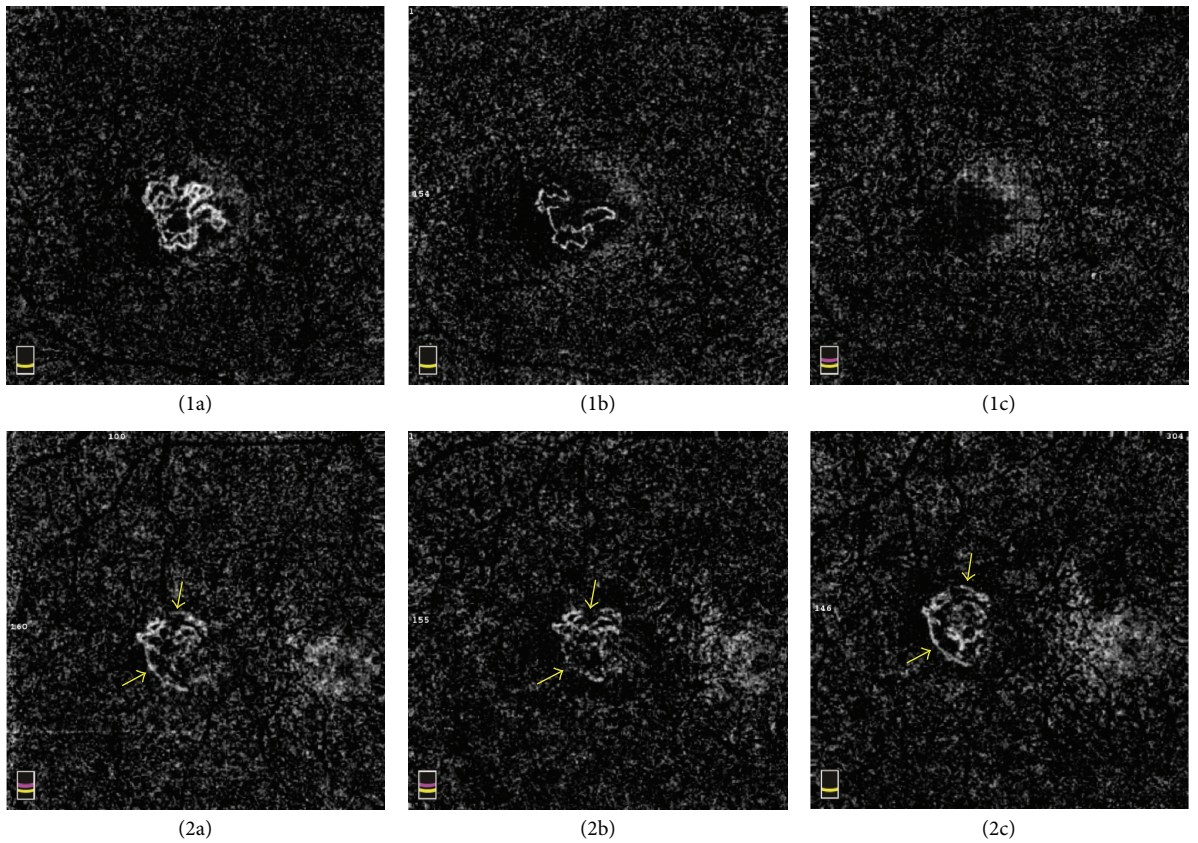

Figure 2: Changes of CNV after intravitreal anti-VEGF treatment of 2 patients 1-2: 3 × 3 OCTA images of each subject. ((a)–(c)) CNVs form before treatment, 1 day after treatment, and 1 month after treatment on OCTA. ((1a)-(1b)) Visible shrinkage of lesion from peripheral vessels and reduction in number and density of vessels at 1 day after treatment. (1c) After 1 month, no detected CNV flow. ((2a)–(2c)) The CNV changes of one female patient whose small abnormal vessels reappeared in previous lesion 1 month after treatment comparing to 1 day (yellow arrows).

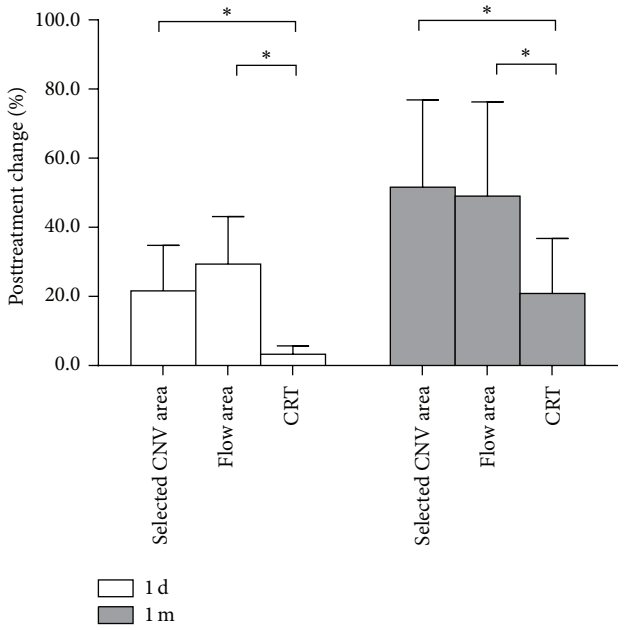

Figure 3: Comparison of 1-day and 1-month posttreatment changes on selected CNV area, flow area, and CRT. * P value < 0.01.

a hyperdense frame. That may be why there were short and discontinuous linear branching flow signals.

The "tree-in-bud" structure is different from the large central trunk-like or "sea fan" vessels in AMD [17–19]. In this study, about 11% of the eyes (2/17) had "medusa-shaped" lesions, and the rate of this structure was lower than those in AMD patients [20]. Previous trials proved that ICNV was treated more effectively by anti-VEGF drugs than AMD, because the former needed fewer injections and gained better vision [6, 21]. Although the size of the lesion and duration of disease were related to treatment effects, we speculate that different neovascular morphology, such as "tree-in-bud" in ICNV and other structures in AMD, will cause different outcomes and prognosis after anti-VEGF therapy.

Some eyes were found to have highlighted peripheral blood flow around the CNV membrane. It was indicated that these lesions might have an anastomotic vessel bounding the outer border of the vascular lesions, which have played an important role in the pathophysiology of CNV [18]. After the treatment, CNV in most eyes continued to shrink and microvascular flow was rarefaction, although large internal vessels persisted, which was mentioned in another study [17]. This implies that anti-VEGF treatment is more effective in

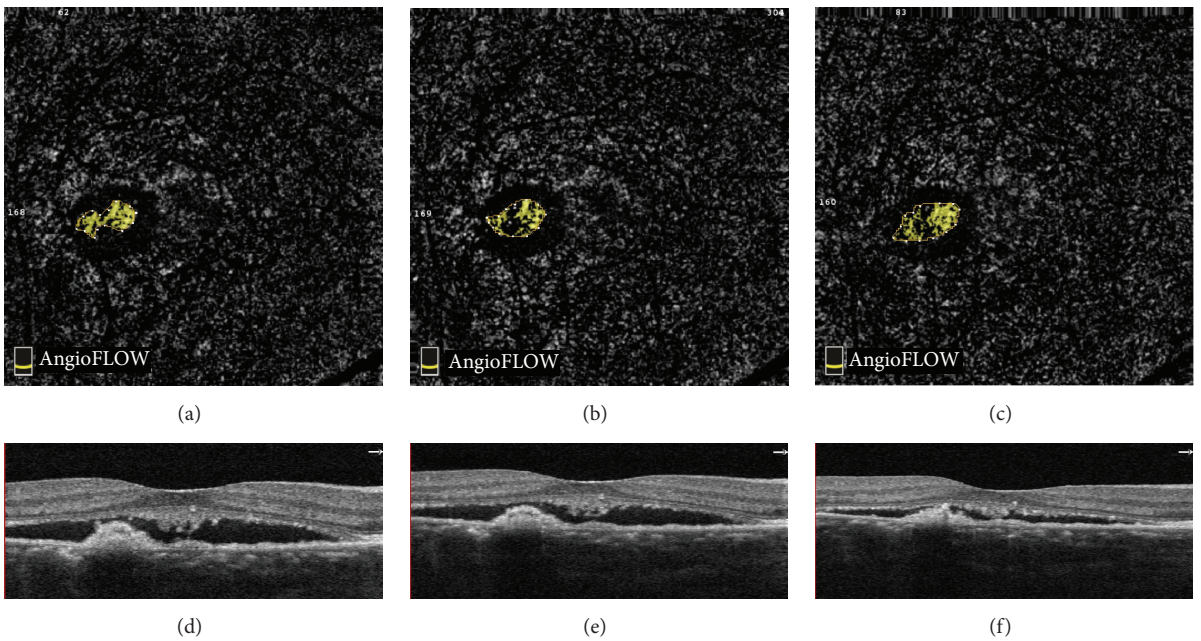

Figure 4: OCTA images with associated B-cans of a female patient. ((a)–(c)) CNVs form before treatment, 1 day after treatment, and 1 month after treatment on OCTA. The selected CNV areas were 0.089 mm^2, 0.097 mm^2, and 0.116 mm^2. The flow areas were 0.048 mm^2, 0.045 mm^2, and 0.060 mm^2. ((d)–(f)) B-scans of 3 detections. The CRT was 367 μm, 354 μm, and 287 μm. The subretinal fluids were decreased continuously.

causing the vanishing of small vessels than large, mature vessels. The sensitivity of smaller capillaries to anti-VEGF therapy may be associated with the mechanism of VEGF in angiogenesis [22, 23]. We believed that the decrease of vessels density was mainly due to the loss of smaller capillaries [24], which were not visible because of collapse or very slow flow. For 3 of 17 eyes in this study, the OCTA images showed that small internal vessels reappeared 1 month after treatment, and CNV flow areas increased compared to the 1-day posttreatment exam. This suggested that the patients should be treated once again. Since OCTA can be repeated often while FFA or ICGA should not be, OCTA can be a better way to monitor CNV development after anti-VEGF treatment. In the future, more research with OCTA is needed to find the timing for retreatment on OCTA.

Currently, SD-OCT is used regularly in evaluating clinical effect of anti-VEGF treatment in patients with CNV. OCT examination provides valuable data to confirm the characteristics of CNV, especially intraretinal and subretinal fluid, pigment epithelium detachment, and central retinal thickness [25]. As a noninvasive examination, OCT is essential at every visit after the treatment. Nowadays, OCTA is a useful tool to detect CNV area and flow. Muakkassa et al. reported that the area and greatest linear dimension (GLD) of CNV were simple measurements to quantify the CNV size after treatment [12]. Jia et al. also used quantitative measurements of CNV flow and area to evaluate treatment effects in neovascular AMD [26].

With the clinical application of OCTA, the assessments of treatment for CNV can be more developed and diverse. In this study, selected CNV area and detected vessel flow were measured with analysis software that was developed for OCTA, and the responses to treatment were basically consistent with OCT images and ETDRS letter exams. In addition, the rates of change of CNV size and detected vessel flow as shown on OCTA were higher than the CRT change on SD-OCT. One day after intravitreal injection, there were no obvious changes of fluid on OCT, but the selected CNV area and flow area were significantly smaller than those before treatment. The mean rate of changes on OCT and on OCTA presented a larger significant difference between the two detection methods. This study showed that the selected CNV area and flow area could be more sensitive for evaluating treatment outcomes, instead of relying solely on visual acuity and OCT B-scans. Additionally, the quantitative analysis confirmed that intravitreal ranibizumab is an effective treatment for ICNV. In the future, CNV size and vessel area in ICNV patients will be examined regularly to monitor the response to treatment, especially in early stage after treatment.

In 1 of the 17 eyes, it was found that the selected CNV area and flow area were increased after treatment, and BCVA decreased. Although these changes indicated that the condition of CNV had worsened, the OCT image showed reduction of subretinal fluid and CRT. In another one eye, OCTA showed that the CNV vessel area decreased with increased CRT value, and the BCVA improved after treatment. This suggested that OCTA performance did not correspond to OCT in some cases but did correspond to vision changes.

Retina fluid is caused by the increase of vascular permeability and leakage, so subretinal fluid and the CRT value on SD-OCT do not accurately reflect CNV structure or abnormal blood flow. OCTA might better reflect the state of

CNV, because it can detect the vessel flow directly. Future studies are needed to assess the two measurements for monitoring the therapeutic effect of ICNV.

There were several limitations to this study. Firstly, this observational study had a limited number of patients, and patients with poor fixation or imaging quality were excluded, which may have caused selection bias. Secondly, the follow-up period after treatment was short, which only included 1 day and 1 month. Additional observation phases might help to explain the atrophy and reperfusion of CNV vessels. Moreover, the selected CNV area was performed manually. Although trained and qualified personnel drew every area twice, the possibility of measurement error existed. With OCTA, SSADA software can only detects blood flow in a certain range of speeds [9, 15]. The blood flow is too slow or too fast, such vessels will not be displayed in the OCTA. Therefore, OCTA could not completely reflect the changes of vessels in this study. CNV was observed and detected only at the outer retinal layer that was usually avascular in the background, which did not accurately reflect CNV vessels overall. In the future, improved software for three-dimensional volumetric analysis would be an ideal measurement for quantifying CNV lesion.

5. Conclusion

In summary, OCTA enables the observation of abnormal vascular morphology of ICNV from the horizontal section, examines changes of CNV after anti-VEGF treatment, and quantitatively analyzes variation in selected CNV areas or flow areas with specific analysis software. By using OCTA as an assessment method, intravitreal injection of ranibizumab was shown to be effective for idiopathic choroidal neovascularization, and CNV shrinkage from the periphery as well as vessel density reduction was observable after 1 day of treatment. OCTA provides a useful approach for monitoring and evaluating the treatment effects of intravitreal anti-VEGF for ICNV.

Competing Interests

The authors declare that there are no competing interests regarding the publication of this paper.

References

[1] H.-J. Qi, X.-X. Li, and Y. Tao, "Outcome of intravitreal bevacizumab for idiopathic choroidal neovascularization in a Chinese population," *Canadian Journal of Ophthalmology*, vol. 45, no. 4, pp. 381–385, 2010.

[2] S. N. Shah, Q. Y. Kang, X. J. Fan, and F. Shahbaz, "Microstructural effects of intravitreal bevacizumab in idiopathic choroidal neovascularisation," *Journal of Ayub Medical College, Abbottabad*, vol. 27, no. 2, pp. 259–263, 2015.

[3] P. A. Campochiaro, "Ocular neovascularization," *Journal of Molecular Medicine*, vol. 91, no. 3, pp. 311–321, 2013.

[4] L. Jian, Y. Panpan, and X. Wen, "Current choroidal neovascularization treatment," *Ophthalmologica*, vol. 230, no. 2, pp. 55–61, 2013.

[5] R. A. Cheema, J. Mushtaq, and M. A. Cheema, "Intravitreal bevacizumab as a primary treatment for idiopathic choroidal neovascularization," *Middle East African Journal of Ophthalmology*, vol. 18, no. 3, pp. 220–223, 2011.

[6] E. Carreño, T. Moutray, K. Fotis et al., "Phase IIb clinical trial of ranibizumab for the treatment of uveitic and idiopathic choroidal neovascular membranes," *British Journal of Ophthalmology*, 2015.

[7] T. E. de Carlo, A. Romano, N. K. Waheed, and J. S. Duker, "A review of optical coherence tomography angiography (OCTA)," *International Journal of Retina and Vitreous*, vol. 1, article 5, 2015.

[8] Y. Jia, S. T. Bailey, T. S. Hwang et al., "Quantitative optical coherence tomography angiography of vascular abnormalities in the living human eye," *Proceedings of the National Academy of Sciences of the United States of America*, vol. 112, no. 18, pp. E2395–E2402, 2015.

[9] Y. Jia, O. Tan, J. Tokayer et al., "Split-spectrum amplitude-decorrelation angiography with optical coherence tomography," *Optics Express*, vol. 20, no. 4, pp. 4710–4725, 2012.

[10] R. Mastropasqua, L. Di Antonio, S. Di Staso et al., "Optical coherence tomography angiography in retinal vascular diseases and choroidal neovascularization," *Journal of Ophthalmology*, vol. 2015, Article ID 343515, 8 pages, 2015.

[11] B. Lumbroso, M. Rispoli, and M. C. Savastano, "Longitudinal optical coherence tomography-angiography study of type 2 naive choroidal neovascularization early response after treatment," *Retina*, vol. 35, no. 11, pp. 2242–2251, 2015.

[12] N. W. Muakkassa, A. T. Chin, T. De Carlo et al., "Characterizing the effect of anti-vascular endothelial growth factor therapy on treatment-naive choroidal neovascularization using optical coherence tomography angiography," *Retina*, vol. 35, no. 11, pp. 2252–2259, 2015.

[13] L. A. Yannuzzi, "Indocyanine green angiography: a perspective on use in the clinical setting," *American Journal of Ophthalmology*, vol. 151, no. 5, pp. 745–751.e1, 2011.

[14] A. M. Wu, C. M. Wu, B. K. Young, D. J. Wu, C. E. Margo, and P. B. Greenberg, "Critical appraisal of clinical practice guidelines for age-related macular degeneration," *Journal of Ophthalmology*, vol. 2015, Article ID 710324, 5 pages, 2015.

[15] B. Lumbroso, D. Huang, Y. Jia, J. G. Fujimoto, and M. Rispoli, *Clinical Guide to Angio-OCT: Non Invasive, Dyeless OCT Angiography*, Jaypee Brothers Medical Publishers, New Delhi, India, 2015.

[16] Q. Wang, S. Y. Chan, J. B. Jonas, and W. B. Wei, "Optical coherence tomography angiography in idiopathic choroidal neovascularization," *Acta Ophthalmologica*, vol. 94, no. 4, pp. 415–417, 2016.

[17] L. Kuehlewein, S. R. Sadda, and D. Sarraf, "OCT angiography and sequential quantitative analysis of type 2 neovascularization after ranibizumab therapy," *Eye (Basingstoke)*, vol. 29, no. 7, pp. 932–935, 2015.

[18] R. F. Spaide, "Optical coherence tomography angiography signs of vascular abnormalization with antiangiogenic therapy for choroidal neovascularization," *American Journal of Ophthalmology*, vol. 160, no. 1, pp. 6–16, 2015.

[19] L. Kuehlewein, M. Bansal, T. L. Lenis et al., "Optical coherence tomography angiography of type 1 neovascularization in age-related macular degeneration," *American Journal of Ophthalmology*, vol. 160, no. 4, pp. 739–748.e2, 2015.

[20] A. El Ameen, S. Y. Cohen, O. Semoun et al., "Type 2 neovascularization secondary to age-related macular degeneration

imaged by optical coherence tomography angiography," *Retina*, vol. 35, no. 11, pp. 2212–2218, 2015.

[21] F. Razi, A. Haq, P. Tonne, and M. Logendran, "Three-year follow-up of ranibizumab treatment of wet age-related macular degeneration: influence of baseline visual acuity and injection frequency on visual outcomes," *Clinical Ophthalmology*, vol. 10, pp. 313–319, 2016.

[22] J. Z. Cui, H. Kimura, C. Spee, G. Thumann, D. R. Hinton, and S. J. Ryan, "Natural history of choroidal neovascularization induced by vascular endothelial growth factor in the primate," *Graefe's Archive for Clinical and Experimental Ophthalmology*, vol. 238, no. 4, pp. 326–333, 2000.

[23] A. M. Byrne, D. J. Bouchier-Hayes, and J. H. Harmey, "Angiogenic and cell survival functions of Vascular Endothelial Growth Factor (VEGF)," *Journal of Cellular and Molecular Medicine*, vol. 9, no. 4, pp. 777–794, 2005.

[24] B. Lumbroso, M. Rispoli, M. C. Savastano, Y. Jia, O. Tan, and D. Huang, "Optical coherence tomography angiography study of choroidal neovascularization early response after treatment," *Developments in Ophthalmology*, vol. 56, pp. 77–85, 2016.

[25] F. Coscas, G. Coscas, E. Souied, S. Tick, and G. Soubrane, "Optical coherence tomography identification of occult choroidal neovascularization in age-related macular degeneration," *American Journal of Ophthalmology*, vol. 144, no. 4, pp. 592–599.e2, 2007.

[26] Y. Jia, S. T. Bailey, D. J. Wilson et al., "Quantitative optical coherence tomography angiography of choroidal neovascularization in age-related macular degeneration," *Ophthalmology*, vol. 121, no. 7, pp. 1435–1444, 2014.

Hindawi Publishing Corporation
Journal of Ophthalmology
Volume 2016, Article ID 8271762, 6 pages
http://dx.doi.org/10.1155/2016/8271762

Research Article

Biomechanical Measurement of Rabbit Cornea by a Modified Scheimpflug Device

Bo Zhang,[1] Jianjun Gu,[1] Xiaoxiao Zhang,[1] Bin Yang,[1] Zheng Wang,[2] and Danying Zheng[1]

[1]*State Key Lab of Ophthalmology, Zhongshan Ophthalmic Center, Sun Yat-Sen University, Guangzhou 510060, China*
[2]*Guangzhou Aier Eye Hospital, Guangzhou 510288, China*

Correspondence should be addressed to Zheng Wang; gzstwang@gmail.com and Danying Zheng; zhengdyy@163.com

Received 25 March 2016; Accepted 15 May 2016

Academic Editor: George M. Saleh

Purpose. To explore the probability and variation in biomechanical measurements of rabbit cornea by a modified Scheimpflug device. *Methods*. A modified Scheimpflug device was developed by imaging anterior segment of the model imitating the intact eye at various posterior pressures. The eight isolated rabbit corneas were mounted on the Barron artificial chamber and images of the anterior segment were taken at posterior pressures of 15, 30, 45, 60, and 75 mmHg by the device. The repeatability and reliability of the parameters including CCT, ACD, ACV, and CV were evaluated at each posterior pressure. All the variations of the parameters at the different posterior pressures were calculated. *Results*. All parameters showed good intraobserver reliability (Cronbach's alpha; intraclass correlation coefficient, α, ICC > 0.96) and repeatability in the modified Scheimpflug device. With the increase of posterior pressures, the ratio of CCT decreased linearly and the bulk modulus gradually reduced to a platform. The increase of ACD was almost linear with the posterior pressures elevated. *Conclusions*. The modified Scheimpflug device was a valuable tool to investigate the biomechanics of the cornea. The posterior pressure 15–75 mmHg range produced small viscoelastic deformations and nearly linear pressure-deformation response in the rabbit cornea.

1. Introduction

A comprehensive understanding of biomechanical properties of the cornea is crucial for a wide range of clinical applications such as keratoconus, tonometry, and refractive surgeries [1–3]. Corneal biomechanics involves the complex interaction between its lamellar collagen structure and the charged, hydrated proteoglycan gel. Many studies have indicated that the stress-strain response in mammalian corneas is typical for anisotropic collagenous tissues [4–6]. Strip extensometry and inflation tests were still the two important methods in biomechanical studies. The former was relatively simple and had low cost but involved three inherent deficiencies and had less reliability: a strip specimen is originally part of the cornea, its curvature flattens, and the back analysis usually considers the effect of the central cornea thickness and ignores the fact of the natural increase in cornea thickness away from the center [7]. The inflation tests were executed by altering the intraocular pressure (IOP) and measuring the apex displacement or central corneal tangential elongation on the intact eyes or corneal rigs, and then biomechanical parameters were calculated by mathematical analysis. Tissue markers on the epithelial and endothelial surfaces such as mercury droplets, adhesive tape marker, or dark and light contrasting regions of the cornea provided by graphite powder combined with digital cameras were usually needed in the inflation tests; however, these methods could disturb the cornea and had limited metrical parameters [8–10].

Pentacam (Oculus, Germany) using Scheimpflug photography as a basis has become a popular clinical device for measuring and characterizing the anterior segment. Many studies have indicated good repeatability and reproducibility in the measurements of topographic corneal thickness, anterior and posterior corneal curvatures, anterior chamber depth, and angle and corneal aberrations [11–19]. With the update of the software version, it also provides parameters such as corneal volume and keratometric power difference, which offer new and technical analyses of the cornea [20, 21]. At

present, Pentacam has been used in the range of study types including chronic applications over longer periods as well as dose range studies investigating a no-effect level with respect to lens changes in animal models. Rats, rabbits, dogs, cats, and monkeys all have ocular dimensions, which allow recording of optical sections of their eyes by Pentacam in a reproducible way [22]. The use of animal corneas as approximate models to human corneas in mechanical property characterization studies had been necessary because of the difficulties in obtaining enough human donor corneas.

In this study, we investigated the biomechanics of intact corneas of rabbits subjected to altering of posterior inflation pressures by a modified Scheimpflug device and evaluated the probability of this method.

2. Materials and Methods

2.1. Specimen Preparation. Eight fresh rabbit eyes from New Zealand white rabbits (2-3 Kg, female) were obtained. A central disk including the corneal button and a 3 mm scleral ring was removed with a pair of curved scissors and this was followed by the removal of the iris, lens, and ciliary body under microscope within 1 hour of eye enucleation. Prior to specimen preparation the central corneal thickness was measured using a pachymeter (DGH1000, DGH Technologies, Exton, PA). The average value and standard deviation were $397.3 \pm 13.7\ \mu$m. The epithelium of the cornea was kept complete to lessen the effect of hydration in the procedure.

2.2. Inflation Tests. The corneas were mounted onto the artificial pressure chamber (K20-2126, Katena, USA). The pressure chamber was filled with saline solution and connected to a small reservoir, whose vertical movement represented the change of intraocular pressure. The actual pressure in the chamber was measured using a differential pressure transducer (YP101, Xinhang Co., China) and the measurements were recorded automatically in Bio-Signal Acquisition System (Chengdu TME Technology Co., China). The whole apparatus was fixed by two clamps between the two pillars of the Pentacam and moved vertically to attain the appropriate position. The maximum pressure applied was 75 mmHg, which was well above the normal physiological level. Three cycles of loading and unloading up to 75 mmHg at intervals of 5 minutes were applied to recondition and stabilize its behavior of the cornea.

2.3. Experimental Protocol. The posterior inflation pressure was varied stepwise from 15 mmHg to 75 mmHg and the images were taken at 15, 30, 45, 60, and 75 mmHg. The pressure was always increased with the speed of 15 mmHg/min. All images were taken in 5 minutes after the step increase in pressure to allow enough time for the equilibration of cornea creep. The surface of cornea was drenched using the solution (Dextran40 Sodium Chloride) in 10 seconds before taking images. The examiner adjusted the joystick until perfect alignment was shown, and then, the system automatically took images of the cornea within 2-second period. Only those scans that registered as "OK" were included. Three consecutive scans were captured for intraobserver reliability analysis. The same procedures were repeated on a different pressure level.

2.4. Statistical Analysis. Statistical analysis was performed using SPSS software (version 19.0, SPSS, Inc., Chicago, IL, USA). The intraobserver reliability of all parameters was tested using Cronbach's alpha test (α) and the intraclass correlation coefficient (ICC). The intraobserver repeatability for each corneal parameter was assessed by the statistical parameters: the within-subject standard deviation, intraobserver precision, and intraobserver repeatability as previously reported [14]. All the data were tested for normality using the Kolmogorov-Smirnov test. The level of significance was set at 0.05.

3. Results

3.1. Intraobserver Repeatability and Reliability of the Measurements for the Parameters. Like human screening by Pentacam, most parameters such as corneal curvatures, corneal thickness (CCT), anterior chamber depth (ACD), corneal elevations, anterior chamber volume (ACV), and corneal volume (CV) were acquired by the modified Scheimpflug device. With the increase of the inflation pressure, all parameters varied without the loss of high quality of the images, even in high pressure of 75 mmHg.

The modified Scheimpflug device was shown to be highly reliable in the measurements of the parameters such as central corneal thickness, anterior chamber depth, anterior chamber, and corneal volumes ($\alpha > 0.98$; ICCs > 0.96). With the varying of posterior pressure, the reliabilities of the measurements of the parameters did not change significantly ($p > 0.05$, Table 1). High repeatabilities of the measurements of the parameters were also shown and did not alter significantly with the increase of posterior pressures ($p > 0.05$).

3.2. The Measurements of Corneal Thickness. The corneal thickness at posterior pressure of 15 mmHg which is appropriately consistent with normal intraocular pressure of rabbit was viewed as the initial number of CCT. With a rise in posterior pressure, the average corneal thickness diminished. The changes of CCT to the primary corneal thickness at pressures were calculated as $(\mathrm{CCT}_{15\,\mathrm{mmHg}} - \mathrm{CCT}_{\mathrm{posterior\ pressure}})/\mathrm{CCT}_{15\,\mathrm{mmHg}}$, and the ratios were shown linearly with the increase of posterior pressure (Figure 1).

3.3. Corneal Volume Measurements and Modulus of Volumetric Strain. Pachymetry software in the device can calculate the corneal volume within different range around the central cornea. Figure 2 shows the corneal volumes within 10 mm circle decrease with the increase of posterior pressures and the ratios of the decrease of the corneal volume are almost linear. In the inflation test, the stress and volumetric strain values derived from the pressure-deformation experimental results could be used to determine the variation of the bulk modulus with applied posterior pressure. If the cornea at posterior pressure of 15 mmHg was defined as normal primary

Table 1: Summary of intraobserver repeatability and reliability for the parameters.

Parameters	Posterior pressure (mmHg)	Sw	Pr	Rep	C alpha	ICC
CCT	15	0.972	1.904	2.691	1.000	1.000
	30	1.028	2.014	2.847	1.000	1.000
	45	1.374	2.694	3.807	1.000	0.999
	60	1.460	2.863	4.046	1.000	0.999
	75	1.713	3.357	4.744	1.000	0.999
ACD	15	0.032	0.062	0.088	0.998	0.994
	30	0.032	0.062	0.088	0.998	0.995
	45	0.032	0.062	0.088	0.998	0.996
	60	0.032	0.062	0.088	0.999	0.997
	75	0.032	0.062	0.088	0.999	0.998
ACV	15	2.402	4.709	6.655	0.998	0.993
	30	5.911	11.586	16.374	0.988	0.967
	45	2.448	4.799	6.782	0.998	0.995
	60	3.141	6.157	8.701	0.997	0.994
	75	6.011	11.782	16.651	0.994	0.976
CV	15	0.138	0.270	0.382	1.000	0.999
	30	0.118	0.232	0.328	1.000	1.000
	45	0.276	0.540	0.764	0.999	0.997
	60	0.138	0.270	0.382	1.000	0.999
	75	0.443	0.868	1.226	0.997	0.988

Sw: within-subject standard deviation; Pr: precision; Rep: repeatability; ICC: intraclass correlation coefficient; CCT: central cornea thickness; ACV: anterior chamber volume; ACD: anterior chamber depth; CV: corneal volume.

condition, the average bulk modulus was 0.25 megapascals (Mpa) at the posterior pressure of 30 mmHg and decreased to 0.11 Mpa at 75 mmHg. Beyond the pressure 45 mmHg, the modulus was almost attainted at the platform (Figure 3).

3.4. The Measurements of Anterior Chamber. The rabbit corneas were mounted to the artificial chamber for simulating the intact eyeballs. The images of anterior chamber were scanned well by the modified device. With the increase of posterior pressures, both ACV and ACD gradually elevated and the change of ACD was almost linear (Figure 4).

4. Discussion

The present study employed a new modified Scheimpflug device and executed the inflation test to examine the rabbit corneal biomechanics. In the experiment, we mounted the rabbit corneas to the artificial chamber. The base of the artificial chamber was modified by black tape to simulate the iris structure. The light reflex reduced greatly and the back surface of the cornea was shown obviously in the scan of the modified device and high quality of the images of anterior segment was acquired. The objective of this study was to evaluate the intraobserver repeatability and reliability of

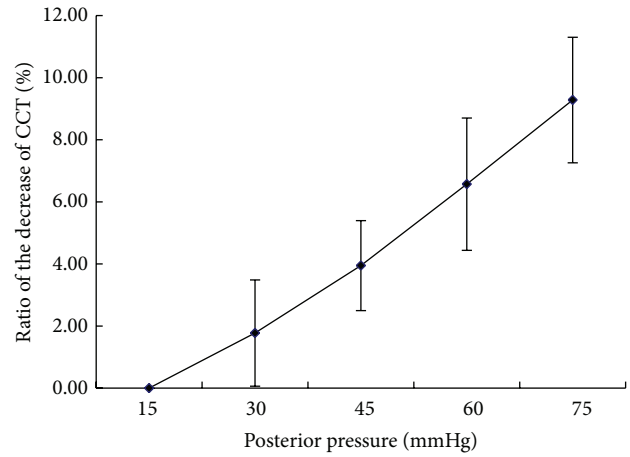

Figure 1: The change of central corneal thickness (CCT) of rabbit eyes with the increase of posterior pressure. The ratios of the decrease of CCT were calculated as $(CCT_{15\,mmHg} - CCT_{posterior\ pressure})/CCT_{15\,mmHg}$, where $CCT_{15\,mmHg}$ was viewed as the initial thickness of the cornea. The ratios were shown linearly with the increase of posterior pressure ($R^2 = 0.9928$).

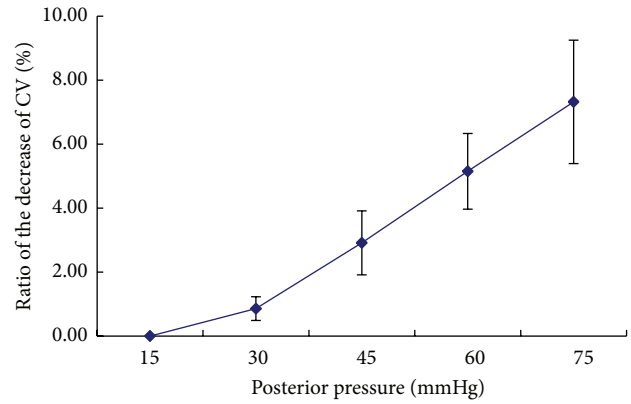

Figure 2: The change of rabbit corneal volume (CV) with the increase of posterior pressure. The ratios of the decrease of CV were calculated as $(CV_{15\,mmHg} - CV_{posterior\ pressure})/CV_{15\,mmHg}$. The ratios were shown linearly with the increase of posterior pressure ($R^2 = 0.98$).

the modified device. In general, a value of 0.70 is considered satisfactory and in clinical applications a value of 0.90 is required. For the ICC, a value above 0.75 indicates good reliability, but most clinical applications require a value of at least 0.90 [13]. In the experiment, the values of ICC and α were almost 1.0 and excellent results even higher than those in human measurements as reported were shown in repeatability analysis [13]. There were two reasons to account for the facts: firstly, the device kept stable without any factors affecting the measurement such as eye movement or blink during the scan. Secondly, several studies reported that the creep was small for the normally hydrated and the swollen corneas and lasted between 30 and 70 seconds [23], so the posterior pressures continued for 5 minutes and ensured the equilibration of corneal creep without effects on

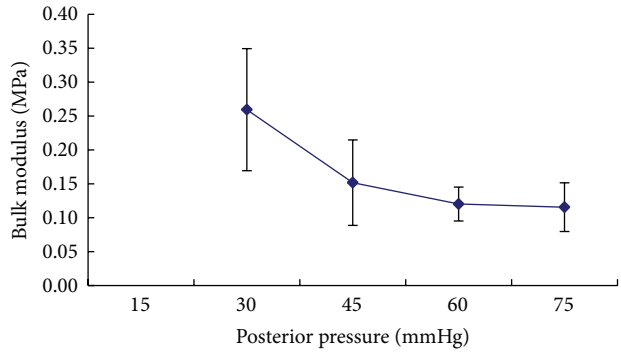

Figure 3: The change of bulk modulus of rabbit corneas with the increase of posterior pressure. The cornea at posterior pressure of 15 mmHg was defined as primary condition (P_0). The bulk modulus was calculated as $\Delta P/\Delta V$, where $\Delta P = (P - P_0)$, $\Delta V = (CV_{15\,mmHg} - CV_{posterior\ pressure})/CV_{15\,mmHg}$.

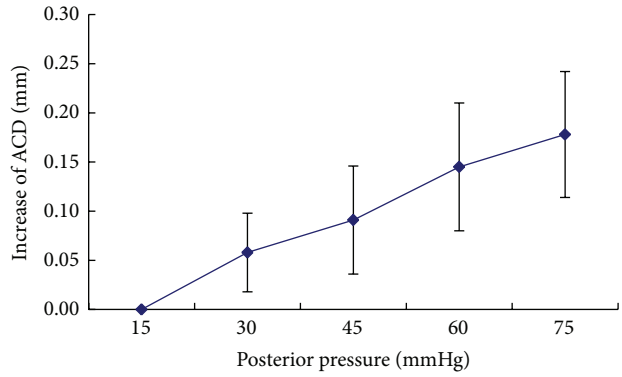

Figure 4: The variation of anterior chamber depth (ACD) of rabbit eyes with the increase of posterior pressure. The increase of ACD was calculated as ($ACD_{posterior\ pressure} - ACD_{15\,mmHg}$). With the increase of posterior pressures, ACD gradually elevated and the change of ACD was almost linear ($R^2 = 0.9913$).

the measurements of the cornea in the study. Our results indicated that the modified device had good reliability and repeatability in the measurements of the parameters, even still kept stable with the increase of posterior pressures. The modified device should be taking advantage of measuring the corneal biomechanics.

Until now corneal biomechanics has been challenging in the ophthalmic field because of difficulties of in vivo accurate measurements. Although two noncontact tonometers (Ocular Response Analyzer and CorVis ST) are currently commercially available to study corneal biomechanics, there are still obvious drawbacks in the two devices. In the former, whether the corneal resistance factor and corneal hysteresis accurately represent corneal biomechanics is questionable, even some studies have found that there is no direct relationship between the modulus of elasticity and the corneal hysteresis and this suggests that conclusions from studies using the ORA should be considered cautiously [24, 25]. In the latter, the Corvis ST does not provide conventional biomechanical parameters such as the elastic modulus and the stiffness. Furthermore, the area of analysis with the two devices is only limited to approximately the central 3.0 mm of the cornea, which does not represent all of the corneal biomechanics [25, 26]. The inflation test is still a valuable method combined with shell theory to calculate stress, strain, and elastic modulus, which ensures the integrity of the corneal tissue in almost normal physiological condition.

Some studies have proved that corneal hydration affects the properties of corneal biomechanics and corneal thickness rises linearly with the increase of corneal hydration [27]. In the study, we kept the intact epithelium and minimize the evaporation on corneal surface drenched using the solution (Dextran40 Sodium Chloride) and the corneal hydration almost maintained normally in the procedure to minimize its effects on the properties of corneal biomechanics. In biomechanical studies, the corneal strain behaviors and corneal apex displacement were usually investigated. One study found that the human cornea showed a negligible extensibility and the rabbit tissue underwent a 9% strain with a curvilinear relationship between stress and strain under low pressures and the relationship was linear at higher pressures [28]. Our data showed the linear relationship between posterior pressures and ACD increase similar with apex displacement beyond the normal physiologic IOP and they were consistent with previous reports.

In this study, we found that the corneal thickness decreased linearly with increasing intraocular pressure and the corneal thickness decreased by 9.28 ± 2.02% for a pressure increase from 15 mmHg to 75 mmHg, which was in good agreement with the results of Hennighausen et al. [23]. According to the incompressibility assumption, corneal volumetric considerations reveal that the relative change in stromal thickness would have been twice the tangential strain of the stroma and the reduction of the corneal thickness is generally viewed as compensation for the corneal surface increase on inflation test. But the average corneal thickness decreased more than expected theoretically; a small reduction in corneal volume did take place during the pressure increase [29]. The modified Scheimpflug device can provide the data of corneal volume in different range from the apex of the cornea and may benefit investigating the interaction of fluid flows within the stroma and corneal load. In the experiment, our data showed that the corneal volume decreased by approximately 7.32% for a pressure increase from 15 mmHg to 75 mmHg and it further supported the idea that local fluid shifts in the stroma are possible within minutes after load changes.

Young's modulus is a measure of property of elastic materials and it is defined as the ratio between stress and strain. Mammalian corneas demonstrated hyperelastic behavior with an initial low stiffness and a final high stiffness under short-term inflation testing. The stress-strain relationship of the cornea is not linear. Therefore, it is inappropriate to use Young's elastic modulus to describe the nonlinear biomechanical properties of the cornea [30]. In this study, bulk modulus defined as the ratio of the infinitesimal pressure increase to the resulting relative decrease of the volume was introduced to describe the corneal biomechanics. The changes of the corneal bulk modulus were investigated with

the posterior pressure increase and we found that the bulk modulus decreased gradually to the platform. It suggested that the cornea was almost viewed as an incompressible soft tissue especially with the stress of more high posterior pressure.

In conclusion, the modified Scheimpflug device is a valuable method to measure the parameters of anterior segment on the inflation tests and has more advantages of the measurements of biomechanics of the cornea. The variations of the corneal biomechanics due to the refractive corneal surgeries or corneal transplantation may be further investigated by this device.

Competing Interests

The authors state that they have no commercial or proprietary interest in the products named in the paper.

Acknowledgments

This study was supported by Guangdong Science and Technology Project Fund (2002C30902).

References

[1] J. Liu and C. J. Roberts, "Influence of corneal biomechanical properties on intraocular pressure measurement: quantitative analysis," *Journal of Cataract and Refractive Surgery*, vol. 31, no. 1, pp. 146–155, 2005.

[2] T. T. Andreassen, A. H. Simonsen, and H. Oxlund, "Biomechanical properties of keratoconus and normal corneas," *Experimental Eye Research*, vol. 31, no. 4, pp. 435–441, 1980.

[3] V. Alastrué, B. Calvo, E. Peña, and M. Doblaré, "Biomechanical modeling of refractive corneal surgery," *Journal of Biomechanical Engineering*, vol. 128, no. 1, pp. 150–160, 2006.

[4] D. A. Hoeltzel, P. Altman, K. Buzard, and K.-I. Choe, "Strip extensiometry for comparison of the mechanical response of bovine, rabbit, and human corneas," *Journal of Biomechanical Engineering*, vol. 114, no. 2, pp. 202–215, 1992.

[5] A. Elsheikh, D. Alhasso, and P. Rama, "Biomechanical properties of human and porcine corneas," *Experimental Eye Research*, vol. 86, no. 5, pp. 783–790, 2008.

[6] A. Elsheikh and D. Wang, "Numerical modelling of corneal biomechanical behaviour," *Computer Methods in Biomechanics and Biomedical Engineering*, vol. 10, no. 2, pp. 85–95, 2007.

[7] A. Elsheikh and K. Anderson, "Comparative study of corneal strip extensometry and inflation tests," *Journal of the Royal Society Interface*, vol. 2, no. 3, pp. 177–185, 2005.

[8] J. O. Hjortdal, "Biomechanical studies of the human cornea: development and application of a method for experimental studies of the extensivility of the intact human cornea," *Acta Ophthalmologica Scandinavica*, vol. 73, no. 4, pp. 364–365, 1995.

[9] S. L.-Y. Woo, A. S. Kobayashi, W. A. Schlegel, and C. Lawrence, "Nonlinear material properties of intact cornea and sclera," *Experimental Eye Research*, vol. 14, no. 1, pp. 29–39, 1972.

[10] P. D. Jaycock, L. Lobo, J. Ibrahim, J. Tyrer, and J. Marshall, "Interferometric technique to measure biomechanical changes in the cornea induced by refractive surgery," *Journal of Cataract and Refractive Surgery*, vol. 31, no. 1, pp. 175–184, 2005.

[11] Ö. Ö. Uçakhan, M. Özkan, and A. Kanpolat, "Corneal thickness measurements in normal and keratoconic eyes: pentacam comprehensive eye scanner versus noncontact specular microscopy and ultrasound pachymetry," *Journal of Cataract and Refractive Surgery*, vol. 32, no. 6, pp. 970–977, 2006.

[12] U. de Sanctis, A. Missolungi, B. Mutani, L. Richiardi, and F. M. Grignolo, "Reproducibility and repeatability of central corneal thickness measurement in keratoconus using the rotating Scheimpflug camera and ultrasound pachymetry," *The American Journal of Ophthalmology*, vol. 144, no. 5, pp. 712–718.e1, 2007.

[13] D. Chen and A. K. C. Lam, "Reliability and repeatability of the Pentacam on corneal curvatures," *Clinical and Experimental Optometry*, vol. 92, no. 2, pp. 110–118, 2009.

[14] D. P. Piñero, C. Saenz González, and J. L. Alió, "Intraobserver and interobserver repeatability of curvature and aberrometric measurements of the posterior corneal surface in normal eyes using Scheimpflug photography," *Journal of Cataract and Refractive Surgery*, vol. 35, no. 1, pp. 113–120, 2009.

[15] D. Chen and A. K. C. Lam, "Intrasession and intersession repeatability of the Pentacam system on posterior corneal assessment in the normal human eye," *Journal of Cataract and Refractive Surgery*, vol. 33, no. 3, pp. 448–454, 2007.

[16] C. A. Utine, F. Altin, H. Cakir, and I. Perente, "Comparison of anterior chamber depth measurements taken with the Pentacam, Orbscan IIz and IOLMaster in myopic and emmetropic eyes," *Acta Ophthalmologica*, vol. 87, no. 4, pp. 386–391, 2009.

[17] J.-H. Yi, S. Hong, G. J. Seong, S. Y. Kang, K. T. Ma, and C. Y. Kim, "Anterior chamber measurements by pentacam and AS-OCT in eyes with normal open angles," *Korean Journal of Ophthalmology*, vol. 22, no. 4, pp. 242–245, 2008.

[18] M. A. Miranda, C. O'Donnell, and H. Radhakrishnan, "Repeatability of corneal and ocular aberration measurements and changes in aberrations over one week," *Clinical and Experimental Optometry*, vol. 92, no. 3, pp. 253–266, 2009.

[19] H. Shankar, D. Taranath, C. T. Santhirathelagan, and K. Pesudovs, "Repeatability of corneal first-surface wavefront aberrations measured with Pentacam corneal topography," *Journal of Cataract and Refractive Surgery*, vol. 34, no. 5, pp. 727–734, 2008.

[20] J.-D. Ho, C.-Y. Tsai, R. J.-F. Tsai, L.-L. Kuo, I.-L. Tsai, and S.-W. Liou, "Validity of the keratometric index: evaluation by the Pentacam rotating Scheimpflug camera," *Journal of Cataract and Refractive Surgery*, vol. 34, no. 1, pp. 137–145, 2008.

[21] S. Doganay, P. Bozgul Firat, S. Emre, and S. Yologlu, "Evaluation of anterior segment parameter changes using the Pentacam after uneventful phacoemulsification," *Acta Ophthalmologica*, vol. 88, no. 5, pp. 601–606, 2010.

[22] A. Wegener and H. Laser-junga, "Photography of the anterior eye segment according to Scheimpflug's principle: options and limitations—a review," *Clinical and Experimental Ophthalmology*, vol. 37, no. 1, pp. 144–154, 2009.

[23] H. Hennighausen, S. T. Feldman, J. F. Bille, and A. D. McCulloch, "Anterior-posterior strain variation in normally hydrated and swollen rabbit cornea," *Investigative Ophthalmology and Visual Science*, vol. 39, no. 2, pp. 253–262, 1998.

[24] D. H. Glass, C. J. Roberts, A. S. Litsky, and P. A. Weber, "A viscoelastic biomechanical model of the cornea describing the effect of viscosity and elasticity on hysteresis," *Investigative Ophthalmology and Visual Science*, vol. 49, no. 9, pp. 3919–3926, 2008.

[25] D. P. Piñero and N. Alcón, "Corneal biomechanics: a review," *Clinical and Experimental Optometry*, vol. 98, no. 2, pp. 107–116, 2015.

[26] A. K. C. Lam, Y. Hon, L. K. K. Leung, and D. C. C. Lam, "Repeatability of a novel corneal indentation device for corneal biomechanical measurement," *Ophthalmic and Physiological Optics*, vol. 35, no. 4, pp. 455–461, 2015.

[27] N. Ehlers, "The fibrillary texture and the hydration of the cornea," *Acta Ophthalmologica*, vol. 44, no. 4, pp. 620–630, 1966.

[28] B. Jue and D. M. Maurice, "The mechanical properties of the rabbit and human cornea," *Journal of Biomechanics*, vol. 19, no. 10, pp. 847–853, 1986.

[29] J. O. Hjortdal, "Extensibility of the normo-hydrated human cornea," *Acta Ophthalmologica Scandinavica*, vol. 73, no. 1, pp. 12–17, 1995.

[30] B. L. Boyce, R. E. Jones, T. D. Nguyen, and J. M. Grazier, "Stress-controlled viscoelastic tensile response of bovine cornea," *Journal of Biomechanics*, vol. 40, no. 11, pp. 2367–2376, 2007.

Hindawi Publishing Corporation
Journal of Ophthalmology
Volume 2016, Article ID 4680621, 8 pages
http://dx.doi.org/10.1155/2016/4680621

Research Article

Visualization of IOL Material-Induced Changes in Retinal Color Stimulus

Stephan Reiss,[1,2] Karsten Sperlich,[1,2] Martin Kunert,[2] Rudolf F. Guthoff,[2,3] Heinrich Stolz,[1] Anselm Jünemann,[2] and Oliver Stachs[2]

[1]*Institute of Physics, University of Rostock, Albert-Einstein-Straße 23-24, 18059 Rostock, Germany*
[2]*Department of Ophthalmology, University of Rostock, Doberaner Straße 140, 18057 Rostock, Germany*
[3]*Institute for Biomedical Engineering, University of Rostock, Friedrich-Barnewitz-Straße 4, 18119 Rostock, Germany*

Correspondence should be addressed to Stephan Reiss; sreiss@beuth-hochschule.de
and Karsten Sperlich; karsten.sperlich@uni-rostock.de

Received 26 January 2016; Accepted 23 May 2016

Academic Editor: Mehmet Borazan

Purpose. Different IOL materials, particularly blue-light filtering materials, have different spectral transmittance characteristics. The color stimuli, which influence retinal receptors objectively, have consequently implications for color perception. We report on the quantitative determination of IOL-specific transmittance characteristics and present a method visualizing the resultant changes in color stimulus. *Methods*. A setup was realized to quantify IOL-absorption in a range of 390–780 nm. To visualize the influence of the different spectral transmittance characteristics an algorithm was developed, which converts RGB-pixel values of images into spectra, which performs the corresponding transmittance correction, reconverts to RGB, and reconstructs the image. IOLs of hydrophobic acrylate and hydrophilic acrylate with a hydrophobic surface in each case with/without blue-light filter were examined. *Results*. Assessment of the reference images verifies the suitability of the pipeline. Evaluation of the transmittance spectra reveals differences of material- and manufacturer-specifics, which are capable of inducing considerable changes in color perception, particularly in the blue color range and mixed colors involving blue. *Conclusions*. The developed technique provides an approach for determining IOL-specific transmittance behavior and subsequently its influence on the retinal color stimulus. Problems of altered color perception are occasionally reported after cataract surgery and these become obvious with the visualization procedure developed here.

1. Introduction

Color perception is a complex process in which a chain of signals consisting of physical, physiological, and psychological components evokes the actual impression of color. Radiation in a wavelength range from 390 nm to 780 nm is designated as visible light. The relative spectral distribution of the primary light sources or light bodies in the perception of color will be affected by the respective spectral transmittance characteristics of the individual optically refracting media of the eye, namely, the cornea, aqueous humor, lens, and vitreous humor. A color stimulus is induced on the retina and is converted by the specific response of the retina into a color intensity.

Cataract surgery using intraocular lenses (IOLs) with different spectral transmittance characteristics is known to affect the retinal color stimulus. This effect is to be expected in the light of previously published IOL transmittance curves [1–3], and yet its impact is difficult to quantify. The present study therefore sets out to calculate the changes in color stimuli on the retina by quantitatively determining the spectral transmittance characteristics of IOLs made from different materials and supplied by different manufacturers. The main aim of this study was to understand how IOL implantation using different optic materials influences the retinal color stimulus.

2. Method

To visualize the retinal color stimulus change due to the spectral transmittance characteristics of different IOL materials, it is necessary to determine transmittance in the wavelength range of visible light.

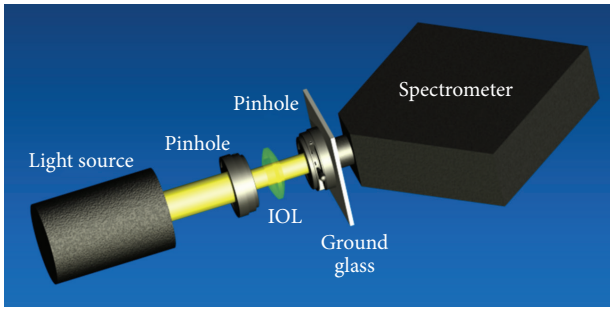

Figure 1: Setup for determining transmittance properties.

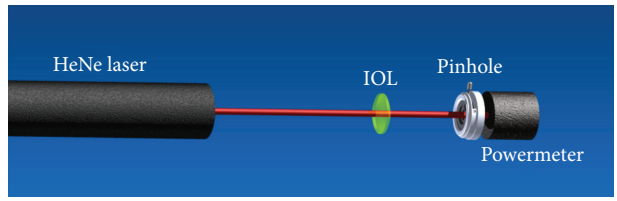

Figure 2: Schematic illustration of the experimental setup for normalization of the intensity spectrum with IOL (for the wavelength 633 nm). The pinhole ensured that no stray light was incident on the power meter (Powermeter 1918-R, Newport Corporation, Irvine, CA/USA).

2.1. Transmittance Measurement. With a light source (KL1500, Schott, Mainz/Germany) radiating in a wavelength range from 390 nm to 780 nm, two pinhole apertures ensured that transmittance was measured through the IOL in a diameter of 4.5 mm (Figure 1). A ground glass (SM5, Edmund Optics, Karlsruhe/Germany) was used to generate homogeneous light distribution and to bypass any influence of IOL focus. A high-resolution spectrometer (HR4000, Ocean Optics, Dunedin, FL/USA) was used to determine spectral intensity distribution in the investigated wavelength range.

The spectral transmittance curve $T(\lambda)$ is a relative quantity. In an initial step the spectral intensity of the light source was measured, background-corrected, and normalized to $I_L(\lambda)$ as reference.

In the next step the intensity spectrum with IOL inserted was measured, background-corrected, and scaled using the same normalization factor to obtain $I_{\mathrm{IOL}}(\lambda)$. The spectral transmittance curve $T(\lambda)$ was then defined as the ratio of $I_{\mathrm{IOL}}(\lambda)$ divided by $I_L(\lambda)$.

However, this approach was invalidated because the focusing characteristic of the IOL resulted in an incorrect intensity spectrum of transmitted light compared with the spectrum of the light source. This potentially leads to a transmittance greater than 1, which is contrary to the laws of physics.

To circumvent this problem we needed to scale $I_{\mathrm{IOL}}(\lambda)$ correctly. With the aid of a HeNe laser at 633 nm and a powermeter, we determined transmittance T_{PM} at this specific wavelength. Since the powermeter has a large detector area, this measurement has the advantage of not being affected by the focusing characteristic of the lens, compared with the entrance slit of a spectrometer, and hence permits laser light to be collected entirely (see Figure 2).

For $\lambda = 633$ nm the scaling parameter S can easily be calculated from $T_{\mathrm{PM}} = SI_{\mathrm{IOL}}/I_L$. The following general equation is therefore valid:

$$T(\lambda) = \frac{SI_{\mathrm{IOL}}(\lambda)}{I_L(\lambda)}. \quad (1)$$

Figure 3 illustrates the spectrum of the light source $I_L(\lambda)$ and the now correctly scaled spectrum of light transmitted through the IOL $I_{\mathrm{IOL}}(\lambda)$, while the derived transmittance $T(\lambda)$ is depicted in Figure 4.

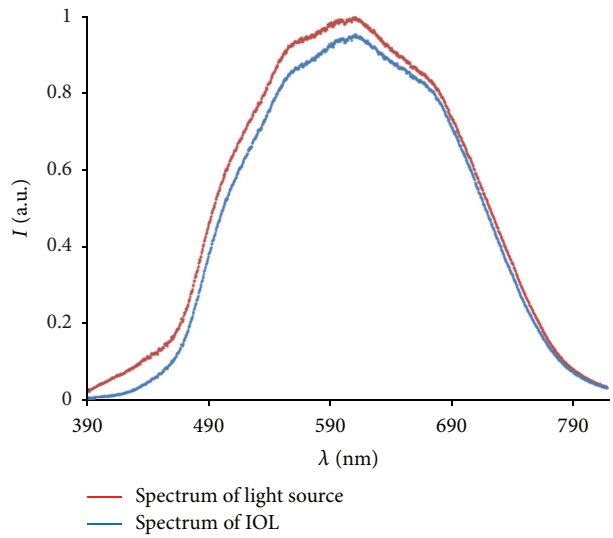

Figure 3: Background-corrected and normalized intensity distributions in the wavelength range from 390 nm to 780 nm for the light source (red) only and an IOL example (Hoya NY60) (blue).

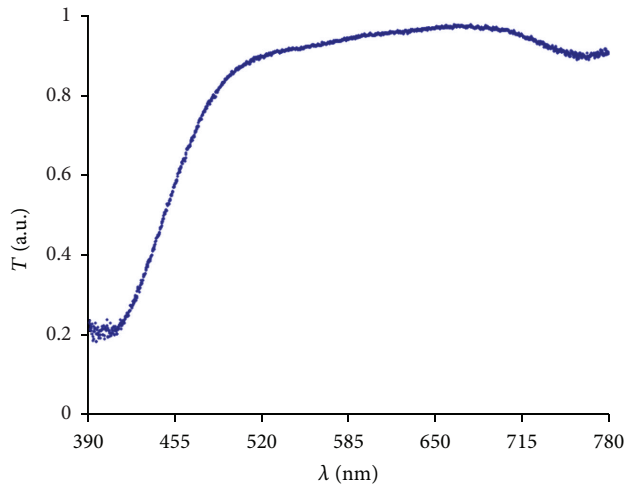

Figure 4: Example of a measured transmittance curve for an IOL (Hoya NY60).

2.2. Visualization. We set out to visualize the retinal color stimulus changes induced by the measured transmittance spectra of the artificial IOLs. The analysis involved calculating the influence of the IOL-specific transmittance on a reference image on a monitor. Each pixel corresponds to a triple of color values, namely, Red Green Blue (RGB), and has to be recalculated according to the measured transmittance curve. To apply the RGB value of a pixel to the transmittance spectrum, this must be transformed into the corresponding wavelength. The literature contains equations that enable wavelength values to be converted to RGB values [4]. However, these equations are not suitable since each pixel corresponds to a spectrum instead of one single wavelength, a disadvantage that is especially obvious for mixed colors, such as pink or white. In order to obtain a spectrum for each pixel we adopted a different approach.

A spectrometer (HR4000, Ocean Optics, Dunedin, FL/USA) was used to measure separately the intensity spectrum of each RGB color of a monitor (Flatron IPS235P, LG Electronics Inc., Seoul, South Korea) (Figure 5). The most intense color (blue) was selected to be normalized to 1 and the other two colors were normalized using the same factor. Addition of these three spectra yielded the spectrum for white. Measuring the spectrum for white itself yielded the same spectrum and, since the two curves were identical, we plotted only one curve for white.

Having identified a spectrum for each color, a spectrum for every RGB value was obtained simply by multiplying the spectra for red, green, and blue with the corresponding RGB value and summing these spectra. This yielded a spectrum for each pixel of the reference image and each pixel spectrum could then be multiplied by the spectral transmittance of the specific IOL. Under these conditions the pixel spectra are altered in the same way as would be experienced by a patient with an implanted IOL. The final task was to identify the new RGB values corresponding to the new modified pixel spectra. Since the spectra for red, green, and blue are of fixed shape, it is impossible to achieve RBG values that match the new spectrum exactly. Therefore we implemented an iterative algorithm in Mathematica 10.0 (Wolfram Research, Champaign, IL/USA) to identify the RGB set whose pixel spectrum best matched the modified pixel spectrum. These values correspond to the transmittance properties of the specific IOL. This approach allowed visualization of the change in retinal receptor color stimulus caused by an implanted artificial lens.

2.3. Setup Verification. In a subsequent verification step the conversion algorithm and the experimental setup were tested using a neutral density filter. With its known spectral transmittance of 70% it is obvious how the "modified" image has to look like. This is a simple way to test whether or not the program and our experimental setup were operating as intended. Subsequently, the same routine was applied to the reference image using IOL transmittance curves.

2.4. Material Selection. The color stimulus change induced by IOLs from different materials and manufacturers (Alcon, Hoya, Zeiss, Polytech, Domilens, and Medicontur) was investigated according to the procedure outlined above. IOL selection was performed to address the influence of hydrophobic acrylate materials and hydrophilic acrylate materials with a hydrophobic coating. The following material groups were investigated:

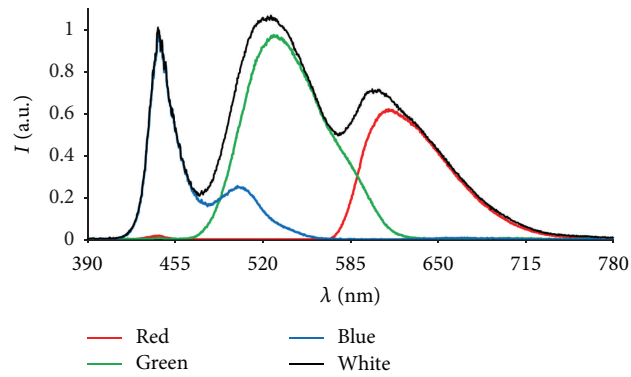

Figure 5: Intensity spectra of RGB colors and white of an LED monitor (Flatron IPS235P, LG Electronics Inc., Seoul, South Korea) measured with a spectrometer (HR4000, Ocean Optics, Dunedin, FL/USA).

(1) Hydrophobic acrylate materials without blue-light filter (Hoya VA-65BB, Alcon MA60AC).

(2) Hydrophobic acrylate materials with blue-light filter (Alcon SN60AT, Hoya NY60).

(3) Hydrophilic acrylate with a hydrophobic coating without blue-light filter (Zeiss 209M, Polytech Opti Vis).

(4) Hydrophilic acrylate with a hydrophobic coating with blue-light filter (Domilens Domicryl 677ABY, Medicontur 677MY).

3. Results

Figure 6 shows the transmittance curve of the neutral density filter. As anticipated, an almost constant transmittance pattern was recorded across the entire wavelength range from 390 nm to 780 nm.

As expected, there was no selective change in brightness of any one color or wavelength. Instead, the brightness of the entire image was reduced (by about 30%) (Figure 7).

On the basis of these validating results, the IOL transmittance spectra were measured (see Figure 8).

The two raw materials tested (hydrophobic acrylate, hydrophilic acrylate with a hydrophobic coating) are both manufactured with and without blue-light filter. All lenses showed similar transmittance curves with more or less constant transmittance between 480 nm and 700 nm and a decline of 60% below 480 nm, except IOLs made from hydrophilic acrylate with a hydrophobic coating without blue-light filter.

In the wavelength range from 390 nm to 780 nm the hydrophilic IOLs with a hydrophobic coating without blue-light filter showed an almost constant high transmittance of

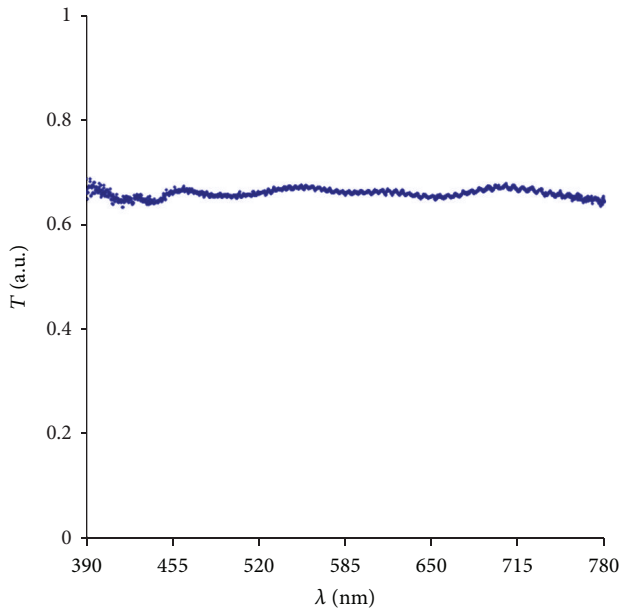

Figure 6: Measured transmittance spectrum of the 70% neutral density filter.

Figure 7: Effect of neutral density filter transmittance on the reference image: (a) reference image and (b) reference image affected by neutral density filter transmittance curve.

about 80% to 90%. The hydrophobic lenses without blue-light filter had a transmittance edge at about 410 nm; at that point transmittance increased from about 20% within 20 nm to 80% and then remained relatively constant at about 95%.

The hydrophobic IOLs with blue-light filter revealed a transmittance of 20% at 390 nm. Over a wavelength range of roughly 110 nm the intensity of the transmitted radiation through the lens increased to approximately 95%. However, the hydrophilic IOLs with a hydrophobic coating and blue-light filter achieved this change in transmittance within a wavelength range of approximately 40 nm.

Visualization of retinal color stimuli changes, based on the IOL-specific transmittance curves, was determined and is shown in Figures 9 and 10. The transmittance characteristics were applied to the reference image according to the conversion algorithm described above. Minimal color stimulus changes were found to be induced by hydrophobic acrylate without blue-light filter as well as by hydrophilic acrylate with a hydrophobic coating without and with blue-light filter (Figures 9 and 10, resp.). Hydrophobic acrylate lenses with blue-light filter, however, showed a significant change, especially in the blue color range (Figure 10).

These results were also evident in the representation of the difference images. A black difference image signifies that there was no change at all. However, intense blue regions, for example, denote a major change in the blue wavelength range due to the IOL. The more intense a color is, the more it is affected by the IOL. The intensity of difference images has been increased by a factor of two for enhanced visualization of the differences.

4. Discussion

The aim of the present study was to visualize changes in retinal color stimulus induced by different lens materials, including the effect of incorporated blue-light filters. For this purpose, a simple measurement method was developed to determine the transmittance behavior of IOLs in the wavelength range from 390 nm to 780 nm. Since spectral transmittance was determined as a percentage value (1 corresponds to 100%), specific IOL design parameters such as thickness or refractive index are no longer important in our measurement. Initial experiments with a neutral density filter demonstrated the validity of the experimental setup and the visualization algorithm.

As illustrated in Figure 8, different material- and manufacturer-dependent transmittance characteristics were detected. IOLs manufactured from the same material (hydrophobic acrylate or hydrophilic acrylate with a hydrophobic coating) by the same manufacturer exhibited identical transmittance behavior (data not presented) whereas divergent patterns may be present between different manufacturers. For example, Alcon SN60AT and Hoya NY60 are both manufactured from hydrophobic acrylate and include a blue-light filter, but their transmittance behaviors differed. A similar difference was found between Domilens Domicryl 677ABY and Medicontur 677MY for hydrophilic acrylate with a hydrophobic coating. Surprisingly, these different transmittance behaviors have a negligible effect on the retinal color stimulus, as shown in Figure 10.

In general, in the range from 390 nm to 500 nm, hydrophilic acrylate IOLs with a hydrophobic coating (with or without blue-light filter) are characterized by significantly better transmittance than hydrophobic acrylate lenses. They display almost constantly high transmittance of about 85% across the entire wavelength range of the visible spectrum. This property can also be recognized in the visualization of the color stimulus.

The blue-light filter influence on the retinal color stimulus is not insignificant. The transmittance curves of the IOLs

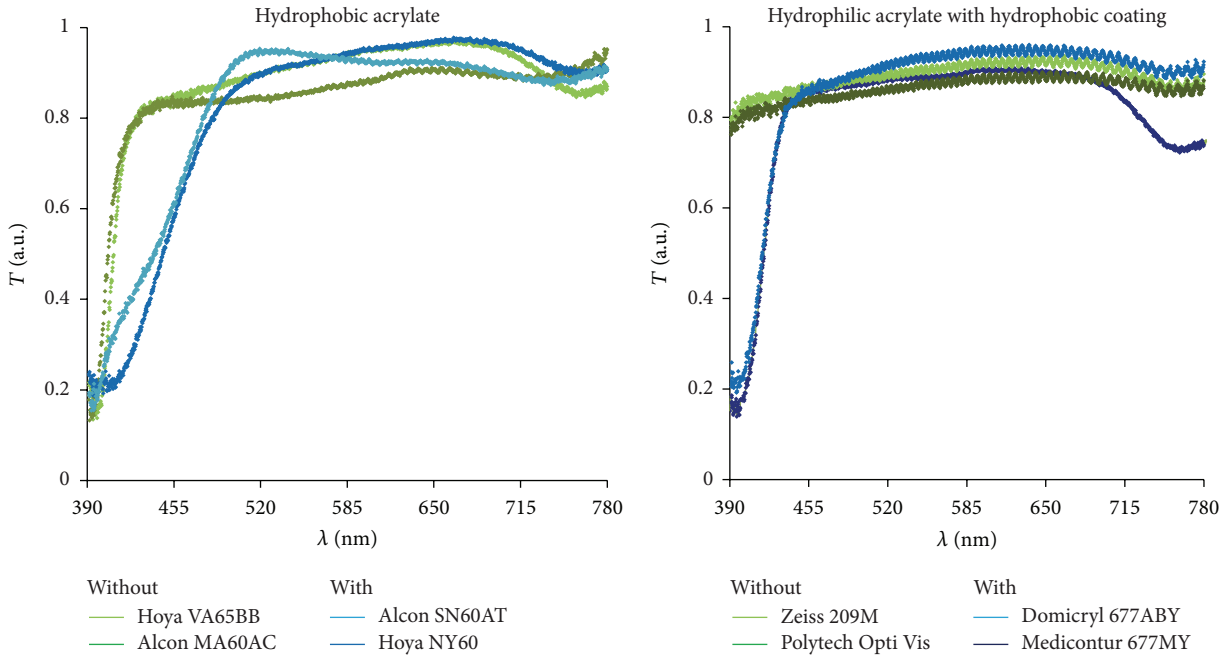

Figure 8: Transmittance spectra of IOLs made from different materials with (blue) and without blue-light filter (green).

tested show the expected difference between materials with and without blue-light filter. Both material groups (hydrophobic acrylate, hydrophilic acrylate with a hydrophobic coating) show lower transmittance in the range from 390 nm to 450 nm when the IOLs have a blue-light filter: similar findings have already been published elsewhere [1–3].

This difference has an effect in terms of the retinal color stimulus. In the case of hydrophilic lenses with a hydrophobic coating with and without blue-light filter, the visualization of transmittance curve effects on the reference image (see Figures 9 and 10) shows that there is only a small change in color stimulus compared with the initial reference image. This is confirmed in the difference images where all colors are represented almost equally dark or equally bright, respectively.

In contrast, transmittance differences between hydrophobic acrylate IOLs with blue-light filter (Alcon SN60AT, Hoya NY60) and without blue-light filter (Hoya VA-65BB, Alcon MA60AC) are responsible for significant color stimulus changes (see Figures 9 and 10). In particular, hydrophobic acrylate IOLs with blue-light filter provide a significant change in blue and mixed colors involving blue compared with hydrophobic acrylate IOLs without blue-light filter.

The calculated difference images reflect this. Both investigated hydrophobic acrylate IOLs without blue-light filter reveal approximately the same brightness changes in the difference images. However, the difference images for hydrophobic IOLs with blue-light filter show an increased brightness level for blue, which indicates a strong influence on the blue-affected colors due to the transmittance characteristics of these IOLs. The blue color stimulus changes considerably, while the other colors of the visible spectrum remain unaffected. In this context, it is understandable that other studies have demonstrated generally larger color discrimination with blue-light filter IOLs than with clear IOLs [5–10].

The present study also has some limitations. The influence of the cornea, aqueous humor, and vitreous body has not been investigated. However, their transmittances do not change on IOL implantation and they can be considered as constant factors having no influence on the color stimulus.

It is worth mentioning that our method implies the use of continuous spectra without spectral intensity peaks or jumps; that is, a patient looking at an image on a present-day LED monitor fulfills the continuous spectrum requirement.

Furthermore, the stimulus on the retina does not equate to color perception processed by the visual pathway. We might also be criticized for not investigating IOL transmittance behavior in the UV-A (315 nm–380 nm) and UV-B (280 nm–315 nm) ranges. The cornea, aqueous fluid, and vitreous body absorb most ultraviolet radiation below 300 nm in the phakic eye. Moreover, information between 300 nm and 380 nm does not contribute to color vision and our investigation relates only to IOL material-induced changes in retinal color stimulus. Protection or safety aspects are not addressed in this study because the transmittance behavior of IOLs in the UV-A and UV-B ranges has already been investigated by Laube et al. [2].

5. Summary

To the best of our knowledge this is the first study to investigate the implications of different IOL materials on color perception. The technique developed here provides a simple approach for determining IOL-specific transmittance behavior and subsequently its influence on the retinal color

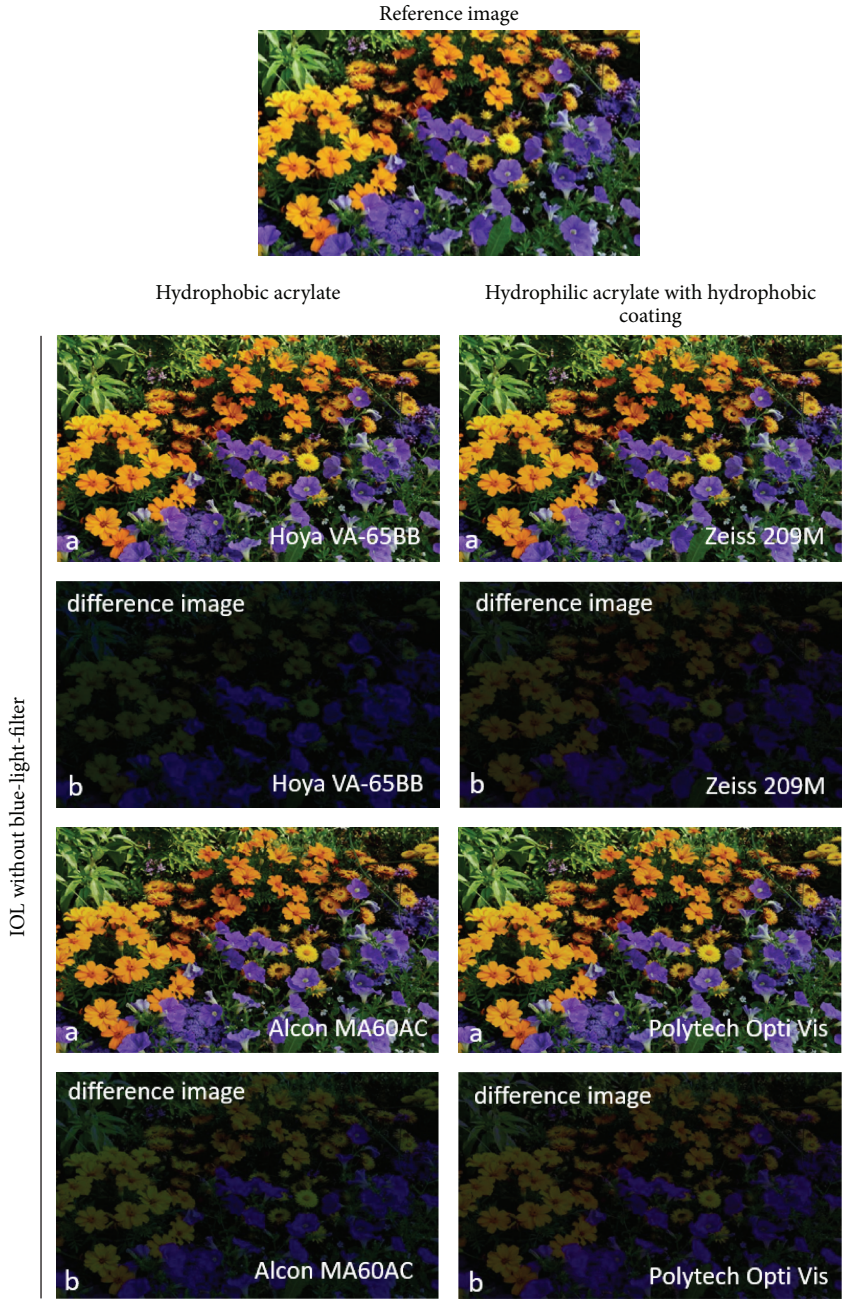

Figure 9: (a) Influence of the specific transmittance curves on the reference image for hydrophobic IOL materials and hydrophilic IOL materials with a hydrophobic coating, in each case without blue-light filter. (b) Difference between reference image and the image affected by a specific transmittance curve for each IOL (for enhanced visualization, the brightness value was increased by a factor two).

stimulus. Problems of altered color perception are occasionally reported by patients after cataract surgery and these become obvious and understandable with the visualization procedure developed here. Major differences exist between IOL optic materials and these may be responsible for not insignificant changes in retinal color stimulus. For blue-light filter IOLs, due to their relatively constant transmittance of about 85% in the visible wavelength range, hydrophilic acrylate IOLs with a hydrophobic coating have significantly less influence on retinal color stimulus than hydrophobic acrylate IOLs. In summary, IOLs of any manufacturer without blue-light filter have no significant influence on the retinal color stimulus.

Competing Interests

The authors declare that there is no conflict of interests regarding the publication of this paper.

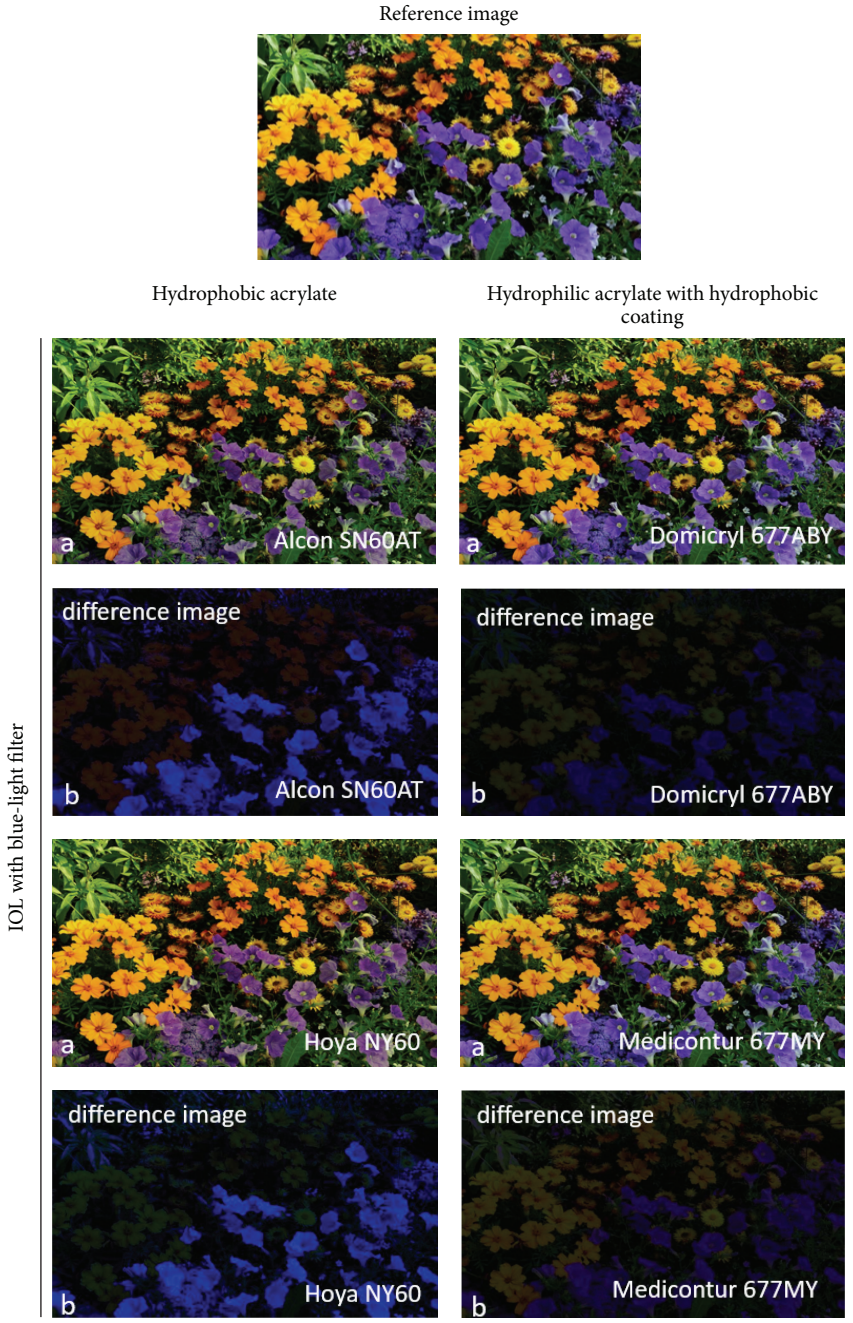

Figure 10: (a) Influence of the specific transmittance curves on the reference image for hydrophobic IOL materials and hydrophilic IOL materials with a hydrophobic coating, in each case with blue-light filter. (b) Difference between reference image and the image affected by a special transmittance curve for each IOL (for enhanced visualization, the brightness value was increased by a factor two).

Authors' Contributions

Stephan Reiss and Karsten Sperlich contributed equally to this paper.

Acknowledgments

The authors are grateful to D. Beattie (medical writer, UK) for editorial assistance in preparing the paper for publication.

This work was financially supported by the Federal Ministry of Education and Research within the REMEDIS and RESPONSE.

References

[1] N. Schrage, "Spektrale Durchlässigkeit bei Blaufilter-Intraokularlinsen," *Der Ophthalmologe*, vol. 109, no. 2, pp. 142–148, 2012.

[2] T. Laube, H. Apel, and H.-R. Koch, "Ultraviolet radiation absorption of intraocular lenses," *Ophthalmology*, vol. 111, no. 5, pp. 880–885, 2004.

[3] C. Brockmann, M. Schulz, and T. Laube, "Transmittance characteristics of ultraviolet and blue-light-filtering intraocular lenses," *Journal of Cataract and Refractive Surgery*, vol. 34, no. 7, pp. 1161–1166, 2008.

[4] U. Kern, "Darstellung sichtbarer Wellenlängen in üblichen Farbmodellen," *Die TEXnische Komödie*, vol. 4, no. 16–25, 2005.

[5] Z. Yuan, P. Reinach, and J. Yuan, "Contrast sensitivity and color vision with a yellow intraocular len," *American Journal of Ophthalmology*, vol. 138, no. 1, pp. 138–140, 2004.

[6] J. Landers, T.-H. T.-H. Tan, J. Yuen, and H. Liu, "Comparison of visual function following implantation of Acrysof Natural intraocular lenses with conventional intraocular lenses," *Clinical and Experimental Ophthalmology*, vol. 35, no. 2, pp. 152–159, 2007.

[7] C. Wohlfart, K. Tschuschnig, P. Fellner et al., "Visual function with blue light filter IOLs," *Klinische Monatsblätter für Augenheilkunde*, vol. 224, no. 1, pp. 23–27, 2007.

[8] A. Rodríguez-Galietero, R. Montés-Micó, G. Muñoz, and C. Albarrán-Diego, "Comparison of contrast sensitivity and color discrimination after clear and yellow intraocular lens implantation," *Journal of Cataract and Refractive Surgery*, vol. 31, no. 9, pp. 1736–1740, 2005.

[9] H. Wang, J. Wang, W. Fan, and W. Wang, "Comparison of photochromic, yellow, and clear intraocular lenses in human eyes under photopic and mesopic lighting conditions," *Journal of Cataract and Refractive Surgery*, vol. 36, no. 12, pp. 2080–2086, 2010.

[10] M. Schürer, A. Walter, H. Brünner, and A. Langenbucher, "Effect of transparent yellow and orange colored contact lenses on color discrimination in the yellow color range," *Ophthalmologe*, vol. 112, no. 8, pp. 670–678, 2015.

Hindawi Publishing Corporation
Journal of Ophthalmology
Volume 2016, Article ID 4182693, 4 pages
http://dx.doi.org/10.1155/2016/4182693

Clinical Study

Passive Removal of Silicone Oil with Temporal Head Position through Two 23-Gauge Cannulas

Zhong Lin, Zhi Sheng Ke, Qian Zheng, Zhen Quan Zhao, and Zong Ming Song

The Eye Hospital, School of Ophthalmology and Optometry, Wenzhou Medical University, Wenzhou, Zhejiang 325027, China

Correspondence should be addressed to Zhi Sheng Ke; kzs7417@163.com

Received 24 January 2016; Revised 14 May 2016; Accepted 30 May 2016

Academic Editor: Yannis Athanasiadis

Purpose. To report a new approach for removal of silicone oil. *Methods*. All surgeries were performed using 23-gauge vitrectomy system with two transconjunctival sutureless cannulas. At the beginning, most of the silicone oil was removed by traditional microinvasive vitrectomy system through inferior-temporal cannula. Then, the blood transfusion tube is removed from the inferior-temporal cannula, and the fluid-air exchange is performed. A passive fluid-air exchange was performed to aspirate the residual silicone oil after gradually turning the patient's head temporally by approximately 90° gradually. *Results*. After the surgery, all patients had a clear anterior chamber and vitreous cavity on slit lamp and B scan examination, respectively. The mean time taken for silicone oil removal and total surgery was 8.0 ± 1.4 minutes and 12.4 ± 2.5 minutes, respectively. The mean intraocular pressure 1 day, 3 days, 1 week, 1 month, and 3 months after surgery was 9.0 ± 5.8 mmHg, 11.3 ± 7.6 mmHg, 16.1 ± 6.9 mmHg, 17.7 ± 4.8 mmHg, and 17.1 ± 3.5 mmHg, respectively. *Conclusion*. This new approach may provide a safe and fast method to remove the silicone oil.

1. Introduction

The 23-gauge cannula transconjunctival sutureless vitrectomy has been widely used for treatment of vitreous and retinal diseases, including intraocular silicone oil removal. As compared to conventional 20-gauge cannula, the 23-gauge cannula system has some advantages, such as more secure surgical procedure and faster wound healing [1, 2]. New approaches for injecting and removing silicone oil in sutureless vitreoretinal surgery have been developed accordingly [1–5]. However, the silicone oil is difficult to be completely removed from the vitreous chamber even when using the 23-gauge cannula system. Many postoperative complications related to intraocular silicone oil have been reported, including secondary glaucoma [6], corneal endothelial decompensation [7], and intraconjunctival oil inclusion cysts [8]. Furthermore, the patients often complain about floaters, which interfere with their vision and quality of life. In order to remove the silicone oil and emulsified silicone oil drops completely, we report a new surgical approach with temporal head positioning and passive fluid-air exchange through two 23-gauge cannulas.

2. Methods

Twenty-four silicone oil eyes of 24 patients, from the Eye Hospital of Wenzhou Medical University, were enrolled between December 2013 and June 2014. The study followed the tenets of the Declaration of Helsinki and was approved by the Ethics Committee of Wenzhou Medical University. All participants signed a written and informed consent.

All patients with primary vitreous or retinal disease, such as vitreous hemorrhage, rhegmatogenous retinal detachment, and proliferative vitreoretinopathy, who previously underwent 23-gauge transconjunctival sutureless vitrectomy and silicone oil (5,000 cSt) injection in the Eye Hospital of Wenzhou Medical University, were included in this study. Silicone oil was used as tamponade for all eyes for at least 3 months before removal. The binocular indirect ophthalmoscope, optical coherence tomography (OCT), and B-scan all indicated that the retina was attached preoperatively.

All procedures were performed by the same surgeon (Zhi Sheng Ke) using 23-gauge (Midlaps, US) valve casing transconjunctival sutureless vitrectomy system after retrobulbar anesthesia with a 50% mixture of 2% lidocaine and

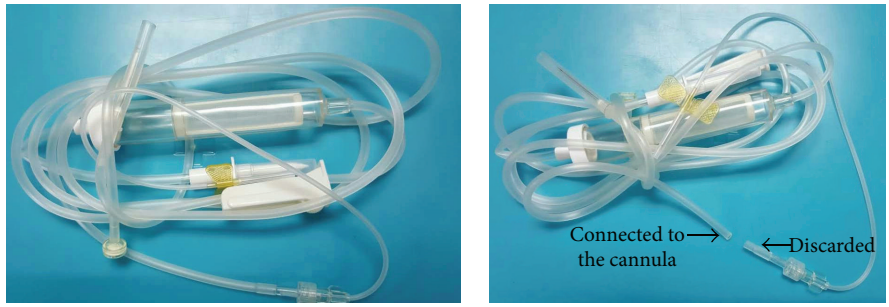

(a) (b)

Figure 1: (a) Blood transfusion tube (model: IS-V9; Shanghai Kindly Enterprise Development Group, Shanghai, China). (b) The adaptor of the blood transfusion tube was cut. One side of the blood transfusion tube was connected to the inferior-temporal cannula after removing the valve.

0.75% bupivacaine. To begin the surgery, two 23-gauge cannulas, that is, the superior-nasal infusion cannula and the inferior-temporal operation cannula, were established. A trocar was inserted into the intended sclerotomy site at an angle of approximately 30° parallel to the limbus with the bevel up. Once past the trocar sleeve, the angle was made perpendicular to surface and the cannula was inserted into the eye. A scleral tunnel incision was made. The cannula was held in place with forceps, and then the trocar was removed. The infusion tube was attached to the superior-nasal cannula. The infusion was opened and adjusted to approximately 60 cm. The adaptor of a blood transfusion tube (model: IS-V9; Shanghai Kindly Enterprise Development Group, Shanghai, China) was cut with scissors (Figure 1). The inferior-temporal cannula valve was removed and connected to one side of the blood transfusion tube. The diameter of the cannula without the valve was 1.96 mm, and the diameter of the blood transfusion tube was 2.00 mm. The other side of the blood transfusion tube was connected to the vitrectomy instrument. The negative pressure of the vitrectomy instrument was adjusted to approximately 600 mmHg (1 mmHg = 0.133 kPa). The silicone oil removal was started through the blood transfusion tube. During the oil removal, anterior chamber wash was performed to assist the removal of oil drops when necessary. After that, the fundus status was examined by inserting a 23G light probe. Additional procedures, such as endolaser and membrane peeling, were performed as needed through the cannula(s). If the fundus was in good condition, the blood transfusion tube was removed from the inferior-temporal cannula. At the same time, the patient's head was gradually turned temporally by approximately 90°. A passive fluid-air exchange was started to remove the residual silicone oil as well as balanced salt solution (BSS) out of vitreous cavity (Figure 2). The air irrigation pressure was reduced to 10–15 mmHg. At this time, the temporal sclera and cannula were observed directly, since they were turned out of the visual field of microscope. Finally the superior-nasal cannula was removed. The scleral incisions were pressed with cotton swab to close them. If leakage was noticed and continued beyond 1 minute, a suture was placed to close the wound.

The time taken for silicone oil removal and total surgery was recorded. Postoperative residual silicone oil in the anterior chamber and vitreous chamber was verified by slit lamp examination and B-scan, respectively, within 2 days after surgery. Preoperative IOP and postoperative IOP at one day, three days, one week, one month, and three months were recorded. Patients' postoperative complaints were also recorded.

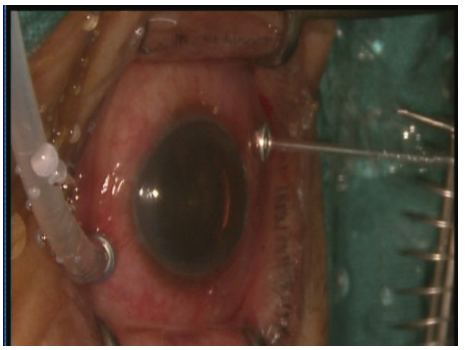

Figure 2: The passive fluid-air exchange was performed after removing the blood transfusion tube from the inferior-temporal cannula. At the same time, the patient's head was gradually turned temporally by approximately 90°.

All statistical analyses were performed with Statistical Analysis System for Windows version 9.1.3 (SAS Inc., Cary, NC). A P value of <0.05 was considered statistically significant.

3. Results

Overall, 10 male and 14 female patients were included. The average age was 50.5 ± 18.2 years. The mean time interval between pars plana vitrectomy with silicone oil tamponade and removal of silicone oil was 3.5 ± 0.8 months. Fifteen eyes were aphakic, 8 eyes were pseudophakic with an intact posterior capsule, and 1 eye was phakic.

Silicone oil was removed successfully in all these 24 cases. No severe postoperative complications were noted, such as severe decrease of intraocular pressure, corneal edema and opacity, intraocular tissue damage, intraocular hemorrhage, and retinal detachment. Postoperatively, all the patients had

Figure 3: B-scan ultrasonography showed a clear vitreous cavity of a patient after the surgery of silicone oil removal.

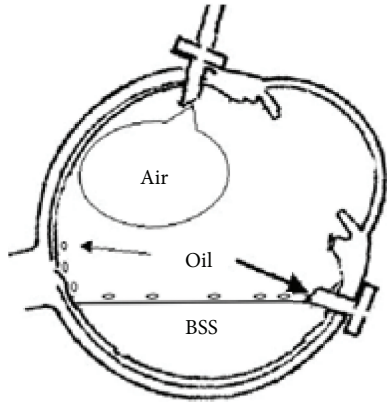

Figure 4: The emulsified silicone oil droplets adhering to the retinal surface would be pushed into the vitreous cavity, while the air entered into the vitreous cavity. The silicone oil droplets would float up because of buoyancy and finally form a thin oil layer between the air (upper layer) and the balanced salt solution (BSS, bottom layer). At that time, the patient's head was gradually turned temporally by approximately 90°, so that the silicone oil layer together with BSS would flow out of the eyeball through the inferior-temporal cannula due to gravity.

a clear anterior chamber and vitreous cavity on slit lamp and B-scan examination, respectively (Figure 3). One patient with sutured scleral incisions complained of foreign body sensation (4.2%) and 1 (4.2%) patient complained of floaters postoperatively.

The mean time taken for silicone oil removal and total surgery was 8.0 ± 1.4 minutes and 12.4 ± 2.5 minutes, respectively. Besides, 8 eyes underwent posterior capsulotomy, intraocular lens was implanted in 10 aphakic eyes, 1 eye underwent phacoemulsification, 7 eyes underwent an additional cannula to peel epiretinal membrane, and 6 eyes underwent retinal laser photocoagulation.

The mean IOP before surgery and 1 day, 3 days, 1 week, 1 month, and 3 months after surgery was 13.7 ± 3.9 mmHg, 9.0 ± 5.8 mmHg, 11.3 ± 7.6 mmHg, 16.1 ± 6.9 mmHg, 17.7 ± 4.8 mmHg, and 17.1 ± 3.5 mmHg, respectively. At 3 months postoperatively, the BCVA improved compared to that preoperatively (Snellen, 0.28 ± 0.31 versus 0.12 ± 0.15).

4. Discussion

Previous studies reported that residual silicone oil may cause keratopathy [7] and secondary glaucoma [6] and even migrate along the intracranial portion of the optic nerve and into the lateral ventricles of the brain [9]. Therefore, complete removal of silicone oil is important. Compared to conventional 20-gauge cannula transconjunctival suture to remove silicone oil, silicone oil removal by 23-gauge cannula transconjunctival sutureless vitrectomy system has some advantages, such as better eye closure and less incision leakage [1, 2]. However, the main problem of silicone oil removal is still the residue of silicone oil.

In this study, we proposed an improved method for silicone oil removal. Most of the silicone oil was removed by traditional microinvasive vitrectomy system. The principle behind this method is related to the physical property of silicone oil itself. First, the silicone oil easily floats above water, since its density (0.97 g/cm^3) is lower than water (1.0 g/cm^3) [10]. Second, the silicone oil tends to form oil droplets above water when it coexists with air, since its surface tension is lesser (35 mN/m) than that of air (approximately 80 mN/m) [10]. Third, silicone oil droplets tend to fuse together above water, since it has high viscosity (5000 cSt) [10]. The present silicone oil removal approach was performed not only through 23G transconjunctival sutureless vitrectomy system, but also combined with the passive fluid-air exchange. At the beginning of the passive fluid-air exchange operation, the vitreous cavity was filled with BSS. The residual silicone oil drops at the bottom of the vitreous cavity rose up, while the BSS went into the vitreous cavity. The emulsified silicone oil droplets adhering to the retinal surface would be pushed into the vitreous cavity, while the air entered into the vitreous cavity. The silicone oil droplets would float up because of buoyancy and finally form a thin oil layer between the air (upper layer) and the BSS (bottom layer). At that time, the patient's head was gradually turned temporally by approximately 90°, so that the silicone oil layer together with BSS would flow out of the eyeball through the inferior-temporal cannula due to gravity (Figures 2 and 4).

In this study, the mean time intervals of silicone oil removal and total surgery were 8.0 ± 1.4 minutes and 12.4 ± 2.5 minutes, respectively. Since the passive fluid-air exchange of this approach does not require the use of corneal contact lens, noncontact observation lens, vitrectomy probe, or backflush needle, the time is apparently shorter than traditional method. After surgery, all patients had a clear anterior chamber and vitreous cavity. Besides, only 1 (4.2%) patient complained of floaters postoperatively. Moreover, no severe intra- or postoperative complications were noted. Postoperative intraocular pressure remained stable, and the BCVA improved. However, the small sample size, lack of controlled group, and relatively short follow-up time are the limitations. Large controlled samples and long-period follow-up are warranted.

There were several advantages of this new approach besides less residual of silicone oil. First, the intraocular pressure was stable intraoperatively. Second, there is no need for the vitrectomy probe or backflush needle to be inserted into the vitreous cavity during the fluid-air exchange operation of

this approach. Hence, it reduces the change of lens, choroid, and retinal injury. Third, the fluid-air exchange operation can be performed even without transparent refractive media. This is especially advantageous in patients with corneal lesion.

In summary, this new approach of silicone oil removal uses negative pressure of traditional microinvasive vitrectomy system to aspirate most of the silicone oil. The technique also uses passive fluid-air exchange to remove the remaining emulsified silicone oil droplets. This new approach is safe, facilitated, fast, and with wider indications.

Competing Interests

All authors certify that they have no affiliations with or involvement in any organization or entity with any financial interest (such as honoraria; educational grants; participation in speakers' bureaus; membership, employment, consultancies, stock ownership, or other equity interest; and expert testimony or patent-licensing arrangements) or nonfinancial interest (such as personal or professional relationships, affiliations, knowledge, or beliefs) in the subject matter or materials discussed in this paper. The authors have no proprietary or commercial interest in any materials discussed in this paper.

Acknowledgments

The study was supported by research grants from the Science Plan Funds of Wenzhou (Y20090276), the Innovation Research Project of the Eye Hospital of Wenzhou Medical University (YNCX201308), and the Research Startup Project for doctors of the Eye Hospital of Wenzhou Medical University (KYQD131101).

References

[1] M. R. Romano, C. Groenwald, R. Das, T. Stappler, D. Wong, and H. Heimann, "Removal of densiron-68 with a 23-gauge transconjunctival vitrectomy system," *Eye*, vol. 23, no. 3, pp. 715–717, 2009.

[2] Z.-M. Song, D. Chen, Z.-S. Ke et al., "A new approach for active removal of 5,000 centistokes silicone oil through 23-gauge cannula," *Retina*, vol. 30, no. 8, pp. 1302–1307, 2010.

[3] R. C. Siqueira, A. D. C. Gil, and R. Jorge, "Retinal detachment surgery with silicone oil injection in transconjunctival sutureless 23-gauge vitrectomy," *Arquivos Brasileiros de Oftalmologia*, vol. 70, no. 6, pp. 905–909, 2007.

[4] Z. Kapran and N. Acar, "Active removal of silicone oil with 25-gauge sutureless system," *Retina*, vol. 27, no. 8, pp. 1133–1135, 2007.

[5] Z. Kapran, N. Acar, Y. B. Unver, T. Altan, and B. Ocak, "Passive removal of silicone oil with a 25-gauge sutureless system," *Japanese Journal of Ophthalmology*, vol. 52, no. 1, pp. 63–66, 2008.

[6] J. Moisseiev, A. Barak, T. Manaim, and G. Treister, "Removal of silicone oil in the management of glaucoma in eyes with emulsified silicone," *Retina*, vol. 13, no. 4, pp. 290–295, 1993.

[7] B. C. Norman, J. Oliver, L. Cheeks, D. S. Hull, D. Birnbaum, and K. Green, "Corneal endothelial permeability after anterior chamber silicone oil," *Ophthalmology*, vol. 97, no. 12, pp. 1671–1677, 1990.

[8] S. P. Donahue, T. R. Friberg, and B. L. Johnson, "Intraconjunctival cavitary inclusions of silicone oil complicating retinal detachment repair," *American Journal of Ophthalmology*, vol. 114, no. 5, pp. 639–640, 1992.

[9] A. W. Eller, T. R. Friberg, and F. Mah, "Migration of silicone oil into the brain: a complication of intraocular silicone oil for retinal tamponade," *American Journal of Ophthalmology*, vol. 129, no. 5, pp. 685–688, 2000.

[10] F. Barca, T. Caporossi, and S. Rizzo, "Silicone oil: different physical proprieties and clinical applications," *BioMed Research International*, vol. 2014, Article ID 502143, 7 pages, 2014.

Hindawi Publishing Corporation
Journal of Ophthalmology
Volume 2016, Article ID 3578617, 10 pages
http://dx.doi.org/10.1155/2016/3578617

Research Article

Computational Simulation of Scleral Buckling Surgery for Rhegmatogenous Retinal Detachment: On the Effect of the Band Size on the Myopization

Elena Lanchares,[1,2] María A. del Buey,[1,3,4,5] José A. Cristóbal,[1,3,4,5] Begoña Calvo,[1,2] Francisco J. Ascaso,[3,4,5] and Mauro Malvè[1,2,6]

[1] *Aragón Institute of Engineering Research (I3A), University of Zaragoza, Campus Río Ebro, Calle Mariano Esquillor s/n, 50018 Zaragoza, Spain*
[2] *Biomedical Research Center in Bioengineering, Biomaterials and Nanomedicine (CIBER-BBN), Aragón Health Sciences Institute, Calle Mariano Esquillor s/n, 50018 Zaragoza, Spain*
[3] *Department of Ophthalmology, Hospital Clínico Universitario "Lozano Blesa", Avenida San Juan Bosco 15, 50009 Zaragoza, Spain*
[4] *Department of Surgery, School of Medicine, University of Zaragoza, Domingo Miral s/n, 50009 Zaragoza, Spain*
[5] *Aragón Health Research Institute (IIS Aragón), Aragón Biomedical Research Center (CIBA), Avenida San Juan Bosco 13, 50009 Zaragoza, Spain*
[6] *Department of Mechanical Engineering, Energetics and Materials, Public University of Navarra, Campus Arrosadía, 31006 Pamplona, Spain*

Correspondence should be addressed to Mauro Malvè; mauro.malve@unavarra.es

Received 15 March 2016; Revised 9 May 2016; Accepted 22 May 2016

Academic Editor: Yannis Athanasiadis

A finite element model (FE) of the eye including cornea, sclera, crystalline lens, and ciliary body was created to analyze the influence of the silicone encircling bandwidth and the tightness degree on the myopia induced by scleral buckling (SB) procedure for rhegmatogenous retinal detachment. Intraocular pressure (IOP) was applied to the reference geometry of the FE model and then SB surgery was simulated with encircling bandwidths of 1, 2, and 2.5 mm. Different levels of tightening and three values of IOP were applied. The anterior segment resulted as unaffected by the surgery. The highest value of Cauchy stress appeared in the surroundings of the implant, whereas no increment of stress was observed either in anterior segment or in the optic nerve head. The initial IOP did not appear to play any role in the induced myopia. The wider the band, the greater the induced myopia: 0.44, 0.88, and 1.07 diopters (D) for the 1, 2, and 2.5 mm bandwidth, respectively. Therefore, patients become more myopic with a wider encircling element. The proposed simulations allow determining the effect of the bandwidth or the tightness degree on the axial lengthening, thus predicting the myopic increment caused by the encircling surgery.

1. Introduction

The conventional surgical treatment for rhegmatogenous retinal detachment (RRD) is 360-degree scleral buckling (SB). It is an effective procedure to achieve retinal reattachment and has been used over 60 years [1, 2]. Since the introduction of *pars plana* vitrectomy (PPV) in 1971 [3], the surgical treatment of RRD consists of these two procedures: encircling procedure and posterior *pars plana* vitrectomy, either alone or combined.

The SB surgery begins with the application of locoregional or, in some cases, general anesthesia. After having hooked the eye muscles using silk surgical thread, the encircling silicone band is guided under the muscle insertions. The encircling element is secured to the sclera 12-13 mm posterior to the limbus with monofilament nylon mattress sutures placed in the four quadrants between the muscles. The encircling implant is fastened with a sleeve with moderate tightness and the surplus end is cut from the band. Then, PPV would be performed if it was planned.

The increment of myopic defect observed in eyes that underwent encircling scleral buckle is due to an increase of the anteroposterior axial length caused by circumferential indentation. Some works in the literature [4, 5] found that the encircling band surgery does not modify the anterior segment of the eye and therefore the degree of myopia induced during the surgery would be exclusively due to the lengthening of the posterior segment of the eye. Although other authors observed a significant modification of the anterior chamber depth after surgery [6, 7], recovery of its normal value in 9–12 months was reported [7].

Finite element (FE) models will help to predict the surgical results and determine the influential parameters [8–14]. Numerical models of the eye have been used to analyze the mechanical response of the eye to different ocular surgeries such as arcuate and limbal relaxing incisions for astigmatism correction, photorefractive keratectomy for the correction of myopia [8–10], and specifically scleral buckling (SB) surgery [11–14]. Before the SB surgery, the size of the encircling band and the position and pull tightening must be established. The more tightened the band, the more the possibilities of bringing the retinal pigment epithelium in contact with the detached sensory retina. Nevertheless, the increment of the axial length will be greater, and thus it will induce higher levels of myopia.

Idealized numerical models of the eye created from average dimensions provide qualitative information on the response of the eye to surgery [8, 15]. Patient specific models would supply quantitative results applicable to a specific patient [16, 17]. In both cases, the accuracy of results will depend on the quality of the model, which must reproduce the geometry of the eye and the mechanical behavior of the tissues.

This work is not intended to simulate retinal attachment achieved by the SB surgery. Assuming that the operation is successful, the aim of this study is to investigate, by means of a numerical model of the eye, the degree of myopia induced by the SB surgery according to the width and the tightening of the encircling element, in order to minimize this collateral effect.

In particular, the scope of this work is to predict and quantify the effect of the main parameters related to the scleral buckling. For this reason, a numerical model based on average data of a large number of patients is provided. The proposed investigation is more parametric than patient specific. The advantage of this numerical model of the eye is that it is possible to perform many variations of the different parameters without altering the patient functionalities and considerably reducing the animal experimental tests.

We simulated two commonly employed bandwidths: 2.0 mm and 2.5 mm, respectively. Besides these two sizes, we also used a 1 mm width to analyze the efficiency of such a narrow band, since it may induce lower myopia increment. Three values of IOP (11, 15, and 18 mmHg) were considered.

2. Materials and Methods

2.1. Finite Element Model. A spherical three-dimensional finite element model of the eyeball was created using Rhinoceros v.4.0 (McNeel & Associates, Indianapolis, IN, USA). This idealized model is based on average eye dimensions and was validated with other surgical techniques in previous works [8–10].

Figure 1 shows the parts of the model, namely, cornea, limbus, sclera, lens, zonules, and ciliary body and the optic nerve. The model of the cornea was based on a nonrevolution ellipsoid with semiprincipal axes of lengths $a = 10.43$, $b = 10.27$, and $c = 14.26$ mm [18] with a sagittal corneal diameter of 11.26 mm and transversal diameter of 11.51 mm; the central corneal thickness was 550 microns. The crystalline lens had an anterior radius of 11 mm, while the posterior radius was −6.5 mm. The eyeball was modelled with a nonspherical geometry, whose dimensions were 25.43 mm (sagittal), 25.76 (transverse), and 24.86 mm (axial). The thickness of the sclera varies with the distance to the limbus and was modelled following Olsen et al. [19].

The created geometry was meshed using the commercial software Ansys ICEM CFD v.14.5 (Ansys Inc., Canonsburg, PA, USA). The numerical model, composed of 34430 nodes, was obtained after an appropriate grid sensitivity analysis. This independence study was conducted comparing the displacements obtained under the same conditions to different mesh refinements.

The human eye is composed of porous tissues with high water content. Approximately 80 percent of the corneal weight is due to water. Cornea and sclera are composed of long collagen fibres embedded in a ground substance mainly formed of proteoglycans and water. In the cornea, collagen fibres lie parallel and run along the whole length of the lamella. In the central region of the cornea, fibres are orthogonally disposed along the superior-inferior and nasal-temporal directions whereas they are predominantly circumferential near the limbus. Moreover, there are other randomly oriented fibres throughout the cornea. This microstructure and the different distributions of collagen fibres give the corneal tissue an anisotropic mechanical behavior [20]. According to this, the cornea was considered as an anisotropic hyperelastic material with two preferred material directions. The two families of fibre directions were as follows: one along the nasal-temporal direction and the other one along the superior-inferior direction (see Lanchares et al. [8]). A circumferential direction of collagen fibres was defined in the limbus, whose material parameters have been assumed identical as for the cornea. The sclera was considered as an isotropic material [21].

The human crystalline lens is composed of nucleus, cortex, and capsule. The fibres in the nucleus are not clearly arranged; therefore the nucleus is considered as an isotropic material. In spite of the clear arrangement of the fibres in the cortex [22], it was modelled as an isotropic material due to the lack of data for the specific material parameters. Isotropy was also assumed for the neural tissue of the optic nerve. The capsular tissue of the lens is increasingly stiffer circumferentially towards the equator [23]; therefore a preferential circumferential direction of deformation was considered.

An appropriate strain energy density function Ψ is required from which stress-strain relations and local elasticity

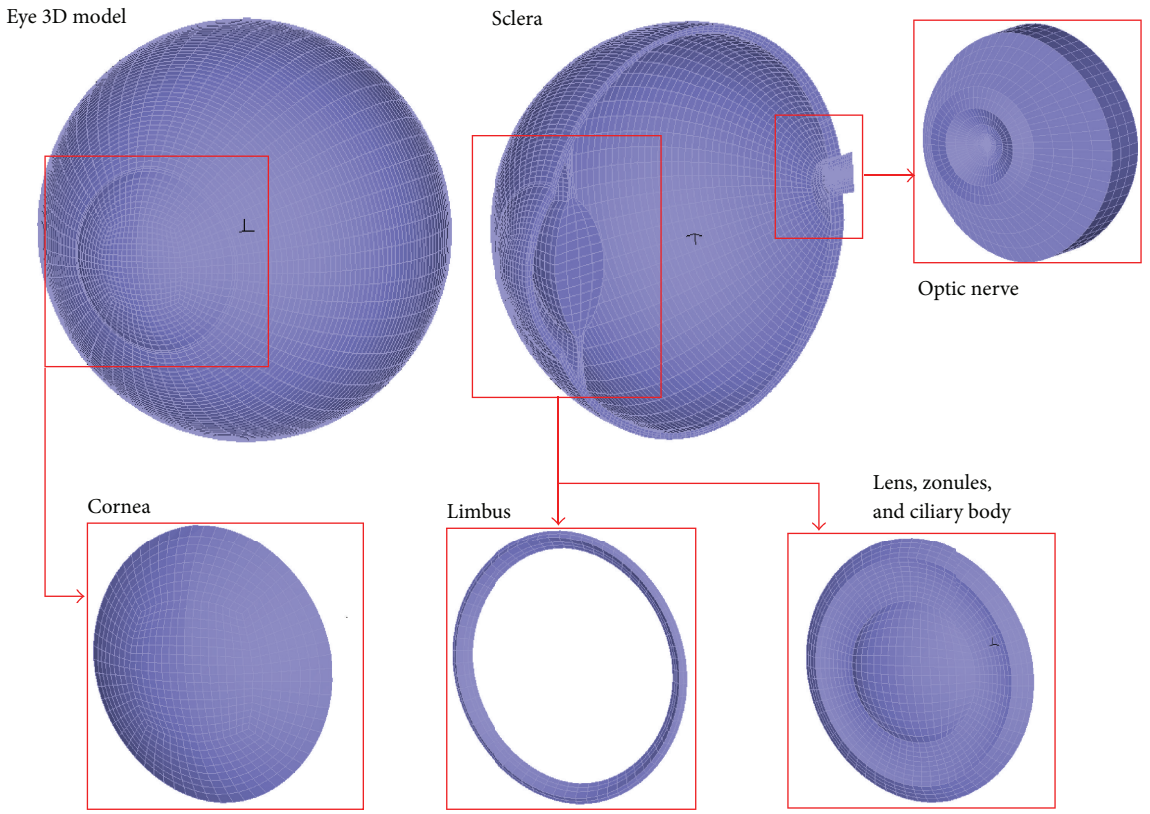

FIGURE 1: Finite element model of the eye. Components of the model used in this work for the simulation of the scleral buckling surgery.

tensors are derived [24]. Because of the directional dependence on the deformation of the tissues, we use a unique decoupled representation of Ψ [25] which depends on the right Cauchy-Green tensor $\mathbf{C} = \mathbf{F}^T\mathbf{F}$ with $\mathbf{F}$ being the deformation gradient tensor. To represent the dependence of Ψ on the directions of the fibres in the reference configuration $\mathbf{m}_0$ and $\mathbf{n}_0$, the structural tensors $\mathbf{M} = \mathbf{m}_0 \otimes \mathbf{m}_0$ and $\mathbf{N} = \mathbf{n}_0 \otimes \mathbf{n}_0$ are used:

$$\Psi(\mathbf{C}) = \Psi_{\text{vol}}(J) + \overline{\Psi}\left(\overline{\mathbf{C}}, \mathbf{M}, \mathbf{N}\right), \tag{1}$$

where $\Psi_{\text{vol}}(J)$ characterizes the change in volume and $\overline{\Psi}(\overline{\mathbf{C}}, \mathbf{M}, \mathbf{N})$ characterizes the change in shape, with $J = \det(\mathbf{F})$ and $\overline{\mathbf{C}} = \overline{\mathbf{F}}^T\overline{\mathbf{F}}$ the modified right Cauchy-Green tensor, with $\overline{\mathbf{F}} = J^{-1/3}\mathbf{F}$.

Then, we use the following strain energy function Ψ:

$$\begin{aligned}\Psi &= \Psi_{\text{vol}} + \overline{\Psi}_{\text{matrix}} + \overline{\Psi}_{\text{fibres}} \\ &= \frac{1}{2D}\ln(J)^2 + \frac{C_1}{2}\left(\overline{I}_1 - 3\right) + \frac{C_2}{2}\left(\overline{I}_2 - 3\right) \\ &\quad + \frac{k_1}{2k_2}\left\{\exp\left[k_2\left(\overline{I}_4 - 1\right)^2\right] - 1\right\} \\ &\quad + \frac{k_3}{2k_4}\left\{\exp\left[k_4\left(\overline{I}_6 - 1\right)^2\right] - 1\right\},\end{aligned} \tag{2}$$

where $1/D$ is a penalty coefficient for numerical purposes; $\overline{\Psi}_{\text{matrix}}$ corresponds to the isochoric change of the matrix of the tissue; and $\overline{\Psi}_{\text{fibres}}$ represents the isochoric change due to the fibres in the tissue. $\overline{I}_1$ and $\overline{I}_2$ are the first two modified strain invariants of the symmetric modified right Cauchy-Green tensor $\overline{\mathbf{C}}$. The pseudoinvariants $\overline{I}_4$ and $\overline{I}_6$ characterize the constitutive response of the fibres. They have a clear physical meaning, the square of the stretch λ along the fibre directions [26]. C_1, C_2, k_1, k_2, k_3, and k_4 are the parameters of the model that characterize each tissue. These material properties of the tissues were taken from several authors [8, 27–29] and are listed in Table 1.

2.2. Simulation of the Surgery and Analysis of Results. The process of simulation was performed using the commercial software Adina v8.5 (ADINA R&D Inc., Watertown, MA, USA). To set the model in physiological conditions, the dimensions must reproduce those measured of the eye *in vivo*. Nevertheless, such geometry belongs to a deformed configuration of the eye due to the effect of the IOP but the tissue prestress is neglected in the model. Consequently, in a first step, both the boundary conditions and the physiological internal stress distribution must be introduced in the FE model in order to balance the IOP. An iterative process was then used to incorporate into the model the initial strains by means of the deformation gradient $\mathbf{F}_0{}^n = \mathbf{F}_{n-1}{}^n\mathbf{F}_0{}^{n-1}$ which balances the IOP. At the end of the process, the final configuration of the model matches the initial one. This methodology is explained in detail in Lanchares et al. [8].

Table 1: Material parameters of the tissues in the anisotropic fibred model of the eye. D is a penalty coefficient for computational purposes; C_1 and C_2 are the material parameters of the extracellular matrix. The parameters k_1 and k_2, k_3, and k_4 correspond to the two families of fibre directions, respectively.

Tissue	D (MPa^{-1})	C_1 (MPa)	C_2 (MPa)	k_1 (MPa)	k_2	k_3 (MPa)	k_4
Cornea	10^{-5}	10^{-1}	0	0.234	29.917	23.4×10^{-2}	29.917
Limbus	10^{-5}	10^{-1}	0	0.234	29.917	0	0
Sclera	10^{-5}	35	−32	0	0	0	0
Lens cortex	34.54	58.295×10^{-5}	0	0	0	0	0
Lens nucleus	214.96	93.667×10^{-6}	0	0	0	0	0
Lens capsule	28.35×10^{-2}	21.60×10^{-2}	0	3.39×10^{-2}	9.7406	0	0
Nerve	4	50.335×10^{-4}	0	0	0	0	0

In a second step we resolved the surgery. The simulation of the band implantation consists of the imposition of a given value of displacement in the negative radial direction (inwards) of the nodes positioned at the equator of the eyeball where a band of that width would be implanted (12-13 mm posterior to the limbus) causing elongation of the eye (Figure 2). The value of displacement u_r is calculated according to the tightening pressure to be applied to the band: $u_r = R_f - R_i$, where R_i is the radius of the eyeball in the initial model at the meridian where the band is going to be implanted, before any simulation, and R_f is the radius of the eyeball under the band after the surgery, obtained from $2\pi R_i - 2\pi R_f = 10$ mm, where 10 mm is the length of the surplus end cut from the band. The bands considered for this study were Mira silicone band-40 (2.0 mm wide and 0.75 mm thick) and Mira silicone band-240 (2.5 and 0.60 mm, resp.) (Mira, Inc., Waltham, MA, USA). Three values of IOP, 11, 15, and 18 mmHg, were applied to evaluate any influence of IOP on the final result.

To determine the change in myopia caused by the SB surgery, the process described by Wang et al. [12] was followed. The initial dioptric power of the eye (D_0) is calculated according to the theoretical eye model, which considers the eye as a lens system composed of cornea (D_1) and crystalline lens (D_2): $D_0 = D_1 + D_2 - D_1 D_2 d/n_1$, where d is the distance between the anterior corneal apex and the middle surface of the crystalline lens and n_1 is the corneal refractive index. Its value is 1.376, but, given the refractive indexes of the aqueous humor (1.336) and the tear film covering the anterior surface of the cornea (1.337), and since the cornea is very thin (0.55 mm thick), it is reasonable to simplify this optical system and consider only the curvature of the anterior surface and the refractive index of 1.336 for the refractive power of the cornea [12].

The degree of myopia induced by the surgery (ΔD) is obtained as the subtraction of the final refraction of the eye (D_{0f}) from the initial refraction (D_0): $\Delta D = D_0 - D_{0f} = D_0 - (n_1/\mathrm{AL})$, where AL is the postoperative axial length of the model.

3. Results

Figure 3(a) shows the line graph of myopia induced *versus* IOP. With increasing IOP, each band shows a different behavior. While the 2 mm wide band has a lower effect at 15 mmHg than at 11 mmHg, the 1 mm wide band shows a slight increase in its effect between these two values of IOP; both of them achieve a higher myopic change at 18 mmHg. The 2.5 mm wide band induces approximately the same myopic change for the three values of IOP. Thus, no clear trend can be inferred. The graph in Figure 3(b) represents the myopic change obtained by numerical simulation *versus* the bandwidth for the three values of IOP considered. Although only the 2.5 mm wide band gives the same results for the three values of IOP, no trend can be inferred from the results corresponding to the other two bandwidths. Thus, we assumed no relationship between myopic change and IOP, so the myopic changes obtained by numerical simulation were averaged for all the three values of IOP (11, 15, and 18 mmHg).

The modification of the axial length and myopic change after the simulation of the surgery for all the cases considered are compiled in Table 2. The mean axial length increment was 0.21 ± 0.07, 0.42 ± 0.06, and 0.51 ± 0.01 mm for the 1.0, 2.0, and 2.5 mm wide bands, respectively. The mean myopic increment for the 1.0, 2.0, and 2.5 mm wide bands was −0.44 ± 0.15, −0.88 ± 0.12, and −1.07 ± 0.03 D, respectively.

Table 3 shows the increment of myopia caused by three levels of tightening of the encircling band, *that is,* 33%, 67%, and 100%, of the final tightening for all nine cases (see Figure 3(c)). In agreement with the assumption made above, no correlation of the induced myopia with IOP was observed. Thus, the resulting data obtained for the three bandwidths and the three values of IOP at each level of tightening were averaged and included in Table 3 and depicted in Figure 3(d). The 1 mm wide band had a considerably lower effect than the 2.0 and 2.5 mm bands. For all the bandwidths considered, the observed trend predicts substantially greater increments of induced myopia for levels of tightening over 100%. In order to estimate these increments, we used a power function of the form $a * x^b + c$ that fits the outcoming data, where x represents the percentage of tightening applied to the encircling band. Using Matlab R2013a (The MathWorks, Natick, MA, USA), we obtained the following functions for the three bandwidths: $-4.80 \cdot 10^{-11} \cdot x^{4.899} - 0.1387$ (1 mm), $-1.12 \cdot 10^{-06} \cdot x^{2.901} - 0.1716$ (2 mm), and $-1.051 \cdot 10^{-06} \cdot x^{2.96} - 0.1972$ (2.5 mm). Changes of −1.04, −1.52, and −1.89 D were obtained, respectively, for a tightening of 125%. That means that an increment of 25% in the tightening of the band causes increments in myopia

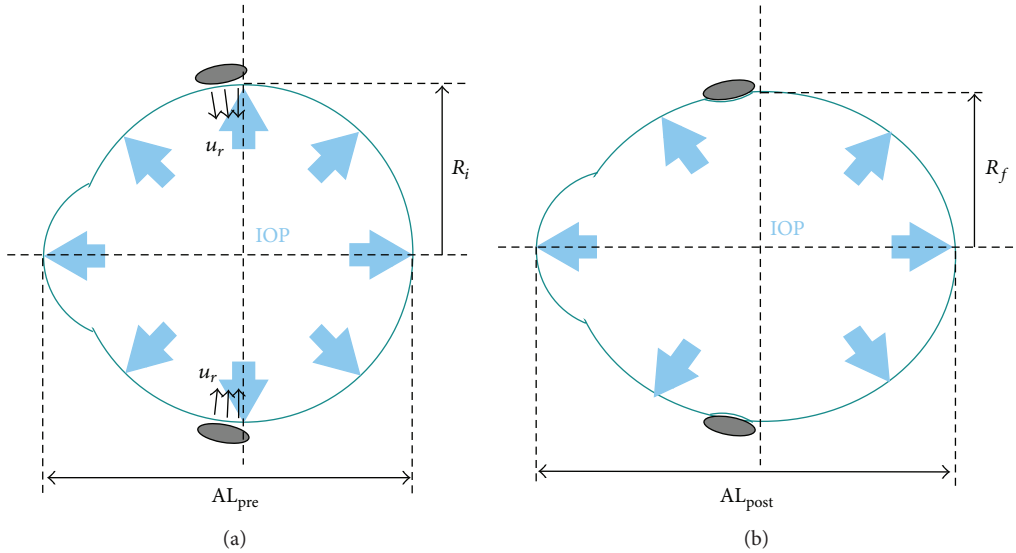

FIGURE 2: Eyeball before (a) and after (b) encircling scleral buckling surgery. The light-blue bold arrows represent the IOP acting on the inner surface of the eye. R_i is the radius of the eyeball at the position where the band is planned to be attached, u_r (line arrows) is the radial displacement towards the inner of the eye at the tightening of the band, AL_{pre} is the axial length of the eye before the surgery, R_f is the radius of the sclera under the band after the implantation, and AL_{pos} is the postsurgical axial length.

TABLE 2: Increment of myopia (ΔD) in diopters (D) induced by the scleral buckling surgery in the numerical model. Nine cases are considered. IOP is the intraocular pressure, BW is the width of the band implanted, AL_{pre} is the axial length before the simulation of the surgery, AL_{pos} is the axial length after the simulation, and ΔAL is the increment of axial length. The mean value of ΔAL and ΔD for each of the three bandwidths is also shown.

Case	IOP (mmHg)	BW (mm)	AL_{pre} (mm)	AL_{pos} (mm)	ΔAL (mm)	ΔD (D)
1	11	2.5	24.860	25.382	0.522	−1.11
2	15	2.5	24.860	25.356	0.496	−1.05
3	18	2.5	24.860	25.359	0.499	−1.06
	Mean ± SD	2.5	—	—	0.51 ± 0.01	−1.07 ± 0.03
4	11	2	24.860	25.273	0.413	−0.88
5	15	2	24.860	25.219	0.359	−0.76
6	18	2	24.860	25.334	0.474	−1.01
	Mean ± SD	2	—	—	0.42 ± 0.06	−0.88 ± 0.12
7	11	1	24.860	25.022	0.162	−0.35
8	15	1	24.860	25.029	0.169	−0.36
9	18	1	24.860	25.149	0.289	−0.62
	Mean ± SD	1	—	—	0.21 ± 0.07	−0.44 ± 0.15

of 136%, 73%, and 76% for the 1, 2, and 2.5 mm wide bands, respectively.

Figure 4 shows the maximal principal stress distribution and the logarithmic strain in the model (15 mmHg) following the simulation of surgery, for the three bandwidths (1.0, 2.0, and 2.5 mm). The highest values of both parameters appear in the area where the band was implanted. Neither the anterior segment nor the optic nerve head area was affected by the simulated surgery.

The anterior segment of the eye model was not altered by the SB simulation in any of the cases since no change was observed in corneal refraction, corneal thickness, and anterior chamber depth.

4. Discussion

Numerical simulation of blunt trauma causing retinal detachment has been accomplished by some authors [30, 31] as well as scleral buckling surgery either from a mechanical approach or by coupling fluid mechanics with structural mechanics [12–14]. Kim et al. [14] simulated encircling SB surgery with a spherical FE model of the eye composed of two layers, outer sclera and inner choroid-retina, using a linear elastic constitutive model to characterize the tissues. Wang et al. [12] studied the effect of segmental SB surgery with FE model of the eye that included the vitreous humor. All the tissues were modelled as hyperelastic materials but considered isotropic.

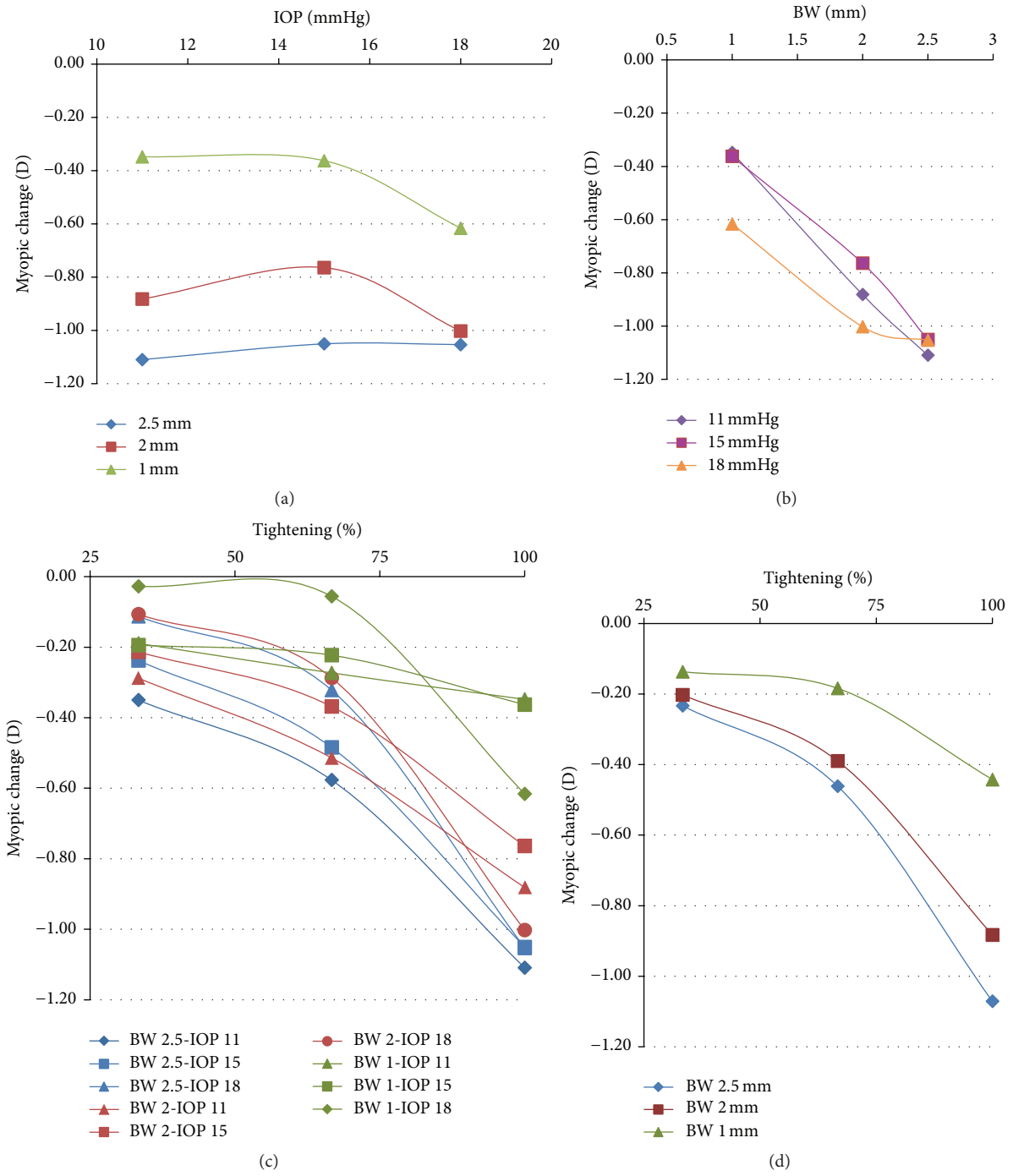

Figure 3: Influence of (a) IOP (mmHg) and (b) BW (mm) on the myopia induced, in diopters (D). No clear tendency of the induced myopia is observed with increasing IOP. On the contrary, bandwidth has a role in the postsurgical myopia change. The wider the band is, the greater the degree of myopia is induced. (c) Myopic changes obtained for all the simulated cases. (d) Mean values of the myopic change induced by the three bandwidths considered: 1, 2, and 2.5 mm.

In this work, we introduced anisotropy in those parts of the FE corresponding to tissues with fibres preferentially aligned in given directions [8, 27].

The encircling scleral buckling procedure enlarges the axial length of the eye, resulting in an increment of myopia, which has been the object of the present study. A finite element model of the eye was developed to evaluate the myopic effect of this technique by means of numerical simulation. The purpose is to present a numerical tool to analyze the encircling SB surgery in a numerical approach for predicting its effect on the human eye before the surgery. All the parameters involved, such as bandwidth, IOP value, and

Table 3: Increment of myopia (ΔD) in diopters (D) induced by the scleral buckling surgery in the numerical model for the nine cases considered (bandwidths of 1, 2, and 2.5 mm; IOP of 11, 15, and 18 mmHg) at three different levels of tightening (33%, 67%, and 100%). Since no relation is observed with IOP, the mean value of the myopia induced for each of the three bandwidths is also shown.

Case	IOP (mmHg)	BW (mm)	ΔD (D) 33%	ΔD (D) 67%	ΔD (D) 100%
1	11	2.5	−0.35	−0.58	-1.11
2	15	2.5	−0.24	−0.48	-1.05
3	18	2.5	−0.11	−0.32	-1.06
	Mean ± SD	2.5	−0.23 ± 0.12	−0.46 ± 0.13	−1.07 ± 0.03
4	11	2	−0.29	−0.51	-0.88
5	15	2	−0.21	−0.37	-0.76
6	18	2	−0.11	−0.29	-1.01
	Mean ± SD	2	−0.20 ± 0.09	−0.39 ± 0.11	−0.88 ± 0.12
7	11	1	−0.19	−0.27	-0.35
8	15	1	−0.19	−0.22	-0.36
9	18	1	−0.03	−0.06	-0.62
	Mean ± SD	1	−0.14 ± 0.09	−0.18 ± 0.11	−0.44 ± 0.15

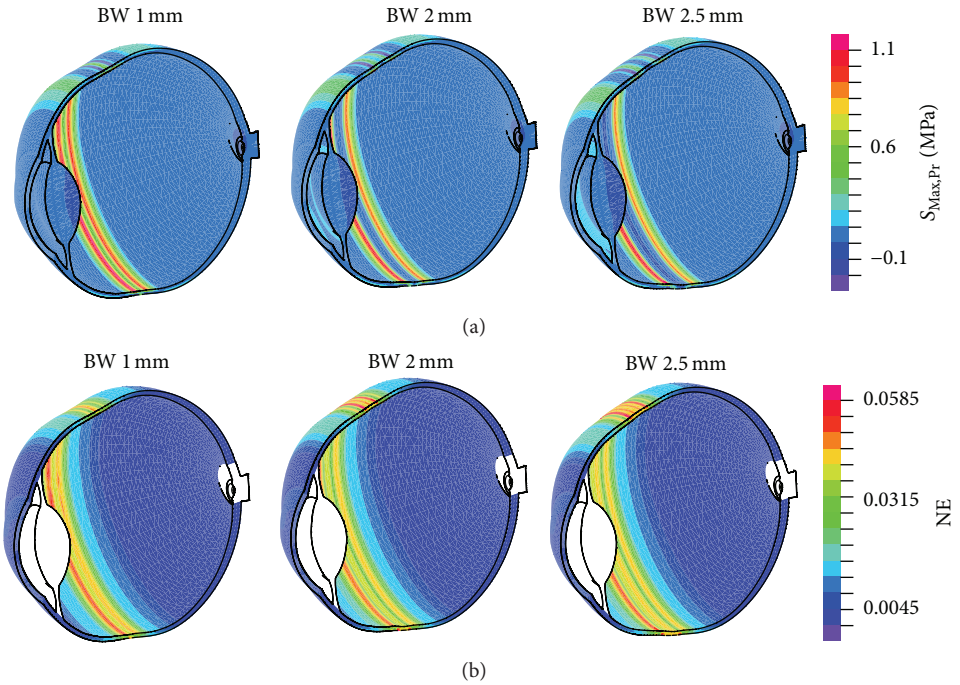

Figure 4: Stress and strain distribution in the model after surgery. The three upper images show the maximal principal stress ($S_{Max,Pr}$) distribution (in MPa) in the model of the eye after the simulation of 1, 2, and 2.5 mm wide bands at an IOP of 15 mmHg. The images at the bottom show the logarithmic strain NE (nondimensional) in the model after the simulation of the surgery for the same three cases.

tightening of the encircling silicone element, can be modified and their effects can be analyzed, while the eye features remain invariable. For this reason, a parametric model is necessary to firstly assess the effect of each variation on the human eye. This type of model has the advantage that many variations can be performed without compromising the patient functionality. This would also considerably reduce the number of experimental animal models.

In a future step, once clinically validated, the numerical simulations could be applied to a patient specific model for predicting the effect of the surgery on a specific subject before performing the encircling. This validation is crucial before the numerical tool can be accepted and introduced in the daily clinical praxis. However, this validation is not provided in this work because it is out of the aim of the study, which is oriented to providing qualitative results of the SB surgery.

Our conclusions must be considered from a qualitative point of view. If particular values were required, then a patient specific model should be developed, which entails an accurate modelling of both the geometry and the tissue mechanical response. In the clinical practice, each eyeball presents different dimensions; therefore the same values of

the treatment parameters (bandwidth, etc.) induce a different degree of myopia on each patient. Those results obtained by numerical simulation can help the ocular surgeon to choose the optimal parameters while planning the surgery.

However, it has to be noted that different surgeons normally used different techniques when performing ocular surgery. For this reason, the application in the clinics of the results coming from the numerical simulations, which may provide a kind of numerical tool for surgical planning, may strongly depend on the surgeon and on the variability of the surgical technique. In this sense, the results presented in this work have to be considered as a first step into the future application of numerical techniques for clinical scopes. Considering that some surgeries are nowadays standard, we can reasonably assume this point as limitation of this study.

The numerical simulation showed no significant change in the anterior segment morphology (corneal curvature, corneal thickness, and anterior chamber depth) following the surgery. Therefore, the anterior segment resulted as unaltered after the simulation of SB. This conclusion is consistent with the clinical findings of previous studies in the literature [4, 5]. Other authors found a significant modification of the anterior chamber depth after the encircling band surgery [6, 7] but reported that the anterior chamber depth returned to normal at 1 year after surgery [7].

We analyzed the influence of silicone bandwidth, tightening degree, and IOP value on the myopic increment induced by the SB surgery. Regarding the bandwidth, the widest band (2.5 mm) caused the highest increment in myopia (1.07 D); hence we can conclude that the bandwidth plays a relevant role in the final myopia. The induced myopia due to the axial length increment is directly related to the width of the band. Moreover, other studies also found a strong relation with the thickness of the encircling silicone element [14], which we did not consider in our study.

We used a noncommercial 1 mm wide band to analyze the effect of the bandwidth on the eyeball lengthening. As expected, axial length was increased while the anterior segment dimensions remained intact. Nevertheless, the stress distribution in the scleral tissue next to the band was acutely concentrated, causing local effects which may lead to scleral tissue damage. This effect observed in the numerical model after the SB simulation reproduces a described complication of the technique pioneered by Arruga [32] who performed equatorial cerclage with a nylon, silk, or supramid suture, which in some patients produced a necrosis of the scleral tissue leading to intrusion of the suture into the eye [33].

The effect of the tightening of different bandwidths on the myopia change induced was also analyzed. Figure 3(d) shows a nonlinear relation between the tightening level and the increment of myopia induced. At 75% of the total tightening, the level of induced myopia is lower than half of the value of myopia at 100% tightening. The fitting function predicts considerable increments of induced myopia for levels of tightening over 100%, for all the bandwidths considered. An increment of 25% in the tightening of the band causes increments in myopia of more than 70% in all the three cases considered. From a clinical point of view, our results suggest that the surgeon should avoid overtightening of the implant. Moreover, it may also affect the anterior segment of the eye. These considerations should be validated with clinical studies.

Regarding IOP, we found no relation of the increment in myopia with this parameter. The variations considered here for the IOP (from 11 to 18 mmHg), that is, 7 mmHg, have shown to be negligible for this study. This result is consistent with Wang et al. [12] who observed a minimal effect of IOP values on the stress of the tissue following surgery. The values of IOP evaluated in our cases of simulation correspond to typical values in case of rhegmatogenous retinal detachment, which is usually preoperatively decreased. The IOP variation caused by the surgery cannot be measured by the numerical simulation process since the IOP value is an input parameter for the model.

With respect to the level of myopia induced by the surgery, the maximal value of myopia change in this study was obtained for the 2.5 mm wide band and IOP of 11 mmHg. In that case, the axial length was enlarged 0.52 mm corresponding to an increment of myopia of −1.1 D. In order to assess these outcomes, we only found a similar work in the literature (Kim et al. [14]). In contrast to our results, their model showed modification of the corneal curvature as well as shortening of the optical length of the eye; therefore the refractive error was modified following surgery. These results, opposite to ours, may be due to the absence of crystalline lens and ciliary body in their model, thus making it weaker. Moreover, the difference in the initial geometry of the model (they considered a spherical shape of the eye) may also cause differences between the two works. However, as it was explained above, the postsurgical values supplied by the simulation with our model correspond to the dimensions assigned to the preoperative model, and patient specific values would give more accurate results. The same value of inner radial displacement in a smaller eyeball would cause a greater effect since it would mean a greater tightening of the band. Kim et al. [14] reached the same conclusion in their study when the eyeball size was reduced by 15%. They observed an increment in the maximum stress in the sclera with respect to the reference size model under the same value of indentation force and IOP.

An important limitation of the presented work is that additional clinical studies are necessary to validate the refractive changes predicted by our model. The increment in myopia found here is slightly lower than the clinical outcome obtained by Smiddy et al. [34] in 75 eyes whose average induced myopia was 2.75 D with an average increased axial length of 0.99 mm. Some of these eyes were also implanted with a radial element, which would increase the myopia induced by the encircling surgery. Goezinne et al. [7] reported in a clinical study with 38 eyes a myopic change of 2.6 D for an axial length increment of 0.7 mm. This greater effect of the surgery on the induced myopia may be due to the use of a radial or segmental buckle associated with the encircling band in the reported cases. To achieve clinical validation of our results, patient specific models will help in the future, but it is out of the aim of this paper.

We also analyzed the stress distribution in the tissue after the surgery. The maximal level of stress obtained in our study

is considerably lower than that considered to cause tissue damage. We obtained a maximal value of stress of 1.1 MPa in the most unfavorable of the cases (2.5 mm wide band with an IOP of 18 mmHg). According to Uchio et al. [35], the failure of the scleral tissue happens at a 6.8% strain, corresponding to a stress value of 9.5 MPa, and the linear elastic behavior ends at about 6.6 MPa. That means that between both values the tissue is damaged. Therefore, the stress value after the surgery is considerably lower than the elastic limit of the sclera, which means that no damage was caused.

One obstacle to overcome when modelling the eyeball is deciding the boundary conditions to impose. In this work, both the anterior segment and the optic nerve insertion of the model were free to move, whereas the eyeball in physiological conditions is fitted into the socket and surrounded by tissues in such a way that backward movement would be almost negligible. If we reproduce that situation in our model, that is, the backward movement set to zero, then the stress distribution in the retinal area computed by simulation would give unreasonable maximal values of stress, which would mean an overestimation of the damage caused by the SB surgery. Since this work was not intended to study the squashing of the back of the eye or the optical nerve, we assumed this as limitation of the model. Wang et al. [12] constrained the exterior posterior wall of the eyeball, nevertheless, they did not analyze the stress in the optical nerve head area but in the surroundings of the encircling implant, and hence the local effect of this boundary condition did not affect their area of interest.

In this study, we presented a numerical tool to estimate the myopic effect of the SB surgery on the human eye. In this sense we provided qualitative results based on different parameters of the encircling procedure. For an exact quantification of the myopic effect, a clinical validation based on clinical cases would be necessary to contrast the provided results. In particular, the design of models based on patient specific geometries instead of parametric values such as those used in this work will help improving the quality of the results and will help assessing the reliability of the clinical outcomes.

Abbreviations

FE: Finite element
SB: Scleral buckling
IOP: Intraocular pressure
RRD: Rhegmatogenous retinal detachment
PPV: *Pars plana* vitrectomy.

Disclosure

The authors alone are responsible for the content and writing of the paper.

Competing Interests

The authors declare no conflict of interests.

Acknowledgments

The authors wish to acknowledge the research support by the Spanish Ministry of Education and Science Research Project DPI2014-54981R, the CIBER initiative, Instituto de Salud Carlos III (ISCIII) Platform for Biological Tissue Characterization of the Centro de Investigación Biomédica en Red en Bioingeniería, Biomateriales y Nanomedicina (CIBER-BBN), and the Department of Industry and Innovation (Government of Aragón) through the research group Grant T88 (Fondo Social Europeo).

References

[1] E. Custodis, "Treatment of retinal detachment by circumscribed diathermal coagulation and by scleral depression in the area of tear caused by imbedding of a plastic implant," *Klinische Monatsblätter für Augenheilkunde*, vol. 129, pp. 476–495, 1956.

[2] C. L. Schepens, I. D. Okamura, and R. J. Brockhurst, "The scleral buckling procedures. I. Surgical techniques and management," *A.M.A. Archives of Ophthalmology*, vol. 58, no. 6, pp. 797–811, 1957.

[3] R. Machemer, H. Buettner, E. W. Norton, and J. M. Parel, "Vitrectomy: a pars plana approach," *Transactions of the American Academy of Ophthalmology and Otolaryngology*, vol. 75, no. 4, pp. 813–820, 1971.

[4] M. Citirik, C. Batman, G. Acaroglu, C. Can, O. Zilelioglu, and F. Koc, "Analysis of changes in corneal shape and bulbus geometry after retinal detachment surgery," *International Ophthalmology*, vol. 25, no. 1, pp. 43–51, 2004.

[5] E. Ruiz–De-Gopegui, F. Ascaso, M. Del Buey, and J. Cristóbal, "Efecto del cerclaje escleral en la cirugía vítreo-retiniana sobre la morfología y biomecánica de la córnea," *Archivos de la Sociedad Española de Oftalmología*, vol. 86, no. 11, pp. 363–367, 2011.

[6] E. Cetin, Z. Ozbek, A. O. Saatci, and I. Durak, "The effect of scleral buckling surgery on corneal astigmatism, corneal thickness, and anterior chamber depth," *Journal of Refractive Surgery*, vol. 22, no. 5, pp. 494–499, 2006.

[7] F. Goezinne, E. C. La Heij, T. T. J. M. Berendschot et al., "Anterior chamber depth is significantly decreased after scleral buckling surgery," *Ophthalmology*, vol. 117, no. 1, pp. 79–85, 2010.

[8] E. Lanchares, B. Calvo, J. A. Cristóbal, and M. Doblaré, "Finite element simulation of arcuates for astigmatism correction," *Journal of Biomechanics*, vol. 41, no. 4, pp. 797–805, 2008.

[9] J. A. Cristóbal, M. A. D. Buey, F. J. Ascaso, E. Lanchares, B. Calvo, and M. Doblaré, "Effect of limbal relaxing incisions during phacoemulsification surgery based on nomogram review and numerical simulation," *Cornea*, vol. 28, no. 9, pp. 1042–1049, 2009.

[10] E. Lanchares, B. Calvo, M. A. Del Buey, J. A. Cristóbal, and M. Doblaré, "The effect of intraocular pressure on the outcome of myopic photorefractive keratectomy: a numerical approach," *Journal of Healthcare Engineering*, vol. 1, no. 3, pp. 461–476, 2010.

[11] Z. G. Sun and A. Makinouchi, "FEM program for a coupling analysis of a hyperelastic solid and static liquid to simulate the retinal detachment operation on an eyeball," in *Proceedings of the Riken Symposium*, pp. 80–93, 2000.

[12] F. Wang, H. P. Lee, and C. Lu, "Biomechanical effect of segmental scleral buckling surgery," *Current Eye Research*, vol. 32, no. 2, pp. 133–142, 2007.

[13] W. J. Foster, N. Dowla, S. Y. Joshi, and M. Nikolaou, "The fluid mechanics of scleral buckling surgery for the repair of retinal detachment," *Graefe's Archive for Clinical and Experimental Ophthalmology*, vol. 248, no. 1, pp. 31–36, 2010.

[14] Y. Kim, Y. Na, J. Kim, and J. Seo, "Quantitative analysis of ocular structure after scleral buckle encircling," in *Proceedings of the 5th European Conference of the International Federation for Medical and Biological Engineering*, Á. Jobbágy, Ed., vol. 37, pp. 267–270, Budapest, Hungary, 2011.

[15] A. Pandolfi, G. Fotia, and F. Manganiello, "Finite element simulations of laser refractive corneal surgery," *Engineering with Computers*, vol. 25, no. 1, pp. 15–24, 2009.

[16] H. P. Studer, H. Riedwyl, C. A. Amstutz, J. V. M. Hanson, and P. Büchler, "Patient-specific finite-element simulation of the human cornea: a clinical validation study on cataract surgery," *Journal of Biomechanics*, vol. 46, no. 4, pp. 751–758, 2013.

[17] I. Simonini and A. Pandolfi, "Customized finite element modelling of the human cornea," *PLoS ONE*, vol. 10, no. 6, Article ID e0130426, 2015.

[18] R. Navarro, L. González, and J. L. Hernández, "Optics of the average normal cornea from general and canonical representations of its surface topography," *Journal of the Optical Society of America A*, vol. 23, no. 2, pp. 219–232, 2006.

[19] T. W. Olsen, S. Y. Aaberg, D. H. Geroski, and H. F. Edelhauser, "Human sclera: thickness and surface area," *American Journal of Ophthalmology*, vol. 125, no. 2, pp. 237–241, 1998.

[20] K. M. Meek and R. H. Newton, "Organization of collagen fibrils in the corneal stroma in relation to mechanical properties and surgical practice," *Journal of Refractive Surgery*, vol. 15, no. 6, pp. 695–699, 1999.

[21] A. Eilaghi, J. G. Flanagan, I. Tertinegg, C. A. Simmons, G. W. Brodland, and C. R. Ethier, "Biaxial mechanical testing of human sclera," *Journal of Biomechanics*, vol. 43, no. 9, pp. 1696–1701, 2010.

[22] J. R. Kuszak, R. K. Zoltoski, and C. E. Tiedemann, "Development of lens sutures," *International Journal of Developmental Biology*, vol. 48, no. 8-9, pp. 889–902, 2004.

[23] R. M. Pedrigi, G. David, J. Dziezyc, and J. D. Humphrey, "Regional mechanical properties and stress analysis of the human anterior lens capsule," *Vision Research*, vol. 47, no. 13, pp. 1781–1789, 2007.

[24] G. A. Holzapfel, *Nonlinear Solid Mechanics: A Continuum Approach for Engineering*, John Wiley & Sons, New York, NY, USA, 2000.

[25] J. C. Simo and R. L. Taylor, "Consistent tangent operators for rate-independent elastoplasticity," *Computer Methods in Applied Mechanics and Engineering*, vol. 48, no. 1, pp. 101–118, 1985.

[26] A. J. M. Spencer, "Theory of invariants," in *Continuum Physics*, Academic Press, New York, NY, USA, 1954.

[27] E. Lanchares, R. Navarro, and B. Calvo, "Hyperelastic modelling of the crystalline lens: accommodation and presbyopia," *Journal of Optometry*, vol. 5, no. 3, pp. 110–120, 2012.

[28] A. J. Bellezza, R. T. Hart, and C. F. Burgoyne, "The optic nerve head as a biomechanical structure: initial finite element modeling," *Investigative Ophthalmology & Visual Science*, vol. 41, no. 10, pp. 2991–3000, 2000.

[29] I. A. Sigal, J. G. Flanagan, I. Tertinegg, and C. R. Ethier, "Finite element modeling of optic nerve head biomechanics," *Investigative Ophthalmology and Visual Science*, vol. 45, no. 12, pp. 4378–4387, 2004.

[30] T. Rossi, B. Boccassini, L. Esposito et al., "The pathogenesis of retinal damage in blunt eye trauma: finite element modeling," *Investigative Ophthalmology & Visual Science*, vol. 52, no. 7, pp. 3994–4002, 2011.

[31] R. Bhardwaj, K. Ziegler, J. H. Seo, K. T. Ramesh, and T. D. Nguyen, "A computational model of blast loading on the human eye," *Biomechanics and Modeling in Mechanobiology*, vol. 13, no. 1, pp. 123–140, 2014.

[32] H. Arruga, "Le cerclage equatorial pour traiter le decollement retinien," *Bulletins et Mémoires de la Société Française d'Ophtalmologie*, vol. 71, pp. 571–580, 1958.

[33] A. J. Dark and S. N. M. Rizk, "Untoward sequels of Arruga encirclement for retinal detachment: report on 29 cases," *British Journal of Ophthalmology*, vol. 49, no. 5, pp. 259–263, 1965.

[34] W. E. Smiddy, D. N. Loupe, R. G. Michels, C. Enger, B. M. Glaser, and S. deBustros, "Refractive changes after scleral buckling surgery," *Archives of Ophthalmology*, vol. 107, no. 10, pp. 1469–1471, 1989.

[35] E. Uchio, S. Ohno, J. Kudoh, K. Aoki, and L. T. Kisielewicz, "Simulation model of an eyeball based on finite element analysis on a supercomputer," *British Journal of Ophthalmology*, vol. 83, no. 10, pp. 1106–1111, 1999.

Hindawi Publishing Corporation
Journal of Ophthalmology
Volume 2016, Article ID 5641273, 5 pages
http://dx.doi.org/10.1155/2016/5641273

Clinical Study

Relationship between Peeled Internal Limiting Membrane Area and Anatomic Outcomes following Macular Hole Surgery: A Quantitative Analysis

Yasin Sakir Goker,[1] Mustafa Koc,[1] Kemal Yuksel,[2] Ahmet Taylan Yazici,[2] Abdulvahit Demir,[3] Hasan Gunes,[2] and Yavuz Ozpinar[2]

[1] *Ulucanlar Eye Training and Research Hospital, 06240 Ankara, Turkey*
[2] *Beyoglu Eye Training and Research Hospital, 34420 Istanbul, Turkey*
[3] *Kagıthane Government Hospital, Ophthalmology Department, 34416 Istanbul, Turkey*

Correspondence should be addressed to Yasin Sakir Goker; yasingoker5367@hotmail.com

Received 23 February 2016; Accepted 29 May 2016

Academic Editor: George M. Saleh

Purpose. To quantitatively evaluate the effects of peeled internal limiting membrane (ILM) area and anatomic outcomes following macular hole surgery using spectral domain optical coherence tomography (SD-OCT). *Methods*. Forty-one eyes in 37 consecutive patients with idiopathic, Gass stage 3-4 macular hole (MH) were enrolled in this retrospective comparative study. All patients were divided into 2 groups according to anatomic success or failure. Basal MH diameter, peeled ILM area, and MH height were calculated using SD-OCT. Other prognostic parameters, including age, stage, preoperative BCVA, and symptom duration were also assessed. *Results*. Thirty-two cases were classified as anatomic success, and 9 cases were classified as anatomic failure. Peeled ILM area was significantly wider and MH basal diameter was significantly less in the anatomic success group ($p = 0.024$ and 0.032, resp.). Other parameters did not demonstrate statistical significance. *Conclusion*. The findings of the present study show that the peeled ILM area can affect the anatomic outcomes of MH surgery.

1. Introduction

Internal limiting membrane (ILM) peeling is a crucial part of macular hole (MH) surgery [1], and using ILM peeling to remove and treat epiretinal membrane (ERM) improves anatomical outcomes [2]. Histological examinations show that ERM consists of pieces of the ILM [3]. The importance of the ILM in the pathogenesis of MH was also reported by Yoon et al. [4]. Pars plana vitrectomy (PPV) and ILM peeling are used to treat not only MH, but also ERM, diabetic macular edema, and retinal vein occlusion-related macular edema [5].

Optical coherence tomography (OCT) is the gold standard for diagnosing MH and assessing anatomic outcomes after surgery. OCT also provides prognostic information, such as basal MH diameter, MH height, MH minimum diameter, and other indexes of MH formation [6, 7]. Spectral domain optical coherence tomography (SD-OCT) can also assess structural changes in the macular layers, such as the inner and outer segment (IS/OS) and external limiting membrane [8, 9].

Age, basal MH diameter, MH index (MHI), stage, symptom duration, ILM peeling, and preoperative visual acuity affect the anatomic outcomes of MH surgery [10, 11]. However, no studies assess the relationship between peeled ILM area and anatomic outcomes following MH surgery. This study quantitatively evaluates the effects of peeled ILM area on open and surgically closed MHs.

2. Subjects and Methods

Forty-one eyes in 37 consecutive patients with idiopathic, Gass stage 3-4 MH were enrolled in this retrospective comparative study. The participants were classified as anatomic success or anatomic failure.

All MH cases underwent standard, sutureless, 3-port, 23-gauge vitrectomy surgery between March 2012 and March 2014. All surgeries were performed by the same surgeon (Ahmet Taylan Yazici) at Beyoglu Eye Research and Training Hospital. All patients received a complete ophthalmic examination, including measurement of best corrected visual acuity (BCVA) using an ETDRS chart, biomicroscopy of the anterior segment, and dilated fundus examination; all examinations were performed preoperatively on day 1 and week 1 and 1, 3, and 6 months after surgery. Spectral domain optical coherence tomography (SD-OCT) (SPECTRALIS® Heidelberg Engineering, Heidelberg, Germany) was used preoperatively to assess each patient and postoperatively at 1, 3, and 6 months.

Inclusion criteria were stage 3-4 MH according to the Gass classifications [12]. Exclusion criteria included refractive error > −6.00 D, traumatic MH, and history of ocular surgery (except phacoemulsification). Symptom duration was defined as the number of weeks from diagnosis to surgery. All patients provided informed consent prior to surgery, and this study adheres to the Declaration of Helsinki.

2.1. Surgery. All patients underwent standard, sutureless, 3-port, 23-gauge (G) pars plana vitrectomy (PPV) with triamcinolone acetonide- (TA-) assisted posterior vitreous detachment (PVD) (if not already present). The ILM was grasped using ILM forceps and peeled off the retina using 0.2 mL of brilliant blue G dye (Brilliant Peel; Geuder, Heidelberg, Germany). The area of the removed ILM was intended to reach the vascular arcades of the macula. Fluid-air exchange was performed through an extrusion cannula to flatten the hole, which was followed by the injection of 15% perfluoropropane (C_3F_8) or 20% sulfur hexafluoride (SF_6). Patients were postoperatively maintained in the prone position for 5 days. Anatomic success was defined as complete MH closure and the absence of subretinal fluid on SD-OCT. Anatomic failure was defined as open MH after the first surgery.

2.2. SD-OCT. Every patient's SD-OCT parameters were separately analyzed by 2 observers. The initial set of measurements was recorded by the first observer. A second observer—who was blind to the results of the first observer—performed the same measurements in order to assess inter-observer reproducibility. The first observer then scanned the same patient again to measure the same parameters and thereby assess intraobserver reliability. To reduce the likelihood of intraobserver bias, >10 minutes was allowed to elapse before the first observer repeated the measurements. The observers were not present in the OCT room during each other's examinations and were unaware of each other's final measurements.

Twenty-five horizontal scans through the fovea were preoperatively and postoperatively performed. Only the lowest section of the retinal macula was scanned to evaluate peeled ILM area. The borders of the peeled and nonpeeled ILM were seen and marked on the OCT scan. The software of the device calculates the area of the peeled ILM in square millimeters (Figure 1). The arithmetic means of by both observers were used in further analyses.

Basal MH diameter was defined as the diameter at the widest MH cross-section at the retinal pigment epithelium (RPE) [6, 7]. MH height was measured from the RPE to the top of the MH. MHI (hole height/basal hole diameter) was calculated using previously described methods [6]. Anatomic success was defined by complete MH closure and the absence of subretinal fluid on SD-OCT at month 1 postoperatively.

Table 1: Baseline parameters and demographic data.

Variable	Anatomical success (Group 1)	Anatomical failure (Group 2)	p value
Eyes (N)	32	9	
Gender (N)			
Male	9 (31.0%)	2 (25%)	
Female	20 (69.0%)	6 (75%)	
Age, years			0.762*
Mean ± SD	67.1 ± 7.3	66.3 ± 5.7	
Range	57–85	59–81	
Stage (N)			0.176**
3	11 (34.4%)	1 (11.1%)	
4	21 (65.6%)	8 (88.9%)	

*t-test.
**Mann-Whitney test.

2.3. Statistical Analysis. The statistical analysis was performed using SPSS (Statistical Package for the Social Sciences) (version 16 for Windows; SPSS Inc.). The normality of the data was confirmed using the Kolmogorov-Smirnov test ($p > 0.05$). One-way ANOVA was used to evaluate homogeneity between groups ($p > 0.05$). Groups were analyzed using the parametric t-test or nonparametric Mann-Whitney test. Multiple regression analysis was used to determine if there was a significant association between anatomic outcomes and several factors, including Gass stage, basal MH diameter, peeled ILM area, MHI, symptom duration, and preoperative BCVA. BCVA was converted to logMAR (logarithm of the minimal angle of resolution) equivalents for the statistical analysis. In this study, $p < 0.05$ is considered statistically significant.

3. Results

Thirty-seven patients met our inclusion criteria, and 4 had bilateral MH. The mean follow-up period was 17.4 months (range = 6–30 months). Baseline parameters and patient demographic data are presented in Table 1. Thirty-two cases were included in the anatomic success group, and 9 cases were included in the anatomic failure group. The mean ages of the patients in each group were 67.1 ± 7.3 and 66.3 ± 5.7 years, respectively.

The clinical characteristics of participants are shown in Table 2. Thirty-four eyes were phakic, and 7 eyes were pseudophakic. Three patients developed significant cataracts

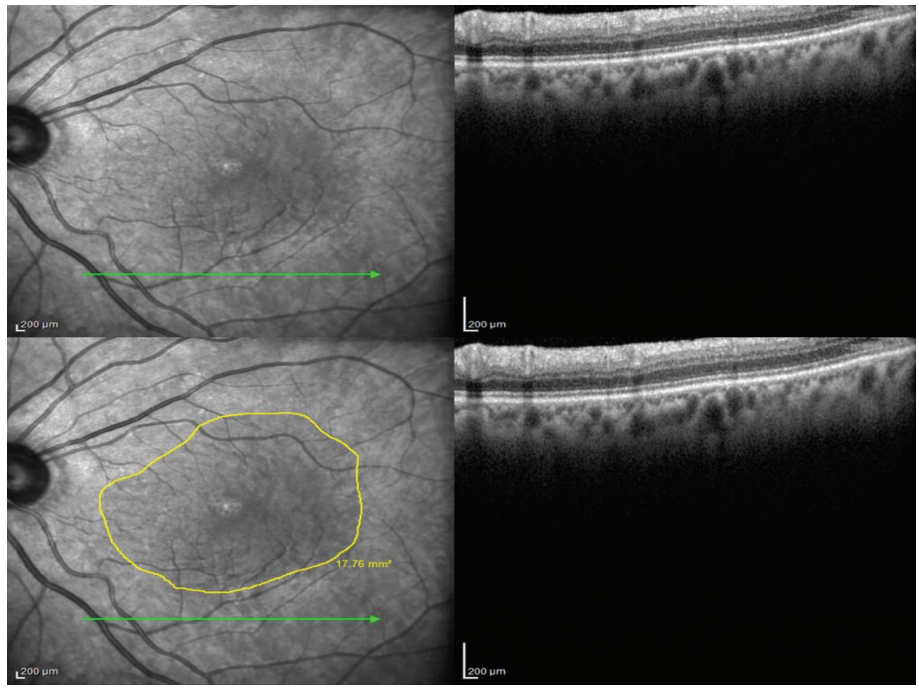

Figure 1: The borders of the peeled ILM area were marked, and the area was calculated using spectral domain optical coherence tomography.

during follow-up and underwent phacoemulsification with intraocular lens implantation. No significant difference in lens status was found between groups ($p = 0.147$). Phacoemulsification with intraocular lens implantation was combined with MH surgery in 2 cases. Therefore, combination surgery did not demonstrate a significant influence ($p = 0.332$). Perfluoropropane (C_3F_8) was used in 33 eyes as tamponade, and sulfur hexafluoride (SF_6) was used in 8 eyes. There was no significant difference between eyes treated with C_3F_8 or SF_6 in terms of anatomic outcomes ($p = 0.616$).

Mean preoperative BCVA was 0.85 ± 0.33 logMAR, which postoperatively improved to 0.66 ± 0.37 logMAR ($p = 0.001$) (0.87 ± 0.36 versus 0.80 ± 0.25 logMAR in patients classified as anatomic success or failure, resp., however, there was no significant difference between groups ($p = 0.936$)). Symptom duration was 18.9 ± 12.8 versus 17.22 ± 14.65 weeks in patients classified as anatomic success or failure, respectively. Therefore, symptom duration did not demonstrate a significant difference between groups ($p = 0.738$).

Mean peeled ILM area was $16.51 \pm 6.15\ mm^2$ (range = 3.90–30.0 mm^2) and $12.8 \pm 4.0\ mm^2$ (range = 6.89–17.67 mm^2) in patients classified as anatomic success or failure. There was a statistically significant difference between groups in terms of peeled ILM area ($p = 0.024$). Mean basal MH diameter was $963.2 \pm 325.1\ \mu m$ (range = 302–1625 μm) and $1426.0 \pm 621.3\ \mu m$ (range = 760–2627 μm) in anatomic success and failure patients, respectively. Basal MH diameter was also significantly different between groups ($p = 0.032$). Furthermore, there was a significant association between anatomic outcomes and 2 factors—basal MH diameter and peeled ILM area ($p = 0.001$ and 0.009, resp.)—according to the multiple regression analysis (shown in Table 3).

The primary and final anatomic success rates were 78% (32 of 41 cases) and 92.7% (38 of 41 cases), respectively. Overall, 9 cases remained open (anatomic failure) after the first surgery, and second surgery was recommended for 8 cases. One case that had not been recommended for second surgery developed wide RPE atrophy and would not have benefited from surgery. Among the open MHs, 2 patients could not postoperatively maintain the prone position for 5 days and subsequently refused additional surgery.

4. Discussion

Over the past 20 years, ILM peeling has played a crucial role in the surgical treatment of a variety of retinal disorders, including epiretinal membrane, MH, diabetic macular edema, and retinal vein occlusions. The available evidence supports using ILM peeling as the treatment of choice for patients with idiopathic stages 2–4 MH [13]. ILM removal relieves the forces around the fovea, including those that are tangential and axial; however, there is no general consensus regarding the extent of the ILM area that should be peeled [5]. In this retrospective study, we found that larger peeled areas demonstrated better anatomic outcomes.

Many factors affect anatomic outcomes, and age, Gass stage, basal MH diameter, MHI, preoperative BCVA, and symptom duration are some prognostic criteria for MH surgery [10, 11]. All could also affect anatomic outcomes. These parameters—including basal MH diameter, MHI, peeled ILM area, Gass stage, symptom duration, and preoperative BCVA—were assessed by our multiple regression analysis, but only MH basal diameter and peeled ILM area were found to be statistically significant.

Table 2: Clinical characteristics of participants.

Variable	Group 1	Group 2	p value
Preoperative BCVA, logMAR			0.936*
Mean ± SD	0.87 ± 0.36	0.80 ± 0.25	
Range	0.4–1.8	0.52–1.3	
Symptom duration, weeks			0.738*
Mean ± SD	18.9 ± 12.8	17.22 ± 14.65	
Range	4–64	4–40	
Lens status, N			0.147**
Phakic	28 (87.5%)	6 (66.7%)	
Pseudophakic	4 (12.5%)	3 (33.3%)	
Tamponade, N			0.616**
C_3F_8	27 (84.4%)	6 (66.7%)	
SF_6	5 (15.6%)	3 (33.3%)	
Surgery, N			0.332**
PPV	31 (96.9%)	8 (88.9%)	
Combined PPV + phaco	1 (3.1%)	1 (11.1%)	
MH basal diameter, μm			**0.032****
Mean ± SD	963.2 ± 325.1	1426.0 ± 621.3	
Range	302–1625	760–2627	
MHI			0.347*
Mean ± SD	0.53 ± 0.25	0.45 ± 0.10	
Range	0.28–1.55	0.30–0.68	
Peeled ILM area, mm^2			**0.024***
Mean ± SD	16.51 ± 6.15	12.8 ± 4.0	
Range	3.90–30.0	6.89–17.67	

Bold values are significant at $p < 0.05$. BCVA, best corrected visual acuity; ILM, internal limiting membrane; MH, macular hole; MHI, macular hole index; PPV, pars plana vitrectomy; phaco, phacoemulsification; μm, micrometer; mm^2, millimeter square.
*t-test.
**Mann-Whitney test.

Table 3: Multiple regression model of variables associated with anatomical outcome.

Variables	95% confidence intervals	p value
MH basal diameter	0.545–0.940	**0.001**
MHI	0.246–0.668	0.137
Peeled ILM area	0.111–0.467	**0.009**
Stage	0.335–0.409	0.461
Symptom duration	0.129–0.601	0.559
Preoperative BCVA	0.358–0.763	0.076

Bold values are significant at $p < 0.01$. BCVA, best corrected visual acuity; ILM, internal limiting membrane; MH, macular hole; MHI, macular hole index.

Balducci et al. reported early and late changes in retinal nerve fiber layer thickness (RNFLT) after ILM peeling for idiopathic macular hole or epiretinal membrane [14]. RNFLT increased at 1 month after surgery, returned to preoperative levels by 3 months, and was lower than basal at 6 months after surgery. Balducci et al. proposed that reduced RNFLT at 6 months after surgery could indicate damage caused by ILM peeling. In addition, according to a retrospective study that used microperimetry, Tadayoni et al. reported that decreased retinal sensitivity was associated with paracentral absolute and relative microscotomas in 8 of 16 eyes following ILM peeling and MH surgery due to large macular holes (>400 mm) [15]. Some authors have proposed that ILM peeling causes the loss of Müller cell footplates and affects retinal function. Terasaki et al. reported delayed implicit time and reduced b-wave amplitude on focal electroretinography (ERG) soon after ILM peeling [16]. Steven et al. reported that ILM peeling may result in retinal weakening via Müller cell damage, which causes structural breakdowns and finally paracentral retinal hole formation. Steven et al., Mason III et al., and Rubinstein et al. have all separately reported the increased risk of secondary paracentral retinal hole formation after ILM peeling [17–19]. On the contrary, Che et al. evaluated 134 eyes in 130 IMH patients who received PPV in combination with ILM peeling (2 disk diameters). Thirteen eyes underwent a second surgery that involved enlarging the peeled ILM area to the vascular arcades of the posterior fundus. MH closure was successfully achieved in 8 of 13 eyes (61.5%) [20].

The surgeon may perform many manipulations to enlarge the peeled ILM area. The retina nerve fiber layers can hemorrhage and iatrogenic retinal holes may develop, and these hemorrhages may result in visual field defects and other retinal alterations. Accordingly, many surgeons do not widen the peeled area, and a smaller peeled ILM results in less of Müller cells loss, stronger retinal structure, lower risk of visual field defects, and paracentral retinal hole formation. On the other hand, small peeled ILM demonstrates worsened anatomic outcomes.

There is tangential traction in the etiology of macular hole formation that is induced by vitreous shrinkage, as observed and reported by Gaudric et al. [21]. We propose that wider ILM peeling relieves this traction more efficiently, therefore resulting in better anatomic outcomes. Here, the mean area of peeled ILM in anatomically successful patients was 16.51 mm^2, whereas patients with anatomic failure demonstrated a mean area of 12.8 mm^2. It is difficult to determine a good cut-off value for the peeled area that confirms the best anatomic outcomes. The surgeon should peel the ILM to as much close to the vascular arcades of the macula as possible.

The limitations of the present study include the relatively small numbers of patients, its retrospective design, and the fact that the peeled ILM borders were only assessed using SD-OCT. Therefore, the peeled area could have been inaccurately measured. Using preoperative ILM markings could improve ILM assessment. Also we did not histologically examine the peeled ILM. A strength of this study is the quantitative assessment of the peeled ILM using SD-OCT. In conclusion, we propose that peeled ILM area is important in MH surgery and that it can affect anatomic outcomes.

Competing Interests

None of the other authors have financial or proprietary interests in any mentioned material or method.

Acknowledgments

This retrospective study was not supported by any of the companies. These data have not been previously published. This retrospective study was accomplished in Beyoglu Eye Training and Research Hospital.

References

[1] H. L. Brooks, "Macular hole surgery with and without internal limiting membrane peeling," *Ophthalmology*, vol. 107, no. 10, pp. 1939–1949, 2000.

[2] O. Liesenhoff, E. M. Messmer, A. Pulur, and A. Kampik, "Treatment of full-thickness idiopathic macular holes," *Ophthalmologe*, vol. 93, no. 6, pp. 655–659, 1996.

[3] E. M. Messmer, H.-P. Heidenkummer, and A. Kampik, "Ultrastructure of epiretinal membranes associated with macular holes," *Graefe's Archive for Clinical and Experimental Ophthalmology*, vol. 236, no. 4, pp. 248–254, 1998.

[4] H. S. Yoon, H. L. Brooks, A. Capone, N. L. L'Hernault, and H. E. Grossniklaus, "Ultrastructural features of tissue removed during idiopathic macular hole surgery," *American Journal of Ophthalmology*, vol. 122, no. 1, pp. 67–75, 1996.

[5] A. Almony, E. Nudleman, G. K. Shah et al., "Techniques, rationale, and outcomes of internal limiting membrane peeling," *Retina*, vol. 32, no. 5, pp. 877–891, 2012.

[6] S. Kusuhara, M. F. Teraoka Escaño, S. Fujii et al., "Prediction of postoperative visual outcome based on hole configuration by optical coherence tomography in eyes with idiopathic macular holes," *American Journal of Ophthalmology*, vol. 138, no. 5, pp. 709–716, 2004.

[7] R. Uemoto, S. Yamamoto, T. Aoki, I. Tsukahara, T. Yamamoto, and S. Takeuchi, "Macular configuration determined by Optical coherence tomography after idiopathic macular hole surgery with or without internal limiting membrane peeling," *British Journal of Ophthalmology*, vol. 86, no. 11, pp. 1240–1242, 2002.

[8] J. Oh, W. E. Smiddy, H. W. Flynn Jr., G. Gregori, and B. Lujan, "Photoreceptor inner/outer segment defect imaging by spectral domain OCT and visual prognosis after macular hole surgery," *Investigative Ophthalmology and Visual Science*, vol. 51, no. 3, pp. 1651–1658, 2010.

[9] E. Ooka, Y. Mitamura, T. Baba, M. Kitahashi, T. Oshitari, and S. Yamamoto, "Foveal microstructure on spectral-domain optical coherence tomographic images and visual function after macular hole surgery," *American Journal of Ophthalmology*, vol. 152, no. 2, pp. 283–290, 2011.

[10] B. Gupta, D. A. H. Laidlaw, T. H. Williamson, S. P. Shah, R. Wong, and S. Wren, "Predicting visual success in macular hole surgery," *British Journal of Ophthalmology*, vol. 93, no. 11, pp. 1488–1491, 2009.

[11] S. Ullrich, C. Haritoglou, C. Gass, M. Schaumberger, M. W. Ulbig, and A. Kampik, "Macular hole size as a prognostic factor in macular hole surgery," *British Journal of Ophthalmology*, vol. 86, no. 4, pp. 390–393, 2002.

[12] J. D. M. Gass, "Reappraisal of biomicroscopic classification of stages of development of a macular hole," *American Journal of Ophthalmology*, vol. 119, no. 6, pp. 752–759, 1995.

[13] K. Spiteri Cornish, N. Lois, N. W. Scott et al., "Vitrectomy with internal limiting membrane peeling versus no peeling for idiopathic full-thickness macular hole," *Ophthalmology*, vol. 121, no. 3, pp. 649–655, 2014.

[14] N. Balducci, M. Morara, C. Veronese, C. Torrazza, F. Pichi, and A. P. Ciardella, "Retinal nerve fiber layer thickness modification after internal limiting membrane peeling," *Retina*, vol. 34, no. 4, pp. 655–663, 2014.

[15] R. Tadayoni, I. Svorenova, A. Erginay, A. Gaudric, and P. Massin, "Decreased retinal sensitivity after internal limiting membrane peeling for macular hole surgery," *British Journal of Ophthalmology*, vol. 96, no. 12, pp. 1513–1516, 2012.

[16] H. Terasaki, Y. Miyake, R. Nomura et al., "Focal macular ERGs in eyes after removal of macular ILM during macular hole surgery," *Investigative Ophthalmology and Visual Science*, vol. 42, no. 1, pp. 229–234, 2001.

[17] P. Steven, H. Laqua, D. Wong, and H. Hoerauf, "Secondary paracentral retinal holes following internal limiting membrane removal," *British Journal of Ophthalmology*, vol. 90, no. 3, pp. 293–295, 2006.

[18] J. O. Mason III, R. M. Feist, and M. A. Albert Jr., "Eccentric macular holes after vitrectomy with peeling of epimacular proliferation," *Retina*, vol. 27, no. 1, pp. 45–48, 2007.

[19] A. Rubinstein, R. Bates, L. Benjamin, and A. Shaikh, "Iatrogenic eccentric full thickness macular holes following vitrectomy with ILM peeling for idiopathic macular holes," *Eye*, vol. 19, no. 12, pp. 1333–1335, 2005.

[20] X. Che, F. He, L. Lu et al., "Evaluation of secondary surgery to enlarge the peeling of the internal limiting membrane following the failed surgery of idiopathic macular holes," *Experimental and Therapeutic Medicine*, vol. 7, no. 3, pp. 742–746, 2014.

[21] A. Gaudric, B. Haouchine, P. Massin, M. Paques, P. Blain, and A. Erginay, "Macular hole formation: new data provided by optical coherence tomography," *Archives of Ophthalmology*, vol. 117, no. 6, pp. 744–751, 1999.

Hindawi Publishing Corporation
Journal of Ophthalmology
Volume 2016, Article ID 6347236, 5 pages
http://dx.doi.org/10.1155/2016/6347236

Research Article

Comparison between a New Optical Biometry Device and an Anterior Segment Optical Coherence Tomographer for Measuring Central Corneal Thickness and Anterior Chamber Depth

Jinhai Huang,[1,2] Weicong Lu,[1,2] Giacomo Savini,[3] Hao Chen,[1] Chengfang Wang,[1] Xinxin Yu,[1] Fangjun Bao,[1,2] and Qinmei Wang[1,2]

[1]*School of Ophthalmology and Optometry, Wenzhou Medical University, Wenzhou, Zhejiang, China*
[2]*Key Laboratory of Vision Science, Ministry of Health, Wenzhou, Zhejiang, China*
[3]*G.B. Bietti Foundation IRCCS, Rome, Italy*

Correspondence should be addressed to Fangjun Bao; bfjmd@126.com and Qinmei Wang; wqm6@mail.eye.ac.cn

Received 19 February 2016; Accepted 9 May 2016

Academic Editor: George M. Saleh

Purpose. To compare between a new optical biometer (AL-Scan, Nidek Co., Aichi, Japan) and an anterior segment optical coherence tomographer (Visante AS-OCT, Carl Zeiss Meditec, Dublin, USA) for measuring central corneal thickness (CCT), anterior chamber depth (ACD), and aqueous depth (AD). *Methods.* Sixty-three eyes of 63 normal subjects were examined with AL-Scan and Visante AS-OCT in this prospective study. One eye per subject was measured three times with both devices to record their CCT, ACD, and AD. All procedures were performed by the same operator. Agreement between the two devices was assessed using paired t-tests, Bland-Altman plots, and 95% limits of agreement (LoA). *Results.* The mean CCT, ACD, and AD measured by AL-Scan were 538.59 ± 27.37 μm, 3.70 ± 0.30 mm, and 3.16 ± 0.30 mm, respectively. The mean values obtained by the Visante OCT were 536.14 ± 26.61 μm for CCT, 3.71 ± 0.29 mm for ACD, and 3.17 ± 0.29 mm for AD. The mean CCT by the AL-Scan was higher than that obtained by the Visante AS-OCT (difference = 2.45 ± 6.07 μm, $P < 0.05$). The differences in ACD and AD measurements were not statistically significant. The 95% LoA of CCT, ACD, and AD were between −9.44 and 14.35 μm, −0.15 and 0.12 mm, and −0.15 and 0.12 mm, respectively. *Conclusions.* Since these two devices were comparable for measuring CCT, ACD, and AD, their results can be interchangeably used in the clinic.

1. Introduction

As cataract and refractive surgery are increasingly performed, the surgeons' skills as well as the precision of ocular measurements are important in order to satisfy patients' expectations. Central corneal thickness (CCT) is critical in designing vision correction surgeries such as laser in situ keratomileusis (LASIK), as well as in glaucoma diagnosis and other corneal diseases [1–6]. Measurements of the anterior chamber depth (ACD), which is defined as the distance from the corneal epithelium to the anterior surface of the crystalline lens, and the aqueous depth (AD), which is defined as the distance from the corneal endothelium to the anterior surface of crystalline lens, have many clinical applications [7]. The ACD measurement is used, for example, by the Holladay 2 formula, whereas the AD measurement is critical for the selection of patients undergoing phakic intraocular lens implantation [8].

Anterior segment optical coherence tomography (Visante AS-OCT, Carl Zeiss Meditec, Dublin, CA, USA) has been clinically used for several years for anterior segment measurement and has high resolution. It is based on low coherence interferometry and uses the light source of a 1310 nm superluminescent light-emitting diode. The Visante AS-OCT is widely used to measure the corneal thickness and ACD. The AL-Scan is a newly introduced optical biometer that can measure six parameters within 10 seconds, including CCT,

ACD, axial length (AL), corneal keratometry (K), white-to-white (WTW), and pupil diameter (PD). It uses the principle of the Scheimpflug imaging to measure CCT and ACD and an 830 nm infrared laser diode for AL. Previous studies had reported highly repeatable and reproducible measurements of AL, K values, and ACD with this new device [9–14].

Few studies have investigated the accuracy and agreement of AL-Scan with other instruments [9, 10, 13–15]. This is the first study to compare the ocular measurements obtained by the AL-Scan and the Visante AS-OCT.

2. Patients and Methods

Sixty-three eyes of 63 healthy subjects (36 men, 27 women) were enrolled in the study. Mean age (standard deviation, SD) was 23 ± 3.83 years (range: 18–32 years). Mean refraction error was −4.41 ± 2.12 D (range: −0.5 D to −9.00 D). The exclusion criteria were age < 18 years, previous ocular surgery, anterior or posterior pathology, contact lens usage (within 4 weeks for rigid contact lens and within 2 weeks for soft contact lens), and astigmatism > 3.0 D. Before enrolment, each patient underwent a complete ophthalmological examination, including visual acuity, intraocular pressure measurement, anterior segment evaluation, and fundus examination. This study was approved by the Review Board of the Eye Hospital of Wenzhou Medical University and performed according to the Declaration of Helsinki. All patients signed an informed consent document.

AL-Scan uses the principle of the Scheimpflug imaging to measure CCT and ACD with 470 nm monochromatic light emitted from an LED. The anterior chamber single-scan mode was used to measure the CCT and ACD with Visante OCT. The depth and width of the scanning field were 6.0 mm and 16.0 mm, respectively. Scans were centered on the pupil and taken along the horizontal meridian. The scan was obtained when a vertical white line along the center of the cornea was visible. The calibrated caliper function was used to calculate the ACD and AD [16, 17].

All measurements were performed by one experienced examiner. Each subject received three consecutive measurements with the AL-Scan and Visante OCT. We randomly chose only one eye for each patient. All measurements were taken between 10:00 and 17:00 and were completed within 15 minutes for each patient. The measurements were performed in a dimly lit room without pupil dilation.

2.1. Statistical Analysis. SPSS software version 21.0 (IBM Corporation, Armonk, NY, USA) and MedCalc Statistical Software V14.8.1 (MedCalc Software, Inc., Belgium) were used for the statistical analysis. The Kolmogorov-Smirnov test was performed to check the data distribution for each device. The paired t-test was used to evaluate the difference between the measurements of each device. $P < 0.05$ was considered to be statistically significant. Bland-Altman plots were used to evaluate the differences between the two devices. The range of agreement was shown with 95% limits of agreement (LoA), which stands for the mean difference ± 1.96 SD. Narrower 95% LoA indicated better agreement [18].

Table 1: Comparison of central corneal thickness (CCT), anterior chamber depth (ACD), and aqueous depth (AD) measured by the AL-Scan partial coherence interferometry and Visante optical coherence tomography.

Device pairings	Mean difference ± SD	P value	95% LoA
CCT (μm)	2.45 ± 6.07	0.002	−9.44 to 14.35
ACD (mm)	−0.01 ± 0.07	0.119	−0.15 to 0.12
AD (mm)	−0.02 ± 0.07	0.077	−0.15 to 0.12

SD: standard deviation.

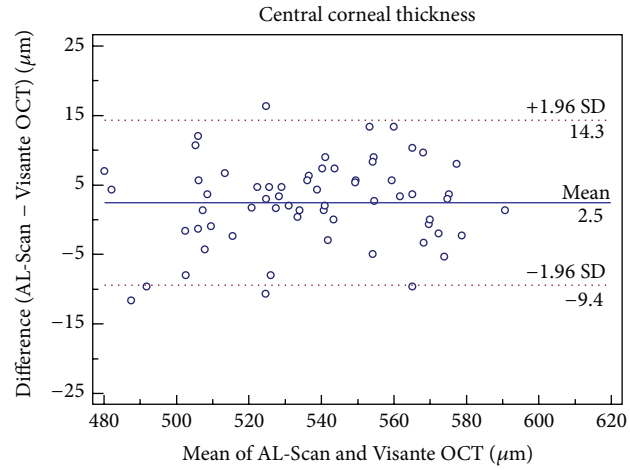

Figure 1: Difference in central corneal thickness measurements between AL-Scan optical biometer and Pentacam rotating Scheimpflug imaging device against their mean values. The solid line indicates the mean difference, and 95% limits of agreement are indicated by solid and dotted lines, respectively.

3. Results

The mean CCT, ACD, and AD measured by AL-Scan were 538.59 ± 27.37 μm, 3.70 ± 0.30 mm, and 3.16 ± 0.30 mm, respectively. The Visante OCT showed 536.14 ± 26.61 μm for CCT, 3.71 ± 0.29 mm for ACD, and 3.17 ± 0.29 mm for AD.

Although there was a statistically significant difference in the mean CCT measurements between the two devices, it was clinically insignificant (Table 1). Good agreement was found between the two devices for CCT with a maximum boundary value of 95% LoA of 14.35 μm (Figure 1). The ACD and AD measurements of AL-Scan and Visante OCT were similar ($P > 0.05$) and had good agreement with the 95% LoA range of −0.15 to 0.12 mm (Figures 2 and 3).

4. Discussion

Accurate quantitative measurements of CCT, ACD, and AD provide valuable clinical information and are important for preoperative assessment, surgical planning, and follow-up in phakic IOL implantation. Ultrasound (US) is typically widely used for measuring these parameters [19, 20]. But, nowadays, noncontact devices such as the Visante AS-OCT are more popular in measuring ocular parameters. The AL-Scan is a recently released, noncontact, imaging instrument using

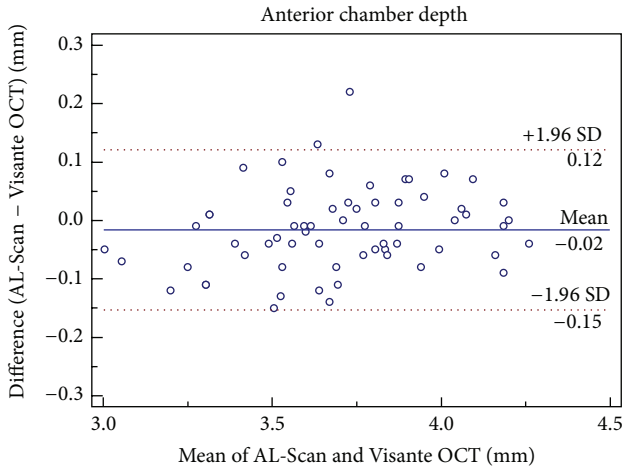

Figure 2: Difference in anterior chamber depth measurements between AL-Scan optical biometer and Pentacam rotating Scheimpflug imaging device against their mean values. The solid line indicates the mean difference, and 95% limits of agreement are indicated by solid and dotted lines, respectively.

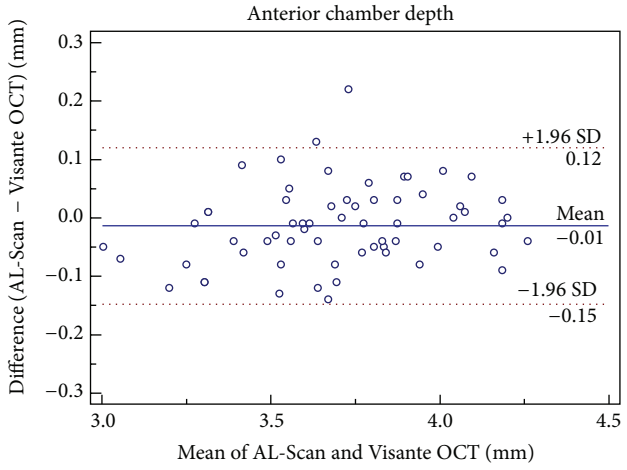

Figure 3: Difference in aqueous depth measurements between AL-Scan optical biometer and Pentacam rotating Scheimpflug imaging device against their mean values. The solid line indicates the mean difference, and 95% limits of agreement are indicated by solid and dotted lines, respectively.

partial coherence interferometry (PCI) and the Scheimpflug principle with good repeatability and reproducibility. The Scheimpflug camera with a 470 nm LED is used for measuring the CCT and anterior chamber in the AL-Scan. Our data is the first study to suggest that the Visante AS-OCT and the AL-Scan have good agreement for measuring CCT, ACD, and AD.

Previous studies have investigated the AL-Scan and compared it to other instruments, mainly the IOLMaster. Since the IOLMaster is unable to directly measure the corneal thickness, no prior data for comparing CCT were available. Ethnic variation was found in previous studies when CCT values were measured; Chinese, Caucasians, Hispanics, and Filipinos had comparable CCT measurements, whereas Japanese had significantly thinner corneas than Caucasians, Chinese, Filipinos, and Hispanics. The CCT of African Americans was the thinnest. The differences also existed between the anterior chamber of Chinese and Caucasians [21–23]. So we are more focused on the repeatability results rather than the mean measurement values. Yagci et al. showed high repeatability of CCT values by the AL-Scan in both normal and keratoconic groups. Although its reproducibility was not better than other available Scheimpflug systems, the AL-Scan showed excellent and comparable repeatability and reproducibility in most ocular parameters' measurements [10–12, 24, 25]. Thus, it was useful to review and compare the currently used devices such as Pentacam (Oculus, Wetzlar, Germany), Galilei (Ziemer, Port, Switzerland), and Sirius (Costruzione Strumenti Oftalmici, Florence, Italy) as they all use the principle of the Scheimpflug imaging to measure the CCT despite the lack of direct comparison between the AL-Scan and other Scheimpflug systems. Nam et al. [26] showed that Pentacam can provide comparable and high repeatability of CCT. High CCT repeatability of Sirius was reported by Savini et al. and Huang et al. [27, 28]. A recent analysis showed that the total measurement error of Visante OCT for CCT was 7.88 μm, while the error was 9.85 μm, 7.05 μm, 2.64 μm, and 4.76 μm for ultrasound, Pentacam, Galilei, and Sirius, respectively [29]. Mohamed et al. [30] showed low coefficients of repeatability and reproducibility and high intraclass correlation coefficients of the CCT measurement by Visante OCT. In our recent prospective studies on three different Scheimpflug imaging systems and one OCT, high repeatability and good agreement for CCT measurement were also demonstrated [28, 31]. However, O'Donnell et al. [32] showed that the 95% LoA for Pentacam and Visante OCT were 25.61 to −49.11 μm. In the current study, the Visante OCT provided slightly thinner CCT than AL-Scan, which was also seen between Visante and Pentacam by Nemeth et al. [33], and our max boundary of 95% LoA was 14.35 μm, demonstrating very good agreement between the two devices. The Scheimpflug and OCT measure CCT by different optical and physical techniques: the Pentacam used 475 nm blue light, Visante OCT used 1310 nm diode laser, and AL-Scan used 470 nm LED, which might contribute to the differences in the results [34]. Besides, the anterior corneal surface also influences the demarcating boundary, which results in differences.

A previous study had shown that the total measurement error of IOLMaster for ACD was 0.06 mm and the error of Visante OCT, Pentacam, and Galilei was all approximately 0.05 mm [29]. As compared to the IOLMaster 500, the ACD was 3.17 ± 0.12 mm by AL-Scan and 3.12 ± 0.11 mm by IOLMaster, with a minor difference of 0.13 ± 0.04 mm and high correlation between AL-Scan and IOLMaster 500 in measuring ACD [9]. Srivannaboon et al. [13] also showed a small difference indicating good agreement between AL-Scan and IOLMaster with a LoA range of −0.24 to 0.19 mm, which was similar to the results of our previous comparison between the AL-Scan and IOLMaster [10]. Nemeth et al. [17], Wang et al. [16], and Lavanya et al. [35] showed that the ACD measurements by OCT were 3.11 ± 0.33 mm, 3.76 ± 0.21 mm, and 3.14 ± 0.34 mm, respectively, in normal adults and presented good agreement with ultrasound or Scheimpflug or

IOLMaster. Bueno-Gimeno et al. [36] also reported similar results in teenagers. Lavanya et al. [35] demonstrated that ACD measured by Visante OCT had deeper but not clinically important values than IOLMaster. Dinc et al. [37] reported high correlation between Pentacam and Visante OCT in measuring ACD, which was similar in keratoconus in a study by Yazici et al. [34]. In our current study, the 95% LoA range was even narrower for ACD or AD measurements indicating better agreement between AL-Scan and Visante OCT than that between AL-Scan and IOLMaster or between AL-Scan and Galilei [14].

In our current study, three parameters of anterior segment were evaluated. We simultaneously measured ACD and AD modes, which is more comprehensive than other studies that only analyzed one mode. In clinical settings, ACD and the intraocular pressure are important parameters for glaucoma screening and diagnosis. However, the ACD values are the summation of CCT and AD values. Since ACD values can be affected by CCT measurement, the method used for measuring CCT, the accuracy of CCT measurement, corneal edema, and other aspects related to CCT results will influence the precision of ACD. Thus, it was meaningful to assess the agreement of these parameters between the two devices in a single study.

This study had some limitations. We only included healthy unoperated eyes and further investigations are needed to assess both instruments for other categories of patients (such as those affected with keratoconus or previous refractive surgery). Mydriasis would influence changes in the cornea and anterior chamber, so further studies will be performed to evaluate the performance of the biometer after pupil dilation.

This study found a clinically insignificant difference between the two devices for the measurement of CCT. The AL-Scan and Visante AS-OCT have good agreement in measuring CCT, ACD, and AD, and their results can be interchangeably used in the clinical setting.

Disclosure

The authors have no proprietary or commercial interest in any materials discussed in this paper.

Competing Interests

The authors declare that they have no competing interests.

Authors' Contributions

Jinhai Huang and Weicong Lu contributed equally as first authors.

Acknowledgments

This paper is supported in part by the National Natural Science Foundation of China (81300807); Foundation of Wenzhou City Science & Technology Bureau (J20140014, Y20150076); Zhejiang Provincial & Ministry of Health Research Fund For Medical Sciences (WKJ-ZJ-1530); and Health Bureau of Zhejiang Province (2016RCB013). The contribution of G.B. Bietti Foundation IRCCS was supported by the Italian Ministry of Health and Fondazione Roma.

References

[1] M. O. Gordon, J. A. Beiser, J. D. Brandt et al., "The Ocular Hypertension Treatment Study: baseline factors that predict the onset of primary open-angle glaucoma," *Archives of Ophthalmology*, vol. 120, no. 6, pp. 714–720, 829–730, 2002.

[2] F. W. Price Jr., D. L. Koller, and M. O. Price, "Central corneal pachymetry in patients undergoing laser in situ keratomileusis," *Ophthalmology*, vol. 106, no. 11, pp. 2216–2220, 1999.

[3] N. C. Wheeler, C. M. Morantes, R. M. Kristensen, T. H. Pettit, and D. A. Lee, "Reliability coefficients of three corneal pachymeters," *American Journal of Ophthalmology*, vol. 113, no. 6, pp. 645–651, 1992.

[4] J. W. McLaren, C. B. Nau, J. C. Erie, and W. M. Bourne, "Corneal thickness measurement by confocal microscopy, ultrasound, and scanning slit methods," *American Journal of Ophthalmology*, vol. 137, no. 6, pp. 1011–1020, 2004.

[5] T. Mimura, S. Yamagami, T. Usui, N. Honda, F. Araki, and S. Amano, "In vivo confocal microscopy of human cornea covered with human amniotic membrane," *Japanese Journal of Ophthalmology*, vol. 52, no. 6, pp. 493–496, 2008.

[6] T. Avitabile, F. Marano, M. G. Uva, and A. Reibaldi, "Evaluation of central and peripheral corneal thickness with ultrasound biomicroscopy in normal and keratoconic eyes," *Cornea*, vol. 16, no. 6, pp. 639–644, 1997.

[7] K. J. Hoffer, "Definition of ACD," *Ophthalmology*, vol. 118, no. 7, article 1484, 2011.

[8] K. J. Hoffer, "Clinical results using the Holladay 2 intraocular lens power formula," *Journal of Cataract and Refractive Surgery*, vol. 26, no. 8, pp. 1233–1237, 2000.

[9] G. Kaswin, A. Rousseau, M. Mgarrech, E. Barreau, and M. Labetoulle, "Biometry and intraocular lens power calculation results with a new optical biometry device: comparison with the gold standard," *Journal of Cataract and Refractive Surgery*, vol. 40, no. 4, pp. 593–600, 2014.

[10] J. Huang, G. Savini, J. Li et al., "Evaluation of a new optical biometry device for measurements of ocular components and its comparison with IOLMaster," *British Journal of Ophthalmology*, vol. 98, no. 9, pp. 1277–1281, 2014.

[11] M. Kola, H. Duran, A. Turk, S. Mollamehmetoglu, A. Kalkisim, and H. Erdol, "Evaluation of the repeatability and the reproducibility of AL-scan measurements obtained by residents," *Journal of Ophthalmology*, vol. 2014, Article ID 739652, 6 pages, 2014.

[12] R. Yagci, E. Güler, A. E. Kulak et al., "Repeatability and reproducibility of a new optical biometer in normal and keratoconic eyes," *Journal of Cataract and Refractive Surgery*, vol. 41, no. 1, pp. 171–177, 2015.

[13] S. Srivannaboon, C. Chirapapaisan, P. Chonpimai, and S. Koodkaew, "Comparison of ocular biometry and intraocular lens power using a new biometer and a standard biometer," *Journal of Cataract and Refractive Surgery*, vol. 40, no. 5, pp. 709–715, 2014.

[14] M. S. Dervişoğullari, Y. Totan, and B. Gürağaç, "Comparison of anterior chamber depth measurements of Nidek AL-Scan and Galilei Dual Scheimpflug Analyzer," *Contact Lens & Anterior Eye*, vol. 38, no. 2, pp. 85–88, 2015.

[15] S. Srivannaboon, C. Chirapapaisan, P. Chonpimai, and S. Koodkaew, "Comparison of corneal astigmatism measurements of 2 optical biometer models for toric intraocular lens selection," *Journal of Cataract and Refractive Surgery*, vol. 41, no. 2, pp. 364–371, 2015.

[16] Q. Wang, X. Ding, G. Savini et al., "Anterior chamber depth measurements using Scheimpflug imaging and optical coherence tomography: repeatability, reproducibility, and agreement," *Journal of Cataract and Refractive Surgery*, vol. 41, no. 1, pp. 178–185, 2015.

[17] G. Nemeth, A. Vajas, A. Tsorbatzoglou, B. Kolozsvari, L. Modis Jr., and A. Berta, "Assessment and reproducibility of anterior chamber depth measurement with anterior segment optical coherence tomography compared with immersion ultrasonography," *Journal of Cataract and Refractive Surgery*, vol. 33, no. 3, pp. 443–447, 2007.

[18] J. M. Bland and D. G. Altman, "Statistical methods for assessing agreement between two methods of clinical measurement," *The Lancet*, vol. 1, no. 8476, pp. 307–310, 1986.

[19] K. Kriechbaum, C. Leydolt, O. Findl, M. Bolz, and W. Drexler, "Comparison of partial coherence interferometers: Acmaster versus laboratory prototype," *Journal of Refractive Surgery*, vol. 22, no. 8, pp. 811–816, 2006.

[20] P.-F. Su, A. Y. Lo, C.-Y. Hu, and S.-W. Chang, "Anterior chamber depth measurement in phakic and pseudophakic eyes," *Optometry and Vision Science*, vol. 85, no. 12, pp. 1193–1200, 2008.

[21] E. Aghaian, J. E. Choe, S. Lin, and R. L. Stamper, "Central corneal thickness of Caucasians, Chinese, Hispanics, Filipinos, African Americans, and Japanese in a glaucoma clinic," *Ophthalmology*, vol. 111, no. 12, pp. 2211–2219, 2004.

[22] E. Dai and C. A. Gunderson, "Pediatric central corneal thickness variation among major ethnic populations," *Journal of AAPOS*, vol. 10, no. 1, pp. 22–25, 2006.

[23] D. Wang, G. Huang, M. He, L. Wu, and S. Lin, "Comparison of anterior ocular segment biometry features and related factors among American Caucasians, American Chinese and mainland Chinese," *Clinical and Experimental Ophthalmology*, vol. 40, no. 6, pp. 542–549, 2012.

[24] G. Savini, P. Barboni, M. Carbonelli, and K. J. Hoffer, "Repeatability of automatic measurements by a new Scheimpflug camera combined with Placido topography," *Journal of Cataract and Refractive Surgery*, vol. 37, no. 10, pp. 1809–1816, 2011.

[25] U. de Sanctis, A. Missolungi, B. Mutani, L. Richiardi, and F. M. Grignolo, "Reproducibility and repeatability of central corneal thickness measurement in keratoconus using the rotating scheimpflug camera and ultrasound pachymetry," *American Journal of Ophthalmology*, vol. 144, no. 5, pp. 712–718, 2007.

[26] S. M. Nam, C. Y. Im, H. K. Lee, E. K. Kim, T.-I. Kim, and K. Y. Seo, "Accuracy of RTVue optical coherence tomography, pentacam, and ultrasonic pachymetry for the measurement of central corneal thickness," *Ophthalmology*, vol. 117, no. 11, pp. 2096–2103, 2010.

[27] G. Savini, M. Carbonelli, A. Sbreglia, P. Barboni, G. Deluigi, and K. J. Hoffer, "Comparison of anterior segment measurements by 3 Scheimpflug tomographers and 1 Placido corneal topographer," *Journal of Cataract and Refractive Surgery*, vol. 37, no. 9, pp. 1679–1685, 2011.

[28] J. Huang, X. Ding, G. Savini et al., "A comparison between Scheimpflug imaging and optical coherence tomography in measuring corneal thickness," *Ophthalmology*, vol. 120, no. 10, pp. 1951–1958, 2013.

[29] J. J. Rozema, K. Wouters, D. G. P. Mathysen, and M.-J. Tassignon, "Overview of the repeatability, reproducibility, and agreement of the biometry values provided by various ophthalmic devices," *American Journal of Ophthalmology*, vol. 158, no. 6, pp. 1111.e1–1120.e1, 2014.

[30] S. Mohamed, G. K. Y. Lee, S. K. Rao et al., "Repeatability and reproducibility of pachymetric mapping with visante anterior segment-optical coherence tomography," *Investigative Ophthalmology and Visual Science*, vol. 48, no. 12, pp. 5499–5504, 2007.

[31] J.-H. Huang, L.-N. Ge, D.-Z. Wen, S.-H. Chen, Y. Yu, and Q.-M. Wang, "Repeatability and agreement of corneal thickness measurement with Pentacam Scheimpflug photography and Visante optical coherence tomography," *Zhonghua Yan Ke Za Zhi*, vol. 49, no. 3, pp. 250–256, 2013.

[32] C. O'Donnell, A. Hartwig, and H. Radhakrishnan, "Comparison of central corneal thickness and anterior chamber depth measured using LenStar LS900, Pentacam, and Visante AS-OCT," *Cornea*, vol. 31, no. 9, pp. 983–988, 2012.

[33] G. Nemeth, Z. Hassan, E. Szalai, A. Berta, and L. Modis Jr., "Anterior segment parameters measured with 2 optical devices compared to ultrasonic data," *European Journal of Ophthalmology*, vol. 23, no. 2, pp. 177–182, 2013.

[34] A. T. Yazici, G. Pekel, E. Bozkurt et al., "Measurements of anterior segment parameters using three different non-contact optical devices in keratoconus patients," *International Journal of Ophthalmology*, vol. 6, no. 4, pp. 521–525, 2013.

[35] R. Lavanya, L. Teo, D. S. Friedman et al., "Comparison of anterior chamber depth measurements using the IOLMaster, scanning peripheral anterior chamber depth analyser, and anterior segment optical coherence tomography," *British Journal of Ophthalmology*, vol. 91, no. 8, pp. 1023–1026, 2007.

[36] I. Bueno-Gimeno, E. España-Gregori, A. Gené-Sampedro, A. Lanzagorta-Aresti, and C. Dualde-Beltrán, "Anterior chamber depth measurement in teenagers. Comparison of two techniques," *Journal of Optometry*, vol. 6, no. 3, pp. 161–166, 2013.

[37] U. A. Dinc, E. Gorgun, B. Oncel, M. N. Yenerel, and L. Alimgil, "Assessment of anterior chamber depth using visante optical coherence tomography, slitlamp optical coherence tomography, IOL Master, Pentacam and Orbscan IIz," *Ophthalmologica*, vol. 224, no. 6, pp. 341–346, 2010.

Hindawi Publishing Corporation
Journal of Ophthalmology
Volume 2016, Article ID 5260531, 7 pages
http://dx.doi.org/10.1155/2016/5260531

Research Article

Keratorefractive Effect of High Intensity Focused Ultrasound Keratoplasty on Rabbit Eyes

Zhiyu Du,[1,2] Pisong Yan,[2] Qiang Luo,[3] Dan Zhang,[4] and Yu Zhang[1]

[1]*Department of Ophthalmology, The Second Affiliated Hospital, Chongqing Medical University, Chongqing 400010, China*
[2]*Medal Eye Institute, Chongqing 400050, China*
[3]*Key Laboratory of Molecular Biology for Infectious Diseases (Ministry of Education), Institute for Viral Hepatitis, Department of Infectious Diseases, The Second Affiliated Hospital, Chongqing Medical University, Chongqing 400010, China*
[4]*Department of Ophthalmology, Armed Police Hospital of Chongqing, Chongqing 400061, China*

Correspondence should be addressed to Zhiyu Du; dr.duzhiyu@163.com

Received 4 February 2016; Accepted 4 May 2016

Academic Editor: Yannis Athanasiadis

Purpose. To evaluate high intensity focused ultrasound (HIFU) as an innovation and noninvasive technique to correct presbyopia by altering corneal curvature in the rabbit eye. *Methods*. Eighteen enucleated rabbit eyes were treated with a prototype HIFU keratoplasty. According to the therapy power, these eyes were divided three groups: group 1 (1 W), group 2 (2 W), and group 3 (3 W). The change in corneal power was quantified by a Sirius Scheimpflug camera. Light microscopy (LM) and transmission electron microscopy (TEM) were performed to determine the effect on the corneal stroma. *Results*. In the treated eyes, the corneal curvature increases from 49.42 ± 0.30 diopters (D) and 48.00 ± 1.95 D before procedure to 51.37 ± 1.11 D and 57.00 ± 1.84 D after HIFU keratoplasty application in groups 1 and 3, respectively. The major axis and minor axis of the focal region got longer when the powers of the HIFU got increased; the difference was statistically significant ($p < 0.05$). LM and TEM showed HIFU-induced shrinkage of corneal stromal collagen with little disturbance to the underlying epithelium. *Conclusions*. We have preliminarily exploited HIFU to establish a new technique for correcting presbyopia. HIFU keratoplasty will be a good application prospect for treating presbyopia.

1. Introduction

Presbyopia is a progressive loss of crystalline lens accommodation that results in an inability to focus at near vision, which occurs with aging. The aging process affects each individual beginning near 40 years of age [1]. The estimated global prevalence of presbyopia was 1.04 billion people in 2005 [2]. The large number of potential patients who might seek permanent spectacle-free correction of this condition have stimulated the increasing interest in refractive surgery. In recent years, various surgical solutions [3–8] have been developed to effectively treat this condition. However, none has emerged as the final and optimum solution for presbyopia because of complications, invasiveness, and lack of predictability and stability. Thus, it is necessary to seek noninvasive, safe, and effective technique.

High intensity focused ultrasound (HIFU) is a noninvasive or minimally invasive medical procedure which has shown considerable potential for a variety of therapeutic applications [9]. Therapeutic ultrasound, although less well known than ultrasound for diagnostic imaging, has become a topic of growing interest in ophthalmology [10]. In recent years, several experimental and clinical studies for the treatment of glaucoma have been conducted [10–15]. Although several studies have addressed the effects of HIFU on the cornea in the 1980s and 1990s [16, 17], nowadays HIFU has more advantages, such as controlled accuracy, accuracy of positioning in the treatment area, and smaller focal zones [11–13]. Furthermore, a higher operating frequency allows for a steeper transition between the focal zone and the untreated area, thus reducing the risk of heating the neighboring healthy tissue [12].

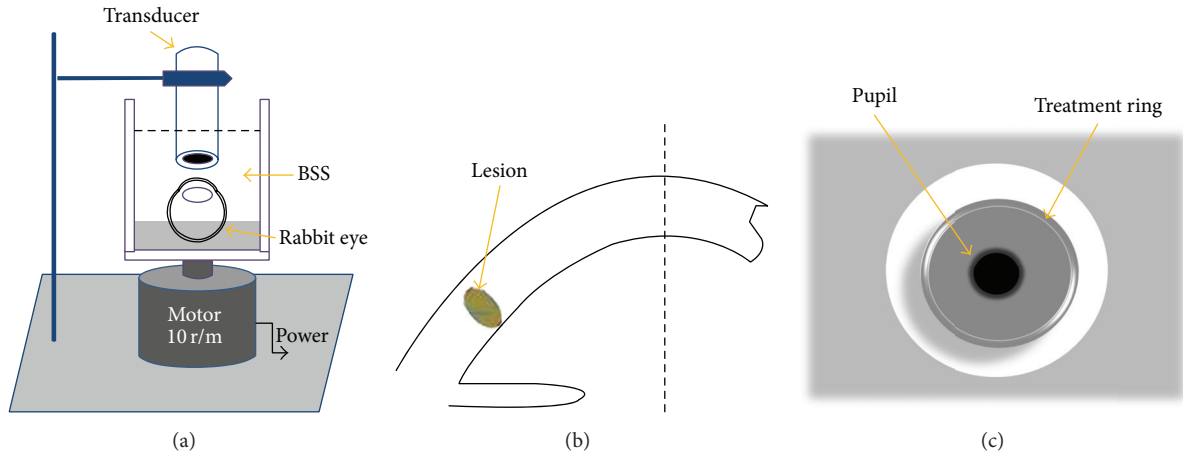

Figure 1: (a) Schematic diagram of HIFU keratoplasty transducer applied to an in vitro rabbit cornea cross section. (b) Cross-sectional view of the lesion of HIFU keratoplasty. (c) End view of the treatment ring.

Therefore, the potential therapeutic applications of HIFU might encompass many present uses of laser therapy in ophthalmology and also offer new methods of treating ocular problems. The primary goal of the present study was to establish a new technique for correcting presbyopia. So, we evaluate the histologic characteristics of corneal stroma lesions induced by HIFU in animals. We also report the change in dioptric power on rabbit eyes in vitro after HIFU corneal circular treatment.

2. Material and Methods

2.1. Experimental Animals. An approval of animal use was granted by the Animal Care and Use Committee at Chongqing Medical University. Whole animal management followed the ARVO Statement for the Use of Animals in Ophthalmic and Visual Research (ARVO Animal Policy). Enucleated eyes from adult New Zealand White rabbits (5-6 months old, 2–2.5 kg) were provided by Laboratory Animal Center of Chongqing Medical University. Rabbits of different sex were included randomly. All rabbits were sacrificed using venous air embolism before ophthalmectomy. Before all animals were sacrificed using venous air embolism, they were anaesthetized using Sumianxin II intramuscular injection (0.1 mL/kg) and all efforts were made to minimize suffering. The fat and muscle were removed from all eyes with scissors after enucleation. Within 1 hour of enucleation, the eyes were stored in isotonic saline on ice until used, not later than 24 hours after enucleation. Eighteen eyes were used.

2.2. Experimental Apparatus. HIFU keratoplasty treatments were delivered with a prototype, which was designed by Chongqing HIFU Technology Co, Ltd., Chongqing, China. Continuous therapeutic energy was emitted from a focal ultrasound transducer (focal length, 5 mm; focal zone, 65 μm) with a working frequency of 10.2 MHz, and therapy power was set at 1 W (group 1, 6 eyes), 2 W (group 2, 6 eyes), and 3 W (group 3, 6 eyes) for an exposure time of 6 seconds. Intact rabbit eye globes were placed in a transparent Plexiglas observation cell, which was put on the rotary motor with uniform velocity (Figure 1(a)). The cell was full of balanced salt solution (BSS). The ultrasound transducer placed perpendicular to the corneal surface and both had no direct contact with each other. The focal length of the transducer was adjusted by Vernier caliper to focus on the same depth of rabbit corneal stroma. The time of running one circle of the rotary motor was also 6 seconds. A stromal treatment ring (8 mm) was produced within the peripheral corneal stroma after HIFU radiation (Figures 1(b) and 1(c)).

2.3. Corneal Topography. The Sirius Scheimpflug camera (CSO, Firenze, Italy) was used for corneal topographic imaging and characterized the treatment effects of the eye before and after HIFU keratoplasty application immediately. The rabbit eye was fixed with a fixed bracket, and it positioned in the front of the Sirius Scheimpflug camera. Three measurements were taken before and after HIFU keratoplasty application. BSS was applied to the cornea before all Scheimpflug measurements. The simulated keratoscope readings (Sim-K) in central 3 mm zone of the rabbit cornea were analyzed.

2.4. Histologic Examination. For histologic examination, the corneas were fixed in 4% buffered formaldehyde, dehydrated in alcohol solutions of increasing concentration, cleared in xylene, embedded in paraffin, and sectioned into 5 μm thick sections. The sections were stained with hematoxylin-eosin and examined under a light microscope (LM). Digimizer software (version 3.1.1.0) was used for measuring the maximum width and length of the focal region.

2.5. Transmission Electron Microscopy (TEM). For TEM examination, the corneas were placed into a glutaraldehyde 2.5% in 0.1 mol/L cacodylate buffer (pH 7.3) at 4°C, for at least 24 hours, and then postfixed in 1% osmium tetroxide in 0.1 mol/L cacodylate buffer (pH 7.3) at 4°C for 1 hour. After dehydration and embedding, samples were sectioned and examined under a TEM.

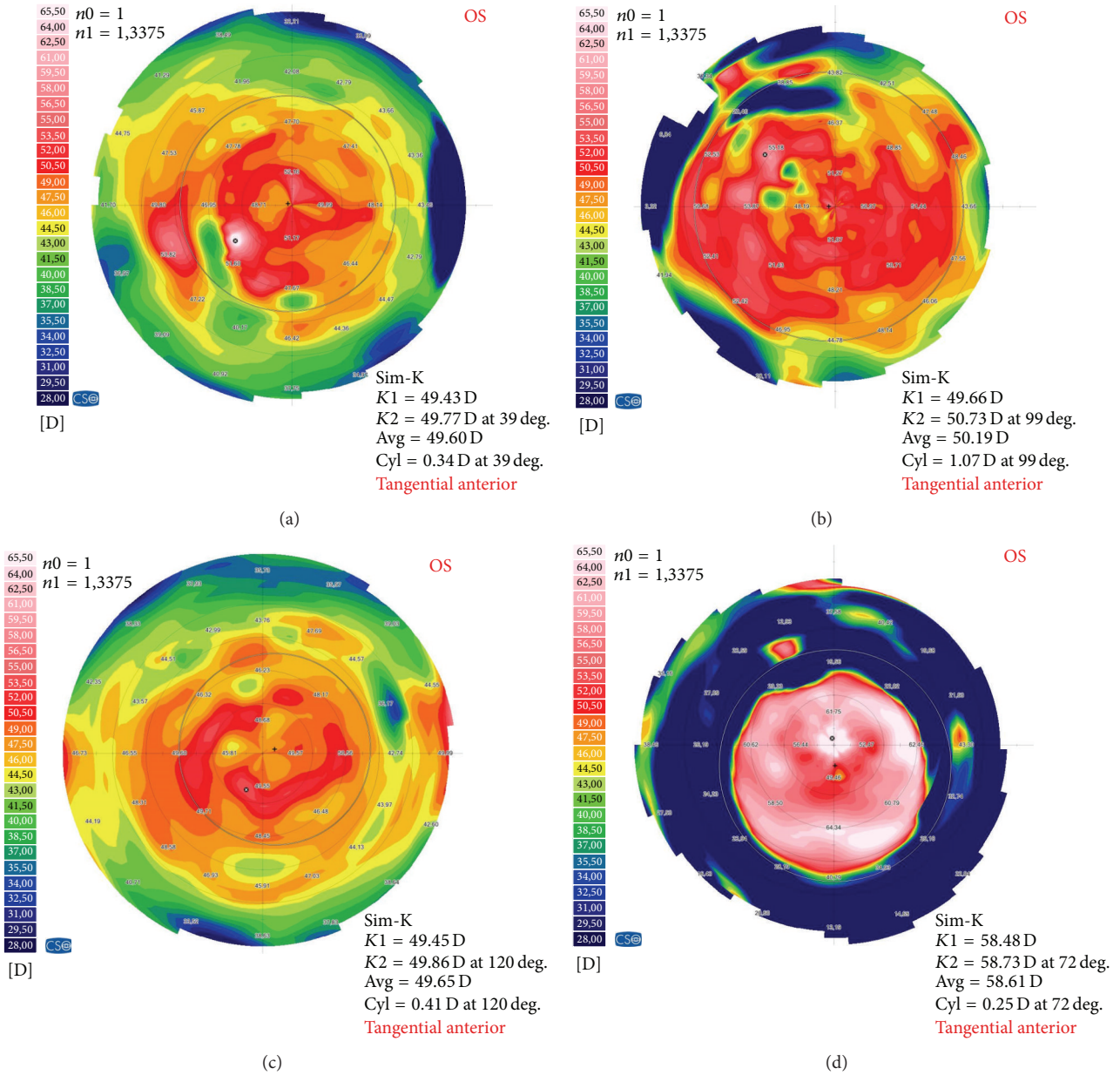

FIGURE 2: Topography display of treated cornea (Sirius, CSO, Firenze, Italy). (a) Group 1 (therapy power, 1 W). (c) Group 3 (therapy power, 3 W). Tangential curvature of the anterior corneal surface before HIFU treatment. (b, d) Tangential curvature of the same cornea after HIFU treatment. It shows steepening in the central cornea and flattening outside. Sim-K: simulated keratoscope readings, *K*1: the curvature in the flat meridian, *K*2: the curvature in the steep meridian, Avg: the mean curvature, Cyl = cylinder, deg.: degree, D: diopter, OS: left eye, and tangential anterior: tangential curvature of the anterior corneal surface.

3. Results

3.1. Corneal Topography. Group 1 (1 W) and group 3 (3 W) were measured before and after HIFU keratoplasty application by using the Sirius Scheimpflug camera. The mean keratometric power (Sim-K value) for corneas before treatment was 49.42 ± 0.30 D and 48.00 ± 1.95 D in groups 1 and 3, respectively. The mean keratometric power (Sim-K value) after treatment was 51.37 ± 1.11 D and 57.00 ± 1.84 D in groups 1 and 3, respectively. Figure 2 shows the corneal topographic variation in the tangential corneal curvature induced by HIFU treatment in a rabbit eye.

3.2. Histology and Electron Microscopy. As shown in Figure 3, the stroma cornea was mostly affected by HIFU keratoplasty. The area of alterations had been similar to the oblique elliptical shape in cornea. The mean major axis of the oblique elliptical shape in cornea of group 1 was 284 ± 18 μm, 431 ± 7 μm in group 2, and 532 ± 33 μm in group 3. The mean minor axis of the oblique elliptical shape in cornea of group 1 was

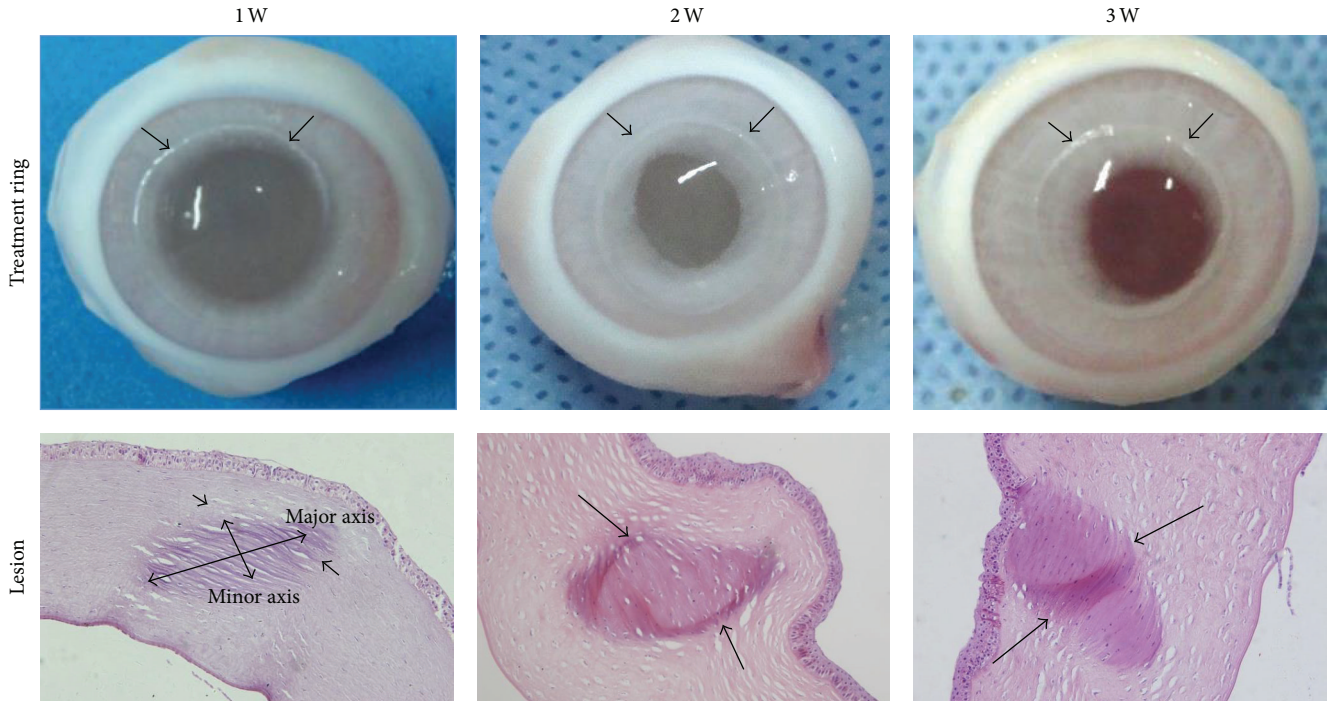

	1 W	2 W	3 W
Major axis (μm)	284 ± 18 (n = 6)	431 ± 7 (n = 6)	532 ± 33 (n = 6)
Minor axis (μm)	122 ± 24 (n = 6)	245 ± 33 (n = 6)	274 ± 68 (n = 6)

Figure 3: Photograph display of treatment ring in the rabbit cornea after HIFU keratoplasty treatment and photomicrograph of a rabbit cornea cross section after HIFU treatment. The loose stromal area (lesion) corresponds to a region of HIFU-induced collagen shrinkage, ×200. The table displays the major and minor axes of the oblique elliptical lesion.

122 ± 24 μm, 245 ± 33 μm in group 2, and 274 ± 68 μm in group 3. Meanwhile, the major axis and minor axis of the focal region got longer when the powers of the HIFU got increased; the difference was statistically significant ($p < 0.05$).

TEM of HIFU-treated zones demonstrated that the morphologic appearance of the keratocytes was close to normal (Figure 4(b)). Within the HIFU-affected area, the keratocytes were situated between the crumpled collagen layers, like "sandwich." Thus the morphology and the structure of keratocytes would be affected by the crumpled collagen layers. According to Figure 4(d), the collagen layers crumpled significantly within the HIFU treatment area. Besides the typical structure of stromal collagen, microfibrillar aggregations can also be observed throughout the area of crumpled collagen layers.

4. Discussion

In the present study, the histologic changes and the variation in dioptric power induced by HIFU treatment in rabbit corneas were evaluated. Since 1898, using heat to change the morphology of the cornea has been employed for different therapeutic and surgical objectives. The best known of these techniques is probably thermokeratoplasty (TKP), which is based on the principle that heating corneal tissue causes collagen fibers to shrink and hence changes the corneal curvature [18]. To date, 3 main TKP technologies have emerged: laser thermokeratoplasty (LTK), conductive keratoplasty (CK), and microwave keratoplasty. However, due to complications, invasiveness, and lack of predictability and stability [19], none has emerged as the optimum solution for presbyopia. Thus, it is necessary to seek noninvasive, safe, and effective technique.

HIFU thermal treatment is a novel, minimally invasive medical procedure which has shown considerable potential for a variety of therapeutic applications [9]. The conception of HIFU was firstly brought forward by Lynn and Putnam in 1944 [20]. In 1960, W. J. Fry and F. J. Fry [21] applied HIFU technology to experimentally treat nervous system diseases and suggested the potential of HIFU in surgical operations. In ophthalmology, HIFU for the treatment of glaucoma and ultrasonic drug delivery are the two main areas of research and potential clinical application [10]. Nevertheless, HIFU keratoplasty was first described in 1990 by Rutzen et al. [17] as a theoretical option for inducing collagen shrinkage in corneas. They commented that HIFU could be used to heat the peripheral cornea with great precision because of the small focal zone and the excellent aiming capabilities of HIFU. However, with the development of high-frequency miniaturized transducer, HIFU enables

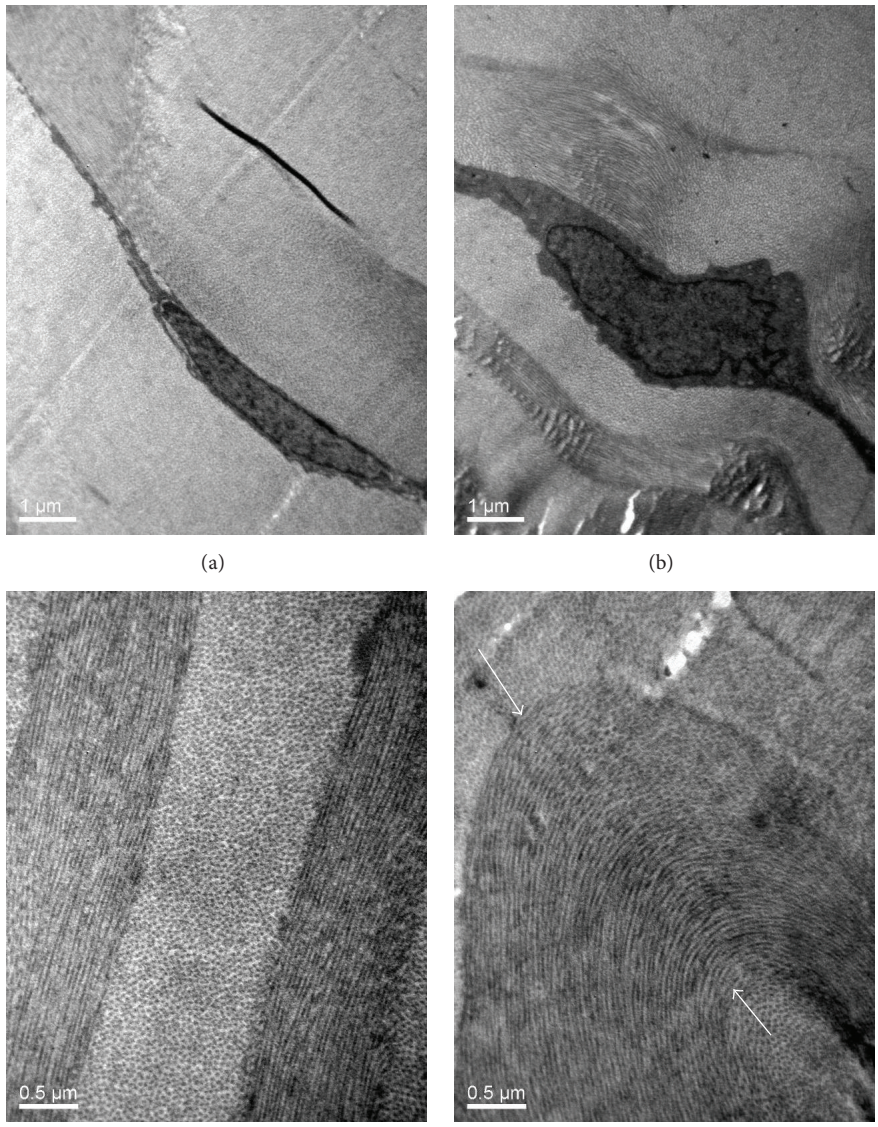

(a) (b)

(c) (d)

Figure 4: (a, c) Blank control group. (b) TEM of HIFU-treated zones demonstrated that the morphologic appearance of the keratocytes was close to normal. (d) The typical structures of stromal collagen shrinkage (white arrows) are within the HIFU treatment zone.

the creation of smaller focal zones (65 μm) that better target the treatment areas, particularly for small organs such as clear cornea. The higher operating frequency (10.2 MHz) also allows for a steeper transition between the focal zone and the untreated area. In addition, HIFU also enables a defined and adjustable tissue volume to be heated and treated at any depth or location within the eye [10]. Therefore, our group evaluated the histologic characteristics of corneal stroma lesions induced by HIFU in rabbits and also report the change in dioptric power of the procedure.

In the present study, our results demonstrated that HIFU keratoplasty increased the power of the rabbit corneas from 49.42 ± 0.30 D to 51.37 ± 1.11 D in group 1 and from 48.00 ± 1.95 D to 57.00 ± 1.84 D in group 3. The results indicated that the variations of curvature of the rabbit corneas got steeper when the powers of the HIFU got increased. Like other thermal techniques (i.e., LTK [3], CK [4]), HIFU thermal treatment is applied in the periphery of the cornea, it causes peripheral flattening and corresponding steepening in the center (Figures 2(b) and 2(d)). Moreover, compared with CK or LTK, HIFU keratoplasty showed comparable refractive results. In addition, our results show a protective effect of epithelium and basement membrane within the HIFU-treated area (Figure 3). Therefore, it is likely that this procedure would not cause postoperative pain. Moreover, as this study showed, because of the epithelium intactness, the topography examination is possible immediately after surgery. In the clinic, this would allow evaluation of clinical results immediately after the treatment. It is well known that postoperative dry eye can be commonly seen after excimer

laser-based refractive surgery. The reason may be the fact that corneal nerves are cut during the procedure. However, HIFU thermal treatment requires no cutting of the cornea; therefore, the problem of postoperative dry eye and infection would not likely occur.

Our findings demonstrated that HIFU thermal treatment induced annular elliptical treatment zone in the anterior stroma (Figure 3). Although the shape of HIFU thermal lesion differs from CK, which creates a thermal footprint that is uniformly cylindrical, the effect seems to be similar to CK [22]. A full circular elliptical treatment ring of HIFU keratoplasty applied to the peripheral cornea produces a cinching effect that increases the curvature of the central cornea [23]. The stability of the induced changes is a critical point in thermokeratoplasty procedures. For this reason, further studies are necessary to determine whether there is regression of treatment effect. Our long-term goal is to use ultrasound to produce permanent alterations in corneal curvature. In addition, the time and dose of the effect on collagen fibers as well as matrix changes will have to be fully elucidated in in vivo experiment. Our group will continue to develop HIFU keratoplasty to improve repeatability and will compare its performance to existing methods for correcting presbyopia. The development of treatment parameters will be necessary to determine the optimum depth, diameter of treatment ring, and power of treatment to produce specific refractive changes.

In conclusion, the results in our study suggest that HIFU as a noninvasive method for applying in the peripheral cornea could steepen the central cornea. We have initially exploited HIFU to establish a new technique for changing the refractive index of the intermediate cornea to correct presbyopia. There will be a good application prospect for HIFU keratoplasty in the treatment of presbyopia.

Disclosure

Zhiyu Du and Pisong Yan are co-first authors. The authors alone are responsible for the content and writing of the paper.

Competing Interests

The authors report no conflict of interests.

Acknowledgments

The authors gratefully acknowledge grant support from Key Program of Chongqing Municipal Health Bureau, Chongqing, China (2010-1-25).

References

[1] M. P. Holzer, A. Mannsfeld, A. Ehmer, and G. U. Auffarth, "Early outcomes of INTRACOR femtosecond laser treatment for presbyopia," *Journal of Refractive Surgery*, vol. 25, no. 10, pp. 855–861, 2009.

[2] B. A. Holden, T. R. Fricke, S. M. Ho et al., "Global vision impairment due to uncorrected presbyopia," *Archives of Ophthalmology*, vol. 126, no. 12, pp. 1731–1739, 2008.

[3] D. D. Koch, "Histological changes and wound healing response following noncontact holmium: YAG laser thermal keratoplasty," *Transactions of the American Ophthalmological Society*, vol. 94, pp. 745–802, 1996.

[4] M. B. McDonald, D. Durrie, P. Asbell, R. Maloney, and L. Nichamin, "Treatment of presbyopia with conductive keratoplasty®: six-month results of the 1-year United States FDA clinical trial," *Cornea*, vol. 23, no. 7, pp. 661–668, 2004.

[5] R. L. Epstein and M. A. Gurgos, "Presbyopia treatment by monocular peripheral presbyLASIK," *Journal of Refractive Surgery*, vol. 25, no. 6, pp. 516–523, 2009.

[6] T. Kohnen, "Multifocal IOL technology: a successful step on the journey toward presbyopia treatment," *Journal of Cataract and Refractive Surgery*, vol. 34, no. 12, p. 2005, 2008.

[7] Ö. F. Yılmaz, N. Alagöz, G. Pekel et al., "Intracorneal inlay to correct presbyopia: long-term results," *Journal of Cataract and Refractive Surgery*, vol. 37, no. 7, pp. 1275–1281, 2011.

[8] N. Menassa, A. Fitting, G. U. Auffarth, and M. P. Holzer, "Visual outcomes and corneal changes after intrastromal femtosecond laser correction of presbyopia," *Journal of Cataract and Refractive Surgery*, vol. 38, no. 5, pp. 765–773, 2012.

[9] R. K. Banerjee and S. Dasgupta, "Characterization methods of high-intensity focused ultrasound-induced thermal field," in *Advances in Heat Transfer*, Y. I. Cho and G. A. Greene, Eds., vol. 42, Elsevier, Burlington, Mass, USA, 2010.

[10] F. Aptel and C. Lafon, "Therapeutic applications of ultrasound in ophthalmology," *International Journal of Hyperthermia*, vol. 28, no. 4, pp. 405–418, 2012.

[11] T. Charrel, F. Aptel, A. Birer et al., "Development of a miniaturized HIFU device for glaucoma treatment with conformal coagulation of the ciliary bodies," *Ultrasound in Medicine and Biology*, vol. 37, no. 5, pp. 742–754, 2011.

[12] F. Aptel, T. Charrel, X. Palazzi, J.-Y. Chapelon, P. Denis, and C. Lafon, "Histologic effects of a new device for high-intensity focused ultrasound cyclocoagulation," *Investigative Ophthalmology and Visual Science*, vol. 51, no. 10, pp. 5092–5098, 2010.

[13] F. Aptel, T. Charrel, C. Lafon et al., "Miniaturized high-intensity focused ultrasound device in patients with glaucoma: a clinical pilot study," *Investigative Ophthalmology and Visual Science*, vol. 52, no. 12, pp. 8747–8753, 2011.

[14] R. Gaudana, H. K. Ananthula, A. Parenky, and A. K. Mitra, "Ocular drug delivery," *The AAPS Journal*, vol. 12, no. 3, pp. 348–360, 2010.

[15] U. B. Kompella, R. S. Kadam, and V. H. L. Lee, "Recent advances in ophthalmic drug delivery," *Therapeutic Delivery*, vol. 1, no. 3, pp. 435–456, 2010.

[16] D. B. Mark and R. Beuerman, "Intracorneal lesions produced with focused ultrasound," *Current Eye Research*, vol. 2, no. 5, pp. 323–326, 1982.

[17] A. R. Rutzen, C. W. Roberts, J. Driller et al., "Production of corneal lesions using high-intensity focused ultrasound," *Cornea*, vol. 9, no. 4, pp. 324–330, 1990.

[18] E. J. Berjano, E. Navarro, V. Ribera, J. Gorris, and J. L. Alio, "Radiofrequency heating of the cornea: an engineering review of electrodes and applicators," *The Open Biomedical Engineering Journal*, vol. 1, no. 1, pp. 71–76, 2007.

[19] J. S. Ehrlich and E. E. Manche, "Regression of effect over long-term follow-up of conductive keratoplasty to correct mild to moderate hyperopia," *Journal of Cataract and Refractive Surgery*, vol. 35, no. 9, pp. 1591–1596, 2009.

[20] J. G. Lynn and T. J. Putnam, "Histological and cerebral lesions produced by focused ultrasound," *The American Journal of Pathology*, vol. 20, pp. 637–649, 1944.

[21] W. J. Fry and F. J. Fry, "Fundamental neurological research and human neurosurgery using intense ultrasound," *IRE Transactions on Medical Electronics*, vol. 7, no. 3, pp. 166–181, 1960.

[22] T. L. Naoumidi, I. G. Pallikaris, I. I. Naoumidi, and N. I. Astyrakakis, "Conductive keratoplasty: histological study of human corneas," *American Journal of Ophthalmology*, vol. 140, no. 6, pp. 984–992.e2, 2005.

[23] M. B. McDonald, "Conductive keratoplasty: a radiofrequency-based technique for the correction of hyperopia," *Transactions of the American Ophthalmological Society*, vol. 103, pp. 512–536, 2005.

Hindawi Publishing Corporation
Journal of Ophthalmology
Volume 2016, Article ID 2623719, 7 pages
http://dx.doi.org/10.1155/2016/2623719

Research Article

Differences in Central Corneal Thickness between Spectral Domain-Optical Coherence Tomography and Ultrasound Pachymetry in Patients with Dry Eye Disease

Ali Riza Cenk Celebi[1] and G. Ertugrul Mirza[2]

[1]*Department of Ophthalmology, Acibadem University School of Medicine, 34303 Istanbul, Turkey*
[2]*Department of Ophthalmology, Erciyes University School of Medicine, 38030 Kayseri, Turkey*

Correspondence should be addressed to Ali Riza Cenk Celebi; arcenkcelebi@gmail.com

Received 8 March 2016; Accepted 17 May 2016

Academic Editor: George M. Saleh

Purpose. To compare central corneal thickness (CCT) values via Spectral Domain-Optical Coherence Tomography (SD-OCT) and ultrasonic pachymetry in patients with severe dry eye disease (DED) to determine the level of agreement between these 2 methods. *Methods*. The paired samples t-test was used to compare CCT values in severe DED patients. Matching analysis between methods was performed using intraclass correlation coefficient (ICC). Intrasession reliability of the measurement methods was calculated via the concordance correlation coefficient (CCC), variation equivalent, and Pearson's correlation coefficient. The Bland-Altman procedure was used to graphically represent the differences between CCT values. *Results*. The study included 56 eyes of 24 female and 4 male patients. Mean age of the patients was 50.9 ± 11.3 years. Mean CCT via Cirrus SD-OCT was 523.82 ± 30.98 μm versus 530.050 ± 31.85 μm via ultrasonic pachymetry (paired samples t-test, $P < 0.001$). The Bland-Altman plot showed good agreement between the examiners. The ICC for repeatability was 0.974. The CCC between the 2 methods' CCT values was 0.973. The variation equivalent was 0.976 and Pearson's correlation coefficient was 99.3%, which also indicated high correlation between the 2 methods' measurements. *Conclusions*. The present findings show that in patients with severe DED Cirrus SD-OCT provides reliable intraobserver CCT values.

1. Introduction

Dry eye disease (DED) is a multifactorial disease that negatively affects tears and the ocular surface, resulting in potential corneal injury [1]. Epidemiological data have shown that dry eye becomes more frequent with age in both sexes. Women are at a higher risk of dry eye than men [2]. The mechanisms of DED include tear film instability, increased tear osmolarity, and a cascade of inflammatory events in the corneal epithelial surface [1]. In order to plan refractive surgery, detect corneal changes due to corneal disease, or measure intraocular pressure (IOP), it is important to measure corneal thickness precisely [3]. Evaluation of corneal thickness provides clinically useful information related to the physiological status of the cornea [4]. Significant alterations in central corneal thickness (CCT) have the potential to alter IOP measurement. Underestimation of IOP because of a thin cornea can potentially delay diagnosis and treatment of glaucoma [5]; therefore, evaluation of CCT is essential in cases of glaucoma, contact lens wear, corneal refractive surgery, and dry eye disease [4].

As CCT is an important indicator of corneal health, various studies have investigated CCT and dry eye disease—some reporting thin CT in patients with DED [6–9]. Furthermore, Karadayi et al. [9] suggested that CCT might be used for the diagnosis and follow-up of patients with DED. Reliable CCT measurement can be obtained using a variety of methods, including ultrasonic pachymetry, scanner slit technology, rotating Scheimpflug imaging, interferometry, corneal confocal microscopy, and optical coherence tomography

(OCT) [10]. Ultrasonic pachymetry is currently the gold standard for measuring CCT; however, use of its contact probe is associated with patient discomfort and microbial contamination [10]. It was reported that patients with DED are more susceptible to corneal infections than healthy individuals [11]. Furthermore, ultrasonic pachymetry can easily produce corneal epithelial damage over the ocular surface which is much more severe in patients with DED and it can produce measurement error due to the pressure exerted over the cornea and due to inadequate alignment of the terminal, which must be positioned absolutely perpendicular to the corneal surface [12]. Because of these drawbacks associated with ultrasonic pachymetry, OCT has been recently applied to the measurement of CCT.

OCT was originally used to diagnose retinal pathologies. Technological advancements in OCT have made it possible to use Spectral Domain-Optical Coherence Tomography (SD-OCT) to image corneal tissue. The Cirrus SD-OCT device is among the latest generation of Fourier domain OCT devices and can imagine anterior segment structures by changing the focus of the OCT beam. Previous studies have evaluated the accuracy and reliability of SD-OCT measurement of CCT [10, 13]. In general, mean CCT values obtained via SD-OCT were lower than those obtained via ultrasonic pachymetry. In an earlier study of ours [13] mean CCT measured via SD-OCT was 3.37 μm less than that via ultrasonic pachymetry. The reliability of measurements obtained using any ophthalmic instrument should be determined, so that misdiagnosis based on the readings can be avoided. To the best of our knowledge, the reliability of Cirrus SD-OCT measurement of CCT in patients with DED has not been studied; as such, the present study aimed to compare CCT measurement via SD-OCT and ultrasonic pachymetry in patients with DED to determine the degree of systematic difference and the level of agreement between the 2 methods. The possible mechanisms and theoretical explanations regarding the difference of CCT measurements obtained by SD-OCT and ultrasonic pachymetry in dry eye patients were also discussed. Therefore, it was also discussed that, in clinics using Cirrus SD-OCT as a diagnostic imaging method, this device could be used as a reliable noncontact pachymeter when assessing dry eye patients. This study also aimed to determine the intraexaminer reproducibility of CCT values via the two methods in patients with DED.

2. Materials and Methods

This prospective observational study included 28 patients diagnosed as severe DED. The study protocol was approved by the Local Ethical Committee and was performed in accordance with the Declaration of Helsinki, and each patient provided written informed consent for imaging and DED assessment at the time they visited our clinic. DED was diagnosed based on tear film breakup time with ocular surface staining <5 s, Schirmer's test result (with topical proparacaine anesthesia) <5 mm, and significant symptoms of dryness at presentation as confirmed with OSDI score which is over 40 [1]. Patients with a history of corneal surgery and those with evidence of active infection in the cornea and/or conjunctiva, localized corneal scar, and reported use of contact lenses were excluded from the study. Patients with any type of corneal dystrophy and/or rheumatic disease were also excluded as were those with a history of any ocular or systemic disease other than DED. All patients underwent comprehensive examination of the anterior and posterior segment structures using slit-lamp biomicroscopy, indirect fundoscopy, and applanation tonometry; patients with any type of posterior segment abnormality were also excluded from the study.

The central part of the cornea was found using calipers. The horizontal and the vertical diameter of the cornea were measured and the center of the distance was pointed. Both SD-OCT and ultrasonic measurements of the central corneal thicknesses were obtained from that central point.

CCT measurement via Cirrus SD-OCT was performed in each patient before CCT measurement via ultrasonic pachymetry, because ultrasonic pachymetry can cause corneal epithelial defects. Corneal images were acquired using the Cirrus SD-OCT device in anterior segment 5-line raster mode, which utilizes 5 horizontal scan lines—each 3 mm long—with a distance of 250 μm between each two lines. Each scan line is composed of 4096 A scans s^{-1}. This mode can easily image the upper (upper border of epithelia) and lower (inner border of endothelia) boundaries of the cornea with great clarity. In addition, the digital caliper can be placed very accurately between these boundaries.

After being seated and properly aligned in front of the device, each patient was instructed to focus on the device's internal fixation target during image acquisition. CCT anterior segment 5-line raster images were obtained for both eyes in each patient. Only images with signal strength ≥7 were evaluated. Examinations were performed between 12.00 and 13.00 to minimize the effect of diurnal variation in corneal thickness [9]. Among the CCT anterior segment 5-line raster images, the image at the center point of the cornea was enlarged. Then, CCT was measured via manual use of a digital caliper in the cross-line scan; the vertical distance between the inner border of endothelia and outer upper border of epithelia of the cornea was considered CCT. The measurements were carried out at the corneal center. CCT measurements were always manually performed at the corneal center point. Five consecutive measurements were obtained from each of the different Cirrus SD-OCT images and the mean CCT value was used for analysis. Immediately following CCT measurement via Cirrus SD-OCT, 1 drop of topical proparacaine 0.5% was placed in the same eye. Then, 5 measurements of the cornea were obtained using a PacScan 300P (Sonomed Escalon, Lake Success, NY, USA) ultrasonic pachymeter, with the ultrasonic probe at the center point of the cornea. Patients were instructed to fixate at a distant object, and then 5 consecutive measurements were obtained and averaged for comparison with Cirrus SD-OCT values.

Cirrus SD-OCT images were obtained and CCT values were calculated by the same physician who was blinded to the ultrasonic pachymetry CCT values to avoid bias. All ultrasonic pachymetry CCT measurements were made by the same ophthalmic technician to avoid interexaminer variability.

2.1. Statistical Analysis. Data were analyzed using SPSS v.16.0 for Windows (SPSS, Inc., Chicago, IL). Quantitative variables, such as CCT, were summarized using descriptive statistics (i.e., sample size frequency, percentage, mean, and standard deviation). Normality of data distribution was tested using the Shapiro-Wilk and Kolmogorov-Smirnov tests. The paired samples t-test was used to compare CCT values. The paired samples t-test was used to determine if there was a significant systematic bias between examiners. Matching analysis between both methods was performed using the intraclass correlation coefficient. Intrasession reliability of the measurement methods was calculated via the concordance correlation coefficient, intraclass correlation coefficient (ICC), variation equivalent, and Pearson's correlation coefficient, which was also used to investigate the correlation between the quantitative measurements of mean CCT.

The Bland-Altman procedure was used to graphically represent the differences between CCT values obtained via the 2 methods, as well as in the matching limits of the 95% limits of agreement (LoA). The 95% LoA was defined as the mean difference in measurements performed by the 2 examiners obtained by the 2 methods ±1.96 SD, with lower values indicating higher interobserver reproducibility. A Bland-Altman plot was generated to assess the difference in individual measurements as a function of the mean of 2 measurements and to evaluate the correlations between the 2 CCT measurement methods (MedCalc Software, Mariakerke, Belgium). In brief, agreement between the measurements obtained via the 2 methods was examined using a Bland-Altman plot and LoA were calculated. Pearson's correlation analysis was used to assess the strength of correlation between the measurements. Reproducibility was evaluated via the intraclass correlation coefficient (ICC); an ICC of 1.00 represents perfect agreement, whereas 0.81–0.99 represents almost perfect agreement. Results were evaluated at the 95% CI and the level of statistical significance was set at $P < 0.05$.

3. Results

The study included 56 eyes of 24 female and 4 male patients. Mean CCT value of the females via Cirrus SD-OCT was 520.67 ± 33.58 μm versus 527.46 ± 35.07 μm via ultrasonic pachymetry. Meanwhile the mean CCT value of the males via Cirrus SD-OCT was 533.00 ± 20.49 μm versus 540.00 ± 20.94 μm via ultrasonic pachymetry. These mean CCT value differences (6.79 μm in females and 7 μm in males) between Cirrus SD-OCT and ultrasonic pachymetry were significant in each sex (paired samples t-test, $P < 0.001$ for females and males). Indeed, the mean CCT value differences (12.33 μm with Cirrus SD-OCT and 12.54 μm with ultrasonic pachymetry) between sexes were substantially different (Mann-Whitney U test, $P < 0.001$).

Mean age of the patients was 50.9 ± 11.3 years. The mean age of female patients was 51.7±11.4 years; however, the mean age for the males was 45.7 ± 10.1 years. All 28 patients had the same Schirmer values in both of their eyes individually.

Mean CCT value of the right eyes via Cirrus SD-OCT was 522.43 ± 32.04 μm versus 529.25 ± 33.41 μm via ultrasonic pachymetry. Meanwhile the mean CCT value of the left eyes via Cirrus SD-OCT was 525.21 ± 30.39 μm versus 530.86 ± 30.79 μm via ultrasonic pachymetry. The mean difference between the 2 methods in left and right eyes separately was statistically significant (paired samples t-test, $P < 0.001$ for left eyes; paired samples t-test, $P < 0.001$ for right eyes). However, the CCT values between eyes were not statistically significant (paired samples t-test, $P > 0.05$). Both eyes were used in analysis because the mean CCT values in right eyes and left eyes for each of the measurement devices showed high correlation [14]. The concordance correlation coefficients of the right eyes and left eyes were 0.97 and 0.98, respectively.

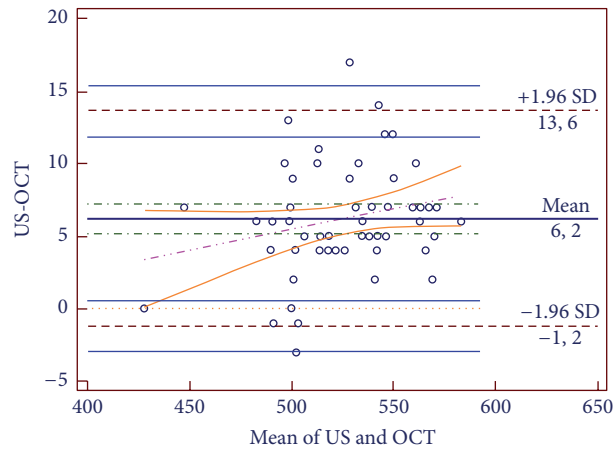

Figure 1: Bland-Altman plot of the difference in mean CCT values based on Cirrus SD-OCT and ultrasonic pachymetry in patients with DED.

Overall mean CCT via Cirrus SD-OCT was 523.82 ± 30.98 μm versus 530.050 ± 31.85 μm via ultrasonic pachymetry; the mean difference between the 2 methods' measurements was significant (6.23 μm) (paired samples t-test, $P < 0.001$). The distribution of the differences between both methods' measurements was normal (Shapiro-Wilk test, $P > 0.05$). The Bland-Altman plot generated to assess the difference in individual measurement as a function of the mean of 2 measurements showed good agreement between the examiners; LoA width was 14.8 μm. The upper limit of LoA was 13.64 (95% CI: 11.90–15.38) and the lower limit was −1.18 (−2.92–0.56) (Figure 1). The ICC for repeatability was 0.974 (95% CI: 0.955–0.984). The correlation coefficient (CCC) between the 2 methods' CCT measurements was 0.973 (95% CI: 0.958–0.983). In addition, the variation equivalent was 0.976 and Pearson's correlation coefficient was 99.3%, which also indicated high correlation between the 2 methods' measurements.

4. Discussion

Evaluation of corneal thickness provides clinically useful information concerning the physiological status of the cornea. Ultrasonic pachymetry has been the gold standard for measuring corneal thickness since 1967 based on a Pubmed search. The primary drawback of this technique is that it is invasive and requires instillation of topical anesthesia [15].

In addition, ultrasonic pachymetry is associated with several potential sources of error in terms of CCT measurement. Its accuracy depends on the cornea, and the perpendicularity of the probe with respect to cornea is often difficult to ascertain. If the probe is placed slightly off center at an oblique angle, corneal thickness can be overestimated. Due to these drawbacks associated with ultrasonic pachymetry, various noncontact methods of CCT measurement have recently come into use [16]. OCT is an in vivo, noncontact technique for obtaining high-resolution, cross-sectional images of biological tissues based on measurement of optical reflections. Recently, the utility of OCT in clinical practice has been extended to the anterior segment of the eye [16]. Moreover, dedicated noncontact SD-OCT devices have become available, offering rapid acquisition of high-resolution, cross-sectional images of the cornea and CCT measurement. Anterior segment optical coherence tomography (AS-OCT) is not associated with the same disadvantages as ultrasonic pachymetry, because it is a noninvasive, noncontact method. Earlier studies evaluated corneal thickness using the OCT intensity profile, in which computer software-controlled cursors are manually placed at the peak of reflectivity corresponding to the tissue interfaces [17]. In the present study, in consideration of the resolution of the OCT images obtained, we directly and manually placed the cursors provided by the SD-OCT software to measure CCT.

DED is a disease of the ocular surface that causes discomfort, visual disturbance, and tear film instability, with the possibility of damage to the ocular surface. DED is accompanied by an increase in osmolarity of the tear film and inflammation of the ocular surface [1]. As the assessment of CCT is an important indicator of corneal health, various studies have investigated CCT in patients with DED [9, 18–20]. Pole and Batzer [18] studied 16 patients with DED and observed a minimal, nonsignificant reduction in corneal thickness in the patients with DED, as compared to healthy controls, whereas Høvding [19] reported a significant reduction in CCT in the absence of marked inflammation in 17 patients with DED.

At the time those earlier studies were performed, ultrasonic pachymetry was the only available method for measuring CCT in patients with DED. A groundbreaking study reported a significant decrease in CCT measured via Orbscan pachymetry in patients with aqueous tear-deficient DED. The researchers measured CCT in 38 eyes of 21 patients with DED and in 34 eyes of 21 healthy controls, and the mean difference between the 2 groups was 35 μm [6]. A more recent study that also used Orbscan pachymetry reported a reduction in CCT in postmenopausal women with DED [8].

The International Dry Eye Workshop [1] modified the definition of DED to include the role of tear film hyperosmolarity and ocular surface inflammation. Regardless of initiating etiological factors, once DED develops inflammation becomes the key mechanism of injury. Excessive inflammation can lead to a vicious cycle, resulting in an increase in tear film osmolarity. In all forms of DED the primary mechanism of ocular surface damage is apparently hyperosmolarity of the tear film, which affects corneal hydration resulting in dehydration of the cornea [20]. In healthy individuals, the aqueous layer of the tear film is isotonic or slightly hypertonic. Hypertonic solutions decrease corneal thickness and it was reported that when tear production decreases tear film osmolarity increases and the cornea becomes thinner [6].

The etiology of decreased corneal thickness in patients with DED is not clearly understood. Among the proposed etiological factors are an increase in tear film evaporation which results in increased osmolarity of the tear fluid, as mentioned above, and a chronic state of desiccation and immune activation that can cause a decrease in tear film thickness, which is normally 1–45 μm [6–8]. It was suggested that drying conditions stimulate cells to cycle and proliferate throughout the entire epithelium as a consequence of apical cell surface damage [19]. In an experimentally induced DED model, Yeh et al. [21] observed apoptosis of keratocytes and suggested that apoptosis might play an important role in the pathogenesis of DED-related epitheliopathy. Hence, it was suggested that excessive apoptosis or shedding of the surface epithelium—if sustained and if there is no compensation for epithelial cycling—might lead to epithelial thinning in patients with DED [22]. Furthermore, a significant reduction in corneal stromal thickness in DED patients was observed via in vivo confocal microscopy. It was hypothesized that apoptosis, as well as an increase in proteolytic activity at the stromal level, might be the cause of this reduction in corneal stromal thickness [23]. An in vivo confocal study reported that the density of superficial corneal epithelial cells and subbasal nerves was significantly lower in patients with DED than in healthy individuals [23]. In addition, the density of superficial and intermediate epithelial cells at the center of the cornea in dry eye patients was less than that in healthy controls, which might have been due to enlargement of the cells as a result of metabolic dysfunction [23].

Another theoretical explanation for the difference in CCT values between ultrasonic pachymetry and SD-OCT methods is corneal edema due to topical anesthetic eye drops [24]. Topical ophthalmic anesthetics are toxic to the cornea; however, they are needed for a number of clinical diagnostic procedures, including ultrasonic pachymetry. The potential adverse effects of topical anesthetics include tear film alteration, epithelial toxicity, microbial contamination, and allergic reactions. Anesthetic eye drops can induce variations in corneal thickness >10 μm, masking the possible effect of dry eye on CCT values in patients with DED. Herse and Siu [25] observed that instillation of a single drop of proparacaine 0.5% induced an increase in CCT which was caused by corneal stromal edema. Mukhopadhyay et al. [26] reported overall corneal swelling following administration of topical proparacaine 0.5% and sodium fluorescein 0.25%, which are commonly used in some of the busy clinics when measuring IOP, and the observed swelling was greatest in the central part of the cornea. They further reported that the increase in CCT was around 10 μm but could be as high as 30 μm. The effect of topical anesthetic should be taken into account when measuring CCT in patients with DED, as it can result in overestimation. In the present study, mean CCT value via ultrasonic pachymetry and topical anesthetic eye drop was approximately 6.23 μm higher than that measured via SD-OCT.

Alcaine®, a topical anesthetic eye drop used during ultrasonic pachymetry, includes the preservative benzalkonium chloride (BAC), which is a quaternary ammonium compound shown to hasten tear film drying, exacerbate preexisting DED, and negatively affect the cornea [27]. BAC at a high concentration such as 0.1% was used to induce a dry eye model in animal studies [28]. Many researchers have investigated the acute toxic effects of high concentrations defined as 0.1% of BAC on the ocular surface [29]. A wealth of clinical and experimental evidence supports the notion that the toxic effect BAC has on the ocular surface is primarily concentration dependent. Topical use of BAC can induce ocular surface changes, such as tear film instability, loss of goblet cells, inflammation, epithelial apoptosis, and corneal endothelial cell edema and disappearance, resulting in loss of barrier function and an increase in corneal stroma, which all result in an increase in corneal thickness [30]. BAC can also cause corneal surface epithelial edema and adversely affect the barrier integrity of the corneal epithelium. Currently, BAC is most often used at a concentration of 0.01% in ophthalmic preparations, which appears to be safe in normal healthy individuals. In a recent study, Chen et al. [28] reported that even low concentrations defined as 0.01% of BAC can induce significant corneal stromal alterations. It was reported that in corneal epithelium (the most clinically significant tissue affected in patients with DED) exposed to a desiccating stress in a mouse model of experimentally induced DED the cell proliferation rate and CCT increased significantly [22]. We did not know the safe concentration of BAC in dry eye patients so CCT value differences between these two devices could be related to BAC preservative, which was used during ultrasonic pachymetry.

The tear system is dynamic and blinking plays an important role in distributing tears across the ocular surface. Blinking redistributes tears to the ocular surface from the tear menisci around the upper and lower eyelids and facilitates tear drainage. Due to reflex tearing, the balance between tear secretion and drainage in normal eyes is altered during delayed blinking. During delayed blinking tear menisci increase significantly. Furthermore, the lack of tears in DED patients can result in abnormal tear distribution across the ocular surface and irregular interaction during blinking [31]; however, in DED patients mean precorneal tear film thickness was higher immediately after delayed blinking than after normal blinking [32]. The increase in precorneal tear film during delayed blinking might also indicate that patients with DED may have some ability to produce tears in response to prolonged eye opening. The effect of delayed blinking was also taken into account during the present study while obtaining CCT values, which in all instances occurred immediately after blinking.

In the present study we carefully sought to avoid the effect of systemic drugs on DED because of the fact that systemic drugs (i.e., anticholinergic drugs and antihistaminic drugs) used to treat several diseases can increase the risk of DED. Furthermore, it is known that tear production is reduced in elderly tear-deficient patients that use systemic medications [33] and, as such, the present study aimed to exclude patients using any type of systemic drug. In addition, DED patients with such systemic illnesses as diabetes mellitus were also excluded, as increased cornea thickness has been reported in diabetic patients [34]. Dry eye in diabetics is known to be due to a decrease in corneal sensation or in the relative numbness of the ocular surface. Mean CCT in the corneas of diabetic patients was 27 μm higher than that in nondiabetic controls [34]. It has been posited that increased corneal thickness in diabetics might be due to increased corneal water content, increased corneal dry weight content, or a combination of both. Moreover, mean CCT in diabetics with DED is lower than that in diabetics without DED. To eliminate all confusion regarding the effect of diabetes on CCT in dry eyes, DED patients with diabetes were excluded in the present study. Contact lens wearers were also excluded from the present study because it is known that dry eye is more prevalent in such patients and that long-term contact lens users have lower mean CCT values than those that do not use contact lenses [35]. Pseudoexfoliation (PEX) material can cause a decrease in tear film secretion and disturb tear film stability. Lower CCT values in eyes with PEX material may be a result of a decrease in corneal stromal cell density [36]. As such, we also excluded the patients with PEX material while interpreting the findings.

One of the limitations of the current study is that we were unable to measure the precorneal tear film thickness due to the lack of imaging spectrograph, ultrahigh resolution optical coherence tomography, noninvasive interferometry, and confocal microscopy. However, there is a wide range of mean precorneal tear film thickness values in healthy subjects. There is not a normal level of tear film thickness in agreement present in the literature. Mean central tear film thickness was reported to be 4.79 μm based on ultrahigh resolution OCT [37]. Prydal et al. [38] observed that precorneal tear film thickness was 34–45 μm based on noninvasive interferometry versus 41–46 μm based on confocal microscopy. Wong et al. [39] reported precorneal tear film thickness as 8.0 μm. King-Smith et al. [40] reported the mean precorneal tear film thickness as 2.7 μm using SpectraPro-150 imaging spectrograph.

Another limitation of the present study is that corneal thickness was only measured centrally. According to a recent study, alteration of epithelial thickness caused by DED affects the peripheral corneal epithelium to a greater extent compared to the central region [32]. To determine why the superior epithelium is thinner in dry eyes, the spatial disparity of epithelial thickness in normal eyes should be determined first. The superior corneal epithelium was shown to be significantly thinner than the inferior in normal eyes [41]. This nonuniform thickness profile was suggested to be induced by the friction that results from the mechanical dynamics of blinking [42]. The wider-range movement and vertical traverse of the upper lid rub more of the ocular surface in the superior corneal region. This friction mechanically damages epithelial cells, causing the thinning of the superior epithelium. DED patients usually do not have enough tears for lubrication and it was proposed that the increase in mechanical friction exacerbates epithelial damage and results in even thinner superior epithelium [32].

The prevalence of dry eye is higher in females; our higher number of female participants supports this finding. The high frequency of woman participants in our study made us consider the possible effect of sex hormones on corneal thickness values. The mean CCT value of female patients in our study was approximately 12 μm thinner than the values of our male patients. The cornea of females can be affected by hormonal changes that occur during the monthly menstrual cycle. Indeed, cyclic variations in corneal thickness have been described. Increased corneal thickness measured during ovulation and at the end of the menstrual cycle is based on a previous study by Goldich et al. [43]. Keskin et al. [44] showed a linear correlation between CCT and serum estradiol levels of their patients. They also showed that menopause causes a decrease in central corneal thickness measurements. The mean age of our female patients was 51.7 years, which can be considered as perimenopause period. The reduced corneal thickness values we encountered in our female patients support this finding. Changes in corneal hydration, together with estrogen-mediated changes in corneal cells and corneal extracellular matrix, can all be possible reasons for these corneal thickness changes in females [43, 44]. The effects of hormones on cornea should be taken into consideration while interpreting the central corneal thickness values.

In the present study, mean CCT measured via Cirrus SD-OCT was 6.23 μm less than that measured via ultrasonic pachymetry, which might have been due to manual adjustment of the Cirrus SD-OCT device's scale. The slightest movement of the Cirrus SD-OCT measurement bar has sensitivity of 4 μm. Decreasing the level of sensitivity of the scale to 1 μm may result in exactly the same CCT measurements as obtained via ultrasonic pachymetry. User-dependent CCT differences can be avoided by future software updates to facilitate automated CCT measurements, as used for retinal examination [14]. It is unclear if ultrasonic pachymetry or SD-OCT measurements more accurately indicate the actual corneal thickness in DED patients. Although it is possible that differences in analysis software might account for the discrepancy observed in the present study, the weight of evidence currently available suggests that a systematic difference does exist between SD-OCT and ultrasonic pachymetry and that the discrepancy is unrelated to intraobserver differences in SD-OCT measurements.

In conclusion, the present findings show that in patients with severe DED Cirrus SD-OCT provides reliable intraobserver CCT values and consistent agreement between independently trained observers. Although potential errors can occur with manual measurements, this present finding can inform researchers and clinicians concerning the expected variability when performing this pachymetry technique in severe DED patients. The difference in CCT based on SD-OCT and ultrasonic pachymetry measurement should always be a consideration when interpreting CCT values in severe DED patients.

Competing Interests

The authors declare that there are no competing interests regarding the publication of this paper.

References

[1] M. A. Lemp, C. Baudouin, J. Baum et al., "The definition and classification of dry eye disease: report of the Definition and Classification Subcommittee of the International Dry Eye WorkShop (2007)," *Ocular Surface*, vol. 5, no. 2, pp. 75–92, 2007.

[2] J. A. Smith, J. Albenz, C. Begley et al., "The epidemiology of dry eye disease: report of the Epidemiology Subcommittee of the International Dry Eye WorkShop (2007)," *Ocular Surface*, vol. 5, no. 2, pp. 93–107, 2007.

[3] T. Schmoll, A. Unterhuber, C. Kolbitsch, T. Le, A. Stingl, and R. Leitgeb, "Precise thickness measurements of Bowman's layer, epithelium, and tear film," *Optometry and Vision Science*, vol. 89, no. 5, pp. E795–E802, 2012.

[4] I. Akyol-Salman, S. Azizi, U. Mumcu, O. Öndaş, and O. Baykal, "Central corneal thickness in patients with meibomian gland dysfunction," *Clinical and Experimental Optometry*, vol. 94, no. 5, pp. 464–467, 2011.

[5] J. B. Jonas, A. Stroux, I. Velten, A. Juenemann, P. Martus, and W. M. Budde, "Central corneal thickness correlated with glaucoma damage and rate of progression," *Investigative Ophthalmology & Visual Science*, vol. 46, no. 4, pp. 1269–1274, 2005.

[6] Z. Liu and S. C. Pflugfelder, "Corneal thickness is reduced in dry eye," *Cornea*, vol. 18, no. 4, pp. 403–407, 1999.

[7] V. Dayanir, R. Sakarya, F. Özcura et al., "Effect of corneal drying on central corneal thickness," *Journal of Glaucoma*, vol. 13, no. 1, pp. 6–8, 2004.

[8] J. A. Sanchis-Gimeno, A. Lleó-Pérez, L. Alonso, M. S. Rahhal, and F. Martínez-Soriano, "Reduced corneal thickness values in postmenopausal women with dry eye," *Cornea*, vol. 24, no. 1, pp. 39–44, 2005.

[9] K. Karadayi, F. Ciftci, T. Akin, and A. H. Bilge, "Increase in central corneal thickness in dry and normal eyes with application of artificial tears: a new diagnostic and follow-up criterion for dry eye," *Ophthalmic and Physiological Optics*, vol. 25, no. 6, pp. 485–491, 2005.

[10] A. Ishibazawa, S. Igarashi, K. Hanada et al., "Central corneal thickness measurements with fourier-domain optical coherence tomography versus ultrasonic pachymetry and rotating scheimpflug camera," *Cornea*, vol. 30, no. 6, pp. 615–619, 2011.

[11] L. Keay, K. Edwards, T. Naduvilath et al., "Microbial keratitis: predisposing factors and morbidity," *Ophthalmology*, vol. 113, no. 1, pp. 109–116, 2006.

[12] C. Lázaro, E. M. Hernández, D. Martínez, and P. Redondo, "Comparison of central corneal thickness measured with anterior segment optical coherence tomography versus ultrasonic pachymetry," *Archivos de la Sociedad Espanola de Oftalmologia*, vol. 88, no. 2, pp. 45–49, 2013.

[13] A. R. Çelebi and G. E. Mirza, "Merkezi Kornea Kalınlığının Değerlendirilmesinde Spektral Domain Optik Koherans Tomografinin ve Ultrasonik Pakimetrinin Karşılaştırılması," *Turkish Journal of Ophthalmology*, vol. 44, no. 4, pp. 259–262, 2014.

[14] R. A. Armstrong, "Statistical guidelines for the analysis of data obtained from one or both eyes," *Ophthalmic and Physiological Optics*, vol. 33, no. 1, pp. 7–14, 2013.

[15] J. A. Sanchis-Gimeno, J. M. Palanca-Sanfrancisco, S. García-Lázaro, D. Madrid-Costa, and A. Cerviño, "The effect of anesthetic eye drop instillation on the distribution of corneal thickness," *Cornea*, vol. 32, no. 5, pp. e102–e105, 2013.

[16] Y. Feng and T. L. Simpson, "Comparison of human central cornea and limbus in vivo using optical coherence tomography," *Optometry and Vision Science*, vol. 82, no. 5, pp. 416–419, 2005.

[17] J. Wang, D. Fonn, T. L. Simpson, and L. Jones, "The measurement of corneal epithelial thickness in response to hypoxia using optical coherence tomography," *American Journal of Ophthalmology*, vol. 133, no. 3, pp. 315–319, 2002.

[18] J. J. Pole and J. K. Batzer, "Central corneal thickness of patients with dry eyes," *Journal of the American Optometric Association*, vol. 56, no. 3, pp. 220–221, 1985.

[19] G. Høvding, "The central corneal thickness in keratoconjunctivitis sicca," *Acta Ophthalmologica*, vol. 70, no. 1, pp. 108–110, 1992.

[20] A. J. Bron, "Diagnosis of dry eye," *Survey of Ophthalmology*, vol. 45, no. 2, pp. S221–S226, 2001.

[21] S. Yeh, X. J. Song, W. Farley, D.-Q. Li, M. E. Stern, and S. C. Pflugfelder, "Apoptosis of ocular surface cells in experimentally induced dry eye," *Investigative Ophthalmology & Visual Science*, vol. 44, no. 1, pp. 124–129, 2003.

[22] C. Fabiani, S. Barabino, S. Rashid, and M. R. Dana, "Corneal epithelial proliferation and thickness in a mouse model of dry eye," *Experimental Eye Research*, vol. 89, no. 2, pp. 166–171, 2009.

[23] E. Villani, D. Galimberti, F. Viola, C. Mapelli, and R. Ratiglia, "The cornea in Sjögren's syndrome: an in vivo confocal study," *Investigative Ophthalmology and Visual Science*, vol. 48, no. 5, pp. 2017–2022, 2007.

[24] S. M. Nam, H. K. Lee, E. K. Kim, and K. Y. Seo, "Comparison of corneal thickness after the instillation of topical anesthetics: proparacaine versus oxybuprocaine," *Cornea*, vol. 25, no. 1, pp. 51–54, 2006.

[25] P. Herse and A. Siu, "Short-term effects of proparacaine on human corneal thickness," *Acta Ophthalmologica*, vol. 70, no. 6, pp. 740–744, 1992.

[26] D. R. Mukhopadhyay, R. V. North, and K. E. Hamilton-Maxwell, "Effect of a proparacaine 0.50%-sodium fluorescein 0.25% mix and contact ultrasound pachymetry on central and midperipheral corneal thickness measured by noncontact optical pachymetry," *Journal of Cataract and Refractive Surgery*, vol. 37, no. 5, pp. 907–913, 2011.

[27] W. S. Wilson, A. J. Duncan, and J. L. Jay, "Effect of benzalkonium chloride on the stability of the precorneal tear film in rabbit and man," *British Journal of Ophthalmology*, vol. 59, no. 11, pp. 667–669, 1975.

[28] W. Chen, Z. Li, J. Hu et al., "Corneal alternations induced by topical application of benzalkonium chloride in rabbit," *PLoS ONE*, vol. 6, no. 10, Article ID e26103, 2011.

[29] A. Labbé, A. Pauly, H. Liang et al., "Comparison of toxicological profiles of benzalkonium chloride and polyquaternium-1: an experimental study," *Journal of Ocular Pharmacology and Therapeutics*, vol. 22, no. 4, pp. 267–278, 2006.

[30] C. Baudouin, A. Labbé, H. Liang, A. Pauly, and F. Brignole-Baudouin, "Preservatives in eyedrops: the good, the bad and the ugly," *Progress in Retinal and Eye Research*, vol. 29, no. 4, pp. 312–334, 2010.

[31] Y. Yuan, J. Wang, Q. Chen, A. Tao, M. Shen, and M. A. Shousha, "Reduced tear meniscus dynamics in dry eye patients with aqueous tear deficiency," *American Journal of Ophthalmology*, vol. 149, no. 6, pp. 932–938.e1, 2010.

[32] X. Cui, J. Hong, F. Wang et al., "Assessment of corneal epithelial thickness in dry eye patients," *Optometry and Vision Science*, vol. 91, no. 12, pp. 1446–1454, 2014.

[33] J. M. Albietz, "Dry eye: an update on clinical diagnosis, management and promising new treatments," *Clinical and Experimental Optometry*, vol. 84, no. 1, pp. 4–18, 2001.

[34] O. M. Oriowo, "Profile of central corneal thickness in diabetics with and without dry eye in a Saudi population," *Optometry*, vol. 80, no. 8, pp. 442–446, 2009.

[35] Z. Liu and S. C. Pflugfelder, "The effects of long-term contact lens wear on corneal thickness, curvature, and surface regularity," *Ophthalmology*, vol. 107, no. 1, pp. 105–111, 2000.

[36] M. O. Akdemir, A. Kirgiz, O. Ayar et al., "The effect of pseudoexfoliation and pseudoexfoliation induced dry eye on central corneal thickness," *Current Eye Research*, vol. 41, no. 3, pp. 305–310, 2016.

[37] R. M. Werkmeister, A. Alex, S. Kaya et al., "Measurement of tear film thickness using ultrahigh-resolution optical coherence tomography," *Investigative Ophthalmology and Visual Science*, vol. 54, no. 8, pp. 5578–5583, 2013.

[38] J. I. Prydal, P. Artal, H. Woon, and F. W. Campbell, "Study of human precorneal tear film thickness and structure using laser interferometry," *Investigative Ophthalmology and Visual Science*, vol. 33, no. 6, pp. 2006–2011, 1992.

[39] H. Wong, I. Fatt, and C. J. Radke, "Deposition and thinning of the human tear film," *Journal of Colloid and Interface Science*, vol. 184, no. 1, pp. 44–51, 1996.

[40] P. E. King-Smith, B. A. Fink, N. Fogt, K. K. Nichols, R. M. Hill, and G. S. Wilson, "The thickness of the human precorneal tear film: evidence from reflection spectra," *Investigative Ophthalmology and Visual Science*, vol. 41, no. 11, pp. 3348–3359, 2000.

[41] E. Hosaka, T. Kawamorita, Y. Ogasawara et al., "Interferometry in the evaluation of precorneal tear film thickness in dry eye," *American Journal of Ophthalmology*, vol. 151, no. 1, pp. 18–23.e1, 2011.

[42] D. Z. Reinstein, R. H. Silverman, S. L. Trokel, and D. J. Coleman, "Corneal pachymetric topography," *Ophthalmology*, vol. 101, no. 3, pp. 432–438, 1994.

[43] Y. Goldich, Y. Barkana, E. Pras et al., "Variations in corneal biomechanical parameters and central corneal thickness during the menstrual cycle," *Journal of Cataract and Refractive Surgery*, vol. 37, no. 8, pp. 1507–1511, 2011.

[44] N. Keskin, S. Cantürk, S. Aydin, H. Saygili, and C. Özgün, "An objective method to determinme corneal changes during menopause," *Clinical and Experimental Obstetrics and Gynecology*, vol. 36, no. 3, pp. 176–178, 2009.

Hindawi Publishing Corporation
Journal of Ophthalmology
Volume 2016, Article ID 3071036, 5 pages
http://dx.doi.org/10.1155/2016/3071036

Research Article

Optical Quality and Related Factors in Ocular Hypertension: Preliminary Study

Yu-jing Wang, Yan-ning Yang, Lin-ying Huang, Bo Wang, Yu-can Han, and Jiang-bo Yan

Department of ophthalmology, Renmin Hospital of Wuhan University, Wuhan, Hubei 430060, China

Correspondence should be addressed to Yan-ning Yang; ophyyn@163.com

Received 27 November 2015; Revised 15 April 2016; Accepted 26 April 2016

Academic Editor: Yannis Athanasiadis

Background. To evaluate the optical quality and related factors in patients with ocular hypertension (OHT). *Methods.* This was a prospective case-control study. A total of 12 eyes with OHT and 20 control eyes underwent testing with Optical Quality Analysis System II (OQAS II) to evaluate the modulation transfer function cut off frequency (MTF cutoff), the Strehl 2D ratio (SR), objective scatter index (OSI), tear-film mean OSI (TFOSI), and the OQAS values (OV100%,OV20%, and OV9%). *Results.* The optical quality of patients with OHT declined, with lower MTF cutoff (OHT 36.86 ± 7.11 cpd , controls 48.50 ± 4.04 cpd, $t = -4.60$, $P < 0.05$), lower SR (OHT 0.22 ± 0.04, controls 0.27 ± 0.05, $t = -2.72$, $P < 0.05$), lower OV100% (OHT 1.26 ± 0.25, controls 1.61 ± 0.14, $t = -4.03$, $P < 0.05$), lower OV20% (OHT 1.27 ± 0.27, controls 1.72 ± 0.20, $t = -4.00$, $P < 0.05$), and lower OV9% (OHT 1.30 ± 0.25, controls 1.69 ± 0.32, $t = -2.28$, $P < 0.05$). There were not any statistically significant differences in OSI and TFOSI. The MTF cutoff in patients with OHT was correlated significantly with age ($r = -0.59$, $P < 0.05$). *Conclusions.* Optical quality of patients with OHT is reduced, with lower MTF cutoff, SR, OV100%, OV20%, and OV9%. MTF cutoff is negatively related to age.

1. Background

Glaucoma is among the leading causes of blindness in the United States and worldwide which is irreversible [1]. OHT is a leading risk factor for the development of primary open-angle glaucoma (POAG) and the only modifiable risk factor at present [2]. The Ocular Hypertension Treatment Study (OHTS) demonstrated that the cumulative incidence of POAG was 9.5% in the patients with OHT [3]. Medications in controlling IOP may decline the incidence of POAG about 50% but increase the complication of cataract [4].

OHT is the condition with an IOP above 21 mmHg without any treatment or use of medications in the absence of optic nerve damage or visual field loss [5]. The optical quality of patients with OHT is not clearly reported so far. Our study analyzed the optical quality with OQAS II (Visiometrics SL, Spain), which provides parameters such as MTF cutoff, SR, OSI, TFOSI, and OVs. In the meantime, we register the general information of the patients with OHT.

2. Methods

2.1. Participants. The patients were diagnosed with OHT in Renmin Hospital of Wuhan University from July 2014 to June 2015. In addition, enrolled eyes fulfilled the criteria, including spherical equivalent refractive error from +2.00 D to −2.00 D and cylinder less than 0.25 D; the corrected visual acuity (BCVA) of all subjects was 1.0 or better measured by standard logarithmic visual acuity chart. All people understand and take the initiative to participate in this study. We have the approval of the Ethics Committee of Renmin Hospital of Wuhan University. And the research was in compliance with the Helsinki Declaration.

Exclusion Criteria. Exclusion criteria was as follows: (a) dry eyes, keratitis, and other ocular surface diseases; (b) uveitis and vitreous turbidity which influence refractive media; (c) histories of eye surgeries; (d) the use of eye drops within one month. A total of 12 OHT eyes and 20 control eyes were enrolled after signing the informed consent.

2.2. OQAS II Measurements. Let the subjects adapt to the dark environment for 3 minutes and then correct the cylindrical defects by external cylindrical lenses; meanwhile the spherical refraction errors were corrected by the double-pass system (±2.00 D). Finally, keep track of the vision quality data for a 4 mm pupil diameter. All subjects underwent three consecutive tests and used the average value. All measurements are performed by an eye specialist.

2.3. Ophthalmologic Examinations. Each examination included autorefraction, best corrected visual (BCVA), Schirmer I test (SIt), tear break-up time (BUT) to exclude dry eyes, and B ultrasonic to exclude vitreous turbidity. The intraocular pressure (IOP) and 24-hour IOP was tested by noncontact tonometry (NCT), including the experimental group and control group. Visual field index (VFI) was assessed using a Humphrey Field Analyzer with the central 30-2 program SITA standard. We also observed the Cup/Disc ratio (CDR) with stereoscopic photography and peripapillary retinal nerve fibre layer, central corneal thickness (CCT) by the use of OCT (Cirrus HD-OCT).

2.4. Statistical Analysis. Data analysis was performed with SPSS 17.0 (Chicago, IL, USA). After normality testing for continuous variables and Chi-square test for nonparametric comparisons, paired Student's t-test was used to compare means of related samples in variables with normal distribution. Paired comparisons included MTF cutoff, SR, OSI, OVs, and TFOSI. Correlation between the MTF cutoff, SR, OSI, and OVs and the age, TFOSI, IOP, CDR, CCT, and VFI was analyzed with Spearman's correlation analysis. The results are expressed as means ± SD, and a P value less than 0.05 was considered statistically significant.

3. Results and Discussion

A total of 32 eyes were enrolled in the study; 20 were men and 12 were women. The mean age was 25.91 ± 6.31 years (range, 14 to 41 years). All subjects had BCVA 1.0 or better. Most of the clinical characteristics of subjects were summarized in Table 1.

3.1. Global Analysis. There were 12 eyes with OHT, 9 males and 3 females, aged 23.33 ± 6.72 years (range: 14 to 32 years old), and 20 control eyes, 11 males and 9 females, aged 27.45 ± 5.67 years (range: 19 to 41 years old). There was no statistically significant difference in gender or age ($P > 0.05$). All the eyes with OHT did not have refractive disorders. The mean spherical equivalent refractive error of manifest refraction in control eyes was −1.32 ± 0.15 D (range, 0 to 1.75 D); the cylinder was −0.07 ± 0.11 D (range, 0 to 0.20 D). It had a statistically significant difference ($P < 0.05$).

3.2. Comparability. Table 2 shows the comparative analysis of the variables between eyes with OHT and control eyes about MTF cutoff, SR, OSI, OVs, and TFOSI. It indicated that patients with OHT have significant decline over MTF cutoff, SR, OV100%, OV20%, and OV9%. However, no other variables presented significant differences.

3.3. Correlation. We found a significant negative correlation between MTF cutoff and age (Spearman's correlation $r = -0.59$, $P = 0.04$), but there were no statistically significant differences between the MTF cutoff and IOP, OSI, CDR, CCT, and VFI. The data were shown in Table 3.

4. Conclusions

4.1. IOP Measurement Reliability Analysis. IOP and CCT were found to be positively correlated by several studies [6, 7], but so far, there is no accurate algorithm for correction. Rahman et al. [7] collected measurements of CCT from 1356 normal individuals; the result showed that the CCT is 540 ± 30 μm presenting normal distribution. All subjects in our study were within normal range. There are a variety of tonometers to evaluate IOP, and the GAT is the current reference standard. Cook et al. [8] evaluated differences between NCT and GAT in 15525 participants. The NCT was with the least amount of variability in IOP. Approximately 66% of measurements with the NCT were estimated to be within 2 mmHg of the GAT measurement. Because all the participants in our study need to repeatedly measure intraocular pressure, consideration of cooperation, and simple operation, we chose the NCT.

4.2. OQAS. Double-pass technique was put forward by Flamant [9] for the first time in 1955. OQAS based on the technique is the only available device that objectively measures the overall optical quality of human eyes [10] and quantitatively analyze the light scatter and aberration in the optical system. It also provides good repeatability and reproducibility [11]. The OQAS had been extensively used for cataract grading [12] and keratitis, dry eyes [13], laser-assisted in situ Keratomileusis (LASIK) [14], and uveitis [15].

OQAS provides parameters such as MTF, SR, OSI, OVs, and TFOSI to simplify the study of the optical quality of the eye. The MTF represents the loss of contrast produced by the eye's optics as a function of spatial frequency. The MTF cutoff is calculated as that corresponding to a 0.01 modulation transfer function value. It is normally assumed that a cutoff frequency of 30 cycles per degree (cpd) in the Contrast Sensitivity Function corresponds to a visual acuity measurement of 20/20 [16]. The SR is often computed in the frequency domain as the ratio between the volume under the MTF curve of the measured eye and that of the aberration-free eye [17]. The SR of normal people is about 30%. The higher the SR value, the smaller the optical system aberration. The three OVs are normalized values of three spatial frequencies, which correspond to MTF values for three contrast conditions commonly used in ophthalmic practice [18]. The system also quantifies intraocular scattered light by means of the OSI parameter [19]. Values of small OSI are usually linked to eyes with low scattering.

The MTF cutoff and OSI measured in this study were close to others found in similar studies. Our results of MTF

Table 1: Clinical characteristics of patients.

Case/age/sex	MD	BCVA	IOP	MTF cutoff (cpd)	SR	OV100%	OV20%	OV9%	OSI	TFOSI
Group 1										
1/14/M	OHT	1.0	24.7	51.10	0.28	1.75	1.92	1.84	0.40	0.69
2/14/M	OHT	1.0	24.0	41.44	0.18	1.38	1.34	1.19	0.33	0.56
3/27/M	OHT	1.0	14.3	29.01	0.20	0.97	1.00	1.13	0.37	0.80
4/25/M	OHT	1.0	16.5	31.75	0.20	1.06	1.00	1.10	0.43	0.85
5/28/F	OHT	1.2	16.2	41.36	0.22	1.38	1.43	1.39	0.30	1.45
6/32/M	OHT	1.2	25.3	33.60	0.25	1.12	1.25	1.46	0.34	0.41
7/28/M	OHT	1.5	13.9	40.39	0.28	1.35	1.48	1.63	0.55	0.81
8/28/M	OHT	1.2	23.8	23.52	0.18	0.78	0.88	1.02	0.67	0.88
9/15/M	OHT	1.0	23.1	36.28	0.25	1.21	1.29	1.44	0.34	0.43
10/15/M	OHT	1.0	22.5	40.11	0.21	1.34	1.15	1.18	0.18	0.51
11/27/F	OHT	1.2	23.4	39.26	0.20	1.37	1.21	1.16	0.54	0.90
12/27/F	OHT	1.2	18.6	34.46	0.19	1.36	1.29	1.10	0.41	0.59
Group 2										
1/24/F	Normal	1.0	15.8	47.03	0.23	1.57	1.69	1.26	0.25	0.61
2/24/F	Normal	1.0	10.3	46.23	0.21	1.43	1.57	1.34	0.22	0.45
3/28/M	Refractive error	1.0	19.7	46.27	0.24	1.54	1.57	1.40	0.64	0.89
4/31/M	Normal	1.0	13.2	53.69	0.32	1.79	2.02	2.04	0.28	0.68
5/22/M	Normal	1.0	12.9	50.60	0.24	1.69	1.53	1.34	0.43	1.29
6/22/M	Normal	1.0	11.5	43.59	0.28	1.45	1.40	1.30	0.39	0.74
7/41/F	Refractive error	1.2	18.2	50.81	0.22	1.69	1.78	1.57	0.19	0.02
8/41/F	Refractive error	1.0	11.6	53.15	0.27	1.77	1.95	1.92	0.20	0.28
9/26/M	Refractive error	1.2	13.9	40.57	0.30	1.35	1.54	1.77	0.66	1.13
10/26/M	Refractive error	1.2	17.1	49.90	0.33	1.66	1.79	1.99	0.65	1.09
11/19/M	Refractive error	1.2	12.6	49.34	0.27	1.64	1.72	1.59	0.43	0.34
12/29/F	Refractive error	1.2	12.7	52.67	0.34	1.76	1.95	2.06	0.55	0.36
13/29/F	Refractive error	1.2	14.1	39.85	0.21	1.33	1.32	1.30	0.38	0.59
14/28/F	Refractive error	1.2	16.9	47.95	0.36	1.60	1.86	2.15	0.19	0.81
15/28/F	Refractive error	1.2	12.5	47.54	0.23	1.58	1.68	1.67	0.24	0.42
16/25/M	Refractive error	1.2	14.3	51.69	0.26	1.72	1.83	1.69	0.27	0.44
17/25/M	Refractive error	1.2	14.2	44.63	0.31	1.49	1.64	1.83	0.29	0.44
18/30/M	Refractive error	1.0	11.1	53.16	0.31	1.77	2.06	2.21	0.56	0.69
19/30/M	Refractive error	1.0	11.3	51.25	0.29	1.71	1.87	1.92	0.37	0.43
20/21/F	Normal	1.0	12.7	50.11	0.22	1.67	1.63	1.38	0.34	0.78

Group 1 = patients with OHT; Group 2 = control; MD = main diagnostic; BCVA = best corrected visual acuity; IOP = mean IOP of 24 h IOP; MTF cutoff = modulation transfer function cutoff frequency; SR = Strehl ratio; OV = OQAS values; OSI = objective scatter index; TFOSI = tear-film mean OSI.

Table 2: Optical quality of OHT and control.

Project	OHT (12 cases) Mean ± SD	Control (20 cases) Mean ± SD	t	P	95% CI Lower bound	95% CI Upper bound
MTF cutoff (cpd)	36.86 ± 7.11	48.50 ± 4.04	−4.60	0.00	−17.44	−6.16
SR	0.22 ± 0.04	0.27 ± 0.05	−2.73	0.02	−0.09	−0.01
OV100%	1.26 ± 0.25	1.61 ± 0.14	−4.03	0.00	−0.55	−0.16
OV20%	1.27 ± 0.27	1.72 ± 0.20	−4.00	0.00	−0.68	−0.20
OV9%	1.30 ± 0.25	1.69 ± 0.32	−2.28	0.04	−0.65	−0.01
OSI	0.40 ± 0.13	0.38 ± 0.16	−0.05	0.96	−0.18	0.17
TFOSI	0.74 ± 0.28	0.62 ± 0.31	0.63	0.54	−0.21	0.37

Table 3: Related factors in MTF cutoff.

Related factors	Correlation coefficient	P
Age	−0.59	0.04
IOP	0.15	0.64
OSI	−0.39	0.20
CDR	−0.05	0.88
CCT	−0.10	0.76
VFI	0.46	0.13

cutoff and OSI were 48.50 ± 4.04 cpd and 0.38 ± 0.16 in control eyes, which is consistent with Matinez et al.'s study of 178 healthy eyes range from 18 to 30 years old showed that normal MTF cutoff is 44.57 ± 7.14 cpd and OSI is 0.38 ± 0.19 [20]. Although there were statistically significant differences in spherical equivalent refractive error and cylinder between these two groups, it had little practical influence on the eye's image quality [20].

Compared with control eyes, patients with OHT had lower MTF cutoff, SR, and OVs, which indicated that the contrast sensitivity in OHT is not as good as healthy one. However, the OSI and TFOSI did not show evident distinction, which means the tear-film and the light scatter are not obvious between these two groups. It can be concluded from the results that the difference between OHT patient and normal is mainly reflected in contrast sensitivity.

Contrast sensitivity function has been accepted widely as a sensitive measure for assessing contrast visual performance in various clinical situations [21]. Some reports have demonstrated that contrast sensitivity function is compromised by optics, such as keratorefractive surgery [22]. It is also influenced by retina and brain processing [23]. Contrast sensitivity was significantly reduced in glaucoma patients with newly diagnosed disease and a good visual acuity [24]. Some studies have concentrated on evaluating whether it would be possible to diagnose glaucoma in patients prior to visual field damage using various contrast sensitivity tests [25]. However, researchers have not determined the diagnostic precision of contrast sensitivity to differentiate between OHT and glaucoma. Our study discovered contrast sensitivity changes in OHT by OQAS prior to visual field damage. And these declines may be mainly attributed to optical and retina changes, because OQAS value reflects the light scatter, aberration [11], and retina [26] changes in the optical system. Nevertheless it is difficult to distinguish between true progression to glaucoma and fluctuation unless the test is repeated for a long time. Xu et al. [27] did not find significant change among patients with higher IOP when evaluating optical quality in patients with thyroid-associated ophthalmopathy. We speculated that their result of IOP was influenced by protopathy.

4.3. Prospect. There are many common functional and structural investigations in detecting progression from OHT to POAG, such as visual field, stereoscopic photography, and OCT [28]. OHTS found the first evidence of glaucomatous damage through visual field (50%) and the optic disc (40%) among those OHT patients [29], and patients with optic nerve head hemorrhage were more likely to turn into POAG. OCT is a high-resolution cross-sectional imaging technique that allows in vivo measurement of tissue thickness. Research has not determined the diagnose precision of ganglion cell complex (GCC) thickness [30] to differentiate between OHT and glaucoma. In our study, we found a decline in optical quality among OHT, especially the contrast visual acuity; we thought the OQAS could be another measurement for those suspected of having POAG, and it was a more sensitive test to measure the contrast sensitivity than VFI. However, long-term monitoring was needed to find out whether the contrast sensitivity would reduce according to the OHT progress and how many patients with OHT would progress to POAG. In terms of complicated pathogenesis and influential factor of IOP, the sample size in our study is relatively small. A larger number of patients would probably result in stronger significance and sensitivity and specificity values.

In summary, OQAS that has the advantages of easy operation and good repeatability quantitatively analyze the optical quality of OHT. It may be another way to study the pathogenetic mechanism, monitor the progress, and guide medication use in OHT.

Abbreviations

OHT: Ocular hypertension
OQAS II: Optical Quality Analysis System II
MTF cutoff: Modulation transfer function cutoff frequency
OSI: Objective scatter index
TFOSI: Tear-film mean OSI
OVs: OQAS values
SR: Strehl 2D ratio
BCVA: Best corrected visual acuity
IOP: Intraocular pressure
VFI: Visual fields index
OCT: Optical coherence tomography
CCT: Central corneal thickness
CDR: Cup/Disc ratio
POAG: Primary open-angle glaucoma
OHTS: The Ocular Hypertension Treatment Study.

Consent

Patient had given their consent for the study to be published. Written informed consent was obtained from the patient for publication of this study and any accompanying images. A copy of the written consent is available for review by the editor of this journal.

Competing Interests

The authors have not received reimbursements, fees, funding, or salary from an organization that may in any way gain or lose financially from the publication of this paper in the past five years, either now or in the future. They have not held any stocks or shares in an organization that may in any way gain or

lose financially from the publication of this paper, either now or in the future. They have not received any patents relating to the content of the paper. There are not any nonfinancial competing interests (political, personal, religious, ideological, academic, intellectual, commercial, or any other competing interests) to declare in relation to this paper.

Authors' Contributions

Yu-jing Wang (AB; FG; ES), Yan-ning Yang (FG; ES), Lin-ying Huang (FG), Bo Wang (FG), Yu-can Han (FG), and Jiang-bo Yan (FG) contributed to this paper.

References

[1] H. A. Quigley, "Number of people with glaucoma worldwide," *British Journal of Ophthalmology*, vol. 80, no. 5, pp. 389–393, 1996.

[2] M. A. Kass, M. O. Gordon, F. Gao et al., "Delaying treatment of ocular hypertension: the ocular hypertension treatment study," *Archives of Ophthalmology*, vol. 128, no. 3, pp. 276–287, 2010.

[3] M. A. Kass, D. K. Heuer, E. J. Higginbotham et al., "The Ocular Hypertension Treatment Study: a randomized trial determines that topical ocular hypotensive medication delays or prevents the onset of primary open-angle glaucoma," *Archives of Ophthalmology*, vol. 120, no. 6, pp. 701–713, 2002.

[4] D. C. Herman, M. O. Gordon, J. A. Beiser et al., "Topical ocular hypotensive medication and lens opacification: evidence from the ocular hypertension treatment study," *American Journal of Ophthalmology*, vol. 142, no. 5, pp. 800–810.e1, 2006.

[5] F. Min, "New progresses in ocular hypertension," *Section OphthalmolForeign Med Sci*, vol. 28, no. 4, pp. 313–315, 2004.

[6] M. G. Uva, M. Reibaldi, A. Longo et al., "Intraocular pressure and central corneal thickness in premature and full-term newborns," *Journal of AAPOS*, vol. 15, no. 4, pp. 367–369, 2011.

[7] M. L. Rahman, C. Bunce, P. R. Healey et al., "Commingling analyses of central corneal thickness and adjusted intraocular pressure in an older Australian population," *Investigative Ophthalmology and Visual Science*, vol. 51, no. 5, pp. 2512–2518, 2010.

[8] J. A. Cook, A. P. Botello, A. Elders et al., "Systematic review of the agreement of tonometers with Goldmann applanation tonometry," *Ophthalmology*, vol. 119, no. 8, pp. 1552–1557, 2012.

[9] F. Flamant, "Distribution of light in the retinal image," *Arch OphthalmolRev Gen Ophthalmol*, vol. 16, pp. 54–66, 1956.

[10] F. Díaz-Doutón, A. Benito, J. Pujol, M. Arjona, J. L. Güell, and P. Artal, "Comparison of the retinal image quality with a Hartmann-Shack wavefront sensor and a double-pass instrument," *Investigative Ophthalmology and Visual Science*, vol. 47, no. 4, pp. 1710–1716, 2006.

[11] A. Saad, M. Saab, and D. Gatinel, "Repeatability of measurements with a double-pass system," *Journal of Cataract and Refractive Surgery*, vol. 36, no. 1, pp. 28–33, 2010.

[12] M. Vilaseca, M. J. Romero, M. Arjona et al., "Grading nuclear, cortical and posterior subcapsular cataracts using an objective scatter index measured with a double-pass system," *British Journal of Ophthalmology*, vol. 96, no. 9, pp. 1204–1210, 2012.

[13] A. Benito, G. M. Pérez, S. Mirabet et al., "Objective optical assessment of tear-film quality dynamics in normal and mildly symptomatic dry eyes," *Journal of Cataract and Refractive Surgery*, vol. 37, no. 8, pp. 1481–1487, 2011.

[14] M. Vilaseca, A. Padilla, J. Pujol, J. C. Ondategui, P. Artal, and J. L. Güell, "Optical quality one month after Verisyse and Veriflex phakic IOL implantation and Zeiss MEL 80 LASIK for myopia from 5.00 to 16.50 diopters," *Journal of Refractive Surgery*, vol. 25, no. 8, pp. 689–698, 2009.

[15] M. A. Nanavaty, M. R. Stanford, R. Sharma et al., "Use of the double-pass technique to quantify ocular scatter in patients with uveitis: a pilot study," *Opthtalmologica*, vol. 225, no. 1, pp. 61–66, 2011.

[16] S. H. Schwartz, *Visual Perception: A Clinical Orientation*, McGraw-Hill, New York, NY, USA, 2nd edition, 1999.

[17] R. Navarro, P. Artal, and D. R. Williams, "Modulation transfer of the human eye as a function of retinal eccentricity," *Journal of the Optical Society of America A: Optics and Image Science, and Vision*, vol. 10, no. 2, pp. 201–212, 1993.

[18] M. Vilaseca, A. Padilla, J. C. Ondategui, M. Arjona, J. L. Güell, and J. Pujol, "Effect of laser in situ keratomileusis on vision analyzed using preoperative optical quality," *Journal of Cataract and Refractive Surgery*, vol. 36, no. 11, pp. 1945–1953, 2010.

[19] P. Artal, A. Benito, G. M. Pérez et al., "An objective scatter index based on double-pass retinal images of a point source to classify cataracts," *PLoS ONE*, vol. 6, no. 2, Article ID e16823, 2011.

[20] J. A. Matinez, M. Vilaseca, J. C. Ondategui et al., "Optical quality and scattering in a healthy young population," *Clinical and Experimental Optometry*, vol. 94, no. 2, pp. 223–229, 2011.

[21] T. Oshika, C. Okamoto, T. Samejima, T. Tokunaga, and K. Miyata, "Contrast sensitivity function and ocular higher-order wavefront aberrations in normal human eyes," *Ophthalmology*, vol. 113, no. 10, pp. 1807–1812, 2006.

[22] S. Mutyala, M. B. McDonald, K. A. Scheinblum, M. D. Ostrick, S. F. Brint, and H. Thompson, "Contrast sensitivity evaluation after laser in situ keratomileusis," *Ophthalmology*, vol. 107, no. 10, pp. 1864–1867, 2000.

[23] D. B. Elliott, "Contrast sensitivity and glare testing," in *Borish's Clinical Refraction*, W. J. Benjamin, Ed., pp. 203–241, WB Saunders, Philadelphia, Pa, USA, 1998.

[24] S. Onal, O. Yenice, S. Cakir et al., "FACT contrast sensitivity as diagnostic tool in glaucoma," *International Ophthalmology*, vol. 28, no. 6, pp. 407–412, 2008.

[25] J. M. Wood and J. E. Lovie-Kitchin, "Evaluation of the efficacy of contrast sensitivity measures for the detection of early primary open-angle glaucoma," *Optometry and Vision Science*, vol. 69, no. 3, pp. 175–181, 1992.

[26] P. Artal and R. Navarro, "Simultaneous measurement of two-point-spread functions at different locations across the human fovea," *Applied Optics*, vol. 31, no. 19, pp. 3646–3656, 1992.

[27] G.-G. Xu, Y.-J. Wu, W. Sheng et al., "Visual quality reduction and related factors in thyroid-associated ophthalmopathy," *Chinese Journal of Optometry Ophthalmology and Visual Science*, vol. 15, no. 2, pp. 98–103, 2013.

[28] P. Y. Boey and S. L. Mansberger, "Ocular hypertension: an approach to assessment and management," *Canadian Journal of Ophthalmology*, vol. 49, no. 6, pp. 489–496, 2014.

[29] J. L. Keltner, C. A. Johnson, D. R. Anderson et al., "The association between glaucomatous visual field and optic nerve head features in the Ocular Hypertension Treatment study," *Ophthalmology*, vol. 113, no. 9, pp. 1603–1612, 2006.

[30] S. Mori, M. Hangai, A. Sakamoto, and N. Yoshimura, "Spectral-domain optical coherence tomography measurement of macular volume for diagnosing glaucoma," *Journal of Glaucoma*, vol. 19, no. 8, pp. 528–534, 2010.

Hindawi Publishing Corporation
Journal of Ophthalmology
Volume 2016, Article ID 6571547, 6 pages
http://dx.doi.org/10.1155/2016/6571547

Research Article

Use of Mechanical Turk as a MapReduce Framework for Macular OCT Segmentation

Aaron Y. Lee,[1,2] Cecilia S. Lee,[1,2] Pearse A. Keane,[2,3,4] and Adnan Tufail[2,3,4]

[1]*Department of Ophthalmology, University of Washington, Seattle, WA 98104, USA*
[2]*Medical Retina Service, Moorfields Eye Hospital NHS Foundation Trust, London EC1V 2PD, UK*
[3]*Institute of Ophthalmology, University College London, London WC1E 6BT, UK*
[4]*National Institute for Health Research Biomedical Research Centre for Ophthalmology, Moorfields Eye Hospital NHS Foundation Trust, London SE1 4TT, UK*

Correspondence should be addressed to Adnan Tufail; adnan.tufail@moorfields.nhs.uk

Received 5 January 2016; Accepted 19 April 2016

Academic Editor: Yannis Athanasiadis

Purpose. To evaluate the feasibility of using Mechanical Turk as a massively parallel platform to perform manual segmentations of macular spectral domain optical coherence tomography (SD-OCT) images using a MapReduce framework. *Methods.* A macular SD-OCT volume of 61 slice images was map-distributed to Amazon Mechanical Turk. Each Human Intelligence Task was set to \$0.01 and required the user to draw five lines to outline the sublayers of the retinal OCT image after being shown example images. Each image was submitted twice for segmentation, and interrater reliability was calculated. The interface was created using custom HTML5 and JavaScript code, and data analysis was performed using R. An automated pipeline was developed to handle the map and reduce steps of the framework. *Results.* More than 93,500 data points were collected using this framework for the 61 images submitted. Pearson's correlation of interrater reliability was 0.995 ($p < 0.0001$) and coefficient of determination was 0.991. The cost of segmenting the macular volume was \$1.21. A total of 22 individual Mechanical Turk users provided segmentations, each completing an average of 5.5 HITs. Each HIT was completed in an average of 4.43 minutes. *Conclusions.* Amazon Mechanical Turk provides a cost-effective, scalable, high-availability infrastructure for manual segmentation of OCT images.

1. Introduction

Crowdsourcing is a relatively novel technique involving the distribution of work to a large group of people, typically through online frameworks [1]. It allows the subdivision of tedious tasks into discrete tasks that can be completed individually. Amazon Mechanical Turk is the largest and most popular of the online crowdsourcing systems [2]. In this system, simple Human Intelligence Tasks (HITs) are submitted to online untrained users for a small compensation. Recently in computer science, the MapReduce programming model has caused a paradigm shift in the way that large data sets are distributed in parallel within a computing cluster [3]. Notably Google used the MapReduce framework to regenerate their index of the Internet, and the MapReduce framework has become popularized as a generic framework to solve big data problems in multicore cluster systems. In this study, our goal was to utilize human intelligence as a MapReduce framework for the segmentation of a macular optical coherence tomography (OCT) volume [4–6].

OCT is an important noninvasive diagnostic tool in the field of ophthalmology [6] and in the management of age-related macular degeneration (AMD), the commonest cause of blindness in the developed world [7, 8]. OCT measurements such as retinal thickness, subretinal fluid, and pigment epithelial detachment are important parameters in the diagnosis and monitoring of various retinal diseases [9, 10] and are thus integral in both large-scale clinical trials and routine clinical practice [11]. However, automated measurements provided by the OCT software result in frequent errors in quantifying critical parameters such as macular thickness and volume [12, 13]. Errors of retinal boundary detection and

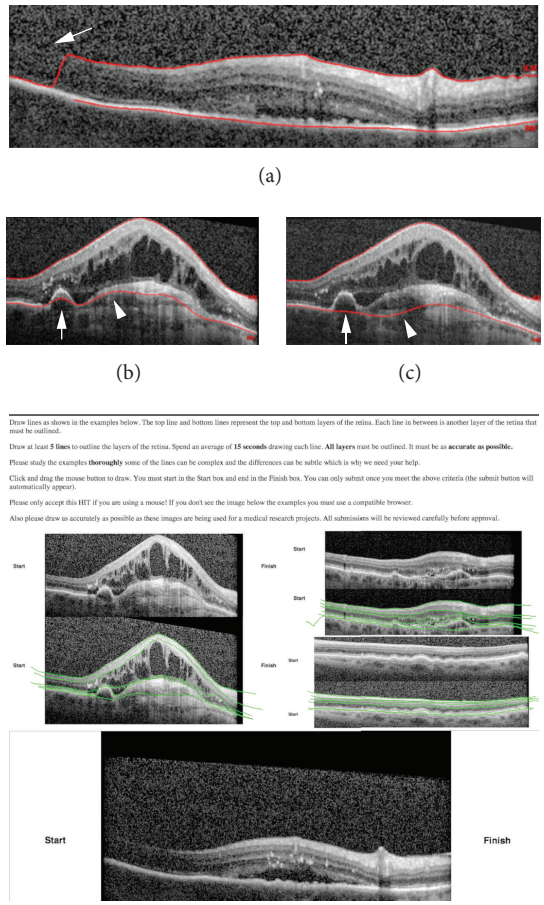

Figure 1: Examples of incorrect segmentations by automated software and user-interface for Mechanical Turk. Panel (a) is an example of a macula SD-OCT image with missing information (arrow) causing a sudden jump in the identification of the Internal-Limiting Membrane (ILM) by automated software included with Heidelberg Spectralis. Panels (b and c) show two similar macular OCT images with different automated segmentations caused by pigment epithelial detachment (arrow) and subretinal fibrosis (arrowhead). Panel (d) is a screenshot of web-based user-interface submitted to Amazon Mechanical Turk for manual segmentations.

thickness measurements have been reported as high as 92% in segmentation performed by the Stratus OCT system (Carl Zeiss Meditec, Germany) [14]. Although spectral domain OCT (SD-OCT) is expected to produce more accurate measurements with higher resolution and less artifacts, the segmentation errors continue to be a significant problem in measuring macular thickness, particularly in eyes with pathology [15–17].

There has been increasing interest in ways to overcome automated segmentation errors. Publicly available image analysis software, OCTOR (Doheny Image Reading Center, Los Angeles), quantifies OCT-derived parameters after a trained OCT grader delineates the retinal boundaries of interest manually. The software calculates the distance in pixels between two manually drawn layers. Then using the dimensions of the B-scan image, the data is converted into a thickness measurement [18]. Even though OCTOR is less subject to segmentation errors, it is time-consuming and impractical for use in large-scale clinical trials.

Automated segmentations have been attempted using dual-scale gradient or intensity information. Then the edges of the boundary were optimized using a shortest path search method [19]. Statistical models have been utilized for a more reliable automatic segmentation system [20]. Retinal layers have been segmented using seven features extracted from the OCT data with a random forest classifier [21]. Despite these achievements in the field of automated segmentations, macular OCT images with complex subretinal pathology, intraretinal/subretinal fluid, or low signal to noise ratio continue to pose a challenge for computer vision (Figures 1(a)–1(c)).

Amazon Mechanical Turk and other modalities of crowdsourcing have been previously used in medical applications and demonstrated high level of accuracy in diagnostic accuracy [22–24]. In ophthalmology, retinal fundus photographs have been recently analyzed and showed an accuracy level at least comparable to automated programs and some trained graders [25]. To our knowledge, it has not been used to

attain segmentations in macular OCT images with complex pathology. We sought to achieve highly reliable segmentation by designing a system for distributed OCT segmentation over a scalable, human based infrastructure and to show proof of concept results.

2. Materials and Methods

Patient identifiers were stripped out completely and pseudoanonymized, and on this basis and for retrospective use of anonymized data in the UK formal ethics committee review is not required. However, consent was still obtained from all patients in this study to use their OCT images for research. This study was conducted in accordance with the Declaration of Helsinki and the United Kingdom's Data Protection Act.

A total of 61 individual macular SD-OCT images were taken using a commercially available SD-OCT device (Spectralis, Heidelberg Engineering, Heidelberg, Germany) as part of routine medical care for AMD. The images were extracted using commercially provided software (Heyex DICOM Interface, Heidelberg Engineering, Heidelberg, Germany), and no image manipulation was performed.

A custom web-based user-interface was created with Hyper Text Markup Language 5 (HTML5) and JavaScript to allow Mechanical Turk users to directly draw on the images through their web browser (Figure 1(d)). This interface gave each user an example image of segmentation by an expert retina trained physician. The JavaScript interface allowed capture of the mouse input to draw segmentation lines on the provided OCT image and captured timing data as the user drew segmentation lines. Each user was instructed to draw 5 lines to segment the provided image and they were required to spend at least an average of 15 seconds per line before they were allowed to submit their work. No image enlargement or zoom was allowed and users were given 3 example segmentations provided by a trained OCT grader using the same system. Each image was created as a separate HIT and the reward was set to \$0.01 (USD). Mechanical Turk users were required to have a prior approval rate of 80% before being allowed to participate in these HITs. In addition to the lines drawn, data was collected on the time spent drawing each line segment and time to completion of segmentation, and each image was submitted twice for segmentation.

After all segmentations were performed, the data was collected and image processing was performed to enhance the accuracy of the manual segmentations. This automated analysis pipeline used adjustments based on finding the consistently highest contrast value within 5 pixels of where the segmentation line was drawn. If there were no improved changes detected, then data from the original manual segmentation was used. Automated quality control heuristics were implemented to ensure that no two segmentations from the same user of the same image crossed paths. The reduction step of combining consensus segmentations of the same image was classified using a linear correlation heuristic, and these segmentation data were used to calculate interrater reliability. The final reduction step was utilized to recreate a three-dimensional segmented model of the retina. Custom Ruby and R code was created to automate the creation, submission, collection, image processing, and data analysis. All custom software is available upon request.

3. Results

The automated analysis pipeline, using a MapReduce framework, was able to create, submit, collect, collate, process, and analyze a total of over 92,500 data points from the 61 macular OCT images that were manually segmented twice over Amazon Mechanical Turk. Time of submission of the 122 HITs to completion of all tasks was 3 days with greater than 75% of HITs finished within the first 24 hours. A total of 22 individual Mechanical Turk users provided segmentations each completing an average of 5.5 HITs.

Each HIT was completed on average of 4.43 minutes (range: 1.83–24.45 minutes) with each segmentation line completed on average of 20.40 seconds (Figure 2(a)). In a subset of users who had segmented four or more HITs, we noted that there was a trend in decreasing time to completion of the task (Figure 2(b)). A total of 646 segmentations were collected, and an average of 5.30 segmentations per macular OCT was provided (range: 5 to 7). The total cost of segmentations of all images was \$1.22 (USD).

Representative segmentations with the associated image processing are shown in Figure 3. All slices from both manual segmentation and the combined final segmentations are shown in the Supplementary Materials (see Supplementary Material available online at http://dx.doi.org/10.1155/2016/6571547). Pearson's correlation of interrater reliability was 0.995 ($p < 0.0001$) and coefficient of determination was 0.991. A Bland-Altman plot was calculated to estimate interrater agreement based on the consensus segmentation lines (Figure 4).

4. Discussion

OCT is a critical tool in clinical practice for ophthalmology, and objective, quantitative OCT parameters have the potential of guiding clinical practice and establishing new endpoints for clinical trials. Automated segmentation approaches have traditionally suffered in the setting of complex retinal pathology such as pigment epithelial detachments, subretinal fibrosis, or intraretinal and subretinal fluid. Indeed the automated segmentation that is provided with the commercial device used in this study failed in many situations (Figures 1(a)–1(c)). With the advent of Mechanical Turk and programming APIs, automating simple human vision tasks through a MapReduce framework has become not only feasible but also cost-effective. The advantages of utilizing manual segmentations using human vision include the ability to complete areas of macular OCT where there is poor signal to noise ratio (Figure 3(a)) or complex pathology (Figure 3(c)).

Next steps of this study would be to compare the accuracy of the Mechanical Turk based segmentation to the ones performed by trained experts. Using the segmentation lines performed by trained experts as the gold standard, we will plan to evaluate the correlation between the accuracy and the time spent by the users, previous experience of the users,

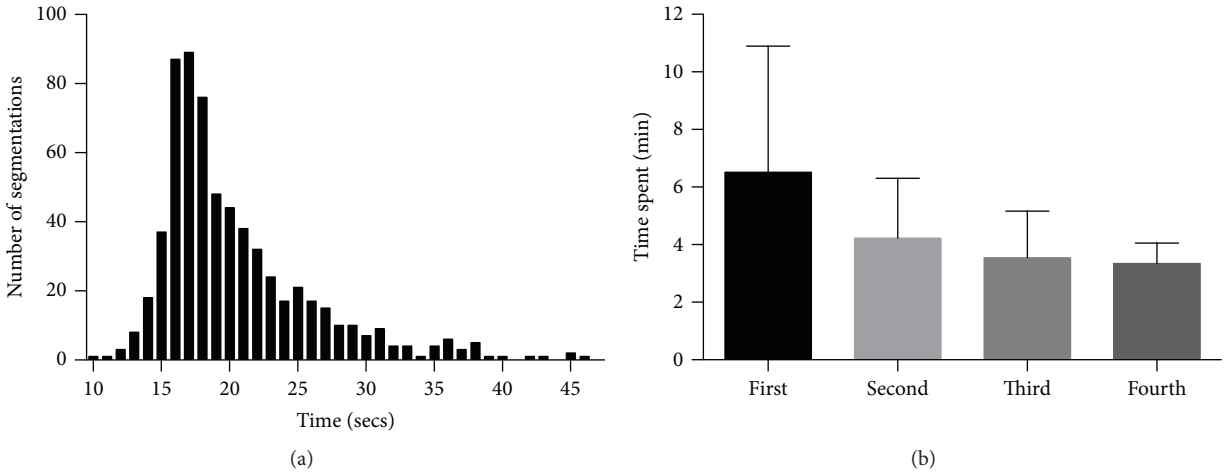

Figure 2: Temporal data of segmentations. Panel (a) shows a histogram of the time spent for each segmentation line. Average was 20.40 seconds with a range of 10.01 to 46.22 seconds. Panel (b) shows the decreasing trend in total time spent in minutes segmenting one SD-OCT image in a subset of users who segmented 4 or more times (7 out of 22 users). Error bars are standard deviation.

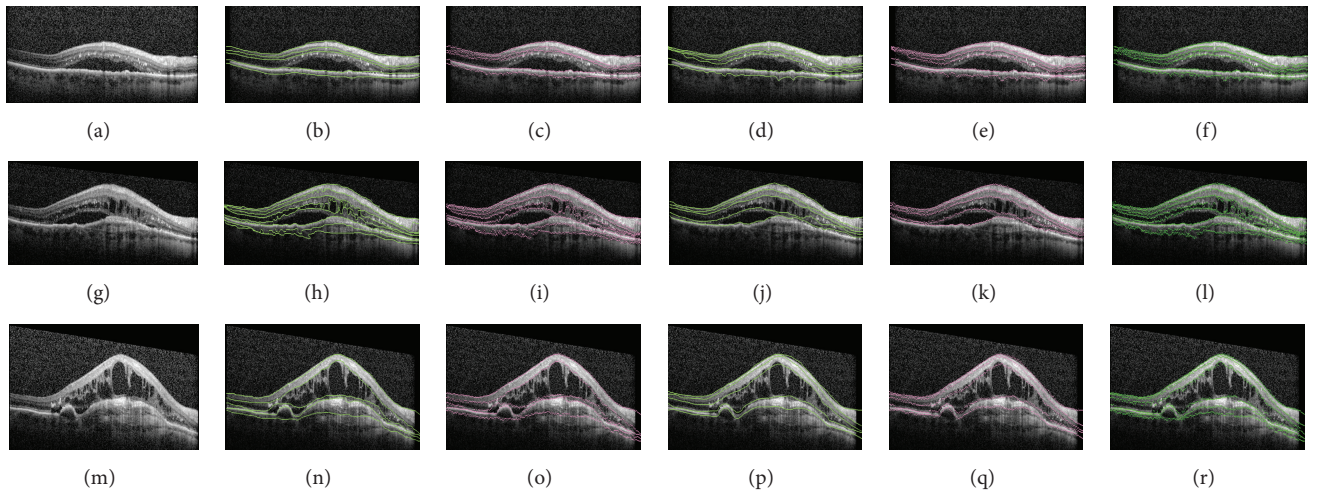

Figure 3: Representative segmentations by Mechanical Turk based manual segmentations with contrast based enhancements. Panels (a, g, m) show three raw SD-OCT macular images. Panels (b, d, h, j, n, p) demonstrate each image segmented by two different people on Mechanical Turk. Manual segmentations are shown as green lines. Panels (c, e, i, k, o, q) show local contrast based enhancement of manual segmentations as magenta lines. Panels (f, l, r) are the final consensus segmentations (green lines) after combining segmentations.

and any learning effect by repetitive performance of the same users.

Limitations of this approach stem from the lack of professionally trained OCT readers and the lack of knowledge or training of the Mechanical Turk users. Future analysis pipelines may include an expert validation step, which reviews the consensus segmentations and decides whether to accept or to reject the submitted segmentations, which then could be resubmitted for another round of segmentation. In addition, future, large-scale studies will be necessary to assess the external validity of this system by submitting macular OCT images for segmentation by expert graders versus Mechanical Turk.

Large data sets are becoming increasingly common with today's clinical studies and multicenter trials. Rapid, reliable, cost-effective methods of interpreting large data will be crucial in the future. Crowdsourcing in OCT segmentation has the potential of minimizing the errors seen in automated segmentation system with less time and cost than manual segmentations performed in reading centers. Additional ways to improve this tool such as more effective training of the users, preselection of qualified users, or creating an automated system based on users' initial segmentation would be important areas to be investigated. Implementation of our current method in the RISE/RIDE study, for example, where 759 patients received monthly OCT imaging, would

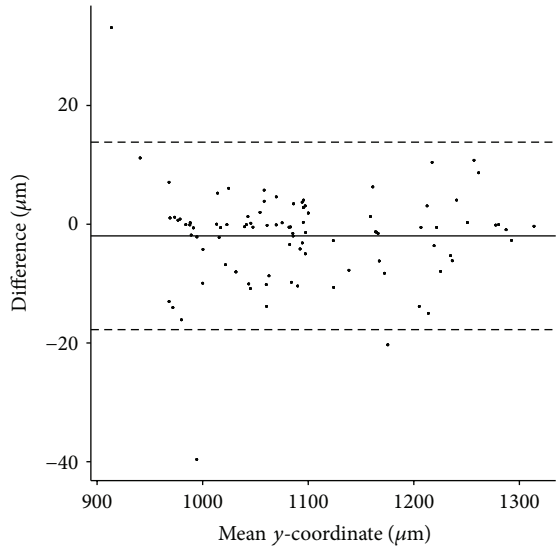

Figure 4: Bland-Altman plot showing agreement between segmentations. Consensus segmentations of the same image between two independent Mechanical Turk users were used to determine interrater reliability. The average y-coordinate value in microns for each consensus line was used and the Bland-Altman plot was created.

cost approximately $273.24 per study month for a standard 18-slice macular OCT.

This study has applied a novel proof of concept of applying manual segmentation of OCT images in a distributed way to nonexpert graders. The retinas with various pathologies provide challenge to currently available automated segmentation systems. Mechanical Turk provides a cost-effective, scalable, high-availability infrastructure for manual segmentation of OCT images of the type which are difficult for automated algorithms to handle. The resulting images can be recombined for high-resolution 3D analysis. This approach may be applied to the analysis of high volumes of OCT images in clinical studies or training of future automated segmentation algorithms.

Competing Interests

The authors declare that they have no competing interests.

Acknowledgments

Cecilia S. Lee was supported by NIH Grant no. 1K23EY-024921.

References

[1] D. C. Brabham, K. M. Ribisl, T. R. Kirchner, and J. M. Bernhardt, "Crowdsourcing applications for public health," *American Journal of Preventive Medicine*, vol. 46, no. 2, pp. 179–187, 2014.

[2] M. J. C. Crump, J. V. McDonnell, and T. M. Gureckis, "Evaluating Amazon's Mechanical Turk as a tool for experimental behavioral research," *PLoS ONE*, vol. 8, no. 3, Article ID e57410, 2013.

[3] R. Bellazzi, "Big data and biomedical informatics: a challenging opportunity," *Yearbook of Medical Informatics*, vol. 9, pp. 8–13, 2014.

[4] R. C. Taylor, "An overview of the Hadoop/MapReduce/HBase framework and its current applications in bioinformatics," *BMC Bioinformatics*, vol. 11, supplement 12, article S1, 2010.

[5] D. Huang, E. A. Swanson, C. P. Lin et al., "Optical coherence tomography," *Science*, vol. 254, no. 5035, pp. 1178–1181, 1991.

[6] I. Voo, E. C. Mavrofrides, and C. A. Puliafito, "Clinical applications of optical coherence tomography for the diagnosis and management of macular diseases," *Ophthalmology Clinics of North America*, vol. 17, no. 1, pp. 21–31, 2004.

[7] R. Klein, T. Peto, A. Bird, and M. R. Vannewkirk, "The epidemiology of age-related macular degeneration," *American Journal of Ophthalmology*, vol. 137, no. 3, pp. 486–495, 2004.

[8] N. Congdon, B. O'Colmain, C. C. W. Klaver et al., "Causes and prevalence of visual impairment among adults in the United States," *Archives of Ophthalmology*, vol. 122, no. 4, pp. 477–485, 2004.

[9] D. M. Brown, P. K. Kaiser, M. Michels et al., "Ranibizumab versus verteporfin for neovascular age-related macular degeneration," *The New England Journal of Medicine*, vol. 355, no. 14, pp. 1432–1444, 2006.

[10] P. J. Rosenfeld, D. M. Brown, J. S. Heier et al., "Ranibizumab for neovascular age-related macular degeneration," *The New England Journal of Medicine*, vol. 355, no. 14, pp. 1419–1431, 2006.

[11] D. M. Brown, Q. D. Nguyen, D. M. Marcus et al., "Long-term outcomes of ranibizumab therapy for diabetic macular edema: the 36-month results from two phase III trials: RISE and RIDE," *Ophthalmology*, vol. 120, no. 10, pp. 2013–2022, 2013.

[12] P. J. Patel, F. K. Chen, L. da Cruz, and A. Tufail, "Segmentation error in Stratus optical coherence tomography for neovascular age-related macular degeneration," *Investigative Ophthalmology and Visual Science*, vol. 50, no. 1, pp. 399–404, 2009.

[13] P. A. Keane, P. J. Patel, S. Liakopoulos, F. M. Heussen, S. R. Sadda, and A. Tufail, "Evaluation of age-related macular degeneration with optical coherence tomography," *Survey of Ophthalmology*, vol. 57, no. 5, pp. 389–414, 2012.

[14] P. A. Keane, S. Liakopoulos, R. V. Jivrajka et al., "Evaluation of optical coherence tomography retinal thickness parameters for use in clinical trials for neovascular age-related macular degeneration," *Investigative Ophthalmology and Visual Science*, vol. 50, no. 7, pp. 3378–3385, 2009.

[15] Y. Song, B. R. Lee, Y. W. Shin, and Y. J. Lee, "Overcoming segmentation errors in measurements of macular thickness made by spectral-domain optical coherence tomography," *Retina (Philadelphia, Pa)*, vol. 32, no. 3, pp. 569–580, 2012.

[16] M. Kim, S. Lee, J. Han, S.-Y. Yu, and H. Kwak, "Segmentation error and macular thickness measurements obtained with spectral-domain optical coherence tomography devices in neovascular age-related macular degeneration," *Indian Journal of Ophthalmology*, vol. 61, no. 5, pp. 213–217, 2013.

[17] P. A. Keane, P. S. Mand, S. Liakopoulos, A. C. Walsh, and S. R. Sadda, "Accuracy of retinal thickness measurements obtained with Cirrus optical coherence tomography," *British Journal of Ophthalmology*, vol. 93, no. 11, pp. 1461–1467, 2009.

[18] S. R. Sadda, S. Joeres, Z. Wu et al., "Error correction and quantitative subanalysis of optical coherence tomography data using computer-assisted grading," *Investigative Ophthalmology & Visual Science*, vol. 48, no. 2, pp. 839–848, 2007.

[19] Q. Yang, C. A. Reisman, Z. Wang et al., "Automated layer segmentation of macular OCT images using dual-scale gradient information," *Optics Express*, vol. 18, no. 20, pp. 21293–21307, 2010.

[20] V. Kajić, B. Považay, B. Hermann et al., "Robust segmentation of intraretinal layers in the normal human fovea using a novel statistical model based on texture and shape analysis," *Optics Express*, vol. 18, no. 14, pp. 14730–14744, 2010.

[21] A. Lang, A. Carass, E. Sotirchos, P. Calabresi, and J. L. Prince, "Segmentation of retinal OCT images using a random forest classifier," in *Proceedings of the Medical Imaging: Image Processing*, vol. 8669 of *Proceedings of SPIE*, Lake Buena Vista, Fla, USA, February 2013.

[22] R. R. Carter, A. DiFeo, K. Bogie, G.-Q. Zhang, and J. Sun, "Crowdsourcing awareness: exploration of the ovarian cancer knowledge gap through Amazon Mechanical Turk," *PLoS ONE*, vol. 9, no. 1, Article ID e85508, 2014.

[23] S. Mavandadi, S. Dimitrov, S. Feng et al., "Distributed medical image analysis and diagnosis through crowd-sourced games: a malaria case study," *PLoS ONE*, vol. 7, no. 5, Article ID e37245, 2012.

[24] T. B. Nguyen, S. Wang, V. Anugu et al., "Distributed human intelligence for colonic polyp classification in computer-aided detection for CT colonography," *Radiology*, vol. 262, no. 3, pp. 824–833, 2012.

[25] D. Mitry, T. Peto, S. Hayat, J. E. Morgan, K.-T. Khaw, and P. J. Foster, "Crowdsourcing as a novel technique for retinal fundus photography classification: analysis of images in the EPIC norfolk cohort on behalf of the UKBiobank eye and vision consortium," *PLoS ONE*, vol. 8, no. 8, Article ID e71154, 2013.